Predicting the fatigue damage evolution in welded steel joints

Zbigniew Jakub Mikulski

Zbigniew Jakub Mikulski

Predicting the fatigue damage evolution in welded steel joints

Doctoral dissertation for the degree *Philosophiae Doctor (PhD)*
at the Faculty of Engineering and Science,
specialization in Civil and Structural Engineering

University of Agder
Faculty of Engineering and Science
2024

Preface

The present thesis is submitted to the University of Agder (UiA) as a partial fulfilment of the requirements for the degree of Doctor of Philosophy (PhD) in Engineering Sciences, specialization in Civil and Structural Engineering.

The research work has been carried out at the Faculty of Engineering and Science under the supervision of Professor Tom Lassen. He is at present the technical manager at Marine Resources Advisory Team and has given important assistance to the present work also from this position. This is highly appreciated.

The research project was part of the SFI Offshore Mechatronics program, associated with work package WP5: Condition Monitoring Technologies.

Acknowledgements

First and foremost, I wish to thank Professor Tom Lassen for providing great supervision throughout my PhD project, for thousands of invaluable discussions, constructive feedback, and guidance in theoretical and experimental work.

I would also like to acknowledge the support given by Vidar Hellum at AS Nymo by providing the welded test specimens applied for the present experimental work. Vidar has later been associated with UiA and has been a good colleague for fruitful discussions.

I also wish to thank Professor Geir Grasmo for valuable comments, discussions, and guidance during the last phase of my project.

I appreciate the interest shown by Det Norske Veritas (DNV) and The Welding Institute (TWI) regarding the application of the present Random Fatigue Limit Model (RFLM) for the fatigue life predictions of girth welds in steel pipes. The meetings with the principal engineers Agnes Horn (DNV) and Carol Johnston (TWI) have been an inspiration for future work.

My heartfelt appreciation also goes out to my family. Especially, I wish to thank my wife, Gosia, for her love, patience, and continuous support.

Finally, I would like to thank Gerrit Surup, Reyn O'Born, Ingrid Lande, Mohammad Ali Mahdavipour, and Guodong Liang with whom I shared the office space for a friendly atmosphere and many discussions.

Summary

The present thesis is investigating the fatigue damage evolution in welded steel joints subjected to dynamic repetitive loading. The work embraces various joint geometries and loading modes. The focus is on the fatigue damage occurring at the weld toe in fillet welded attachments. The work is mainly focusing on joints subjected to constant amplitude (CA) loading but some considerations for variable amplitude (VA) loading are also included. The damage mechanisms involved are discussed and modelled both for the initiation phase and the subsequent crack growth phase. The basic theories for these phases are examined and discussed and new models and prediction methods are proposed. The focus is on the probabilistic modelling such that the large scatter found in the fatigue damage evolution can be accounted for. An advanced probabilistic model for life predictions designated the Random Fatigue-Limit Model (RFLM) is fitted to the experimental data. The model is suggested as a support and even as an alternative to the conventional S-N curves currently recommended for fatigue life predictions in the building codes. The proposed RFLM is enhanced such that it can explicitly account for the mean stress effect for a given applied stress range. A distinction is made between the initiation phase and the crack growth phase regarding the impact from the mean stress. Data from experimental investigations are collected and used to corroborate the proposed models and applied calculation methodologies. Additional experimental work with test series for fillet welded longitudinal attachments is carried out as a supplement to the collected life data. For this test series both the initiation phase and the crack growth phase are monitored by an Alternating Current Potential Drop (ACPD) method. Possible improvements of the models are suggested based on this empirical background. The present work provides new knowledge regarding:

- How to describe and model the entire damage evolution in welded joints.
- The importance and the modelling of the crack initiation phase in the joints.
- Realistic fatigue crack propagation model for cracks emanating from the weld toe region.
- Advanced statistical analysis of life data from tests such that improved fatigue resistance curves under constant amplitude loading are obtained.
- The increased scatter in fatigue lives at very low stress ranges.

- The compatibility between probabilistic models and underlying physical models.
- Damage accumulation modelling under variable amplitude loading.
- How to handle the impact of mean stress effect for a given stress range.

The presentation of the above topics must necessarily be limited in the present summary and overview document. The reader can find more important details for the modelling carried out and more elaborated explanations in the international publications that have been generated from the present research work. These publications are listed in the next section and are also found in the appendices.

Abstrakt

Denne oppgaven undersøker utviklingen av utmattingsskader i sveisede stålforbindelser utsatt for dynamisk gjentatt belastning. Arbeidet omfatter forbindelser med ulike geometrier og ulike belastninger. Fokus er rettet mot utmattingsskaden som oppstår ved sveisetåen i kilsveisede innfestinger. Arbeidet fokuserer hovedsakelig på forbindelser utsatt for belastning med konstant amplitude (CA), men noen betraktninger rundt belastning med variabel amplitude (VA) er også inkludert. De involverte skademekanismene diskuteres og modelleres både for initieringsfasen og den påfølgende sprekkvekstfasen. De grunnleggende teoriene for disse fasene blir undersøkt og diskutert og nye modeller og prediksjonsmetoder foreslås. Fokuset er på modellering basert på sannsynlighets modeller, slik at den store spredningen som finnes i utmattelsesskadeutviklingen kan gjøres rede for. En avansert probabilistisk modell for levetidsberegninger kalt Random Fatigue-Limit Model (RFLM) er tilpasset de eksperimentelle dataene. Modellen er foreslått som en støtte til, og til og med som et alternativ til de konvensjonelle S-N-kurvene som for tiden anbefales for beregning av utmattingslevetid i regelverk for prosjektering av konstruksjoner. Den foreslåtte RFLM er forbedret slik at den eksplisitt kan redegjøre for middelspenningseffekten for en gitt påført spenningsvidde. Det skilles mellom initieringsfasen og sprekkvekstfasen når det gjelder påvirkning fra middelspenningen. Data fra eksperimentelle undersøkelser er samlet inn og brukes til å underbygge de foreslåtte modellene og anvendte beregningsmetoder. Ytterligere eksperimenter på plater med kilsveisede langsgående innfestinger er utført som et supplement til innsamlet levetidsdata. Under disse eksperimentene overvåkes både initieringsfasen og sprekkvekstfasen ved hjelp av ACPD-målinger (Alternating Current Potential Drop). Mulige forbedringer av modellene foreslås basert på denne empiriske bakgrunnen. Dette arbeidet gir ny kunnskap om:

- Hvordan beskrive og modellere hele skadeutviklingen i sveisede forbindelser.
- Viktigheten av og modelleringen av sprekkinitieringsfasen i sveisede skjøter.
- Realistisk sprekkvekst modell for sprekker som har initiert ved sveisetåen.

- Avansert statistisk analyse av levetidsdata fra eksperimenter slik at forbedrede levetidskurver for belastning med konstant amplitude kan foreslås.
- Den økte spredningen i utmattingslevetid ved svært lave spenningsrekkevidder.
- Kompatibiliteten mellom sannsynlighetsmodeller og underliggende fysiske modeller.
- Skadeakkumuleringsmodellering under variabel amplitudebelastning.
- Hvordan håndtere middelspenningseffekten for et gitt spenningsvidde.

Presentasjonen av de ovennevnte temaene må nødvendigvis begrenses i dette sammendraget og oversiktsdokumentet. Leseren kan finne viktige detaljer for den utførte modelleringen og mer utdypende forklaringer i de internasjonale publikasjonene som er generert fra dette forskningsarbeidet. Disse publikasjonene er listet opp i neste avsnitt og finnes også i vedleggene.

Publications

The following articles have been published in peer-reviewed international conference proceedings and journals:

Paper A Z. Mikulski, V. Hellum, T. Lassen, "Modelling the fatigue damage evolution in welded joints", in *Proceedings of the ASME 2017 36th International Conference on Ocean, Offshore and Arctic Engineering, OMAE2017*, Volume 4: Material Technology, ISBN: 978-0-7918-5768-7

Paper B Z. Mikulski, T. Lassen, "Fatigue crack initiation and subsequent crack growth in fillet welded steel joints", in *International Journal of Fatigue*, volume 120 (2019), pp. 303-318

Paper C Z. Mikulski, T. Lassen, Crack growth in fillet welded steel joints subjected to membrane and bending loading modes, in *Engineering Fracture Mechanics*, volume 235 (2020)

Paper D Z. Mikulski, T. Lassen, Probabilistic models for the fatigue resistance of welded steel joints subjected to constant amplitude loading, in *International Journal of Fatigue*, volume 155 (2022)

The articles are appended in their original state. The articles are an integrated part of the thesis and need to be read along with the present document. The PhD candidate has made major contributions to these publications and is consequently listed as the first author in all of them.

Contents

Nomenclature

Abbreviations

ABS	American Bureau of Shipping
ACPD	Alternating Current Potential Drop
CA	Constant Amplitude
CAFL	Constant Amplitude Fatigue Limit
DNV	Det Norske Veritas
ECCS	European Convention for Constructional Steelwork
FCAW	Flux-Cored Arc Welding
FM	Fracture Mechanics
HAZ	Heat Affected Zone
HSE	Health and Safety Executive
IIW	International Institute of Welding
LEFM	Linear Elastic Fracture Mechanics
LRA	Linear Regression Analysis
MLM	Maximum Likelihood Method
MTTF	Mean Time to Failure
P-M	Palmgren-Miner
PoF	Probability of Failure
SAW	Submerged Arc Welding
SCF	Stress Concentration Factor
SIF	Stress Intensity Factor
SIFR	Stress Intensity Factor Range
SLL	Safe Life Limit
SMAW	Shielded Metal Arc Welding
RFLM	Random Fatigue-Limit Model
TSL	Target Service Life
VA	Variable Amplitude

List of tables

List of figures

1. Introduction

1.1. Background

Welding still holds the position as the most important joining technique for large metallic structures. Typical examples are marine structures, ship structures, installations for oil and gas exploitation and large offshore wind turbines. For these steel constructions that are subjected to wind and wave induced dynamic loading one of the major potential failure modes is fatigue fracture. The fatigue damage is often occurring at welded structural details and the damage mechanism is driven by repetitive varying stresses over time. The most common case is that fatigue cracks are emanating from the weld toe. The welded details are vulnerable to fatigue damage at this location due to high local stress concentrations and weld imperfections. Residual stresses caused by the welding process may also often have a negative impact on the fatigue resistance. Hence, the fatigue design criterion will often determine the dimension and the local geometry of such welded details. Life predictions must be carried out at the design stage and safety margins must be chosen to achieve satisfactory reliability against fatigue failure of critical structural details throughout the intended target service life of the structure.

The fatigue damage evolution in welded joints is quite complicated and the damage mechanisms are influenced by many variables and associated sources of uncertainty. The various contributions of uncertainties that may be regarded as the sources for the observed scatter in fatigue lives are listed in Table 1.1. It is often useful to make a distinction between physical, measurement, statistical and model uncertainty. The *physical* uncertainty is related to the fact that important parameters governing the fatigue damage evolution may exhibit large variations within one welded detail such that they must be defined as random variables. *Measurement* uncertainty is related to the problem of determining these variables by given measurement techniques. The *statistical* uncertainty is related to the confidence level obtained for the random variables when applied in the probabilistic models. The *model* uncertainty is given by the limitation of the physical models when used to quantify the fatigue damage evolution. These models will always involve some approximations. In Table 1.1 we have emphasized the physical uncertainties as these are the basic source variables that cause uncertainties in fatigue life predictions. However, some comments are also made for the statistical and model uncertainties. The overview is for fatigue cracks

that emanates from the weld toe region. The overview is thorough but not exhaustive.

Table 1.1. Physical variables that influence the fatigue resistance of as-welded details with cracks emanating from the weld toe

Subject and involved variables	Engineering practices when applying the S-N approach	Assessment of uncertainties Comments
1. Global joint geometry with global geometrical stress concentration effects.	These uncertainties are usually benign and captured in the design calculations by selecting the representative fatigue category for the detail.	Involves both physical and measurement uncertainty but to a limited extent. For welded attachments the plate thicknesses and attachment lengths are important. For full penetration butt welds misalignment may play a role.
2. The local weld toe geometry often characterized by the flank angle and the toe radius. This geometry gives a severe local variable notch effect.	The associated notch effect is usually inherent in the fatigue category when using the nominal stress approach. Extreme unfavourable geometries are defined as non-conformities and rejected during post fabrication inspection. The remaining toe profiles are generally unknown.	These variables involves both physical and measurement uncertainty. The toe angle and the toe radius are random physical variable along the weld seam. These physical uncertainties are usually far more important than the global joint geometry and is also far more difficult to determine by measurements.
3. Weld imperfections such as undercuts, non-metallic inclusions and cold laps.	Non-acceptable flaws and crack like defects are rejected during post fabrication inspection. The remainders are of unknown geometry and size.	Physical and measurement uncertainties are involved. The performance and the extent of the inspection technique are essential. Final condition is related to the workmanship carried out.
4. The presence of residual stresses.	Tensile stresses could typically be above half the yields stress of the steel. They are difficult to measure and are generally unknown in the design calculations.	Physical and measurement uncertainty. Influences both crack initiation and subsequent crack growth.
5. Post-weld material quality, especially in the HAZ.	Tests are carried out during welding procedure qualification. The goal is to eliminate the danger of brittle fracture.	Physical and statistical uncertainty. Several tests must be carried out to reduce the statistical uncertainty.

Subject and involved variables	Engineering practices when applying the S-N approach	Assessment of uncertainties Comments
6. Applied loading modes, associated stress state and stress history over time for VA loading. Shakedown effect on the residual stress level.	Axial and bending loading modes are often dealt with in the same way. The multi-axial stress state is simplified by choosing the largest principal stress range as key variable.	Both physical and model uncertainties are involved. The loading modes and stress state may be difficult to determine in service. Stress direction relative to the weld seam is important.
7. Damage accumulation under VA loading.	Simplified by the linear P-M damage summation rule. Stress block sequence effects and stress cycle interaction effects are generally ignored.	Involves model uncertainty. P-M summation is a simplified model to a complex damage accumulation problem. Several damage mechanisms are often involved.

The global joint geometry listed on the top of the Table 1.1 is generally quite accurately characterized, but exceptions may occur. The so-called thickness effect is only partially understood. However, the uncertainties related to the local weld toe geometry listed in the second line in the table are usually far more important than the uncertainties in the global geometry. Both the weld flank angle and the weld toe radius that are governing the notch stress concentration factor at the potential crack locus, exhibit large variations along a weld seam. Furthermore, these local variables can be difficult both to define and to measure. When the weld imperfections like undercut and inclusion or other flaws are added on in line 3 of the table, it becomes fully understandable that the scatter in damage evolution and final fatigue life become significant. Both the local weld toe geometry and the flaws at the nearby material volume at the weld toe are related to the applied welding procedure and the workmanship during the fabrication process. The size of potential defects and inclusions that escape the quality control is generally non-measurable. Line 4 includes the presence of the residual stresses introduced by the welding process. These stress levels are generally variable and unknown except for stress relieved small specimens in the laboratory tests. The residual stresses may in fact vary from 20% of the yield stress of the steel up to as high as 90% of the yield stress. The impact on fatigue life caused by these differences is significant.

When adding up the contributions from line 2, 3 and 4 it is fully recognized that the sources of uncertainty are plentiful even under CA loading. As all the involved random variables in most cases are unknown to the design engineer, we shall designate them as *Uncontrolled Random Variables* (URV). These URVs make it

difficult to evaluate test results in the laboratory because of the strong influence these variables may have on the fatigue strength. Their variations in one given specimen are significant and they may also change for specimens that are seemingly identical. As these variations and changes are often hidden, their influence may lead to the wrong conclusions when assessing test results. One must be aware of this and be careful not to draw conclusion from one isolated test only. For testing under VA loading, one should preferably have several specimens tested with the same stress spectrum.

Line 5 in Table 1.1 has included the post-weld steel quality, i.e., the microstructure of the heat affected zone (HAZ). This is less emphasized in the present work but is included for the sake of completeness. The two last lines in the table give the main additional uncertainties occurring under VA loading.

1.2. Working method and scope of work

The applied scientific working approach in the present investigation is according to common practice for research within the field of mechanical engineering. The following steps are included:

- Based on literature studies, promising hypotheses and models for the fatigue damage evolution in welded steel joint are selected, examined, and elaborated.

- The selected models are subsequently verified and calibrated against a large amount of collected experimental data from fatigue testing. A part of the experimental data gives both the time to crack initiation, crack growth data and life data. This is a crucial part of the present work.

- The huge database is supplemented with fatigue tests carried out within the framework of the present thesis.

The scope of work is to focus on the damage evolution and final fatigue life for fillet welded steel joints with a geometry and steel grade that are typical for offshore installations and ship structures. A welded detail chosen for extensive studies is a non-load carrying fillet welded attachment. The final goal is to provide tools and recommendations for more accurate predictions of fatigue life and crack growth evolution with good estimates of the scatter to control the safety margins in fatigue life predictions.

1.3. Objectives and research questions

Based on the background described above it is convenient to make a distinction between topics related to the damage evolution and topics related primarily to prediction of the total fatigue life. The research questions are defining the objectives of the work. The research questions regarding the fatigue damage evolution under CA loading are as follows:

- Does there exist a fatigue crack initiation phase for as-welded joints or do there exist crack-like defects already from the start?
- Can the growth model given by the Paris law and established by testing of wide plates with a large central crack be applied for these small semi-elliptically shaped cracks at the weld toe?
- For the crack growth phase, what is the best way to characterize the variable weld toe geometry when determining the stress intensity factor range (SIFR) for small semi-elliptical cracks?
- What is the impact of crack coalescence and how shall the coalescence of multiple cracks be accounted for in the crack growth model?
- What are the most important differences in the crack growth behaviour under the membrane and the bending loading modes?
- How can the mean stress effect for a given stress range be accounted for?

For the prediction of the entire fatigue life based on probabilistic modelling the research questions are:

- Starting with the elementary reliability model for the finite fatigue life at a given stress range, can a conclusion be reached regarding the distribution function that gives the best fit to the life data?
- When establishing the conventional S-N curves with associated lower endurance limit based on CA life data, what are the principal differences between the conventional S-N curves in rules and recommendations and the present resistance curve obtained by Random Fatigue-Limit Model (RFLM)? What will be the practical outcome for fatigue life predictions based on the two approaches?
- The focus of the present analysis will be in the high cycle regime where the RFLM includes all available data whereas the conventional S-N curves do not include these data. How is the RFLM-based resistance curve fitting these experimental data?

- Can any conclusion be reached regarding the existence of the fatigue endurance limit?

- Finally, there shall be a mutual agreement between the RFLM resistance curve and the underlying damage mechanisms. Can the probabilistic curves be explained and supported by physical models for these mechanisms? The question is pursued by an attempt to demonstrate the compatibility between the RFLM resistance curves and the physical based two-phase model for the fatigue damage development.

1.4. Organization of the thesis

Initially, the scope of work and objectives for the thesis are given. Important research questions are formulated as described above. The theoretical part of the thesis starts to present hypotheses and physical models for the fatigue evolution in welded joints based on an extensive literature study, see section 2. In section 3 and 4 these models are discussed and elaborated considering the research questions that have been formulated. To verify the validity of the models, a large sample of crack growth data and life data are collected from literature for a defined population. The focus is on CA loading. Some supplementary experiments (crack growth histories and local weld toe geometry measurements) are also included in the present work, see section 5 and Annex A. The ability of the selected models to predict the fatigue behaviour is investigated. The ability to describe the damage evolution is given in section 6, whereas the probabilistic life prediction models are presented in section 7. Discussion of the results and the conclusions reached are presented in section 8. In section 9, some suggestions for further work are given, particularly for VA loading, and finally, concluding remarks are briefly presented in section 10. The sections 2-8, consisting of theory, methodology, approach, and results, are the revised and shortened chapters that have been previously published in Papers A-D. The thesis form is a compilation of papers, and thus, any references shall not be made to the present document but directly to the original papers.

2. Overview of fatigue damage models and methodologies

2.1. Joint geometry, loading conditions and the associated stress distributions

As discussed in section 1.1 the joint geometry and loading direction are important topics for the fatigue resistance of welded details. The welded details chosen for the present investigation are shown in Figure 2.1. Secondary attachments are attached to a main plate by fillet welds either in the transverse direction or the longitudinal direction. The main plate is subjected to stresses whereas the fillet welds are not carrying any load. The attachments do however create stress concentration at the surface of the main plate such that there is a danger of fatigue cracking from the weld toe region as shown in the lower part of Figure 2.1. The stress concentration is dependent on both the global geometry of these welded details and the local weld toe geometry. As can be seen the crack has a semi-elliptical shape and the crack plane is perpendicular to the applied stress direction. There may be multiple cracks along the weld seam.
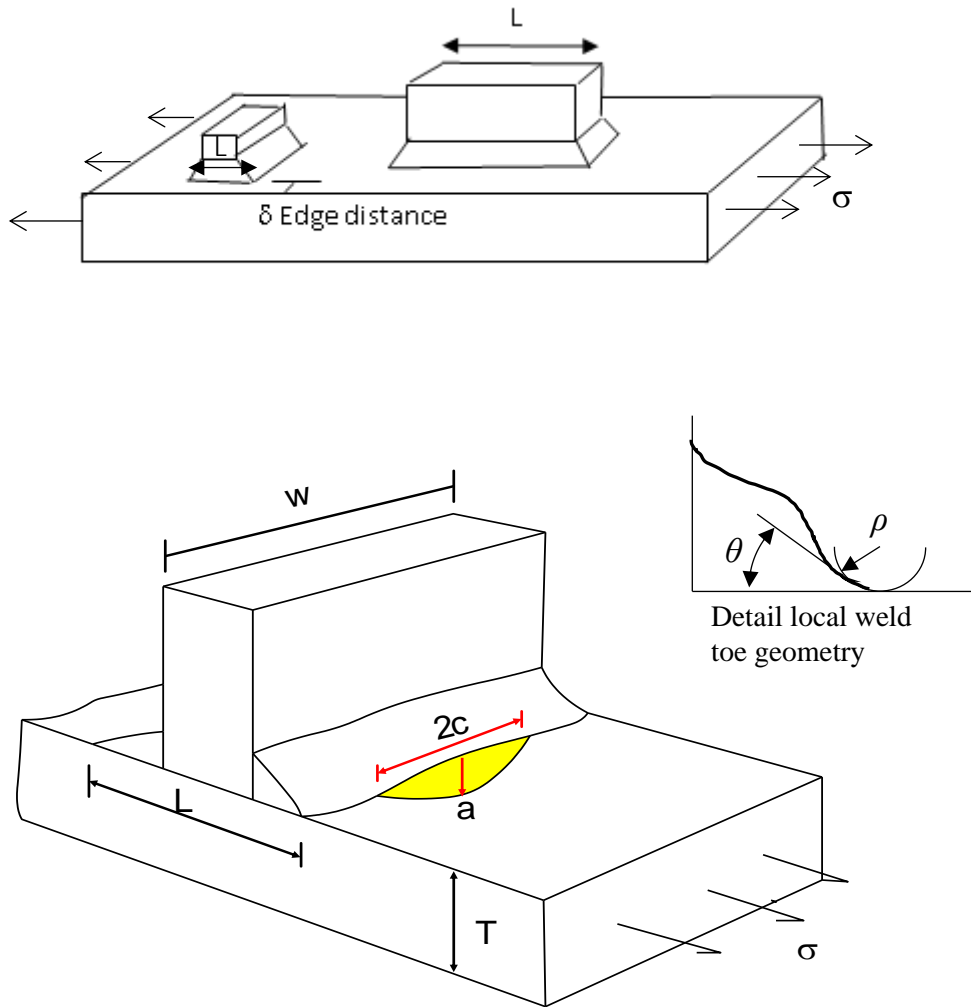
Figure 2.1. Joint geometry [1,2]

There are two main geometrical parameters that govern local stress state at the weld toe – the toe radius ρ and the flank angle θ. It shall be emphasized that both the angle and the radius are random variables varying along the length of the weld seam, see Table 1.1. Characteristic values must be chosen based on statistical considerations. To investigate the local stress concentration occurring at the weld toe and its effect on the SIF related to a crack, an extensive FE parametric study has been performed and presented in Paper B.

In Paper C both the membrane and bending loading modes have been considered for the transverse attachments. It was demonstrated that the two loading modes have a different impact on the fatigue crack evolution in the main plate. This matter is especially interesting as the rules and recommendations for fatigue life prediction do not distinguish between the two loading modes when it comes to the

total predicted life. The differences may be substantial and this is revealed when analysing crack like defects utilizing LEFM [3–6]. This model is described in more detail in section 2.4.

2.2. The evolution of the fatigue damage

The fatigue damage processes related to cracking from the weld toe are quite complicated and involve several sub-phases with different damage mechanisms. A good overview of the possible damage mechanisms at various stages of the damage evolution is given in Figure 2.2. The figure is inspired by work of Baptista et al. [7] and reproduced herein with only small changes. As can be seen from the figure, the three major phases are:

- Phase 1: Crack initiation. The cracks initiate due to repeated irreversible plastic deformation at irregularities in the microstructure, e.g., at dislocations and grain boundaries. The cracks may initiate close to the surface or at the surface in the weld toe region.
- Phase 2: Microcrack propagation. Growth of short cracks with sizes down to the grain size of the microstructure typically in the range from 10 to 100 µm.
- Phase 3: Macrocrack propagation. Growth of larger cracks with depths beyond 100 µm.
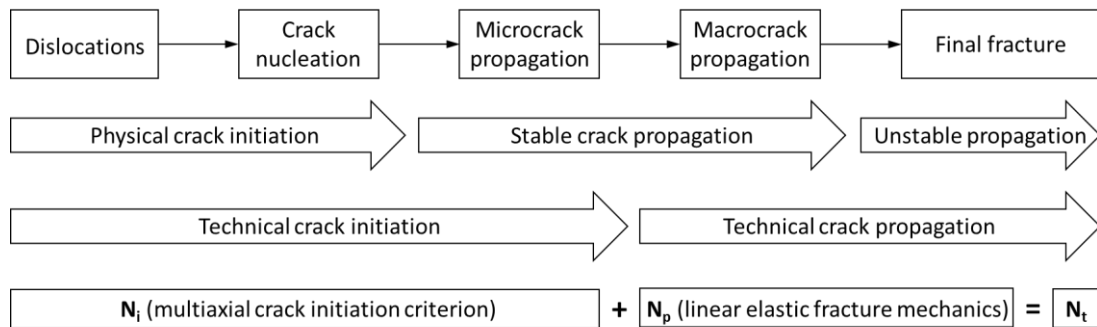
Figure 2.2. Schematic crack stages for the two-phase model [8]

The crack initiation phase is influenced by the quality of the HAZ and the presence of possible weld imperfections. Despite these imperfections there is still an initiation phase, as long as these imperfections are not categorized as crack-like planar defects.

The crack development in various phases has been thoroughly discussed in Paper A, B and Paper C. It is essential to make a distinction between crack initiation and subsequent crack growth. The distinction is important as these two phases involve

different damage mechanisms. The crack initiation phase in flawless alloys is driven by cyclic deviatoric shear stress variation giving dislocation slips and the resistance against this damage mechanism is related to the yield stress of the steel. The growth phase is usually driven by the cyclic principal stresses perpendicular to the crack planes (mode I case) and the resistance against crack growth is not related to the yield stress, but to the Young's modulus E of the alloy. Hence, a distinction between the two phases is crucial to establish a correct model for the entire damage evolution. Each phase must be modelled separately to capture the characteristics of the damage mechanism involved.

In the present work the two early phases designated as nucleation and micro crack propagation are simplified to be a crack initiation phase. The subsequent macro crack growth is then modelled separately. The crack initiation is defined by the number of cycles to reach a fatigue crack with a typical depth close to 0.1 mm. This initiation phase is likely to be influenced by the imperfections (initial flaws) created by the welding process. These flaws are not possible to measure and are not regarded as planar crack-like defects in the present work. Hence, separation of this phase into micro-crack growth modelling as suggested by Zerbst [9] is avoided. The present simplification is chosen to obtain a model that may not be entirely correct, but accurate enough to be a useful tool for the practicing engineer. The subsequent crack growth is simplified as one simple stable crack propagation phase based on the common engineering fracture mechanics approach based on LEFM. It remains to verify if the defined initial crack depth close to 0.1 mm is an appropriate choice for the transition crack depth between the two chosen main phases. Furthermore, it should be verified if the subsequent growth can really be modelled by the common models applied in engineering. The key question to be answered is if an engineering approach based on Paris law with SIFR calculation and growth rate parameters as found in the literature are applicable for small semi elliptical cracks emanating from the weld toe notch.

The chosen crack transition depth of 0.1 mm is mainly based on practical considerations than on theoretical arguments. This crack depth is within the measuring uncertainty of the Alternating Current Potential Drop (ACPD) monitoring equipment that was applied during testing. Furthermore, for the test specimens with plate thickness 25 mm the formulas for the SIFR are valid down to a depth 0.125 mm, so we are just below the application range with the chosen transition crack depth of 0.1 mm. The theoretical argument is that the applied Paris law has never been proven for such small semi elliptical cracks. Attempts in this

field have been made [10]. However, no results from such studies have yet entered rules and recommendations (DNV, BS 7910).

2.3. The existence of a crack initiation phase

It is generally accepted that the crack initiation is an important part of the fatigue damage evolution in high quality machined parts with a smooth surface. It has been a usual assumption that this phase could be neglected for welded joints. However, in the absence of weld imperfections such as slag intrusions, cold laps or undercuts the natural nucleation phase may play an important role even for welded joints. This is a proven fact for welded joints with post weld treatment such as grinding, but the phase may also be important for as-welded joints at low stress ranges. In the present work the experimental results obtained by crack growth monitoring system based on the ACPD method confirm that the initiation phase exists even at moderate and high stress ranges even for as-welded joints. Analyses of the measured growth histories for all investigated test series show that noticeable number of cycles is spent before observing a stable crack growth. It was possible to establish a distribution for reaching a crack depth as small as 0.05 mm, see the example presented in Figure 2.3. Thorough investigations of experimentally obtained growth histories have been presented in Paper B and Paper C. The results demonstrate that the crack initiation phase for welded joints cannot be neglected.

a)

b)
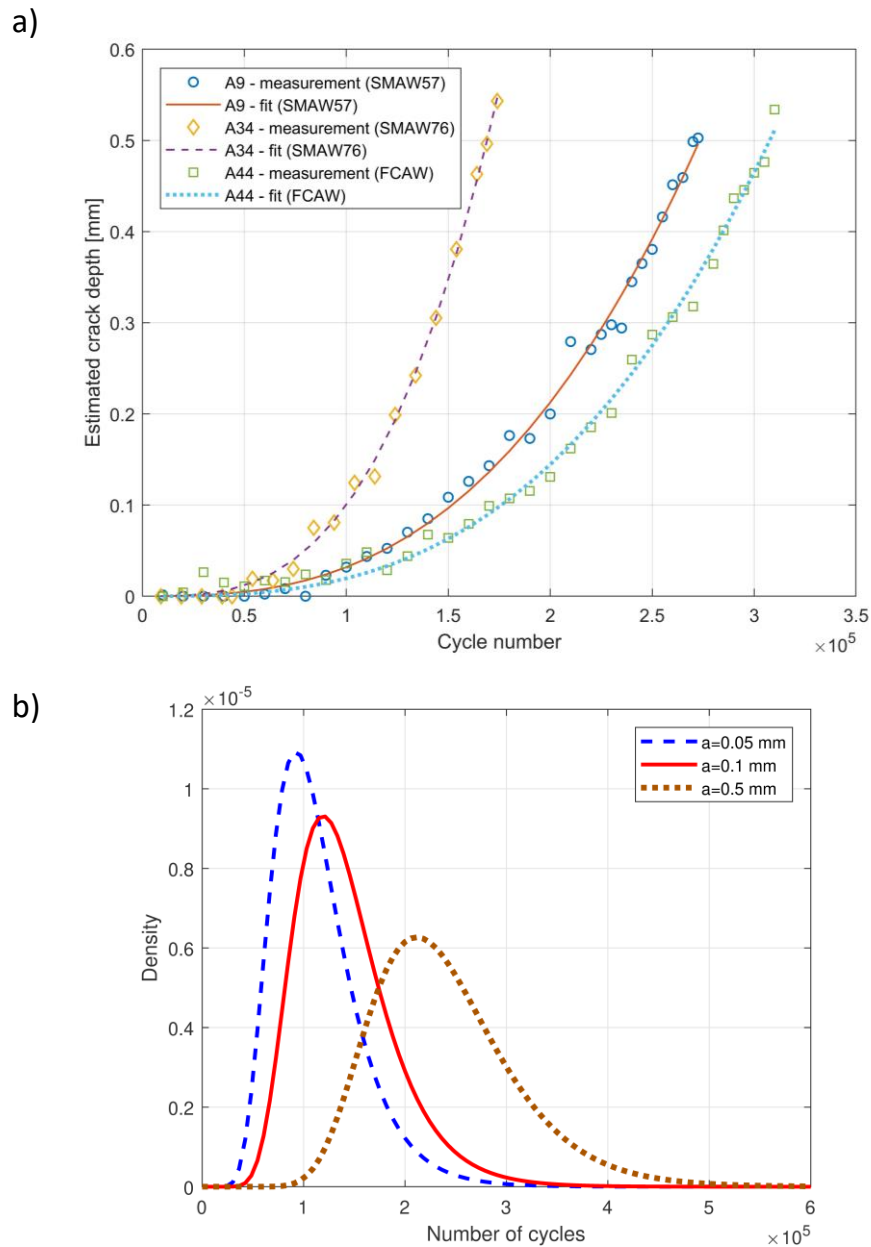
Figure 2.3. Experimental results for Series 1a: a) early crack growth history for representative specimens, b) distribution for the number of cycles to reach given crack depth (more results are presented in section 6, for series details see section 5.1) [8,11]

The existence and importance of the crack initiation phase has been postulated by many researchers. The pioneer work for defining a two-phase model and first attempts for modelling the crack initiation phase was carried out by F.V. Lawrence et al. [12–15]. Crack initiation models usually utilize a local stress-strain approach at the weld toe notch. As an example, the Coffin-Manson equation or the Dang Van criterion can be used for predicting number of cycles spent in this phase. The Coffin-Manson equation is assuming uniaxial stresses, whereas the Dang Van

model can handle a multi-axial stress situation. More details regarding modelling the crack initiation phase are presented in section 4.1.

2.4. Fracture mechanics for the fatigue crack growth phase

The last phase of the damage evolution listed in section 2.2 – Phase 3: macrocrack propagation – is in most cases the last and most important phase for the damage evolution in welded joints. A good review of this propagation phase is given by Fricke [16]. This phase is emphasized in the present work. The applicability of the models, the formulas and the growth parameters recommended in rules and regulations for this phase is at the essence of the present investigation and are covered in all the author's publications, especially in Paper B and Paper C. Numerous simulations of the crack development for the welded detail in question have been performed and corroborated by the experimental results. Establishing formulas for SIF calculation is crucial to predict accurate enough growth histories, especially for shallow cracks at an early growth stage. It is challenging to strike a balance between simplicity and accuracy while dealing with all the involved uncertainties. This is pursued further in section 4.2.2, but to briefly visualize these challenges, an example of the total geometry function $F(a)$ for a plate with surface crack and a T-butt joint with crack at the weld toe is presented in Figure 2.4 ($F = Y*M_k$, see equation (4.9) for more precise definition).

One of the main factors governing predictions of the crack growth – the crack shape evolution – has been investigated thoroughly under membrane and bending loading mode. The findings demonstrate the importance of simulating crack shape development, including crack coalescence, to properly describe crack behaviour in the tested specimens and in real structural details. This approach gives the necessary tool for an engineering critical assessment of welded structural members with crack like defects. Furthermore, the approach is a necessity when carrying out risk-based inspection planning for welded structures. More details are presented in section 4.2.
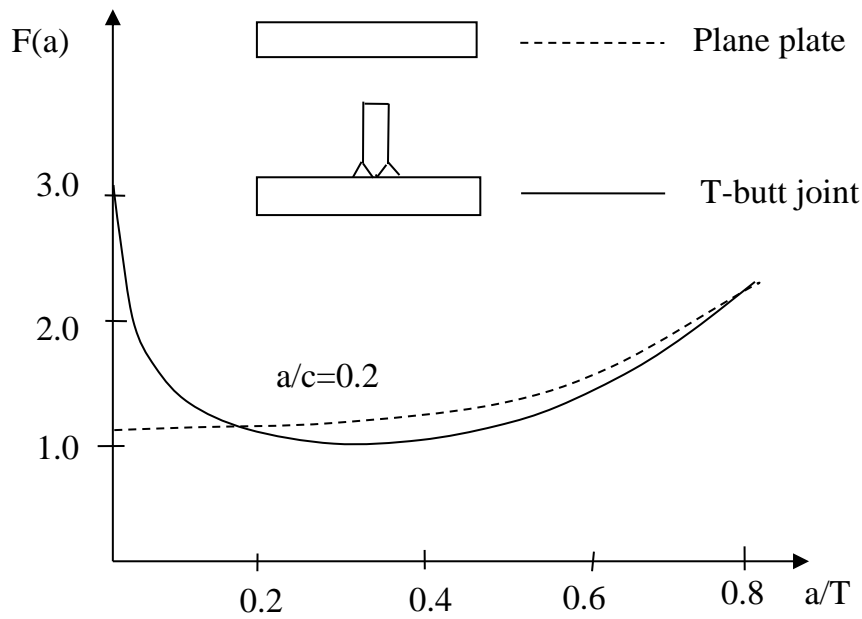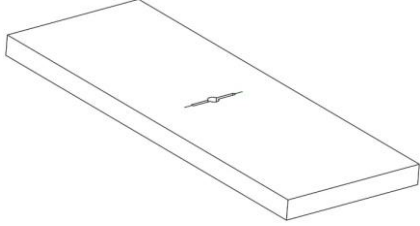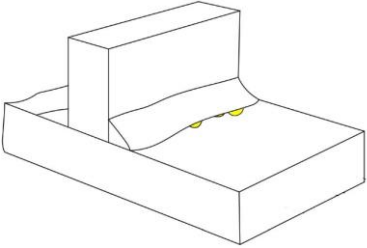
Figure 2.4. Comparison of the total geometry function for a plate with surface crack and a T-butt joint with crack at the weld toe [1]

2.5. Uncertainty and scatter

Physical variables that influence the fatigue resistance of as-welded details were listed in Table 1.1 As elementary fracture mechanics models originate from observations and analyses of crack evolution in simple geometries, it is important to point out differences and challenges related to uncertainties in fatigue crack growth in a welded joint and a wide plate with a central crack. The various types of uncertainties that are introduced when analysing a welded joint compared with a wide plate standard specimen are listed in Table 2.1. As before, a distinction is made between physical, measurement, statistical and model uncertainty, as per ref. [17]. All these uncertainties need to be accounted for when assessing fatigue test results and building a reliable fracture mechanics model for a welded detail.

Table 2.1. Overview of the sources of uncertainties in the fatigue crack growth in welded joints compared with standard wide plate test specimens

Type of uncertainty	Standard test specimen: Wide plate with a single long central crack	Present test specimen: Welded detail with multiple shallow semi-elliptical cracks emanating from the weld toe
Physical	The global geometry and steel properties are well defined and easy to control. The initial crack length is known	The global geometry is well defined. There are large variabilities in the local toe geometry. The steel properties may change during the crack growth. The initial crack depth is unknown
Measurement	The crack growth of a single crack can be measured precisely	The ACPD measurements of the crack depth must be calibrated. Crack coalescence has an important impact. The definition and the measurement of the weld toe geometry are sometimes difficult
Statistical	Little uncertainty due to the many tests carried out	The limited number of tests available give lower confidence in the random variables
Model	The Paris law has a proven validity for these large crack sizes. The threshold value for the SIFR exists and can be determined	The validity of the Paris law for small semi-elliptical cracks at the weld toe is questionable. The threshold value for the SIFR has never been proven. Different loading modes may occur
Stress situation	Stress distribution is well defined. No residual stresses	Significant uncertainty in local stress distribution due to variability in local toe geometry. Residual stresses are unknown

The physical uncertainty in Table 2.1 reflects the uncertainty in physical variables. For the present joints, this type of uncertainty is given by the variability in the local toe profile (i.e. toe angle and radius) and the size of possible initial crack depths and lengths (embedded cracks). The growth parameters characterizing the steel quality may also change along the crack path as the steel microstructure changes when going from the HAZ into the base plate. For this reason, these parameters are treated as random variables [5,6].

The measurement uncertainty is caused by the fact that the exact position of the crack front is hidden during the testing of the joints. The crack depths in the present

case are obtained by ACPD estimates that must be calibrated against true crack depths observed on the fatigue crack planes after the test of the joints. The statistical uncertainty listed in Table 1.1 is related to the limited number of observations available when determining the random variables involved in the crack propagation model. This gives uncertainty when determining the mean values and the associated standard deviations for these variables. This uncertainty is often dealt with by specifying a confidence interval for the estimated mean and variance of the variable.

Finally, the model uncertainty is the most important part of the present investigation. The Paris law applicability has been proven for rather long cracks in well-defined test objects. The law's applicability for very shallow semi-elliptical crack in the weld toe notch stress field is still uncertain. For such small cracks special models must be developed. A good overview of the topic can be found in [18,19].

The uncertainties listed in the right column of Table 2.1 are the same as the uncertainties encountered for a similar structural detail in a load bearing structure in service. An important additional physical uncertainty for structural details in service is of course the magnitude of the acting stresses. Furthermore, significant additional model uncertainty is also introduced caused by the VA loads often occurring in service. Nevertheless, the uncertainties given in the right column of Table 2.1 must be understood, characterized, and modelled in the first place before these additional in-service uncertainties can be dealt with.

3. The S-N approach for fatigue life predictions

3.1. Statistical models for the entire fatigue life

The consequence of the large scatter observed in test data is that the fatigue life t (cycle or calendar time) for a given welded joint must be treated as a random variable. This variable must as usual be characterized by its mean value μ, standard deviation $\hat{\sigma}$ and frequency function $f(t)$. For fatigue problems the time t is usually given in number of cycles N to failure. The model gives the design engineer the possibility to establish a reliability model that gives the fatigue life at a chosen probability of survival. If enough test results are available at a given constant stress range a reliability model can be established at this stress range. The advantage of this approach is that the reliability model can be determined accurately regarding the type of underlying frequency function with modest statistical uncertainty for the involved parameters. Unfortunately, to limit the testing efforts, the tests are usually carried out at various stress ranges with rather few tests at each stress range level. The data are then analysed directly by an S-N approach as we shall discuss in the next section. However, before pursuing the S-N approach it is important to study the behaviour of the fatigue life at a given constant stress range to understand the basic ideas of reliability modelling. In the cases where enough data are collected at a given stress range this can also give important background information for the subsequent S-N analysis at various stress range levels.
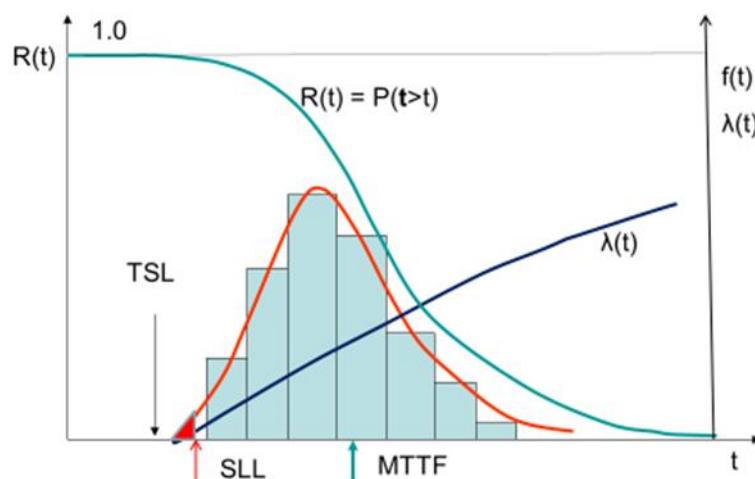
Figure 3.1. Definition of a reliability model for the fatigue life [2]

The basic characteristics for a reliability model at a given stress range are illustrated in Figure 3.1. Based on the histogram describing the life data the frequency function $f(t)$ with associated parameters can be determined. Subsequently the reliability function $R(t)$ and the failure rate function $\lambda(t)$ are obtained. It must be borne in mind that the reliability model shown in Figure 3.1 is valid for:

- A defined damage mechanism (high cycle fatigue in the present case)
- A given quality of the welded joint (joint geometry, steel quality, welding procedures, post weld inspections and post-weld improvement methods)
- A given operating condition (the direction of the stresses, variations of the stresses)

The damage mechanism in the present case is high cycle fatigue, but to make things more subtle one may benefit from making a distinction between crack initiation and subsequent crack growth, see section 2.2, Mikulski and Lassen [11,20], and Lassen and Recho [21]. These two phases are in principle driven by different failure mechanisms.

The quality of the joint is usually given by the definition of the categories in rules and recommendations. However, a category also includes considerations for the direction of the applied stresses relative to the welding direction. Finally, the given operating condition is the stress spectrum to which the welded detail is subjected during service. However, it is quite common to simplify the operating condition by applying various levels of CA stress ranges in laboratory tests. The reliability model is then conditional on an independent free variable such as the CA nominal stress range $\Delta\sigma = S$.

The small red area under the left tail of the frequency function $f(t)$ in Figure 3.1 defines the probability of failure (PoF) which is the complementary probability to the probability of survival. Based on a risk assessment including the consequences of a potential fatigue failure this probability must be chosen at an acceptable low level to define the Safe Life Limit (SLL) for the welded joint in question. The Mean Time to Failure (MTTF=μ) is also indicated on the figure. If additional safety margins are required, this is usually obtained by demanding that the Target Service Life (TSL) of the structure is substantially shorter than the SLL. In cases with severe consequences of failure and when in-service inspections and repair are impossible this additional safety margin is chosen to be high.

The most common frequency functions $f(t)$ applied for reliability models for welded joints are the log-normal function and the Weibull function. A good overview of these models for welded joints is given by Wirsching and Chen [22]. Their work demonstrates the practical application of these functions for welded details in marine structures. The frequency function that gives the best fit to the histogram columns in Figure 3.1 is to be chosen. A common problem is that the two possible functions may fit the histogram columns equally well, but they may give very different results when extrapolated to the important left tail where very few data points exist. Hence, the selection of a model will have a strong influence on the determination of the SLL for a chosen probability of failure. The model depictured in Figure 3.1 is often given by a lognormal distribution or a Weibull distribution. These models are usually defined by two parameters only, in some few cases a third location parameter is introduced. For two-parameters functions the Weibull frequency function has a stronger left tail than the log-normal function. Hence, the log-normal distribution will predict a more optimistic SLL for a given failure probability. This may give a dilemma for the experimentalist when taking the decision on which function to select, see Schijve [23], Engesvik [24] and Wirsching [25]. Neither Engesvik nor Schijve reached any general conclusion on which underlying frequency function to select for the fatigue reliability models. In most rules and recommendations for welded joints the log-normal distribution is applied. However, this selection is usually made as an assumption without any formal proof that justifies this choice.

The probability of failure pertaining to the SLL on the left tail in Figure 3.1 is theoretically obtained by the equation:

$$P(\boldsymbol{t} \leq t) = F(t) = \int_0^t f(t')\mathrm{d}t' \tag{3.1}$$

The acceptable probability of failure is often chosen at 2.5% or 5% in rules and regulations with $t = \text{SLL}$. The reliability $R(t)$ is defined by the probability of surviving the SLL which is the complementary probability to the expression in equation (3.1). If the true theoretical mean value μ and standard deviation σ are known the probability of survival can be found by the reliability function $R(t)$ for a given CA stress range S:

$$P(\boldsymbol{t} > t) = R(t|\mu, \sigma, S|) \tag{3.2}$$

The failure rate function is defined by, Lewis [26]:

$$\lambda(t) = \frac{f(t)}{R(t)} \qquad\qquad (3.3)$$

The failure rate function is a conditional probability function. It gives the probability of failure per time unit just after the time t is reached, given that the joint has survived up to the time t. This function gives important information for the service engineer. The function is particularly included herein because the log-normal distribution and the Weibull distribution may give quite different failure rate functions. The Weibull failure rate is often increasing monotonically, as shown in Figure 3.1, whereas the log-normal model gives a failure rate function that increases from the start, levels off and finally decreases.

In practice the design engineer must work with estimates for the true mean value μ=MTTF and the true standard deviation σ for the time to failure. These model parameters can be found by:

- The method of moments
- The least square method
- The maximum likelihood method

For a description of the two first methods the reader may look into [27]. The estimates are then generally given by a point estimate and an associated confidence interval. For the mean value the interval is determined from Student's t statistics, whereas chi-square statistics are used to determine an interval for the standard deviation. If the life data contain runouts none of the two methods are applicable. For this case a Maximum Likelihood Method (MLM) can be applied to determine the model parameters. A pioneer work for the application of the MLM for fatigue life data was carried out by Bastenaire [28].

3.2. Defining a population

The classical approach in engineering science is to study objects that have very similar properties and behaviour under given operating conditions. These objects define a group often designated a class or category. From a statistical point of view this class is treated as a population. In the present case with welded joint subjected to repetitive loading the population is defined by joints that have the same or very similar fatigue resistance. To define the population, the following parameters play an important role:

- the overall geometry of the joint
- the geometry of the weldment
- the direction of the applied stresses relative to the welding seam
- the steel quality given by chemical composition and mechanical properties
- the applied welding procedure
- the post weld inspection and quality requirements
- the fatigue improvement methods

For a defined population fatigue tests are carried out to determine the fatigue resistance of the welded details belonging to the population. The most common approach in engineering is to establish an S-N curve such that the fatigue life can be predicted at any applied constant stress range.

3.3. Conventional S-N curves for Constant Amplitude loading

To obtain a life model at any constant stress range an S-N curve must be established. The time to fatigue failure given in number of cycles *N* is obtained for any CA nominal stress range *S*. The basic Basquin equation reads:

$$\log N = \log a - m \cdot \log S + \varepsilon \tag{3.4}$$

The basis for this equation is shown in Figure 3.2. The figure includes the data points and the fitted mean curve. In the central part of the diagram the relation between *S* and *N* is assumed linear for a log-log scale as given by equation (3.4). The fatigue damage mechanism in this area is mainly crack growth governed by the stress intensity factor range pertaining to a crack. For higher stress ranges the linear relation is overly optimistic as indicated by the dotted upper curve. This is explained by the fact that the damage mechanism changes to low cycle fatigue which is mainly governed by the plastic strain variation. For lower stress ranges the linear assumption is overly pessimistic as indicated by the dotted lower curve. Again, the explanation is related to the change in damage mechanism as the fatigue life for these low stress ranges is dominated by a crack initiation phase. Based on the data points in the mid region of the diagram a Linear Regression Analysis (LRA) is carried out for a log-log scale. The intercept parameter log *a* and the slope parameter *m* give the mean life at any stress range. A third parameter defined as the standard error is defined by the discrepancy ε for each individual data point relative to the obtained mean curve. The squared sum of the residuals will give an estimate for the standard error defining the standard deviation in the fatigue life. The standard deviation is assumed constant for all stress ranges and the design

curve is found by subtracting a chosen number of standard deviations from the mean curve such that the probability of failure is regarded as acceptable. This curve is shown to the left in Figure 3.2. In some cases, this design curve is chosen to be hyperbola shaped to reflect the increased confidence interval for stress ranges for which the available life data are scarce. This curve is given by the left dashed line in Figure 3.2.
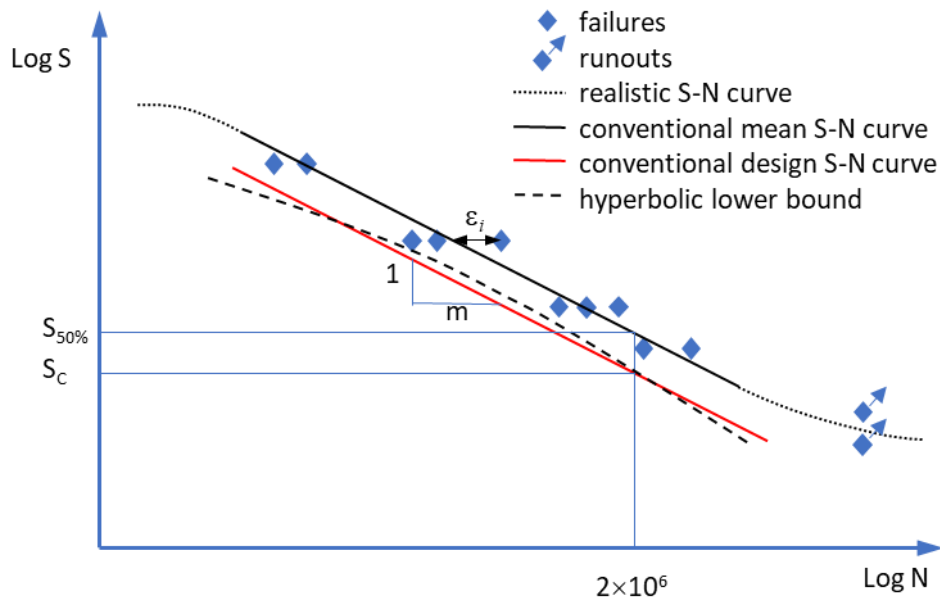
Figure 3.2. An illustration of the basic concepts for the S-N curve [2]

The S-N curves assume that there is a single damage mechanism dominated by crack growth for any stress range. The curve is then cut off at a stress range that is designated the endurance fatigue limit. The damage mechanisms are indeed more complicated. The damage mechanism will mainly be crack growth at high stress ranges, whereas for low stress ranges the crack initiation damage mechanism will be dominant. This is in fact an objection to the basic idea of an S-N curve that assumes the same type of reliability model for any CA stress range level. Schijve [23] argued that scatter in crack initiation and crack growth are different issues. Baptista et al. [7] simulated the damage process in welded joints by three possible phases: crack initiation, micro crack growth and associated crack arrest and the final growth of larger cracks. These possible shifts in damage mechanisms explain why the long life and runout data must be excluded in the conventional analysis. These data do not obey the simple reliability model assumed to be valid for the relatively high stress range levels. This gives doubt with respect to the general validity of the S-N curves when extrapolating them down to lower stress ranges. As the stress ranges decreases, the basic equation (3.4) is no longer valid. The

fatigue life increases in a non-linear manner and the scatter also increases dramatically. To handle this behaviour the RFLM must be applied.

3.4. The resistance curves obtained by Random Fatigue-Limit Model

The RFLM gives a probabilistic resistance curve where both the fatigue life and the fatigue limit are treated as random variables simultaneously. The model is established based on the Maximum Likelihood Method (MLM) such that long lives and runouts are included in the analysis in a logical and rational manner. Another advantage of such a model is that it can be extrapolated into the very high cycle area where very few test results exist. The present work is based on RFLM approach as presented by Pascal and Meeker [29]. The methodology was first applied for welded joint by Lassen et al. [30]. Similar type of analysis has also been carried out by D'Angelo and Nussbaumer [31] that included a Monte Carlo simulation into the model. Toasa and Ummenhofer [32] applied a modified approach based on a general formulation of the probability weighted moments using the three parameter Weibull distribution. This work was further developed by the authors [33] where they focused on how to include the result from retesting of former runouts. Leonetti et al. [34] used the RFLM for welded cover plates on girders. The work suggested to introduce more parameters to the RFLM to enhance the model fitting. Furthermore, the possibility of applying Bayesian interference is emphasized.

The basic equation of the RFLM curve is:

$$\ln N = \beta_0 - \beta_1 \ln(\Delta S - \gamma) + \varepsilon \qquad (3.5)$$

where ln denotes the natural logarithm and $\gamma = \Delta S_0$ is the fatigue-limit defined as a random variable. The parameters β_0 and β_1 are fatigue curve coefficients. As can be seen, equation (3.5) is fundamentally different from equation (3.4). Let $v = \ln(\gamma)$ and assume that v has a Probability Density Function (PDF) given by:

$$f_V(v) = \frac{1}{\sigma_v} \varphi_V \left(\frac{v - \mu_v}{\sigma_v} \right) \qquad (3.6)$$

with location parameter and scale parameter μ_v and σ_v, respectively. $\phi_v(\cdot)$ is the normal frequency function. The normal distribution was chosen because it gave the best fit to present test data. Let $x = \ln(\Delta S)$ and $W = \ln(N)$. Assuming that V is given and that V<x, W$|$V then has a frequency function:

$$f_{W|V}(w) = \frac{1}{\sigma_x} \varphi_{W|V} \left(\frac{w - [\beta_0 - \beta_1 \ln(\exp(x) - \exp(v))]}{\sigma_x} \right) \tag{3.7}$$

with the location parameter $\beta_0 - \beta_1 \ln(\exp(x) - \exp(v))$ and scale parameter σ_x. The marginal frequency function of W is given by:

$$f_W(w) =$$
$$= \int_{-\infty}^{x} \frac{1}{\sigma_x \sigma_v} \varphi_{W|V} \left(\frac{w - [\beta_0 - \beta_1 \ln(\exp(x) - \exp(v))]}{\sigma_x} \right) \varphi_V \left(\frac{v - \mu_v}{\sigma_v} \right) dv \tag{3.8}$$

The marginal Cumulative Distribution Function (CDF) of W is given by:

$$F(w) =$$
$$= \int_{-\infty}^{x} \frac{1}{\sigma_v} \Phi_{W|V} \left(\frac{w - [\beta_0 - \beta_1 \ln(\exp(x) - \exp(v))]}{\sigma_x} \right) \varphi_V \left(\frac{v - \mu_v}{\sigma_v} \right) dv \tag{3.9}$$

where $\Phi_{W|V}(\cdot)$ is the CDF of $W|V$. For given sample data w_i and x_i from various test specimens $i=1,n$, the model parameters can be determined by the Maximum Likelihood (ML) function;

$$L(\boldsymbol{Q}) = \prod_{i=1}^{n} [f_W(w_i, x_i, \boldsymbol{Q})]^{\delta_i} [1 - F_W(w_i, x_i, \boldsymbol{Q})]^{1-\delta_i} \tag{3.10}$$

where $\delta_i = 1$ if w_i is a failure and $\delta_i = 0$ if w_i is a censored observation (runout). The vector $\boldsymbol{Q}$ contains the model parameters:

$$\boldsymbol{Q} = (\beta_0, \beta_1, \sigma_x, \mu_v, \sigma_v) \tag{3.11}$$

Once these parameters have been determined from optimization of equation (3.10), the corresponding confidence intervals can be obtained by a profile likelihood method using the profile ratio of the variables together with chi-square statistics. The details for these calculations can be found in Pascual and Meeker [29]. The integration of equations (3.8) and (3.9) and the optimization of equation (3.10) must be done numerically. When the parameters are determined we can calculate the fatigue life for a chosen probability p of failure using equation (3.9). Hence, the median curve and percentile curves for design purpose are obtained. The RFLM approach eliminates some of the obvious short-comings related to the conventional S-N curves described in section 3.3. These conventional curves are characterized by:

- A simple reliability model with one random variable only is assumed to be valid at any applied stress range above what is believed to be a fatigue limit,

- The linear regression carried out results in a lognormal distribution of the fatigue life as a consequence of the central-limit theorem,
- Long lasting failures and runouts are excluded from the analysis,
- The existence of a fatigue limit at a predetermined number of cycles gives a lower curve segment that becomes horizontal at this CA Fatigue Limit (CAFL),
- For VA loading a lower line segment must be drawn below the CAFL. This raises a discussion of where this knee-point shall be situated and also the slope of the lower line becomes uncertain. It is also a problem that this line is not determined by probabilistic modelling such that the reliability level pertaining to this line is unknown.

In conclusion the major advantages of the RFLM-based resistance curves are two-fold and the short version can be summarized as follows:

- *Physical realities:* A probabilistic model can reflect the fact that there is a change in the fatigue damage mechanism as the stress ranges decreases. The fatigue limit need not exist.
- *Statistical methodology:* A probabilistic model can include long-lasting failures and runouts in rational and logical manner. The frequency function for the fatigue life need not be log-normal. The non-linear relation between the stress range and the number of cycles to failure at low stress ranges should be captured, so shall also the increased scatter in this area.

To illustrate the differences between the conventional S-N curves and the present RFLM resistance curves the data given by Drebenstedt and Euler [35] are plotted in Figure 3.3 together with the two types of curves. The results are discussed in Paper D.
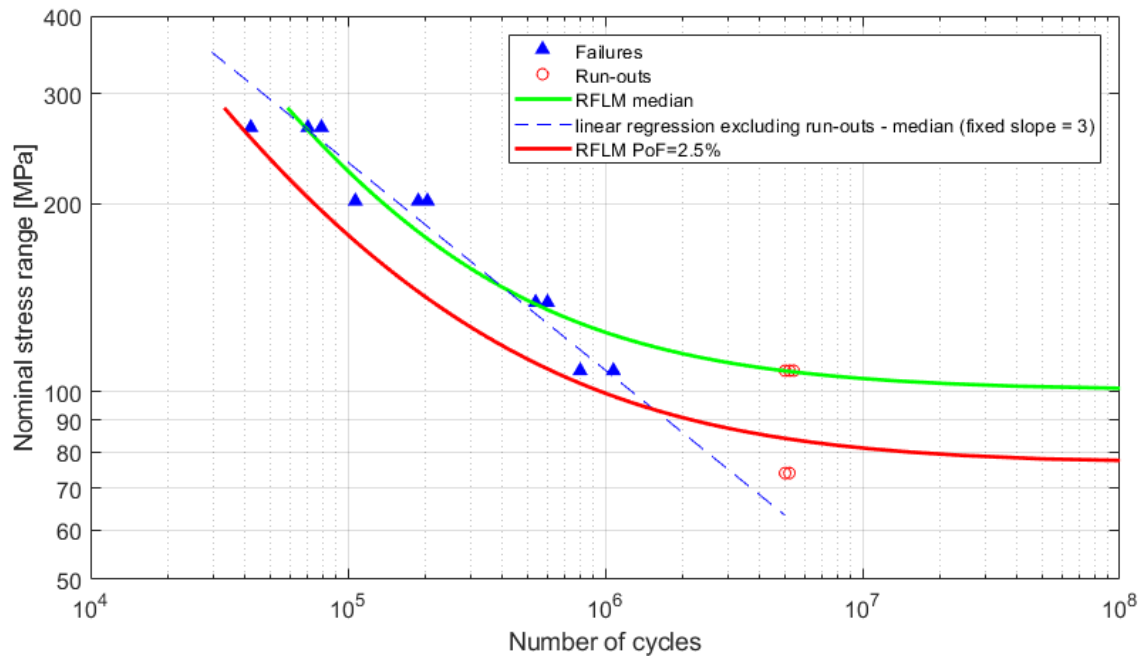
Figure 3.3. RFLM resistance curves and conventional S-N curves fitted to the example data [2] (data sample from [35])

4. Models for the damage mechanisms

4.1. The crack initiation phase, uniaxial and multiaxial stress states

As it was shown in section 2.3, the existence of a crack initiation phase is observed in welded joints subjected to fatigue loading, even for as-welded joints at relatively high stress variations. This phase is even more significant at low stress ranges. Therefore, many approaches have been proposed to simulate damage evolution in this phase, concentrated on predicting lifetime to crack onset. Usually, the crack initiation models are based on a local strain approach at the weld toe notch. The local stress-strain state at the weld toe notch during cyclic loading can be determined by using the Ramberg-Osgood equation for the stress-strain relationship in combination with the well-known Neuber rule and Massing's hypothesis. The approach is visualized in Figure 4.1. Further details can be found in [1].
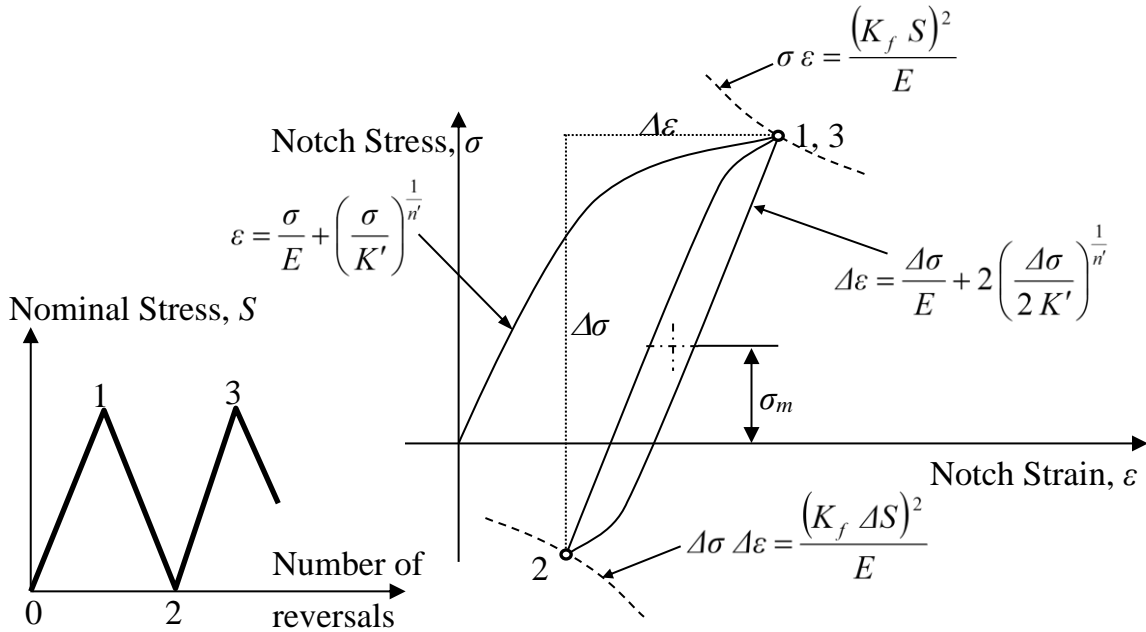
Figure 4.1. Schematic illustration of the local stress-strain hysteresis loop analysis [1]

The relation between local stress and strain range, given by the Ramberg-Osgood equation and Massing's hypothesis concerning the hysteresis loop and established for stabilized cyclic stress-strain curve, can be expressed as:

$$\Delta \varepsilon = \frac{\Delta \sigma}{E} + 2 \left(\frac{\Delta \sigma}{2K'} \right)^{\frac{1}{n'}} \tag{4.1}$$

where $\Delta\varepsilon$ and $\Delta\sigma$ are the local strain and strain range, K' and n' are the cyclic strength coefficient and strain hardening exponent, respectively.

One of the oldest approaches for predicting number of cycles to crack initiation in welded joints is based on the Coffin-Manson equation with Morrow's mean stress correction. In this model the number of cycles N_i to crack initiation can be found from:

$$\frac{\Delta\varepsilon}{2} = \frac{(\sigma'_f - \sigma_m)}{E}(2N_i)^b + \varepsilon'_f(2N_i)^c \tag{4.2}$$

where $\Delta\varepsilon$ is the local strain range, σ_m is the local mean stress, parameters b and c are the fatigue strength and ductility exponents, and σ'_f and ε'_f are the fatigue strength and ductility coefficients respectively. Schematic illustration of the Coffin-Manson equation is presented in Figure 4.2.
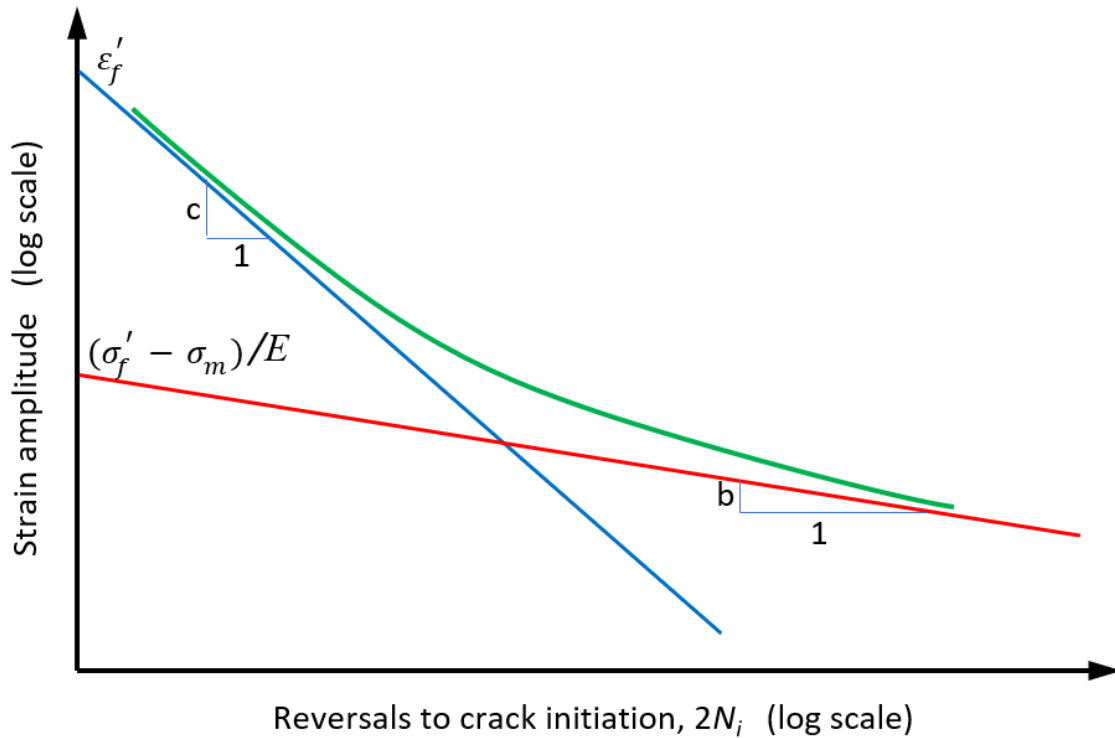
Figure 4.2. Schematic illustration of the Coffin-Manson equation

The application of this model for welded joints was first proposed by Lawrence and Yung [15] and later modified and calibrated against experimental results by Lassen and Recho [21,36].

There is one major disadvantage of this approach – Coffin-Manson equation concerns uniaxial stress state whereas at the weld toe region, even under simple loading conditions, stress state is multiaxial. To overcome this disadvantage

multiaxial fatigue criteria can be used. Such criteria are usually based on critical plane approach and thus are very computationally expensive, thus, criteria that allow to take into consideration stress multiaxiality in a different manner giving better trade-off between accuracy and computational cost are preferable. As an example the Dang Van equivalent shear stress criterion can be used to determine the crack initiation life [37]. According to this approach, for any number of cycles N_i to crack initiation under constant amplitude loading, a critical state can be described as:

$$\tau_{0_i} = \tau_a + \alpha_i \sigma_h \qquad (4.3)$$

where τ_a is the shear stress amplitude, σ_h is the maximum hydrostatic stress, α_i and τ_{0_i} are material parameters obtained by testing. This approach is more in line with the fact that the crack nucleation is driven by the shear stress variations. The Dang Van approach can also take account for a multiaxial stress situation at the weld toe through the hydrostatic stress component occurring in combination with the acting shear stress amplitude. Welding residual stresses often give a multiaxial stress situation. This methodology was originally proposed for determining the fatigue limit for non-welded components [37]. The approach has later been applied for modelling the initiation life for the present test series 1 in Paper A.

4.2. Linear Elastic Fracture Mechanics models

4.2.1. Basic concepts

Fracture mechanics models are usually based on applied LEFM. The Paris law is adopted in rules and regulations for predicting fatigue crack growth in welded joints. The basic concept is linear relation between crack growth rate and stress intensity factor range, for a log-log scale, given by the growth parameters C and m. Furthermore, it is assumed that there exists a threshold value for the SIFR below which a crack does not propagate. This model is suggested in DNV-RP-C210 [5]. In BS 7910 bi-linear model is proposed for better prediction of the crack behaviour at an early crack growth stage. Both approaches do not take account the influence of the stress ratio R explicitly. BS 7910 distinguishes only between two cases, $R<0.5$ and $R\geq0.5$, and gives different values for the C and m material parameters for each of them. An attempt to explicitly take into account the R ratio has been made by Huang et al. [38]. The model is denoted a *unique crack growth model*. The model applies an equivalent SIFR definition and 'a unique crack growth rate

curve method'. Like the previously mentioned models it also contains a threshold term and crack growth rate can be expressed as:

$$\frac{da}{dN} = C(\Delta K_E^m - \Delta K_{th0}^m) \tag{4.4}$$

where ΔK_E is the effective SIFR for the given R ratio, whereas the ΔK_{th0} is the threshold value for the SIFR at $R=0$. The R ratio is defined by the applied SIF:

$$R = \frac{K_{min} + K_R}{K_{max} + K_R} \tag{4.5}$$

The parameters are given by the equations:

$$\Delta K_E = M\Delta K$$

$$\Delta K_{th0} = M\Delta K_{th}$$

$$M = \begin{cases} (1-R)^{-\beta_1} & -5 \le R < 0 \\ (1-R)^{-\beta} & 0 \le R < 0.5 \\ (1.05 - 1.4R + 0.6R^2)^{-\beta} & 0.5 \le R < 1 \end{cases} \tag{4.6}$$

where β and β_1 are parameters dependent on material property and environment, satisfying the following relationship: $0 \le \beta \le \beta_1 \le 1$. Proposed values for medium and high strength steels are: $\beta = 0.7$ and $\beta_1 = 0.84$ ($\beta_1 = 1.2\beta$). A general equation for determining β for structural steels has the following form:

$$\beta = 0.22 + \frac{0.65}{1 + 0.0035\Delta K^4} \tag{4.7}$$

β_1 is typically equal to a constant value of 0.84 for many examined materials [39]. Although the parameters β and β_1 are treated as material properties, proposed empirical formula (4.7) for structural steels assumes a dependency on the stress intensity factor range. It gives higher values in the early crack growth stage and then tends rapidly to a constant value of 0.22. This gives a change in the M factor used in computation of the effective SIFR that, in the case of $R=0.35$, starts from 1.45 for a low nominal SIFR and becomes close to 1.1 for $\Delta K > 10$ MPam$^{0.5}$. The β factor vs. the nominal SIFR is plotted in Figure 4.3 together with the M factor computed for $R=0.35$ and R=0.5.
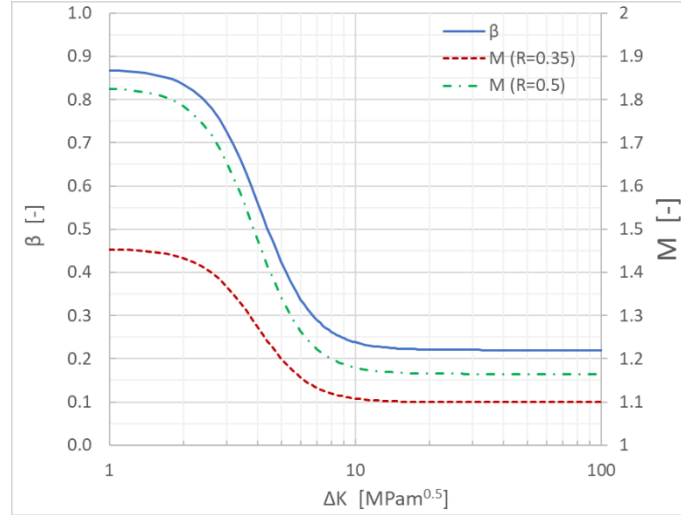
Figure 4.3. β coefficient for structural steels and corresponding M factor for $R=0.35$ and $R=0.5$ [20]

Finally, a unique crack growth rate curve equation recommended for analysis of welded steel structures (mean curve) is given:

$$\frac{da}{dN} = 8.32 \times 10^{-9}\left(\Delta K_E^{2,88} - 7.2^{2,88}\right) \tag{4.8}$$

The equation above uses the following units: MPam$^{0.5}$ for the SIFR values and mm/cycle for the resultant growth rates.

A detailed discussion of advantages and shortcomings of the above model utilized for modelling growth of the shallow cracks in the weld toe notch area has been presented in Paper B and Paper C.

4.2.2. SIF for welded joints

In the present work the formulas adopted in DNV-RP-C210 [5] are used for calculating the SIF. The general expression for the SIF for a given loading mode can be written in the form:

$$K_I = \sigma_0 Y(a, c) M_k(a, c) \sqrt{\pi a} \tag{4.9}$$

where a is the crack depth, $2c$ is the crack surface length and σ_0 is the applied nominal stress. The function Y gives the influence of the global plate and crack geometry, whereas M_k takes account for the effect of the weld notch. The functions Y and M_k also take account for the loading mode. The notch factor M_k is dependent on the crack depth and shape, the welded attachment length and the local toe geometry, see DNV-RP-C210 [5] for further details. The formulas given to determine the geometry factor Y are based on the work of Newman and Raju [40] who proposed empirical parametric equations for the stress intensity factors for

31

semi-elliptical surface cracks in flat plates subjected to membrane and bending loads. These equations have been obtained from a 3D FE analysis. 20 years later Bowness and Lee [41] proposed empirical formulas for a weld toe magnification factors M_k which, together with Newman and Raju formulas, allows us to obtain SIF values for surface breaking semi-elliptical shaped cracks located in the weld toe notch area. Weld toe magnification factors were obtained for the membrane and bending loading modes using the *J*-integral approach and 3D FE simulations. The M_k factor is obtained at the deepest point and at the surface points along the crack front by comparing SIFs for a given crack in a T-butt joint and in a flat plate. Hence, the influence of the local weld toe geometry was determined by comparing the two cases. Only the weld toe flank angle θ is explicitly entering the obtained formulas. The influence of the weld toe radius ρ is considered in a simplified way, by two separate sets of formulas for $\rho=0$ and $\rho=0.1t$ (*t* being the load-carrying plate thickness) corresponding to an as-welded and a ground joint respectively. The assumption of $\rho=0$ is in most cases overly pessimistic as the transition between the weld bead and the plate usually is smoother with $\rho>0$. Hence, although the assumption may be acceptable from the design point of view, it may not be sufficiently accurate for modelling the early crack growth of shallow elliptical cracks. For this reason, a detailed discussion regarding the influence of the weld toe radius on the SIF calculations for shallow cracks is be presented in Paper C. The parametric formulas for the weld notch magnification factor M_k proposed by Bowness and Lee were developed by multiple regression analysis and thus the authors did not recommend extrapolating them outside the validity limit for the crack depth. The lower limit value of the crack depth to thickness ratio in the given formulas is *a/t*=0.005 [41]. In the need of using the formulas below the given validity limit they suggested to use the M_k value at the given lower limit for the crack depth. As the factor M_k has a strong bearing on the calculation of the SIF this aspect is particularly important when dealing with shallow cracks at the weld toe. The problem is illustrated in Figure 4.4. As can be seen from the curves the weld notch magnification factors have a steep gradient when extrapolation is carried out below the validity limit of *a/t*=0.005. If one chooses to keep the factors constant below *a/t*=0.005 this will make an important difference compared to using the extrapolated values when predicting the very early crack growth. Consequently, if fracture mechanics are to be applied to these small cracks it is obviously a need to clarify which values are to be used for the magnification factors when *a/t*<0.005.
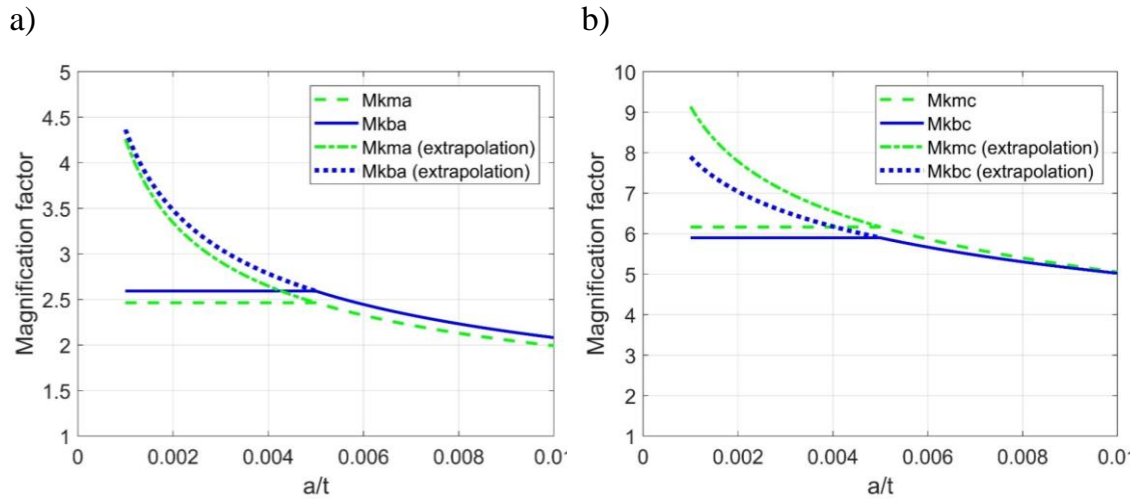
Figure 4.4. Magnification factors, M_k, for shallow cracks for membrane and bending loading: a) at the deepest point, b) at the crack ends; (constant $a/c = 0.2$, $L/t = 2$, $\theta = 45°$, $\rho = 0$) [11]
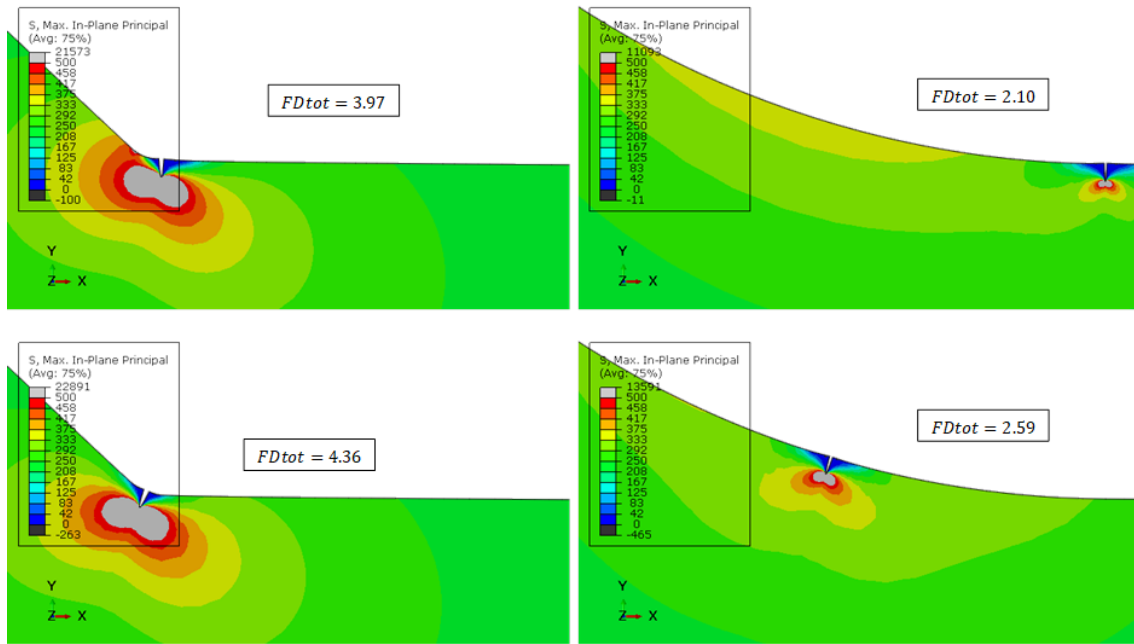
Figure 4.5. Influence of the crack locus and orientation on the SIF; upper/lower figures – different crack location; left/right figures – different toe radius ($FDtot = Y \cdot M_k$ is the total geometry factor, membrane loading mode) [11]
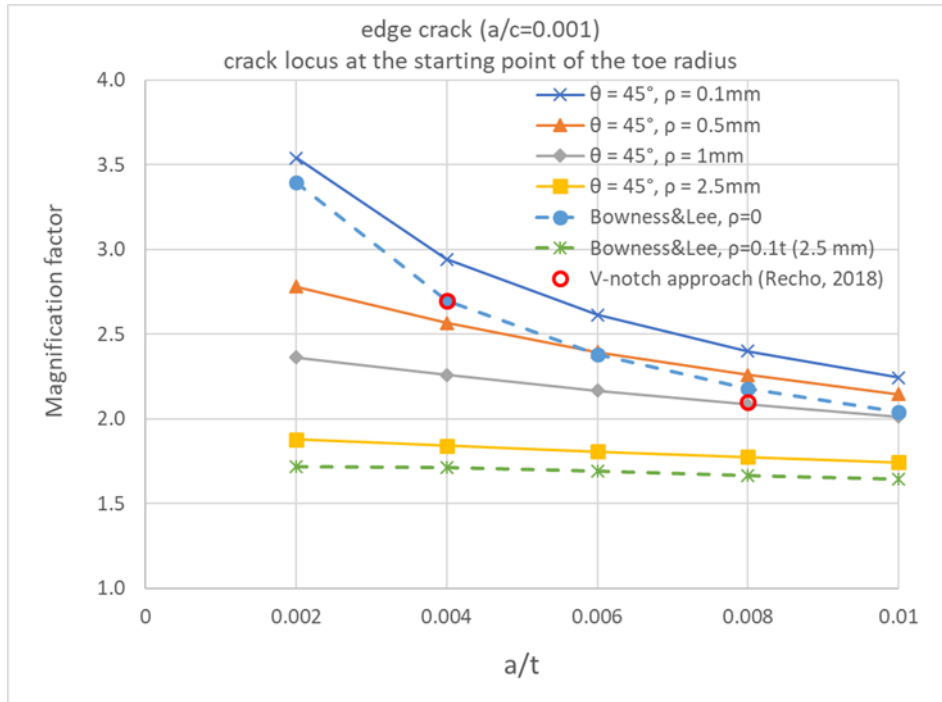
Figure 4.6. Influence of the weld toe radius on the magnification factors M_k for different crack depth to thickness ratios for the membrane loading mode; comparison to extrapolated Bowness and Lee formulas and V-notch results (crack locus at the starting point of the toe radius) [11]

4.2.3. Fitting growth models to measured crack propagation for welded joints

From in-service experience and observations during testing under a nominal stress range of 150 MPa the following crack behaviour is likely:

- Multiple micro cracks initiate at locations where there is a combination of an unfavourable weld toe geometry and a presence of initial flaws. The number of cracks that initiate per length of the weld seam for a given stress range is by nature random and depends on load level. These micro cracks will grow and at a given stage exceed the defined transition depth of 0.1 mm. Based on observations given by the crack monitoring system (ACPD) the number of cracks that initiate along the width of a specimen (60 mm) is between 2 and 3 at an applied stress range of 150 MPa. The number of cracks can be randomized according to a Poisson distribution. The number of cracks will have an influence on when the a/c transition towards an edge crack takes place. At lower stress ranges the number of cracks along the weld seam will decrease.
- The cracks along the weld seam that have passed a depth of 0.1 mm will have a semi-elliptical shape and their aspect ratio a/c is by nature random.

34

- Each of these cracks can be modelled by a single crack fracture mechanics model predicting the crack size and crack shape evolution until crack coalescence takes place.
- After crack coalescence the cracks join to form one crack through the entire specimen width that rapidly propagates to failure.

The goal of LEFM models investigated in this thesis is to simulate all the stages given above, except the first one. Hence, the crack growth from an initial crack depth of 0.1 mm is pursued. The ability of the LEFM models is demonstrated by both comparing the crack depth growth rate and the crack shape evolution with experimental data in Paper B and Paper C and a summary is presented in section 6. A two-stage crack coalescence model utilizing forcing function for crack shape evolution has been proposed in Paper B. The likely difference in shape evolution for the membrane and bending loading mode was also investigated in Paper C. An example for a single semi-elliptical crack under membrane and bending loading modes is presented in Figure 4.7 and Figure 4.8.
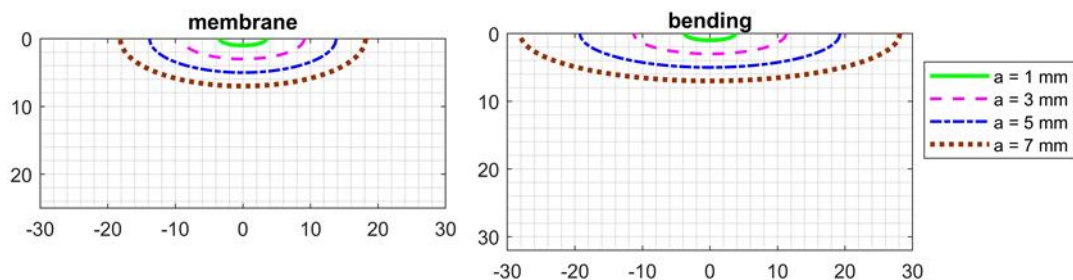
Figure 4.7. Shape evolution of a single semi-elliptical crack under membrane and bending loading modes at different growth stages [11]
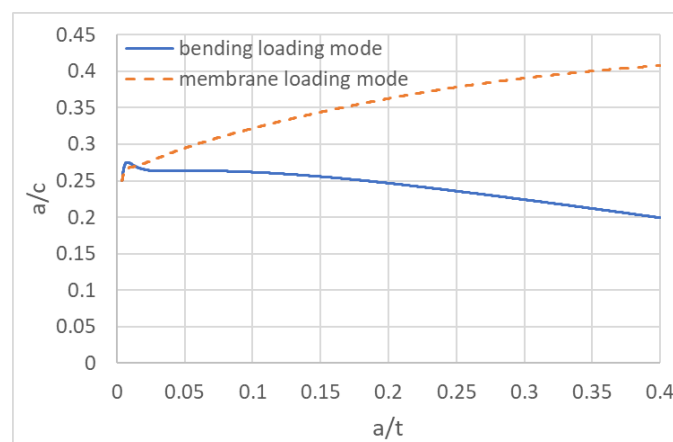
Figure 4.8. Crack shape evolution of a single semi-elliptical crack for the membrane and bending loading mode ($a_0/c_0 = 0.25$, $L/t = 2$, $\theta = 45°$) [11]

The FM models shall be fitted to the crack propagation phase only. Consequently, the number of cycles spent in the initiation phase is subtracted from the fatigue lives. This subtracted portion of the fatigue life is determined from the ACPD measurements up to the point where stable growth begins. Application of LEFM models below this transition depth is questionable and calculation of SIF values using available methods is uncertain. This aspect has been presented in the previous section. Some details of how the growth histories have been extracted for the analysed test series are presented in section 6 and all the details are explained in Paper B and Paper C.

5. Collected data and experimental investigations

5.1. Collected data for stressed plates with transverse fillet welded attachments

The collected life data are from welded joints that belong to the same population. The welded details are designated category 71 in Eurocode 3 Part 1-9 [3], whereas same population is designated as an F class in offshore rules and regulations [4]. Both fatigue life data and crack growth data were collected.

The collected data are divided into two samples:

- Data sample I – the first data sample consists of life data collected at a constant stress range of 150 MPa. All results are for medium strength C-Mn steel with a plate thickness of 25 mm and 32 mm. The specimens with 25 mm thickness were tested under membrane loading mode while specimens with 32 mm thickness were tested under bending loading mode. The effective R ratio was 0.35 and 0.1 for the membrane and bending loading mode, respectively. For the test specimens belonging to this sample both early crack growth histories and final lives are available. The crack growth data in this sample were used as basis for detailed study of the fatigue damage evolution.

- Data sample II – the second data sample is an extended sample. It contains the same life data as the first sample, but the data are now supplemented by tests with other similar test specimens subjected to different constant amplitude stress ranges. The plate thicknesses are ranging from 20 to 32 mm and the steel qualities are mild and medium strength C-Mn steel. For these specimens only life data are available, crack growth was not measured during the testing. This data sample was used for establishing S-N curves and more advanced probabilistic models for the entire fatigue life. These additional data include the two large test series that are also tested at stress range of 150 MPa, giving a large dataset of specimens tested at the same stress range level. This offers a unique possibility for selecting the life model that gives the best fit at that stress range. Various frequency functions were tested. The selected frequency function is based on a goodness-of-fit criterion.

Overview of the collected fatigue test data is presented in Table 5.1.

The data sample I comprises test series marked with grey shading in Table 5.1. Series designations in parentheses are used in Paper C and are included in the table for the sake of clarity. The raw data of crack depth estimates obtained using ACPD monitoring system for test series I-A and II are presented in Figure 5.1 and Figure 5.2, respectively. These data represent entire damage evolution including crack initiation phase as well. To fit and verify the applied fracture mechanics models the crack growth phase has been extracted as explained. For each individual specimen the data have been smoothened, the number of cycles to reach 0.1 mm depth has been estimated. This portion of the fatigue life is subsequently subtracted from the damage history such that the origin-point for crack growth is defined. Thus, the data modified in that way represent the crack growth phase only and it allows to establish a mean crack propagation curve which is used for further investigations. The growth histories from crack depth of 0.1 mm to 10 mm and the mean propagation curve for test series I-A and II are presented in Figure 5.3 and Figure 5.4, respectively.

The data collection presented in [42–44] were examined and results that were representative for the present population were included in data sample II. The runout data was available only in [44]. Some fatigue life data come originally from [45–47]. These additional fatigue life data consist of 88 specimens in total, of which 15 are runouts. Hence, total number of life data in this data sample is 216. The fatigue life data for data sample II is shown in Figure 5.5.

Table 5.1. Collected fatigue data

Test data identification	Geometry	Number of specimens	Thickness [mm]	Steel grade	Welding procedure	Loading mode	R ratio	Life data	Crack growth data	References
Series 1a (Series I-A)	cruciform	34	25	S355	SMAW, FCAW	membrane	0.35	X	X	1) Lassen [48] 2) Mikulski and Lassen [20]
Series 1b (Series I-B)	cruciform	10	25	S355	SAW	membrane	0.35	X	X	Lassen [48]
Series 2	cruciform	42	25	S355	SMAW	membrane	0.1	X		Engesvik and Lassen [49]
Series 3	cruciform	42	32	S235	SMAW	membrane	0.1	X		1) Engesvik [50] 2) Engesvik and Moan [24] 3) Engesvik and Lassen [49]
Series 4 (Series II)	T-joint	10	32	S355	SMAW	bending	0.1	X	X	Mikulski and Lassen [11]
Additional specimens tested at various CA stress ranges	cruciform	36	25	S355	n/a	membrane	n/a	X		Gurney [37]
	cruciform	13	25	n/a	n/a	membrane	0	X		Gurney [38]
	cruciform	5	31	S355	n/a	membrane	n/a	X		Berge [47]
	cruciform	8	20	S355	SMAW	membrane	0.1	X		Friis and Streneroth [51]
	T-joint	26 (15 runouts)	22-32	S355	n/a	membrane, bending	0-0.1	X		Lebas and Fauve [44]
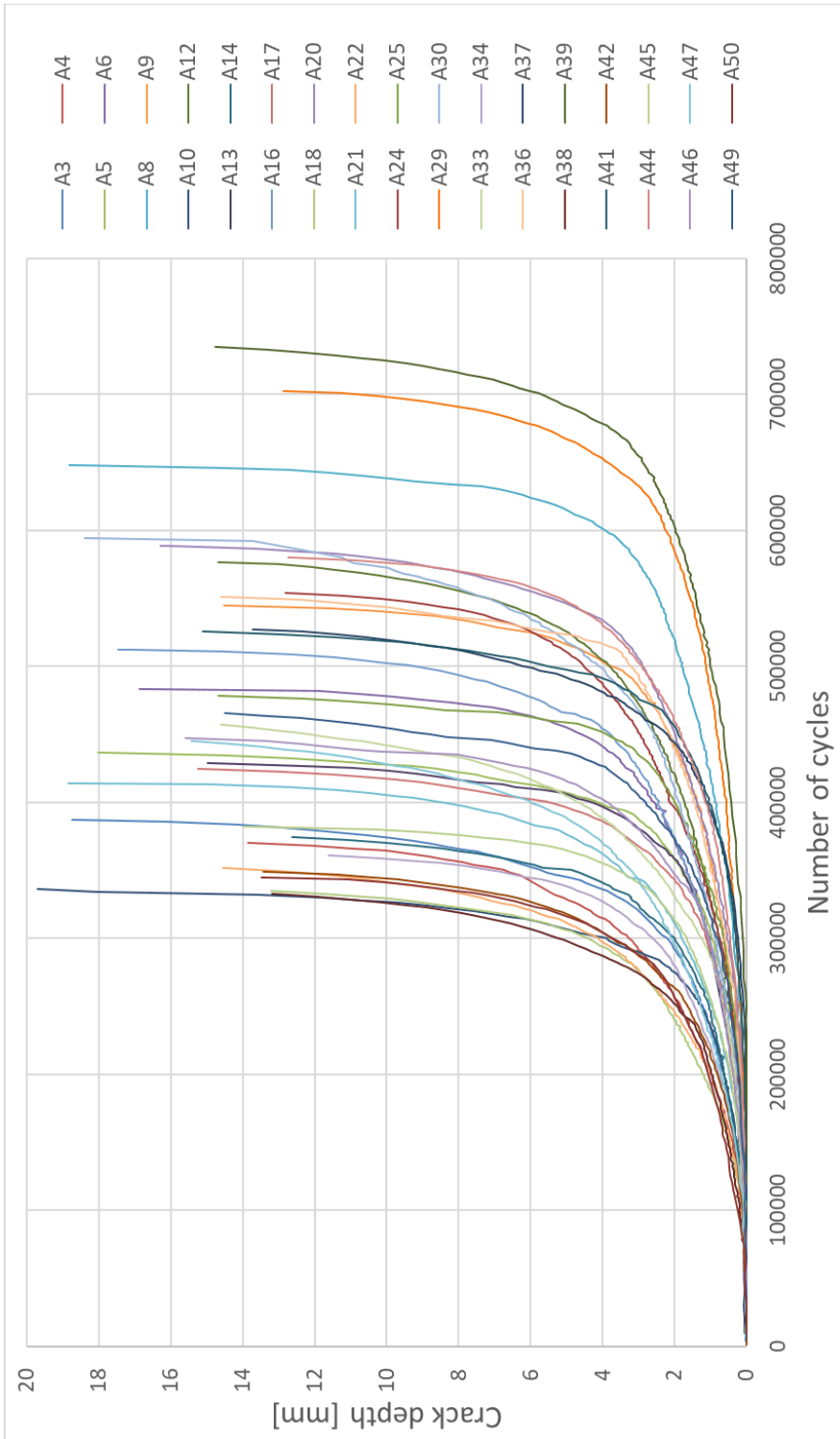
Figure 5.1. Fatigue crack depth as a function of number of cycles for data sample I – test series I-A (membrane loading mode) – raw data including crack initiation period
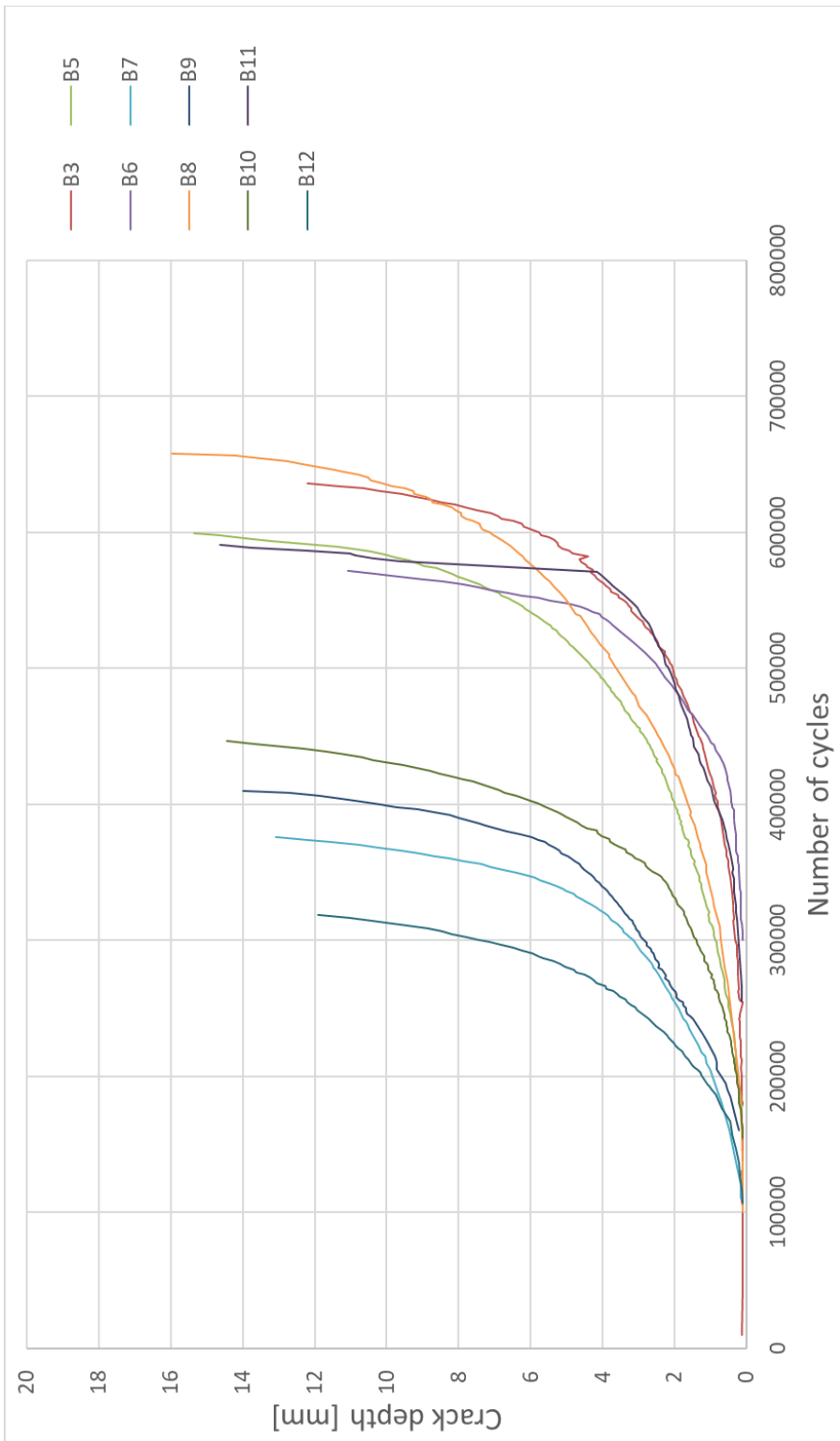
Figure 5.2. Fatigue crack depth as a function of number of cycles for data sample I – test series II (bending loading mode) – raw data including crack initiation period
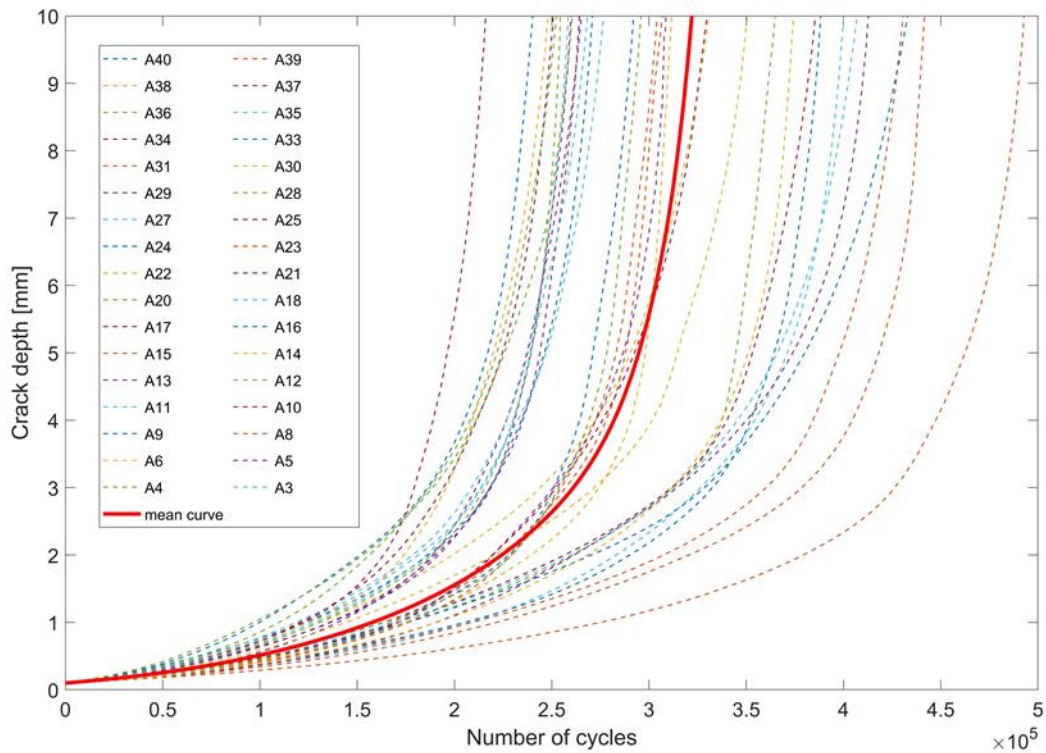
Figure 5.3. Fatigue crack depth as a function of number of cycles for data sample 1 – test series I-A (membrane loading mode) – smoothed data – crack growth form 0.1 mm only [8]
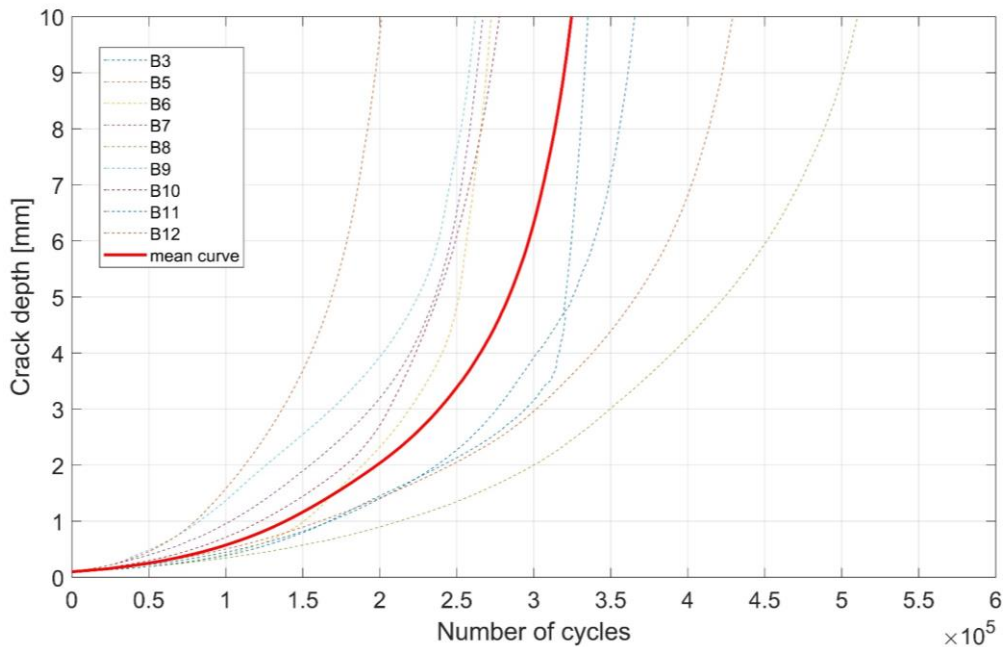
Figure 5.4. Fatigue crack depth as a function of number of cycles for data sample 1 – test series II (bending loading mode) – smoothed data – crack growth from 0.1 mm only
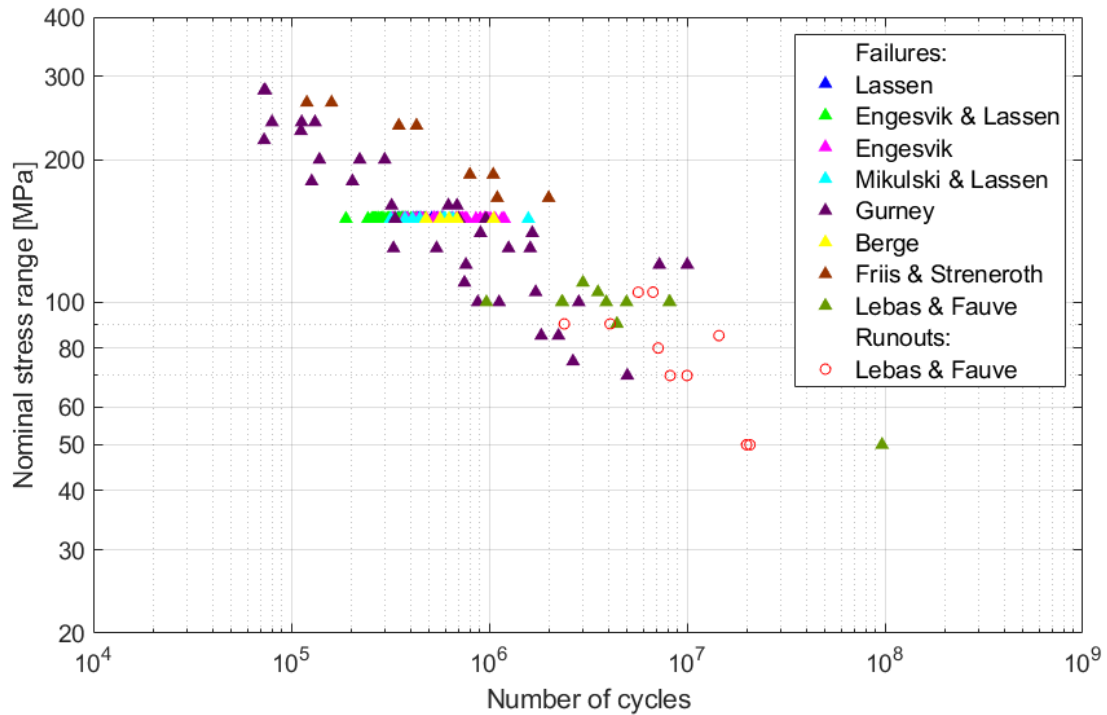
Figure 5.5. Fatigue life data collected in data sample II

5.2. Present experimental investigation of plates with longitudinal attachments

In addition to the data base collected for transverse attachments, some tests were carried out in the present work with longitudinal attachment, see the geometry shown in Figure 5.6. This is also a very common detail in welded structures and the population have a fatigue quality that is very close to F class in the foregoing section. An advanced ACPD monitoring system was set-up to measure the crack growth from the very beginning of the tests. Typical results are shown in Figure 5.7 and Figure 5.8. As can be seen this growth history is very different from the curves shown in Figure 5.3. Whereas the curves in Figure 5.3 have a steep acceleration of the crack growth for larger crack depths, this is not the case for the curve in Figure 5.7 and Figure 5.8. The explanation is that when the surface crack length is exceeding the thickness of the longitudinal attachment, the crack growth will level off. This is because the two end points of the crack front at the surface are no longer influenced by the stress concentration at the end of the longitudinal stiffener. This gives the typical weak S-shape of the curve as shown in Figure 5.7. Hence, the crack growth history can be very different for the two detail types although the final fatigue life can be quite similar. Details from the test set-up are found in Annex A.
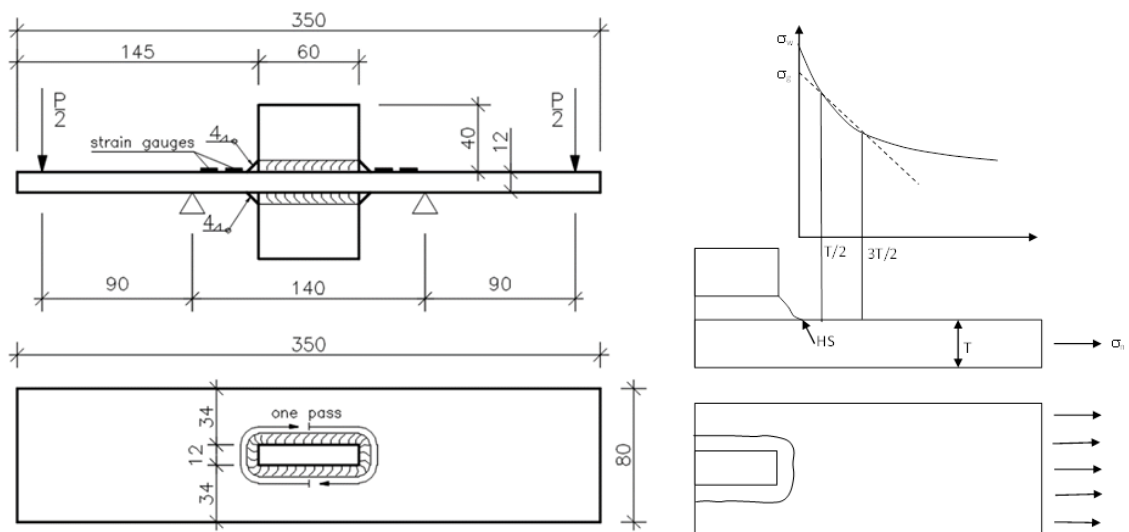
Figure 5.6. Test specimen with longitudinal attachment (left) [52], loading conditions and stress concentration at expected crack locus

Table 5.2. Collected fatigue life data

Specimen	Nominal stress range [MPa]	R-ratio	Fatigue life [cycles]
no. 2	230	0.1	432000
no. 3	230	0.1	385000
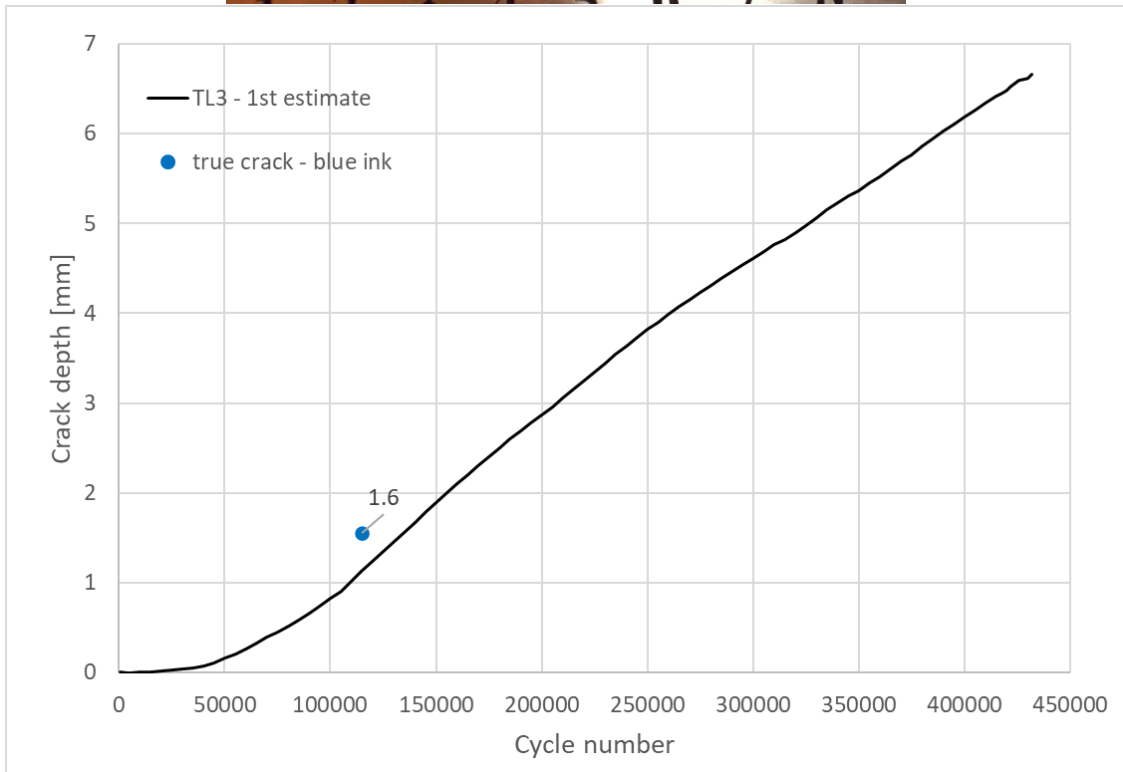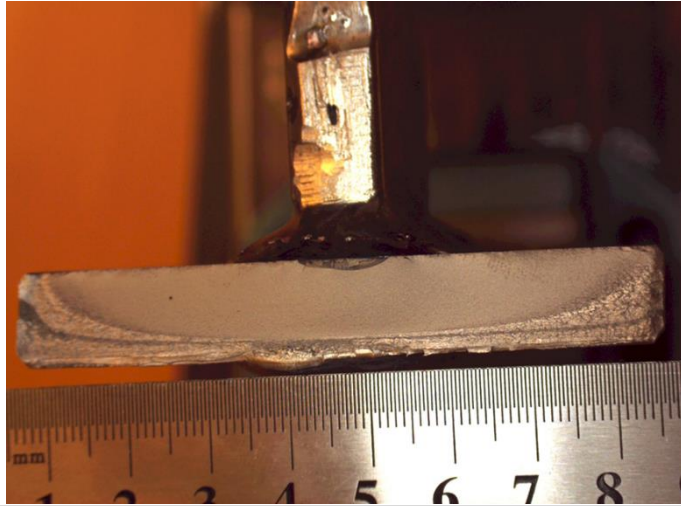
Figure 5.7. Fracture surface and measured crack growth history, specimen no. 2
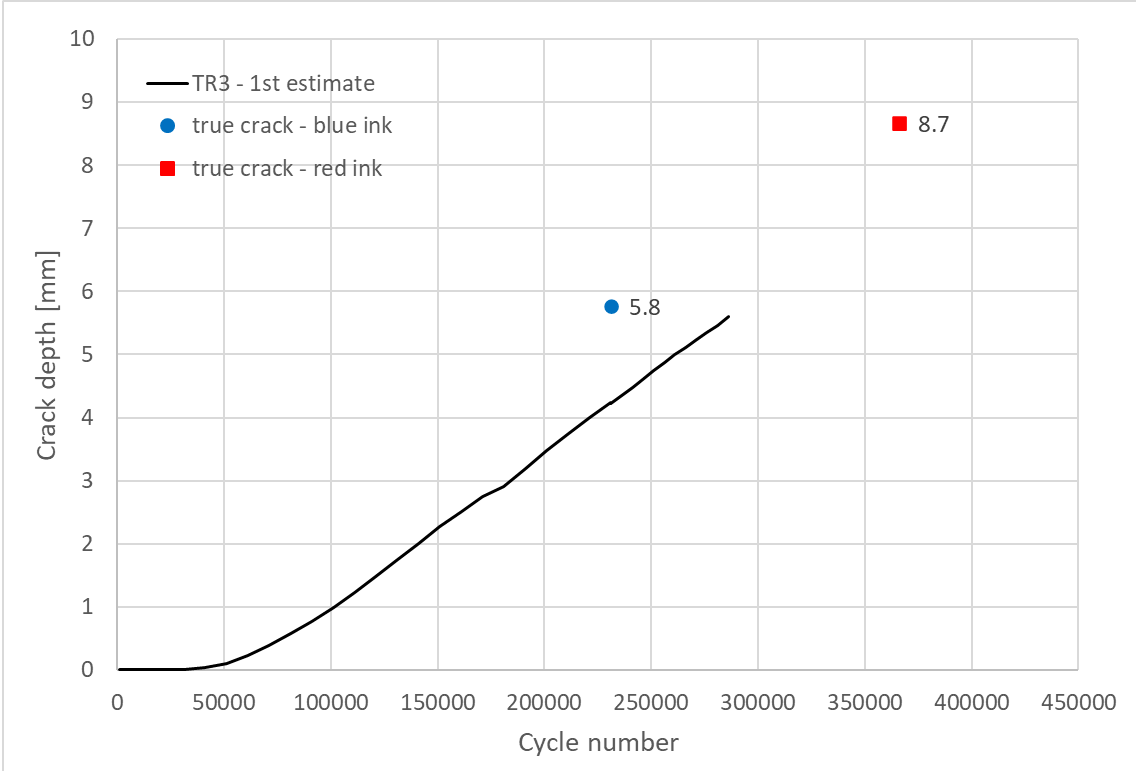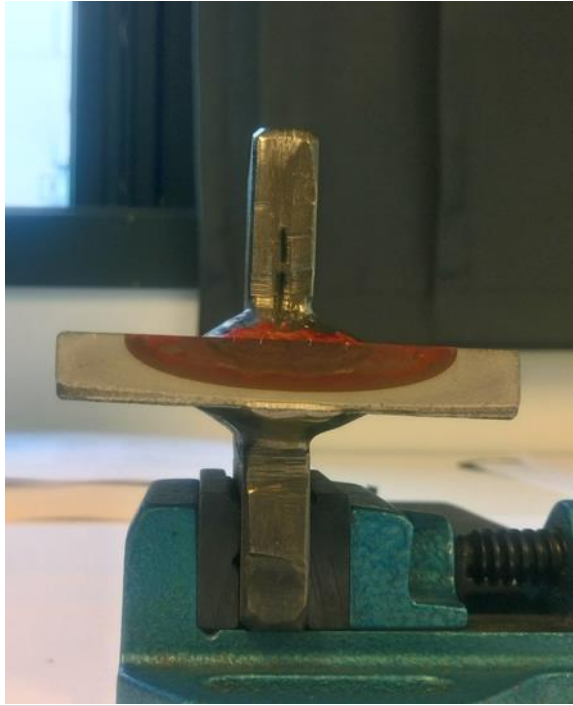
Figure 5.8. Fracture surface and measured crack growth history, specimen no. 3

6. Fitting fracture mechanics models to crack growth data

Fracture mechanics models have been fitted to the measured crack growth data for the plates with transverse attachments. The experimental growth histories have been obtained using ACPD method. From the available test data it was possible to estimate number of cycle to reach a crack depth as small as 0.1 mm for the test series II (bending loading mode) and even 0.05 mm for the test series I-A (membrane loading mode). Details can be found in Paper B and Paper C and the summary is presented in Table 6.1, Table 6.2 and Figure 6.1. Crack growth histories for so small cracks at the weld notch have never been published before. Based on these results an initial crack depth of 0.1 mm has been chosen as input parameter in the fracture mechanics models. Hence, the experimental crack growth histories used for fitting numerical models consist of growth histories from 0.1 mm up to 10 mm. The remaining life after reaching 10 mm crack depth was insignificant comparing to the total fatigue life. Thus, the crack depth of 10 mm has been chosen as final crack depth in numerical simulations. The ACPD depth estimates have been calibrated against true crack depth values obtained by ink staining of the crack faces, see Figure 6.2. The corrected mean *a-N* curves, as presented in Figure 6.3 and Figure 6.4, have been used in further analysis. Details of the calibration procedure is presented in Paper C. Another issue that needs to be considered in the modelling the fatigue behaviour of cracks emanating from the weld toe, is the crack shape evolution and the coalescence of multiple cracks. The likely crack behaviour for welded joints has been described in section 4.2.3. The crack shape evolution is based on the observation that cracks are initiated at several positions along the weld toe within a specimen and in the beginning these cracks grow as individual shallow semi-elliptical cracks. At a later stage these cracks will coalesce, what was observed at a depth between 2 and 3.5 mm. In this depth range a rectangular edge crack is formed and the growth rate is accelerated. To include this phenomenon in numerical simulations of crack growth a two-stage method has been proposed. The method is described in Paper B and further in Paper C. The crack shape evolution and the differences observed under membrane and bending loading modes were studied in detail in Paper C, the results are briefly presented in Figure 6.5.

Table 6.1. Statistics of cycles to reach given crack depths for membrane loading mode (Series I-A, 34 specimens)

Statistical parameter	Number of cycles to reach		
	a = 0.05 mm	a = 0.1 mm	a = 0.5 mm
Mean	113000	142000	239000
Standard deviation	46000	51000	70000
Coefficient of variation	0.40	0.36	0.29

Table 6.2. Statistics of cycles to reach given crack depths for bending loading mode (Series II, 10 specimens)

Statistical parameter	Number of cycles to reach		
	a = 0.1 mm	a = 0.2 mm	a = 0.5 mm
Mean	176000	213000	267000
Standard deviation	73000	83000	93000
Coefficient of variation	0.41	0.39	0.35

a)

b)
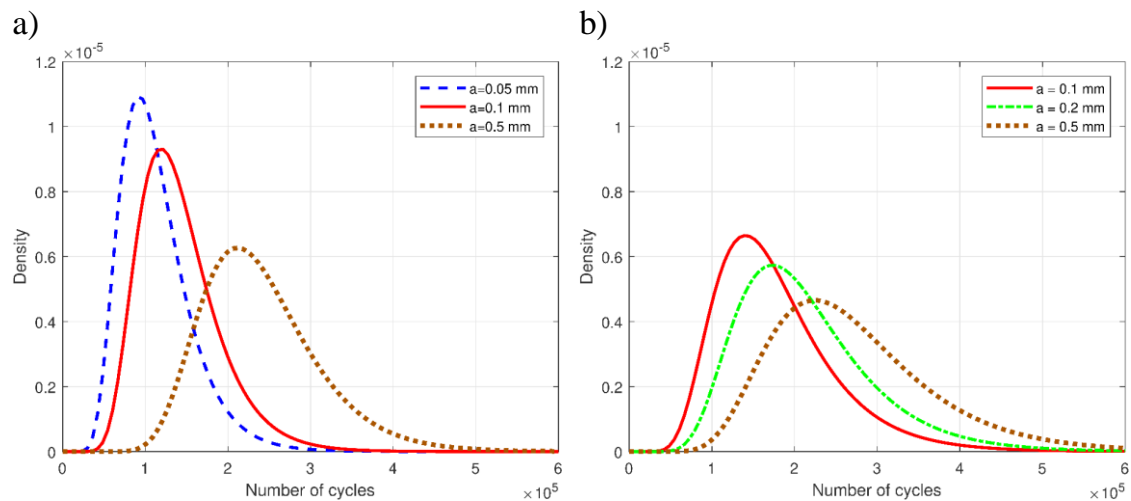
Figure 6.1. Distribution for the number of cycles to reach given crack depth: a) for the membrane loading mode (Series 1a, first estimates), b) for the bending loading mode (Series 2, first estimates) [11]
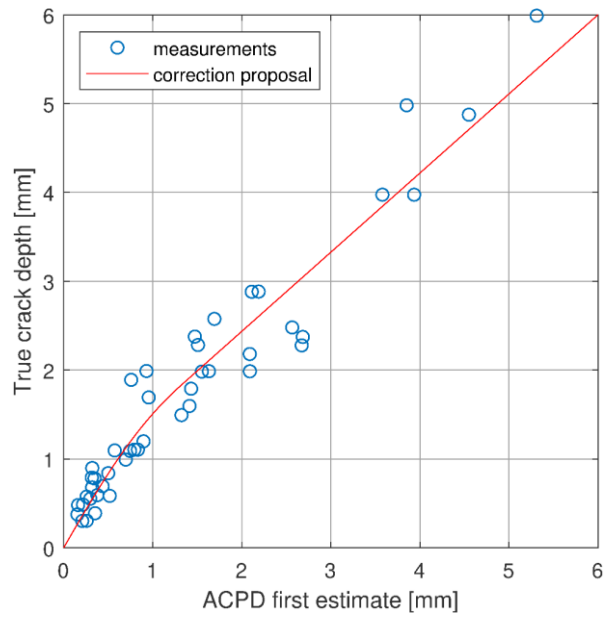
Figure 6.2. True crack depth vs 1st estimate based on ACPD [11]
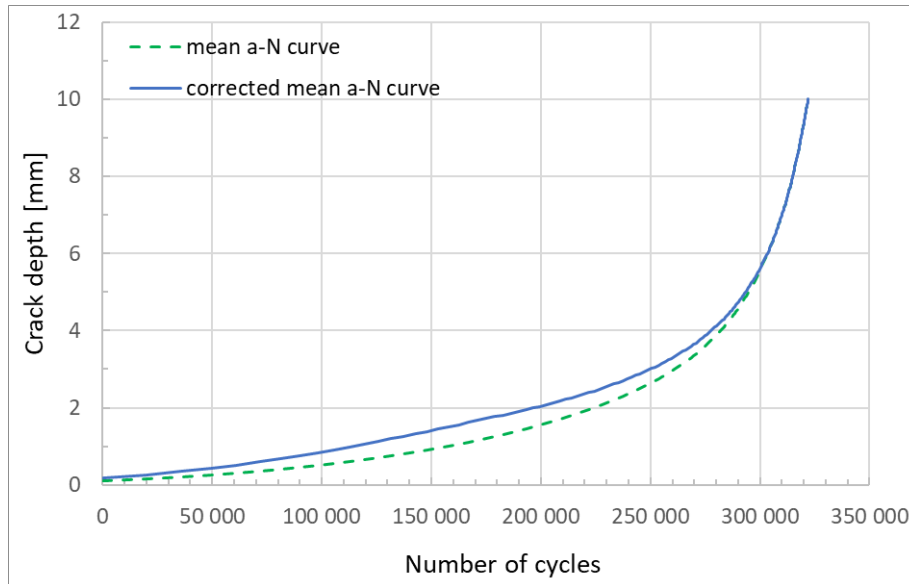
Figure 6.3. Corrected experimental mean *a-N* curve for the membrane loading mode. Uncorrected crack depths are shown for comparison [8]
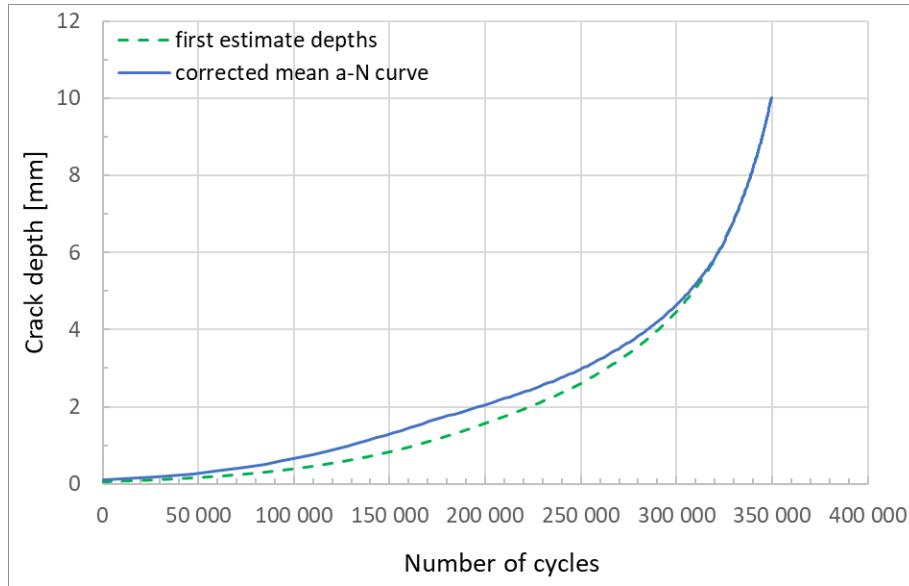
Figure 6.4. Corrected experimental mean *a-N* curve for the bending loading mode. Uncorrected crack depths are shown for comparison [11]
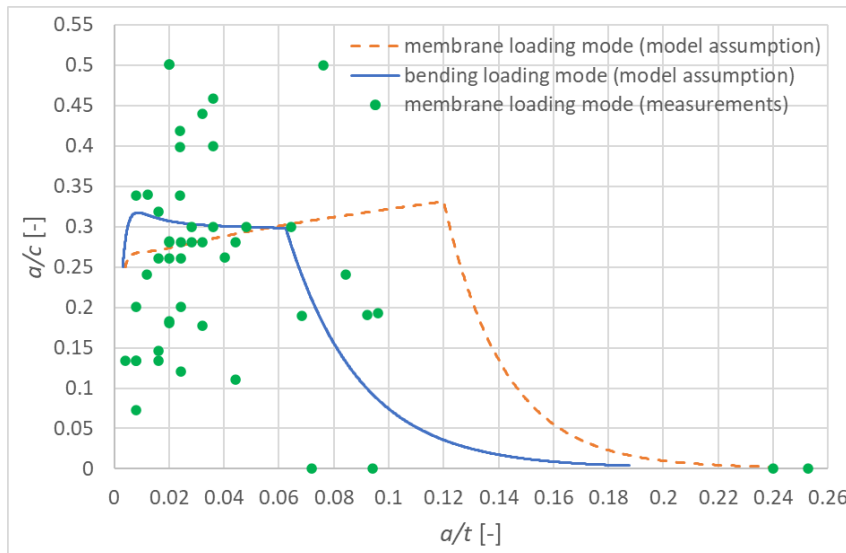
Figure 6.5. Fitted crack shape evolution for the membrane and bending loading modes (all parameters specific for the present test series, $\theta = 58°$, $L/t = 2$ and $\theta = 69°$, $L/t = 1.6$ respectively for the membrane and bending loading mode, $a_{ini}/c_{ini} = 0.25$) [11]

The crack growth histories obtained by the fracture mechanics by using the basic DNV model with recommended *C* and *m* constants have been compared directly to the experimental *a-N* curves and the mean calibrated experimental curves. Both the mean value for *C* and the mean plus two standard deviations have been applied in the analyses, ref. DNV-RP-C210 [5]. The results are presented in Figure 6.6 and Figure 6.7. As can be seen, the impact of crack coalescence is important for the final fatigue life.

50
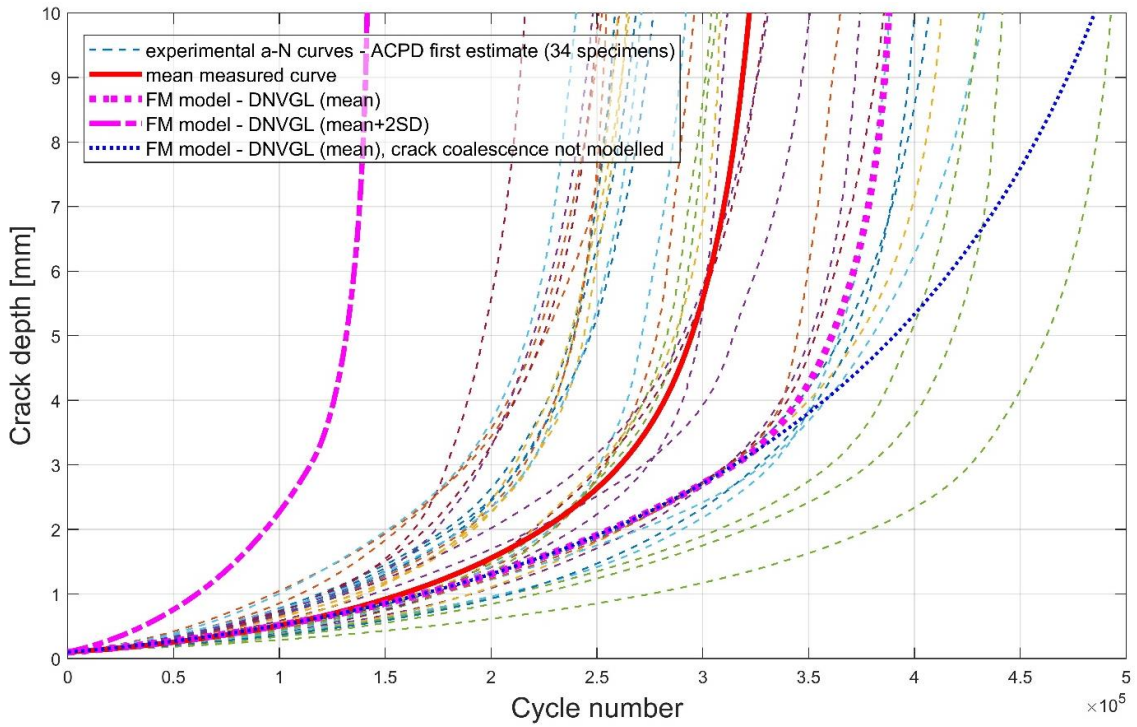
Figure 6.6. Measured individual a-N curves together with the mean curve for all specimens subjected to membrane loading mode (Series I-A, crack depths from 0.1÷10 mm, ACPD first estimate) and model predicted growth histories [11]
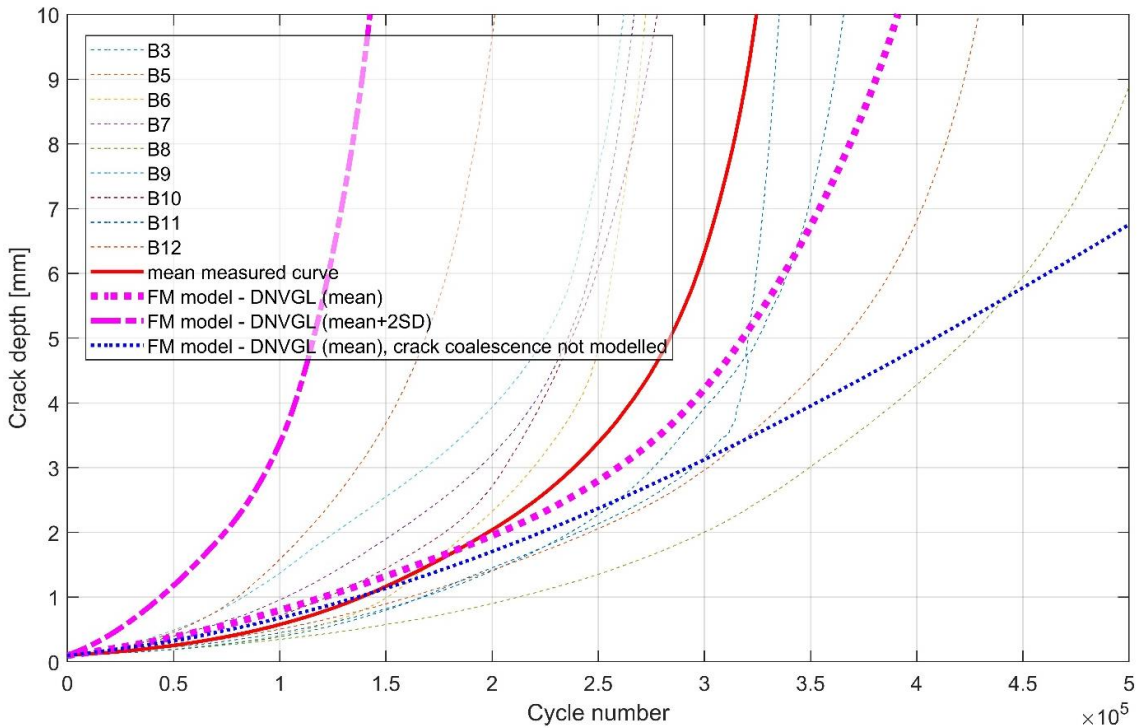
Figure 6.7. Measured individual a-N curves together with the mean curve for all specimens subjected to bending loading mode (Series II, crack depths from 0.1÷10 mm, ACPD first estimate) and model predicted growth histories [11]

To gain more knowledge on the statistics for growth parameters *C* and *m*, an analysis based on the growth rates versus the applied SIFR for a log-log scale was carried out. The exponent *m* is treated as a constant. Crack growth rates obtained from the corrected mean *a-N* curves for both loading modes are plotted versus the SIFR in Figure 6.8. As can be seen the present test data are well within the boundaries given from other investigation based on wide plates and CT specimens. This demonstrates the ability of the Paris law to predict the crack growth at a weld notch.

The fitted growth parameters for the FM model utilizing nominal SIFR values (Model 1a acc. to notation in Paper C) are summarized in Table 6.3.
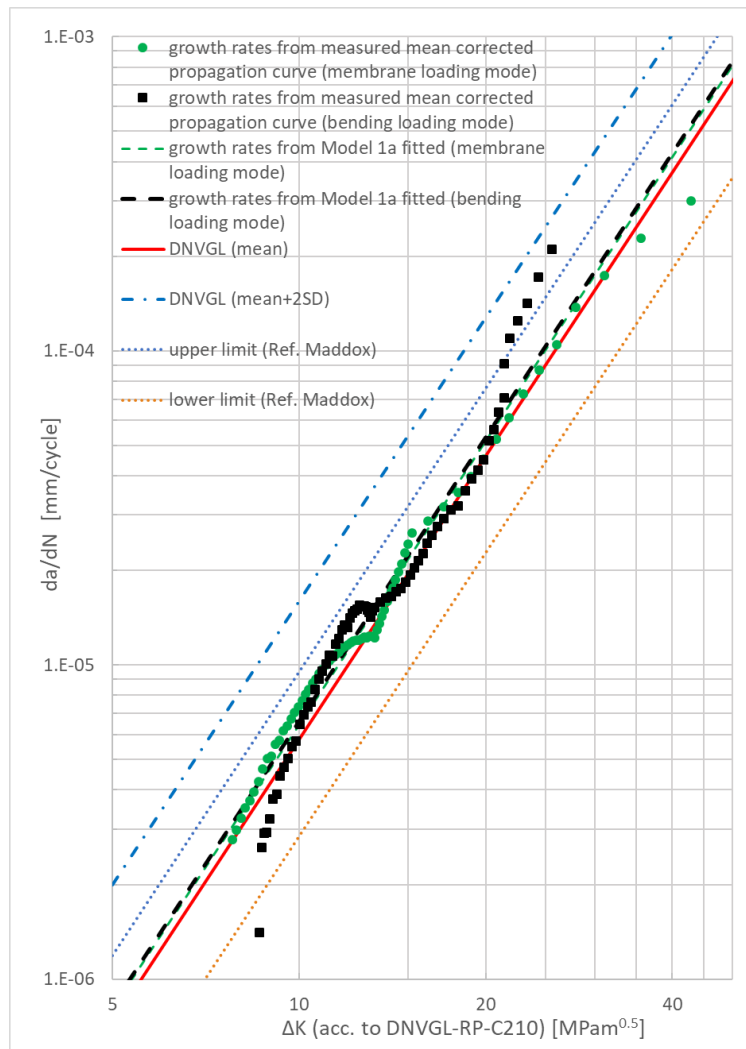
Figure 6.8. Experimental crack growth rates, model 1a predicted growth rates, DNV curves and lower/upper bounds acc. to Maddox, [11]

Table 6.3. Comparison of FM model parameters (fitted values to the mid-section of Figure 6.8)

Loading mode	Model 1a			
	m	C^*	$C_{fitted}/C_{original}$	R^2
All data	3	$6.54 \cdot 10^{-9}$	1.13	0.96
membrane	3	$6.45 \cdot 10^{-9}$	1.11	0.97
bending	3	$6.62 \cdot 10^{-9}$	1.14	0.95

* growth parameter for rate in mm/cycle and ΔK in MPam$^{0.5}$

As can be seen the fitted values for C are quite close to the mean value given in rules and regulations ($5.79 \cdot 10^{-9}$ in DNV-RP-C210 [5]). The discrepancy compared with recommended mean value from the DNV code is also given as fractions in Table 6.3. As can be seen the discrepancy is small, typically 10-20% only. As can be seen from Table 6.3 the correlation factor was as high as 0.96 when all the present data were grouped together. This is close to the same correlation obtained when the two test series are analysed separately. Details and a thorough discussion of the results were presented in Paper C.

7. Fatigue resistance curves for joints with transverse attachments subjected to Constant Amplitude loading

In the present section the RFLM methodology described in section 3.4 is applied to establish fatigue resistance curves under CA loading. For the present analyses a large portion of data (216 samples) were collected at various stress ranges, particularly at lower stress ranges (see section 5.1 for details). Some of these data are runouts such that the conventional linear regression analysis is not capable of including them. An RFLM analysis has been carried out for the collected life data. The fitted model parameters and a comparison to rule-based curves are presented in Paper D. Based on the RFLM analysis the final CA design curve can be defined. The proposed design curve is shown in Figure 7.1 together with the conventional S-N curve obtained from the present data. In the illustration the latter linear curve is chosen to have a fatigue limit at 10^7 cycles and not at $5x10^6$ cycles as in Eurocode 3 Part 1-9 [3]. The RFLM design curve is defined at 97.5% probability of survival. The obtained resistance curve is accepted as it is; however, to the left of $3x10^5$ cycles, the RFLM curve shall be parallel with the conventional linear S-N curve, i.e. $m=3.0$. The chosen point is where the RFLM curve is close to tangential to the conventional linear curve. The argument for this choice is that the conventional analysis is adequate in this high stress range regime. This part of the conventional S-N curve is in the gravity centre of the data included in the linear regression analysis. The conventional design S-N curve gives a fatigue limit of 40 MPa for the present data. As can be seen from the figure the RFLM curve will predict longer CA lives than the conventional curve between 10^6 cycles and 10^9 cycles. For stresses below the conventional fatigue limit of 40 MPa the RFLM will predict finite long lives beyond 10^9 cycles, but not infinitely long as is the case for the conventional curve predictions. It is obvious that the non-linear RFLM curve is more in agreement with the lower data points than the conventional S-N curve. But the RFLM curve has increased uncertainty at very low stresses due to the scarcity of data in this long-lasting life area. As shown, the RFLM curve will give more optimistic CA life predictions than the conventional curve if the fatigue limit is defined at 10^7 cycles. However, this is not the case if the conventional fatigue limit had been drawn at $5x10^6$ cycles as recommended in Eurocode 3 Part 1-9. The design curve suggested by IIW [53] is also included in Figure 7.1. As this curve is keeping $m=3$ down to the knee point at 10^7 cycles and has a constant slope parameter of $m=22$ beyond this point, the curve becomes significantly more

pessimistic than the present RFLM curve. It must be born in mind that the two curves are not obtained from the same data sample.
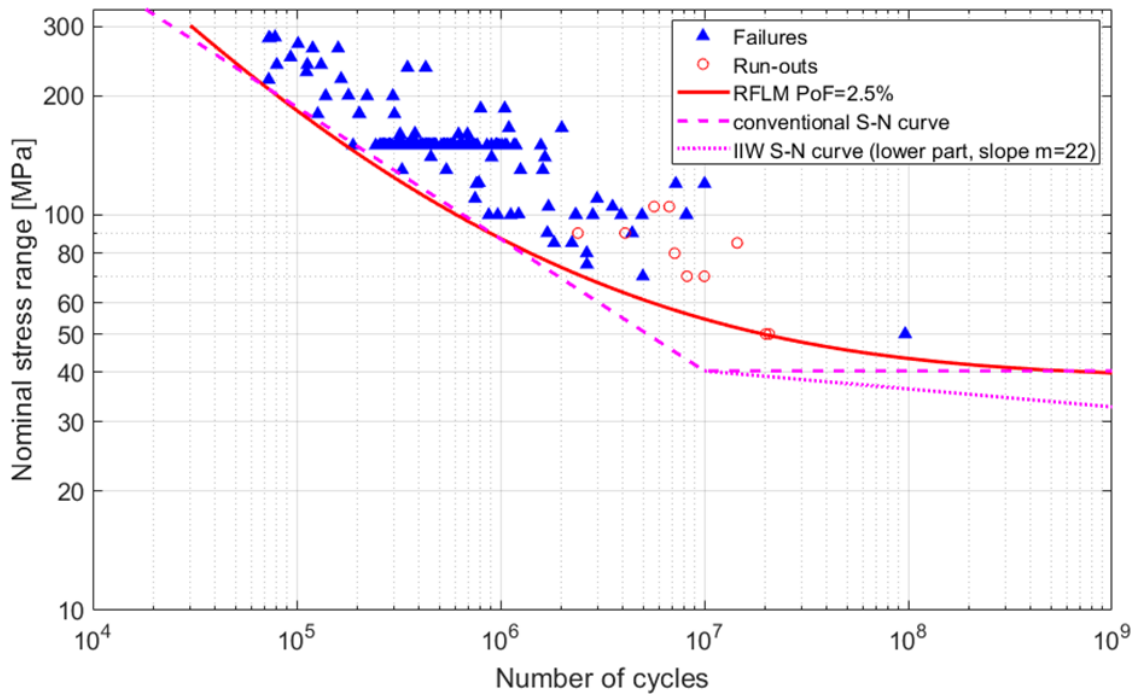
Figure 7.1. Design S-N curves based on RFLM for CA loading together with the conventional S-N curve [2]

As discussed in section 3.3 the chosen probabilistic models and the involved fatigue damage mechanisms shall be compatible. For the high stress ranges the present analysis confirms what is accepted as common knowledge, the upper linear S-N curve has a slope parameter m that coincides with the exponent m in the Paris crack propagation law. Hence, the fatigue life in this area consists mainly of crack growth. At lower stress ranges the RFLM curve continues to fall but the slope of the curve gets more and more shallow. However, the RFLM curve does not turn into a horizontal line. This observation does in fact reject the hypothesis that a fatigue limit exists. The traditional explanation for such a fatigue limit has been the threshold value for the stress intensity factor range for a given initial crack. In the present work the shape of the lower part of the RFLM curve demonstrates that the fatigue damage mechanism is gradually changing from crack growth to a crack initiation mechanism such that the crack initiation phase becomes the dominant part of the fatigue life. It seems that this shift in damage mechanisms is a better description of the physical realities than a cut-off given by the threshold value based on LEFM. If the RFLM curve is linearized between 10^7 and 10^8 cycles the slope parameter m is close to 10. This is in good agreement with the inverse value

of the fatigue strength exponent (-1/*b*) of the elastic part of the Coffin-Manson equation. The equation can be written:

$$\frac{\Delta\sigma}{2} = \sigma_f'(2N_i)^b \tag{7.1}$$

where $\Delta\sigma$ is the weld notch stress range, N_i is the number of reversals to crack initiation, σ_f' is the fatigue strength coefficient and b is the fatigue strength exponent. The equation can be expressed as:

$$N_i = \frac{\left(2\sigma_f'\right)^{-1/b}}{(\Delta\sigma)^{-1/b}} \tag{7.2}$$

The notch stress range $\Delta\sigma$ at the weld toe is directly linear proportional to the nominal stress S under linear elastic conditions. This is assumed to be the case when the number of cycles to failure is longer than 10^7 cycles. To illustrate this graphically, the RFLM curve can be split into two parts as shown in Figure 7.2, more details can be found in Paper D.
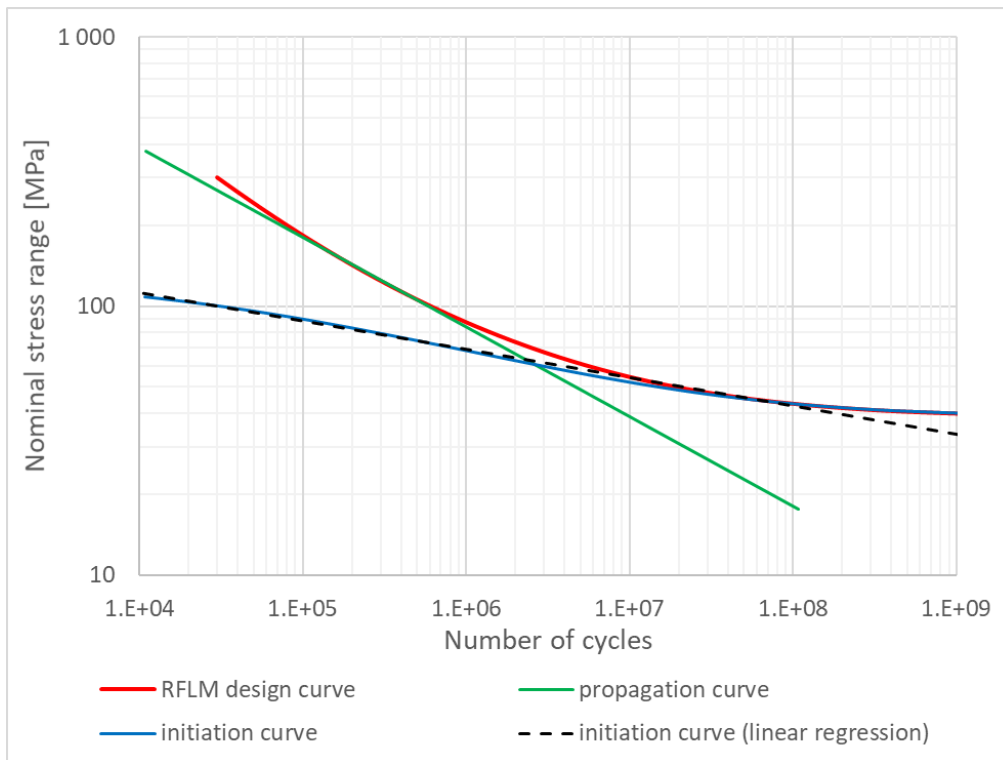
Figure 7.2. Splitting the RFLM design curve into two straight lines for crack initiation and crack growth [2]

The compatibility between the fitted probabilistic models and the underlying fatigue damage mechanisms is summarized in Table 7.1. The low cycle fatigue phenomenon with number of cycles to failure less than 10^4 cycles is not included.

These short lives are not within the scope of the present study. In the medium cycle area with lives between 10^4 and 10^6 cycles both the mechanical models pertaining to the S-N curve and the RFLM curve is given by the Paris propagation law. In the high cycle area where N is between 10^6 and 10^7 cycles the S-N curve is still assuming that the Paris propagation law alone is governing the damage evolution, but now a possible cut-off given by the threshold value for the SIFR is included. In this stress region the RFLM curve is supported by a two-phase model where both the cycles to crack initiation and the cycles spent in crack growth play an important role.

Table 7.1. The reciprocal relation between the probabilistic model and the mechanical models [2]

Fatigue type classification	Damage mechanisms	Segment of conventional S-N curve	Basic physical equation S-N curve	Segment of RFLM resistance curve	Basic physical equation RFLM
medium cycle fatigue, 10^4-10^6 cycles	mainly crack growth	upper straight line	Paris law	upper straight line	Paris law
high cycle fatigue, 10^6-10^7 cycles	crack initiation and crack growth	lower part of straight line	Paris law	transition segment with maximum curvature	Coffin-Manson equation and Paris law
very high cycle fatigue, longer than 10^7 cycles	mainly crack initiation	lower horizontal line from knee point	threshold cut-off in Paris law	lower segment which approaches a straight line	Coffin-Manson equation

The fact that the crack initiation line in Figure 7.2 has a slope parameter m that is close to the linear part of the Coffin-Manson equation ($m = -1/b$) is a necessary condition for assuming that the crack initiation is the dominant damage mechanism at long lives. However, it cannot be considered as sufficient condition.

8. Discussion and conclusions for Constant Amplitude loading

The fatigue damage evolution in welded joints where cracks emanate from the weld toe has been investigated. The investigation was carried out for non-load carrying fillet welded transverse gussets attached to a central load-carrying plate. The collected life data are from welded joints that belongs to the same population. The welded details are designated category 71 in Eurocode 3 Part 1-9, whereas same population is designated as an F class in offshore rules and regulations. The collected data has been presented in section 5.

The damage evolution analysis was based on data sample I by comparing experimental observations with the present engineering fracture mechanics modelling as presented in section 6. The findings do largely answer the first part of the research questions in section 1.3. The following conclusions are drawn:

1) At the given stress range there exists a substantial crack initiation period before crack propagation starts to occur. At 150 MPa this was revealed by captured voltage signals in the ACPD system monitoring the depths during the testing. The ACPD signals did not start to increase before about 20% of the total fatigue life was spent. This was the case for all specimens in both loading modes.

2) If the crack initiation phase is defined by a transition crack depth of 0.1 mm the number of cycles to reach this crack depth is typically 25-30% of the total fatigue life. The crack depths obtained by the ACPD signals were corroborated by ink staining of small crack faces that were measured on the fractured specimens at the end of the test. Based on these measurements the crack depth given by ACPD readings were calibrated.

3) An attempt to model the very early crack growth before a depth of 0.1 mm was reached by a LEFM model failed. The early crack evolution determined experimentally was not possible to simulate by the model.

4) The fatigue crack growth from a crack depth of 0.1 mm up to final failure was successfully modelled by applying a model based on LEFM. The SIFR calculations were based on the parametric formulas suggested by Bowness and Lee. These formulas are also recommended in rules and regulations.

5) The Bowness and Lee formulas are obtained by 3D FEA models of a welded joint with a crack applying the concept of the J-integral to determine the SIF. The results from the formulas were compared and found in good agreement with the results from the more analytically based V-notch approach.

6) When calculating the SIFR entering the fracture mechanics models the weld toe profile shall be characterized by the mean value for the measured toe angle, whereas the toe radius shall be kept at the extreme minimum value close to 0.1 mm. This gives the best fit between the model predicted crack growth and the experimental curves.

7) The Bowness and Lee formulas should be extrapolated and verified for crack depths below $a/t = 0.005$. There is a significant increase in the SIF as a/t decreases below this given limit. However, as a/t gets smaller the application of LEFM becomes dubious as concluded above.

8) The variation in the toe radius has a significant impact on the crack initiation and early crack growth. This variation is not included in any of the formulas established by Bowness and Lee. These formulas are obtained by setting the radius equal to zero.

9) The mean a-N curves from a crack depth of 0.1 mm to failure were modelled by LEFM using the C and m parameters as recommended in rules and regulations. The obtained curves are very close to the experimental mean curves for both the present loading modes. Furthermore, the model design curves based on a growth parameter C defined by the mean value plus two standard deviations are significantly on the safe side of all the experimental curves for both loading modes.

10) For the applied test stress range of 150 MPa the number of crack initiation points along the weld seam is a random variable with an average value between 2 and 3 for the given seam length of 60 mm. A Poisson distribution can be applied to model this discrete variable. As the applied stress range decreases the average number of crack initiation points will decrease.

11) At high stress ranges it is essential to model the effect of crack coalescence of multiple cracks initiating along the weld seam. If crack coalescence is neglected for the tested specimens the fatigue propagation life will be overestimated by close to 30% for the membrane loading mode and up to 100% for the bending loading mode. The significant difference between the loading modes is caused by the different crack shape evolution and associated time to reach crack coalescence for the two loading modes.

12) The mean fatigue growth rate parameter C obtained from the present measured growth rates is close to the suggested values given in rules and regulations if the exponent m is kept fixed at recommended values. If both m and C are treated as free variables the membrane loading mode will still give

60

parameters *m* and *C* close to the recommendations, whereas the exponent *m* will be too high for the bending load mode, typically close to 3.5. This could be explained by the depth measuring uncertainty or inaccuracy in the SIFR calculations for this loading mode. The number of tests is also fewer for the bending loading mode, and this gives a higher statistical uncertainty.

13) The model fitted to the measured growth data did not get significantly better when applying the unique model (Huang et al. [38]) with the concept of an effective SIFR depending on the applied *R* ratio. Introducing a threshold value for the effective SIFR seems to give overly optimistic results for crack retardation of small semi-elliptical cracks. However, these topics must be investigated further.

For the second data sample the focus has been on modelling the total fatigue life. Various elementary life models at a given stress range are studied and the construction of conventional S-N curves are included. Finally, the more advanced resistance curves obtained by the RFLM are fitted to the test data. The results from the various models are compared and discussed. Based on the obtained results the following conclusions can be drawn regarding the probabilistic modelling for prediction of the entire fatigue life:

1) For the fatigue life data collected at a constant stress range of 150 MPa it is demonstrated that the two-parameter log-normal distribution gives the best fit to the test results. The Weibull distribution gives a poorer fit to the life histogram. This finding supports the common life model applied for the S-N curves in current rules and regulations where the underlying linear regression analysis implies a normal distribution for a log-log scale.

2) The acceptance of the log-normal distribution for the fatigue life gives more optimistic safe life predictions than a Weibull distribution does. Furthermore, the log-normal distribution gives a failure rate function that will decay after the mean time to failure (MTTF) has been reached. This is not the case for a Weibull model that gives a steadily increasing failure rate function. The shape of the log-normal failure rate function indicates that when a welded joint has survived many cycles, it has proven its fatigue quality and may continue to be fit for purpose. This is interesting information for aging structures that have passed their fatigue design lives. If the structure has been kept in service by a scheduled program with frequent detailed inspections up to the MTTF, one does not necessarily have to increase the inspection

frequency during a further life prolongation. However, the decrease in the failure rate function should not be used as an argument for omitting in-service scheduled fatigue inspection for such structures.

3) More life data were collected for the actual detail at various stress ranges to establish S-N curves. The conventional linear regression analysis was carried out using the lower prediction bound as basis for defining the design curves at chosen probability of survival. A comparison between the design curves given by the building codes for civil engineering (e.g. Eurocode 3 Part 1-9) and the codes for marine structures (e.g. DNV-RP-C203) was performed. Although somewhat different statistical analysis procedures are applied in these the two codes, no significant differences were found in the obtained design curves. The lower prediction bound defined by a 95% probability of survival is recommended when defining the design curve in Eurocode 3 Part 1-9. If the statistical procedure accounts for the hyperbola shape of the prediction interval, this will give the same design curve as the one obtained when the probability of survival is set to 97.5% with the hyperbola shape neglected. The latter procedure is the basis for DNV recommendations. Both procedures give the same design curve.

4) At lower stress levels the linear regression has the unfortunate limitation that it excludes the long-life failures and the runout results. These data are essentially important in the way that they usually are closer to the magnitudes of the acting stress ranges in-service than the finite life data entering the linear regression analysis. The short-comings of the conventional S-N curves were eliminated by using the Random Fatigue Limit Model.

5) The design curve obtained by the RFLM is non-linear for a log-log scale. The RFLM design curve is defined at a 97.5% probability of survival. The obtained resistance curve is accepted as it is; however, to the left of $3\text{x}10^5$ cycles, the RFLM curve shall be parallel with the conventional linear S-N curve. The chosen point is where the RFLM curve is close to tangential to the conventional linear curve. The RFLM fatigue resistance curve will as a result coincide with the conventional linear S-N curve in the medium cycle fatigue range for stress ranges above 80 MPa. Both curves have a slope parameter $m = 3$. This part of the curve is the area where the gravity centre of the test data is found. At lower stresses where the conventional S-N curve has a knee point, the non-linear RFLM curve has its maximum curvature. This shape gives far better agreement with the long-life data in this area.

Below the conventional S-N knee point the RFLM curve continues to fall with an increasing slope parameter m with a decreasing curvature. The curve becomes almost linear when 10^7 cycles are passed, but the curve does not become horizontal.

6) When comparing with a conventional S-N curve that has a CA fatigue limit at 10^7 cycles, the RFLM curve is very close to tangential to both the upper line segment and the fatigue limit when approaching 10^8 cycles. Consequently, the RFLM curve will almost always give more optimistic CA life predictions compared to predictions based on the conventional curves found for offshore structures.

7) When comparing with a conventional S-N curve that has a CA fatigue limit at 5×10^6 cycles (as the category 71 in Eurocode 3 Part 1-9 for civil engineering), the RFLM curve is still very close to tangential to the upper line segment, but the RFLM curve has a more pessimistic shape compared to the conventional fatigue limit. For a large band of stress ranges the RFLM curve will in fact predict shorter fatigue lives than the conventional curve.

8) The comparison with the conventional curves from the offshore industry and the Eurocode 3 Part 1-9 indicates that a fatigue limit drawn at 10^7 cycles is a better choice than drawing it at 5×10^6 cycles for a category 71 detail. However, the RFLM resistance curve does in fact reject the existence of a fatigue limit. This rejection agrees well with the latest proposal for CA S-N curves from IIW where the CAFL has been removed based on a re-analysis of life data. However, the IIW curve predicts significantly shorter fatigue lives than the RFLM just above and just below the knee-point given by the new IIW curve. There is still a lack of data in this very high cycle regime to support a conclusion on this matter.

9) It has been demonstrated that the shape of the obtained RFLM resistance curve agrees well with a two-phase model for the involved damage mechanisms. An initiation model based on the Coffin-Manson equation and a crack growth model based on the Paris propagation law have been proposed. These models will support the RFLM resistance curve to handle changes in important variables such as the applied stress ratio and the magnitude of the residual stresses.

10) Future work will be focusing on how to handle VA loading with the present RFLM resistance curves. The split into two separate curves and the conclusion drawn in clause 9) above will play an important role in this work.

The support from the underlying physical equations is expected to increase the accuracy of the calculated damage accumulation. This will be the hypothesis for the future work, and some additional thoughts are given in the next section.

9. Suggestion for future work with focus on Variable Amplitude loading

9.1. Basic accumulation models

All the S-N curves and RFLM resistance curves presented in the present work are based on CA test data. To make fatigue life predictions for welded joints that are subjected to variable amplitude (VA) loading the most common approach is to rely on the Miner damage summation rule:

$$D = \sum_{i=1}^{i=k} \left(\frac{n_i}{N_i} \right) \tag{9.1}$$

where n_i is the acting number of cycles with stress range $\Delta\sigma_i$ in the acting stress spectrum and N_i is the number of cycles to failure for a given stress range $\Delta\sigma_i$. The fatigue life is exhausted when the damage summation reaches 1.0. A typical stress spectrum is shown in Figure 9.1. Although it may be an illusion that this simple rule in equation (9.1) may lead to an accurate fatigue life prediction, the approach has survived in almost all rules and regulations for practical engineering fatigue life predictions.

When applying the Miner rule for VA loading the stress ranges below the CA fatigue limit cannot be ignored. These stress cycles under VA loading will give contributions to the damage accumulation. Physically this means that small stress ranges below the CA fatigue limit will do harm if larger stress ranges have already initiated cracks at the weld toe. As the initiated cracks grow, more of the lower stress cycles will become harmful. Consequently, the conventional S-N curve obtained for CA loading must be modified. Haibach [54] suggested an S-N curve with a 2nd slope parameter m_2 beginning at the CA fatigue limit. The proposal gives $m_2 = 2m_1 - 1 = 5$. The knee-point with the transition between the two slopes was originally defined by Haibach at $5\mathrm{x}10^6$ cycles. The second slope was obtained from a fracture mechanics model that involves the threshold value for SIFR for a technical large initial crack assuming that LEFM was applicable. This is not in agreement with the present model where long lives primarily are explained by a long crack initiation phase. Gurney [55,56] suggested a more pessimistic model where the upper slope of $m_1 = 3$ was kept at all stress levels before a life of $2\mathrm{x}10^7$ cycles was reached. Nevertheless, the Haibach approach has been kept in most

rules and regulations up until present, but the knee point has been extended to 10^7 cycles in most recommendations.

However, it has been recognized that the second slope parameter will depend on the distribution of the acting stress spectrum if a reliable Miner sum shall be obtained. The stress spectra are often characterized by a stress range exceedance diagram defined by an underlying Weibull distribution, see Figure 9.1. The Weibull distribution is given by the scale factor q and the shape factor h. If the exceedance diagram is linear (shape factor $h = 1.0$) the Haibach formula seems to give good failure predictions by the Miner's summation rule. For an exceedance diagram with a concave shape upwards (shape factor $h < 1.0$) the Haibach formula gave overly pessimistic predictions whereas the opposite was true for an exceedance diagram with a convex shape upwards (shape factor $h > 1.0$). These two distributions are shown in Figure 9.1 by the blue (concave upwards) and the red (convex upwards) curves. In a recent work by Baptista et al. [7] the second slope parameter m_2 was sought such that the Miner sum was as close as possible to 1.0 at final fracture under VA loading tests. If the stress spectrum is fitted by a Weibull distribution it was shown that the 2nd slope parameter m_2 will depend on the shape parameter of the Weibull distribution:

$$m_2 = m_1 + \frac{2}{h} \tag{9.2}$$

where h is the shape parameter in the Weibull model. The relation was found for welded details in a bridge structure. It is important to be aware that equation (9.2) is assuming that the expected maximum stress range is kept constant. Baptista et al. also supported their work by a full Monte Carlo simulation of the damage process including initiation life and threshold phenomenon for the crack growth. If we adopt the relation in equation (9.2) for welded details in an offshore structure, we will often have a shape factor h close to 1.0 for a long-term wave induced stress spectrum over several years. Hence, the second slope parameter m_2 shall be set to 5 according to the above formula. This is consistent with the Haibach recommendation, but the number of cycles is usually set to 10^7 for the slope change, which is somewhat longer than Haibach recommended. For a short-term stress spectrum over typically 6 hours in a steady state sea condition the shape factor will be close to $h = 2$ (i.e. a Rayleigh distribution). This gives $m_2 = 4$. If the Haibach equation with $m_2 = 5$ is kept this will give overly optimistic prediction for this important case.
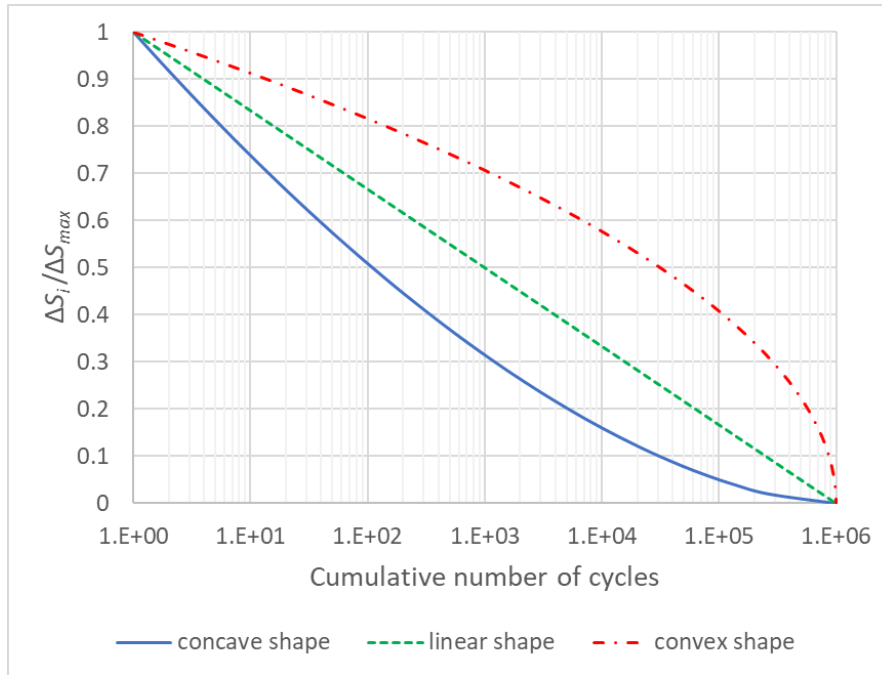
Figure 9.1. Normalised stress range exceedance diagram – spectrum types by shape

When the welded details are subjected to VA loading two phenomena are important. Firstly, stress ranges that were regarded as below the CAFL may now be harmful if they are acting after higher stress levels in the spectrum. The longer time the spectrum is repeated the more harmful will lower stress ranges become. Secondly, there is an interaction between the various stress blocks such that high stress ranges may leave a small plastic zone ahead of the crack front. LEFM must be modified to handle this phenomenon.

9.2. Characterizing the stress spectrum

The equation for the probability of exceedance is according to the Weibull distribution given by:

$$P(\Delta \boldsymbol{S} > \Delta S) = \exp\left(-\left(\frac{\Delta S}{q}\right)^h\right) \qquad (9.3)$$

This equation gives a typical stress spectrum as shown in Figure 9.2. The Weibull distribution is fitted to stress range histogram that is obtained by Rainflow counting technique for a given time series. The stress time history with variable amplitude stresses can then be ordered into groups with the same stress range ΔS_i and with an associated number of occurrences $n_{i.}$ The results can be given by histogram columns as shown to the left on the Figure 9.2 or by an exceedance diagram as

67

shown to the right. Each stress group is usually called a stress block. Each stress block is defined by:

- relative stress range in a spectrum, $p_i = \Delta S_i / \Delta S_{max}$
- stress ratio, $R_i = S_{i,min} / S_{i,max}$
- the maximum (peak) stress range in a spectrum, ΔS_{max}
- the minimum fully damaging stress range, $\Delta S_{0,min}$
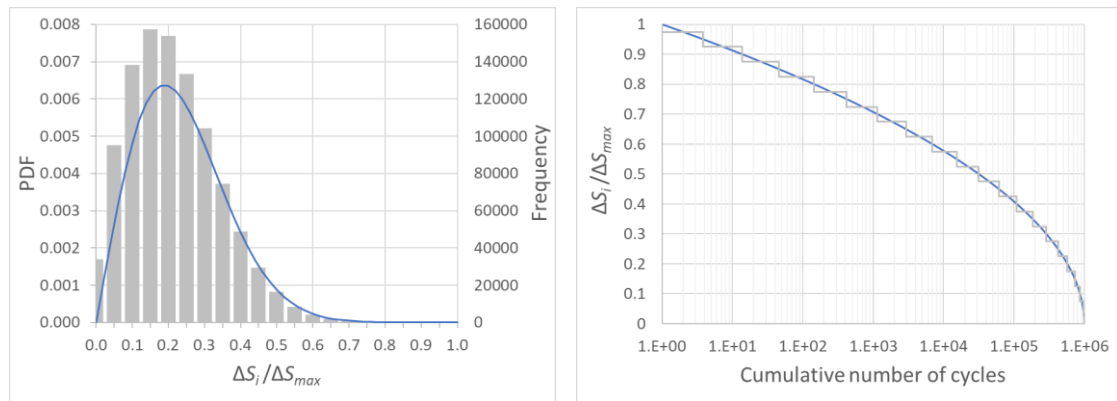
Figure 9.2. Presentation of stress spectrum

9.3. Mean RFLM resistance curve under VA loading

The RFLM resistance curves determined in earlier sections are obtained from tests carried out under CA loading. For VA loading one may pursue the approach used for the conventional S-N curves that we have discussed above. For the S-N curve, a slope parameter $m = 5$ is introduced for the horizontal line pertaining to the CAFL stress range. Hence, smaller stress ranges will become damaging under VA loading as discussed. This approach may also be used for the RFLM curve, see Figure 9.3. An alternative approach is to split the non-linear curve into two separate linear curves. This is visualized in Figure 9.4. The first line (in green) is defined by a crack growth mechanism only. The corresponding curve is obtained by extrapolating the upper linear curve with slope parameter m down to a low stress range level of 1 MPa. When subtracting this crack growth life curve from the total RFLM curve given in Figure 9.4 the other phase of the damage mechanism is obtained. The result is shown by the red curve in Figure 9.4. A conspicuous finding is that this curve obtained by subtracting the crack growth line from the non-linear RFLM curve is also very close to being a straight line for a log-log scale.
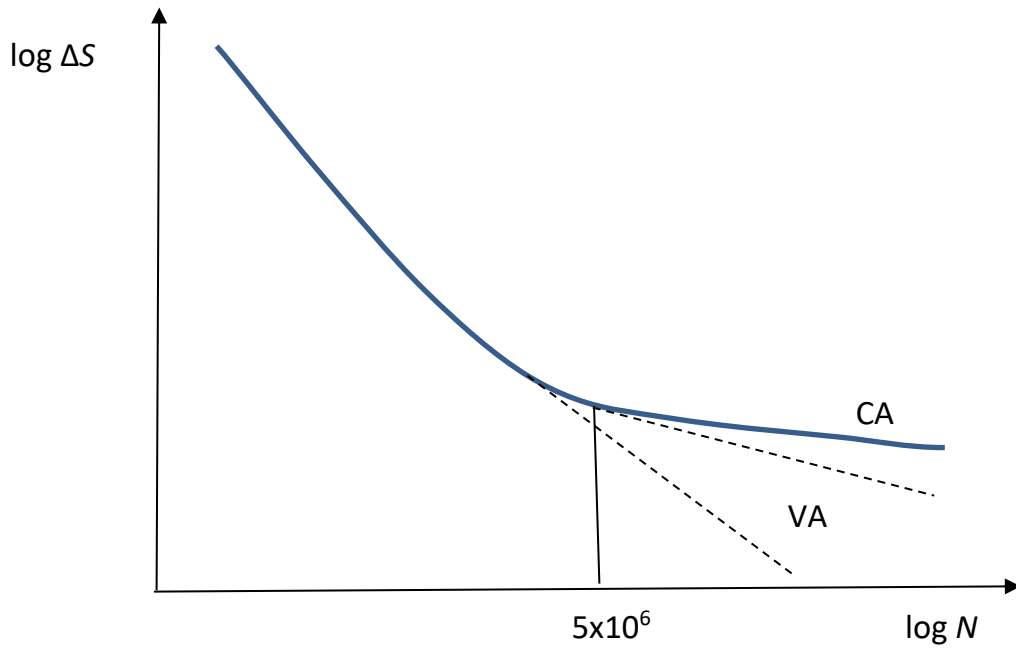
Figure 9.3. Illustration of possible RFLM mean curve for the option 1 model
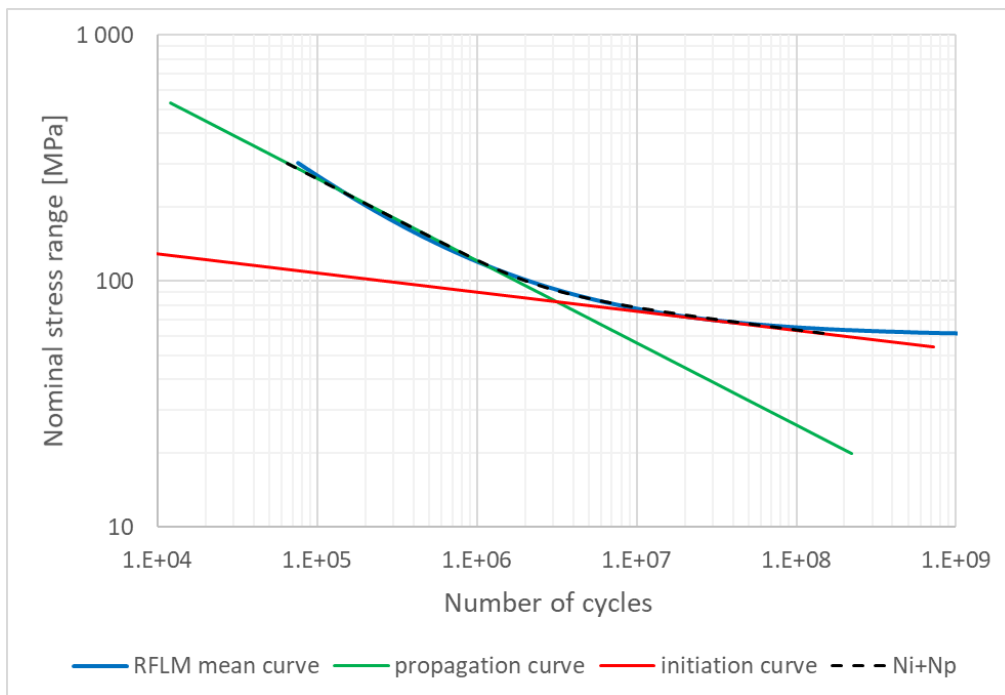
Figure 9.4. Splitting the RFLM mean curve into two straight lines for crack
initiation and crack growth

As underscored earlier the proposed RFLM curve is valid for CA data obtained by
laboratory testing. In the case of an in-service stress spectrum with VA loading the
curve must be modified if used in conjunction with the Miner summation rule.
Based on the discussion given above, there are two alternative ways of doing this
modification:

Option 1 – the RFLM CA curve is modified in the lower region such that the slope is changed depending on the characteristics of the applied stress spectrum. The slope is changed such that the accuracy of the Miner sum criterion for fracture is improved.

Option 2 – the original RFLM CA curve is kept but the curve is split into one curve for crack initiation and one curve for crack growth. The Miner summation rule is applied for each of the curves separately.

Option 1 is not very different from the technique suggested by Baptista et al. [7]. The RFLM curve is identical to the CA curve in Figure 7.1 for lives up to 5×10^6 cycles. At this point the tangential slope parameter of the RFLM curve is very close to 5. The curve can then be linearized and the slope parameter of 5 is kept for all lower stress ranges, see Figure 9.3. This constant slope may subsequently be changed to optimize the accuracy of the Miner summation. There are two ways of doing this optimization; the first one is to keep the linearization point fixed at 5×10^6 cycles such that it is only the slope parameter m_2 that changes. The second way is to change both the position of the tangential point and the slope parameter. The latter alternative gives more freedom during the optimization of the Miner sum accuracy. The rationale for this approach is that various rules and recommendations have not yet reached a consensus on which point on the curve to introduce the fatigue limit. Variations between the points defined by 5×10^6 and 2×10^7 are found in the literature [57]. The proposed methodology is visualized by the sketch in Figure 9.3.

Option 2 where the RFLM curve is split into two linear curves is illustrated in Figure 9.4. After the split the life prediction is based on the double linear summation rule, one summation for each curve. This approach in its original form was first proposed by Manson [57], but it was not coupled to the two phases obtained by linearization of the RFLM. In the present case, the design curve in Figure 7.1 is split into one curve for the initiation phase and another curve for the crack growth phase. The growth phase curve is defined by using the existing straight line above the parallel point at $N=3\times10^5$ cycles. This line is prolonged all the way down to a stress range of 1 MPa. The slope parameter m of this curve coincides with the exponent m in the Paris propagation law, i.e. $m = 3$. The curve for the initiation life is subsequently found by subtracting the lives predicted by the growth curve from the RFLM resistance curve for the total life given in Figure 7.1. As can be seen from Figure 9.4 the initiation curve that is found by the subtraction is also almost linear. It seems convincing that when we carry out a

subtraction of the cycles given by the LEFM crack growth curve from the total number of cycles given by RFLM resistance curve the result is very close to a straight line for a log-log scale. The crack growth curve has its physical explanation by an LEFM model, whereas the second curve has its physical explanation in the Coffin-Manson equation, see discussion in section 4.1. The linearized slope for the initiation curve between 10^7 and 10^8 cycles is close to 11 which also strengthens the possible coupling to the Coffin-Manson equation. This value is close to $-1/b$ where b is the strength exponent in the linear part of the Coffin-Manson equation. This analogy is illustrated by comparing the red line in Figure 4.2 and the red line in Figure 9.4. The curve in Figure 4.2 is obtained by physics, whereas the curve in Figure 9.4 is obtained by stochastic analysis. A more refined model for this initiation phase curve can be based on models that account for the multiaxial stress situation at the weld toe. The Coffin-Manson equation may then be replaced by the Dang Van initiation criterion. This was not pursued in the present work.

The Miner's summation rule is applied for each of the two S-N curves in Figure 9.4 separately in the time domain. When the summation based on the initiation curve has reached 1.0 the crack initiation has been completed. The fatigue lives N will subsequently be taken from the crack growth curve and a new summation starts. The fracture criterion is defined when this latter summation also accumulates to 1.0. The proposed model will avoid that the Miner's rule is used for an S-N curve that involves several damage mechanisms. This enhancement is expected to give less uncertainty in the damage summation failure criterion. It is important to bear in mind that option 1 shown in Figure 9.3 is an empirical numerical manipulation only. Option 2 illustrated in Figure 9.4 has shown to have a more theoretical foundation. It is based on an understanding of the physics of the involved damage mechanisms. It will lead to a Miner sum prediction that is depending on the magnitude and the sequence of the applied stress ranges, not only the shape of the exceedance diagram. This is not the case for option 1. For this reason, it seems that the option 2 is more favourable. However, the final judgement will be carried out when the model's ability to predict fatigue failure for welded joints through double linear summation is proven. This is a goal for future research work.

It should be emphasized that none of the two options proposed above are based on the assumptions that most of the fatigue life at low stress ranges is dominated by a slow crack growth phase. Hence, the use of LEFM to determine the second slope

parameter is avoided. It is the author's opinion that the crack growth threshold is doubtful for small micro semi-elliptical surface cracks emanating from the weld toe [20]. Furthermore, the author has a strong belief that the fatigue damage mechanism in the second slope area of the S-N curve is better explained by the Coffin-Manson equation than by the threshold value in the Paris propagation law. The gradually change in the slope of the fatigue resistance curve obtained by RFLM supports this belief.

9.4. Enhancements of the damage accumulation model – overview of the methodology

9.4.1. Background for the proposed methodology

Based on the discussion in the foregoing sections we are ready to sum-up our planned methodology for life prediction under VA loading. The basis for the methodology is the RFLM resistance curves for crack initiation and crack propagation supported by the underlying physical equations for these two phases. A road map with the necessary and optional steps involved in the life prediction is shown in Figure 9.5. The upper part of the figure illustrates the common rule-based fatigue life predictions. The upper left square is the common engineering procedure, which may be supplemented by a correction for the applied stress ratio and residual stresses as shown in the upper right square in Figure 9.5. The life prediction to the left is usually valid for a rather high R ratio designated R_0, and reasonable corrections are sometimes possible to carry out. The following equation for the stress correction factor is proposed by Zhang and Moan [58]:

$$f_{mean} = \begin{cases} (1-R)^{-B} & \text{for } -5 \leq R < 0.5 \\ (1.05 - 1.4R + 0.6R^2)^{-B} & \text{for } 0.5 \leq R < 1 \\ 6^{-B} & \text{for } R > 1 \text{ or } R < -5 \end{cases} \qquad (9.4)$$

where:

$$\begin{array}{ll} B = 0.4 & \text{for } -5 \leq R_{ef} < 0 \\ B = 0.25 & \text{for } 0 \leq R_{ef} < 1 \end{array} \qquad (9.5)$$

The ratio R_{ef} includes the applied R ratio and the residual stresses. The corrections are made under the assumptions that the S-N curves given in recommendations and codes are valid for $R_{ef} = 0$. This is a simplification when considering all the various load conditions that have been applied for the life data collected to

establish an S-N curve for a given category. In some codes and recommendations, it is also possible to account for the shape of the stress spectrum by adjusting the lower slope of the S-N curve, an example is given by equation (9.2). Although these corrections may improve the accuracy of the conventional S-N life predictions, the two types of correction are usually not carried out by the practicing engineer. The shortcoming of the common practise described above is that the mean stress correction is carried out as if the entire fatigue process is consisting solely of fatigue crack growth. The crack initiation is neglected.

9.4.2. Enhanced procedures for mean stress corrections

In the lower left part of the Figure 9.5 the conventional S-N curve is replaced by the two linear resistance curves for crack initiation and subsequent crack growth obtained from the RFLM. The first life estimates are then carried out directly by using two linear curves separately. The number of cycles to crack initiation and subsequent crack growth is determined by the Palmgren-Miner (P-M) summation rule.

$$D_I = \sum_{i=1}^{k} \frac{n_i}{N_{I,i}} = 1.0 \tag{9.6}$$

$$D_P = \sum_{i=k+1}^{\infty} \frac{n_i}{N_{P,i}} = 1.0 \tag{9.7}$$

The fact that the summation is carried out in two steps in the time domain such that each step is a well-defined damage mechanism is expected to give increased accuracy for the damage summation and life prediction. In both cases the fatigue lives may also be related to the corresponding equivalent stress given by:

$$\Delta\sigma_{eqi0} = \left[\frac{\Delta\sigma_i^m \cdot n_i}{n}\right]^{\frac{1}{m}} \tag{9.8}$$

where the slope parameter m is equal to the initiation slope parameter and the crack growth slope parameter respectively. If the actual R ratio and residual stresses are substantially different from R_0 and σ_{r0} a correction can be done for each damage phase separately as shown down to the right in the bottom of Figure 9.5. These two types of correction are elaborated in the two next sub-sections.

Conventional S-N curve for given R_0 ratio Knee-point at 10^7 cycles Upper slope $m=3$, lower slope $m=5$ Palmgren-Miner summation	Correction of stress range due to the actual applied R ratio and the residual stresses The lower slope of the S-N curve can be adjusted based on the characteristics of the applied stress spectrum

RFLM resistance curve for a given R_0 ratio
The total curve is separated into a
   • crack initiation curve
   • crack growth curve
Linear damage P-M summation for each line with its distinct damage mechanism
	Correction of the initiation life based on the Coffin-Manson equation due to the actual applied R ratio and residual stresses
	Correction of crack growth life based on the Huang-Moan crack growth model due to the actual applied R ratio and residual stresses

Figure 9.5. Methodology for the rule-based and the enhanced life predictions under VA loading

9.4.3. Enhancement of the life prediction for the crack initiation phase

The crack initiation life can be estimated using first term in the Coffin Manson equation (Basquin equation) with the Morrow correction:

$$N_i = \frac{1}{2} \frac{\left(2(\sigma_f' - \sigma_m)\right)^{-1/b}}{(\Delta\sigma)^{-1/b}} \tag{9.9}$$

where σ_m is the local mean stress at the weld toe notch. Then, expressing the notch mean stress σ_m and the notch stress range $\Delta\sigma$ by nominal stress range S, the stress concentration factor SCF and the stress ratio R, equation (9.9) can be re-arranged as:

$$N_i = \frac{1}{2} \frac{\left(2\left(\sigma_f' - \frac{1}{2}SCF \cdot S \cdot \frac{1+R}{1-R} - \sigma_r\right)\right)^{-1/b}}{(SCF \cdot S)^{-1/b}} \tag{9.10}$$

where σ_r is the residual stress at the weld toe notch. The curve is usually established for base material with given mechanical properties. It can be difficult to determine the parameters physically for the HAZ in vicinity of the weld toe where material

properties may vary. Hence, the initiation curve obtained directly by the RFLM model is an achievement. The fraction 1/b is determined by the slope parameter m_i, and a reasonable value must be chosen for the SCF. Finally, the σ'_f is determined such that the curve coincides with the RFLM based initiation curve. The first life estimates can be found from the curve defined at stress ratio R_0 and residual stress level σ_{ro}. This first estimate is then simulated by using equation (9.10) with the same stress ratio and residual stress level for all the stress bins in the spectrum. A life estimate N_{i0} is obtained by adopting the P-M summation rule. The same calculation is subsequently repeated but this time with the actual R ratio and residual stresses for each stress bin. A new life estimate N_{ia} is obtained. The difference in the life estimates N_{i0} and N_{ia} gives an estimate for the correction factor for the acting equivalent stress range that is to be applied in conjunction with the resistance line for the crack initiation:

$$f_{ic} = \left(\frac{N_{i0}}{N_{ia}}\right)^{\frac{1}{m_i}} \tag{9.11}$$

$$\Delta\sigma_{eqic} = f_{ic} \cdot \Delta\sigma_{eqi0} \tag{9.12}$$

This will give an improved initiation life prediction for the actual stress spectrum. The correction can also be applied directly on the life obtained using the original crack initiation curve with the following factor:

$$f_{icN} = \frac{N_{ia}}{N_{i0}} \tag{9.13}$$

The original life prediction obtained by the RFLM crack initiation curve shall be multiplied with this factor to get a more accurate life estimate.

It should be noticed that it is chosen to work with the relative impact on fatigue initiation life due to changes in applied stress ratios and residual stresses. The original RFLM resistance line is then parallelly displaced according to this relative change given in equation (9.13). This choice is made because all the parameters entering the physical equations may not be completely correct. However, the requirement to the equation is that the parameters are accurate enough to capture the correct influence in the local applied effective mean stress.

9.4.4. Enhancement of the life prediction for the crack growth phase

For the crack growth phase the same line of thought is followed, using equations proposed by Huang et al. [38]:

$$\frac{da}{dN} = C(\Delta K_E^m - \Delta K_{th0}^m) \tag{9.14}$$

$$\Delta K_E = M\Delta K \tag{9.15}$$

$$\Delta K_{th0} = M\Delta K_{th} \tag{9.16}$$

$$M = \begin{cases} (1-R)^{-\beta_1} & -5 \leq R < 0 \\ (1-R)^{-\beta} & 0 \leq R < 0.5 \\ (1.05 - 1.4R + 0.6R^2)^{-\beta} & 0.5 \leq R < 1 \end{cases} \tag{9.17}$$

$$R = \frac{K_{min} + K_R}{K_{max} + K_R} \tag{9.18}$$

The crack growth law is integrated in increments:

$$a = a_0 + \sum_{i=1}^{K}\sum_{j=1}^{k} \Delta a_{ij} \tag{9.19}$$

where k is the number of bins in the stress spectrum and K is the number of repetitions of the entire stress spectrum until failure occurs at a predefined crack depth usually close to the plate thickness. The increments in equation (9.19) are found by integration:

$$\Delta a_{ij} = \int_{a_{ij-1}}^{a_{ij}} C(\Delta K_E^m - \Delta K_{th0}^m)dN \tag{9.20}$$

The growth exponent m is equal to the slope parameter of the RFLM growth curve whereas the parameter C is chosen at the mean value found in rules and regulations for the chosen exponent. The initial crack depth a_0 is determined such that the obtained life coincides with the life estimate obtained directly from the RFLM crack growth curve for R_0 and σ_{r0}. The initial crack depth will typically be smaller than 0.1 mm. The calculations are first carried out for the stress spectrum as if $R=R_0$ and $\sigma_r = \sigma_{r0}$ for all stress bins. This gives a life estimate N_{p0} based on fracture mechanics. The same calculations are then repeated for the actual R ratios and residual stress pertaining to each bin. This gives a new life estimate N_{pa}. The difference in the life estimates N_{p0} and N_{pa} gives an estimate for the correction of the acting equivalent stress range that is to be applied in conjunction with the S-N curve:

$$f_{pc} = \left(\frac{N_{p0}}{N_{pa}}\right)^{\frac{1}{m_p}} \qquad (9.21)$$

Such that the life prediction of the original crack growth curve shall use the equivalent stress range:

$$\Delta\sigma_{eqpc} = f_{pc} \cdot \Delta\sigma_{eqp0} \qquad (9.22)$$

The threshold value for the SIFR is neglected in both the fracture mechanics calculations.

The correction can also be applied directly on the life obtained using the original crack growth curve with the following factor:

$$f_{pcN} = \frac{N_{pa}}{N_{p0}} \qquad (9.23)$$

The original life prediction given by the RFLM crack growth curve shall be multiplied with this factor. The correction will improve the accuracy of the estimate because the impact of the sequence effect of the stress blocks and the effective applied R ratio defined by the SIFR is captured.

The above presented methodology will be validated against fatigue life data for VA loading found in the literature. Some preliminary simulations have been performed and the results are promising. An example is presented in the next section. This will be pursued in the future research.

9.5. Application of the enhanced life prediction methodology

9.5.1. The motivation for revisiting these test results

To demonstrate the application of the basic RFLM described in section 9.3 and validate the enhancements proposed in section 9.4 we shall pursue test data for fatigue lives. Zhang and Maddox [59] investigated the fatigue damage accumulation for a longitudinal attachment on a plate surface under VA loading with different applied stress spectra. There were significant variations in the mean stress level in the applied stress spectra. The conventional S-N approach was not capable of capturing the strong influence of the effective R ratios. For that reason, Zhang and Maddox supplemented the S-N predictions using the Paris propagation law such that the sequence effect of the stress blocks could be accounted for. However, the applied crack growth model did not have the ability to account for various effective R ratios in the stress blocks acting on the specimens.

Consequently, many of the interesting test results remained to some degree unexplained.

9.5.2. Test specimen geometry, steel quality and fatigue category

The test specimen geometry is shown in Figure 9.6. As can be seen, the specimen is quite close to the specimens in test series carried out in the present work, see section 5.2. This is a quite widespread welded detail, and the fatigue category is dependent on the length of the attachment. The present test specimen has an attachment length of 150 mm that gives an F1 classification in ref. [4]. The specimens were made in Mn-Si high strength steel with a yield stress of 418 MPa and tensile strength of 554 MPa. The fatigue cracks emanate from the weld toes at the two ends of the attachment. When these specimens are not stress relieved there will aways be significant tensile residual stresses in the direction of the attachment length at these weld toes. A residual stress level between 0.5 and 1.0 of the yield stress is common.
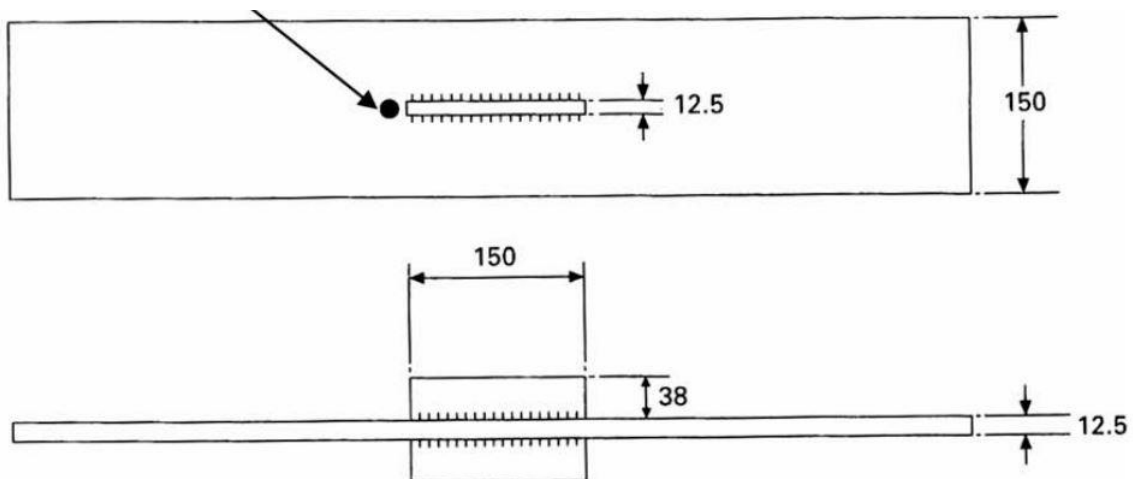
Figure 9.6. Test specimen geometry and location of residual stress measurements [59]

9.5.3. CA fatigue tests and selected S-N curve

Before investigating the VA loading, Zhang and Maddox carried out CA tests with a very high maximum stress. The specimens were not stress relieved. The CA stress ranges varied between 65 MPa and 240 MPa whereas the maximum stress was kept constant at 280 MPa. This gave an average applied stress ratio R close to 0.5. When accounting for the residual stresses that were close to 280 MPa the

average effective R ratio will be as high as 0.8. The fitted median S-N curve based on these tests was given as:

$$\log N = 12.120 - 3.072 \cdot \log S \qquad (9.24)$$

The recommended mean curve for F1 class reads:

$$\log N = 12.099 - 3 \cdot \log S \qquad (9.25)$$

The two curves are depictured in Figure 9.7. As can be seen the two lines are quite close, the F1 curve predicts typically 25-30% longer lives than the curve obtained from the test series carried out by Zhang and Maddox. This difference is assumed mainly to be owed to the fact that the Zhang Maddox curve was obtained by test specimens subjected to an extreme high effective R ratio. The high residual stresses are the main contribution to this high ratio, such that when specimens subjected to an applied stress ratio of R=0.1 no significant difference in tested lives were found. This can in fact be demonstrated by the crack growth model given by equations (9.14) – (9.18). If this model is used with a residual tensile stress higher than 0.8 of the yield stress the number or cycles to failure becomes in practice insensitive to the applied R ratio. Based on the fracture mechanics calculations it can be estimated that the effective R ratio of the F1 category is closed to 0.65. This difference in R ratio can then explain the gap between the two curves in Figure 9.7. An effective R ratio 0.65 is regarded as very high, but it can be explained by the high residual tensile stresses in this specimen geometry when they are not stress relived. For other fatigue categories with significantly different geometry this may not be the case, the residual stresses may even be partly compressive.
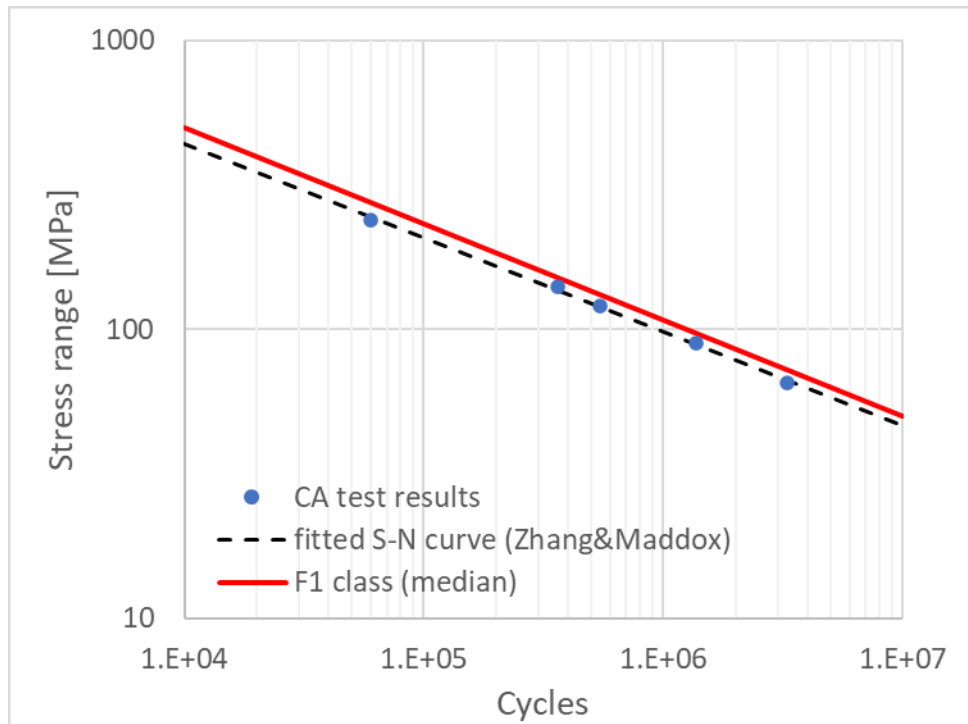
Figure 9.7. S-N curves for the detail

9.5.4. The applied stress spectra

Three stress spectra applied during the testing have multiple number of the following stress sequences:

- Sequence A – the stresses are cycling down from a constant high tensile stress of 280 MPa such that the mean stress increases with decreasing stress range,
- Sequence B – stresses are cycling about a constant mean stress of 175 MPa,
- Sequence C – the stresses are cycling up from a constant minimum stress of 70 MPa such that the mean stress increases with increasing stress range.

Each of the sequences consist of stress blocks with stress ranges as given in Table 9.1. The three stress sequences described above will have, as a result, different applied R ratio for the same applied stress range as shown in Figure 9.8. Due to the shakedown effect the residual stress level was reduced from about 380 MPa to typically 75 MPa at the weld toe after a few stress blocks for all sequences. It is noted that the stress block no. 9, 10, 11 and 12 in Table 9.1 consist of stress ranges that are below the stress ranges used in the CA tests. Not all the sequences included the lowest stress ranges in Table 9.1. The overview of the spectra used for individual specimens is presented in Table 9.2. The tested lives show large systematic variations for the stress spectra that were based on repetition of the three

sequences A, B and C. Sequence A gave the shortest fatigue lives, the sequence B gave the medium lives, whereas Sequence C gave the longest lives. The test lives pertaining to sequence B were closest to the predictions made by the S-N curve obtained by Zhang and Maddox when applying the Miner summation rule. No corrections were carried out for the applied R ratio and residual stresses. The equation (9.1) has been applied by the authors directly and denominators in the sum components have been calculated using equation (9.24) for predicting fatigue life for all stress blocks. The main worry from a design point of view is that stress spectrum A gives significantly shorter fatigue lives than predicted by the S-N approach. The fatigue fracture for 4 specimens occurred at P-M sums that were between 0.4 and 0.6. Due to the little variations in the P-M sums at fracture this discrepancy cannot be explained by the uncontrolled random variables representing uncertainties listed in Table 1.1. P-M summation according to the given S-N curve will systematically overestimate the fatigue life for the stress spectrum where this stress sequence is repeated. The problem in the present case is the biased mean value, not the inherent scatter in the P-M summation. The scatter is within what can be expected in a measure for the inherent scatter in fatigue life under CA loading under controlled laboratory conditions. Hence, it seems obvious that a model error in P-M summation rule is not the root cause of the problem. The problem is that the given S-N curve is not representative for the stress spectrum based on sequence A. Hence, Zhang and Maddox had a challenge when trying to establish an S-N curve that captures the influence of a high R ratio in combination with an applied high maximum stress. The main conclusion by Zhang and Maddox was that the conventional S-N life predictions do not have the ability to do so, but the influence of the mean stress was not investigated when drawing this conclusion. Hence, the reported life results are chosen to be investigated by the present RFLM approach to verify if any progress can be made when accounting for the effective R ratio.

Table 9.1. Stress ranges and cycles in applied stress blocks

Stress block no.	Stress range [MPa]	Relative stress range	Cycles	Exceedance
1	210	1	1	1
2	189	0.9	3	4
3	168	0.8	6	10
4	147	0.7	12	22
5	126	0.6	23	45
6	105	0.5	48	93
7	84	0.4	109	202
8	63	0.3	296	498
9	52.5	0.25	544	1042
10	42	0.2	1125	2167
11	31.5	0.15	2815	4982
12	21	0.1	9500	14482
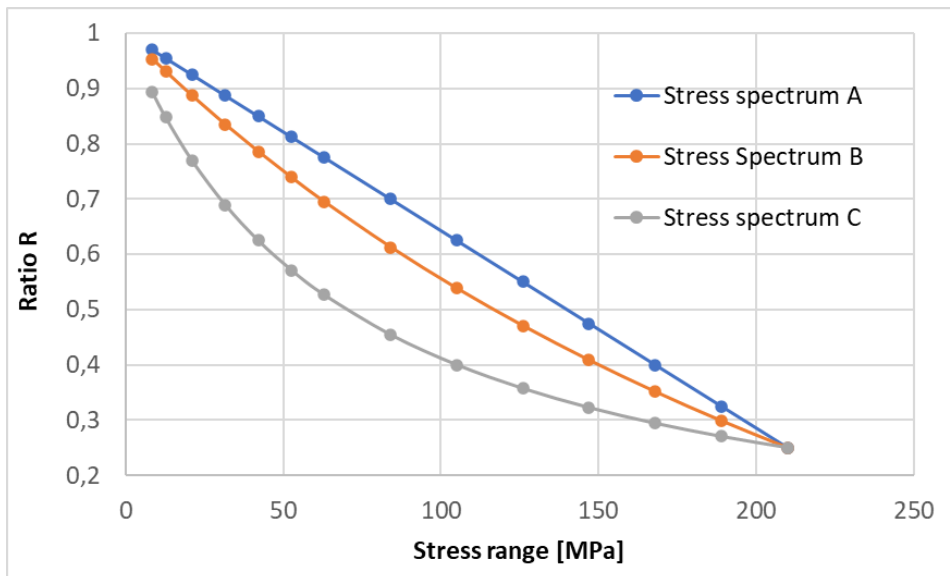
Figure 9.8. Variation of nominal R ratio for increasing stress ranges

Table 9.2. Overview of the tested specimen

Specimen	Spectrum	
	Sequence	Minimum relative stress range
F-03	A	0.25
F-15	A	
F-09	C	
F-10	B	
F-04	A	0.2
F-13	A^e *	
F-06	C	
F-07	B	
F-05	A	0.15
F-08	A	0.1

* stress ranges in spectrum A^e are cycled down from a constant maximum stress 147 MPa

9.5.5. Life predictions by the basic RFLM model

To carry out prediction by the RFLM the two resistance curves in the model must be known. However, due to limited number of CA test data for the welded detail in question some approximations are proposed. Based on experience from the F class detail, the median crack growth line of the RFLM is adopting the S-N curve obtained from the present test series given by equation (9.24). The RFLM initiation line is scaled from the F class initiation line according to the following formula:

$$\log a_{ina} = \log a_{ino} - m_{in} \cdot \log \frac{K_{ga}}{K_{go}} \qquad (9.26)$$

where K_{go} is the geometrical SCF for the original detail (F class), and K_{ga} is the geometrical SCF for the actual detail. Approximation for the geometrical SCF can be found in DNV-RP-C203 [4].

The initiation curve for the F class detail (see Figure 9.4) can be expressed by the following equation:

$$\log N_{inF} = 31.07 - 12.82 \cdot \log S \qquad (9.27)$$

The increase in SCF from F class to F1 class is 1.13. Using this number, an estimate for the actual initiation curve is obtained. Finally, the following equations for crack initiation and crack growth curves are obtained for the actual detail:

$$\log N_{ina} = 30.41 - 12.82 \cdot \log S \qquad (9.28)$$

$$\log N_{cga} = 12.120 - 3.072 \cdot \log S \qquad (9.29)$$

Following the procedure outlined in section 9.3 the analysis started by the P-M summation for the RFLM initiation curve. The highest stress ranges in Table 9.1 gave almost immediately a sum of 1.0. This means that the initiation phase can be neglected for these stress spectra. This would even be true if we had used the original F class initiation curve. Hence, the governing damage mechanism is crack growth only for these stress spectra. This is important information.

The next step in the analysis was to carry out the P-M summation for the crack growth curve. This resulted in the same predictions as obtained by Zhang and Maddox when one single straight S-N curve with slope parameter m=3.072 was chosen. Hence, no progress is made by using the basic RFLM when it comes to improving the life predictions for these stress spectra. But it is learned that the crack initiation phase can be neglected for the present case such that a one slope curve is the best choice for the conventional S-N curve. The predicted life versus tested life is plotted in Figure 9.9 and results for individual specimens are presented

in Table 9.3. On this background the test data give a good opportunity to investigate enhancement of the predictions based on the crack growth model only.
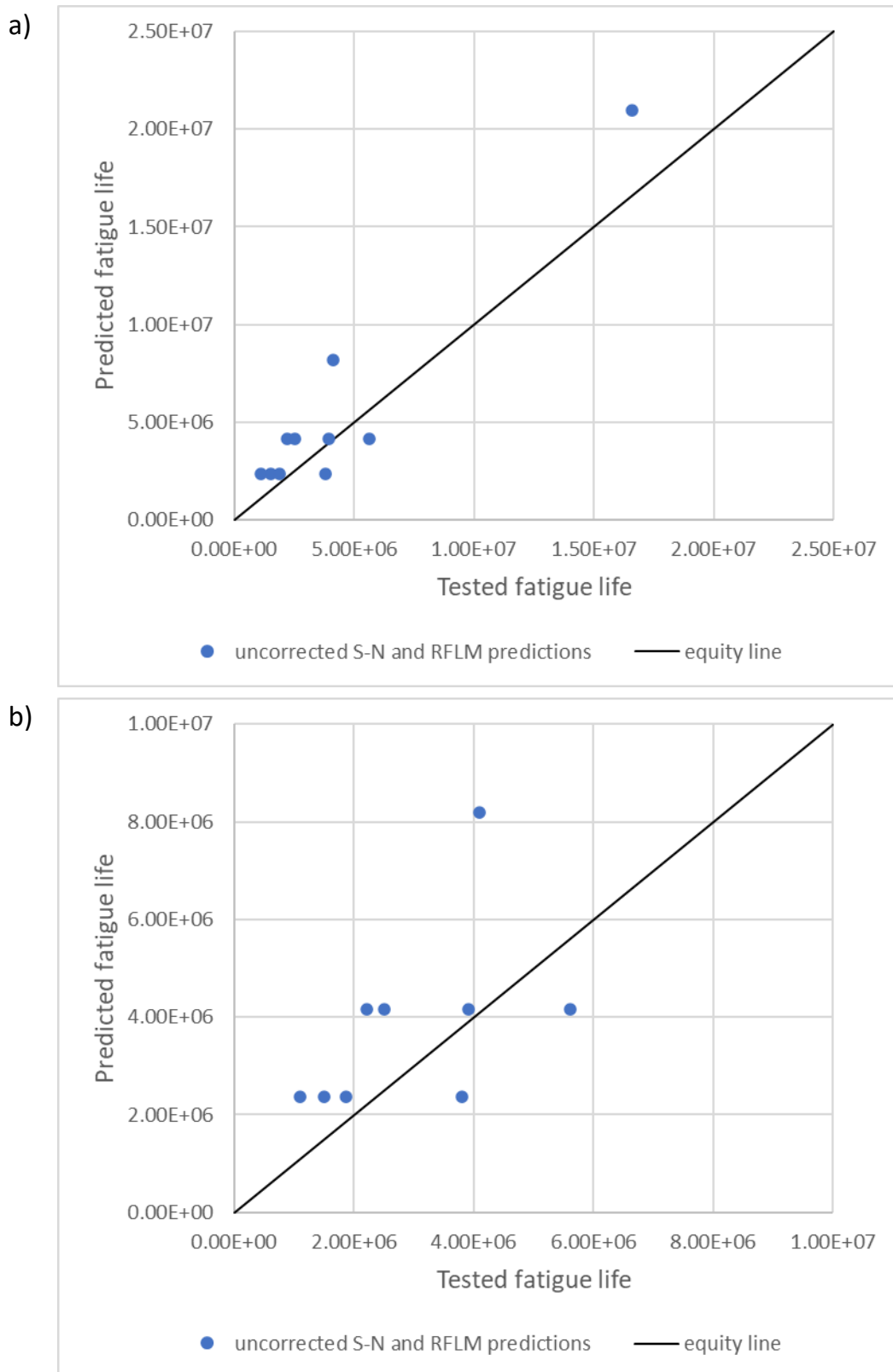
Figure 9.9. Direct fatigue life predictions, a) all specimens, b) magnification of bottom left corner area

Table 9.3. Test results and life predictions with median CA S-N curve

| Specimen | Spectrum | | Tested life [10^6 cycles] | Predicted life [10^6 cycles] | P-M sum at failure |
	Sequence	Minimum relative stress range			
F-03	A		1.10		0.46
F-15	A		1.50		0.63
F-09	C	0.25	3.81	2.38	1.60
F-10	B		1.87		0.79
F-04	A		2.21		0.53
F-13	A^e *		2.51		0.60
F-06	C	0.2	5.62	4.16	1.35
F-07	B		3.92		0.94
F-05	A	0.15	4.10	8.20	0.50
F-08	A	0.1	16.60	20.96	0.79

For all the data point in Figure 9.9 the mean value for the P-M summation at fracture is 0.82 and the standard deviation is close to 0.38. This gives a COV of 0.46. The mean value is acceptable, whereas the COV is above what can be expected for a single test series.

When analysing the 5 specimens for the sequence A alone the mean value for the P-M summation is 0.58 and the standard deviation is as small as 0.13. Hence, the specimens subjected to sequence A give a systematic bias in the life predictions. One of these specimens gave the results as shown up right in Figure 9.9a. This test specimen that endured 16.6×10^6 cycles was the only one subjected to a sequence containing a large amount of block no. 12 in Table 9.1. The stress range was only 21 MPa for this block. The descriptive statistics for the P-M summation are given in Table 9.4. As can be seen spectrum A has significantly different results than the specimens in spectrum B and C. There are also indications of differences between the experimental lives in spectrum B and C that are logical given the difference in applied R ratio for these two spectra. However, the number of specimens in each group is too few to pursue these differences. The main identified problem from a fatigue design point of view is that the life predictions for spectrum A are overly optimistic by a factor close to 2.

Table 9.4. Statistics for P-M summations

| All tests (10 specimens) | | | Spectrum A only (5 specimens) | | | Remaining tests (5 specimens) | | |
P-M sum average	STD	COV	P-M sum average	STD	COV	P-M sum average	STD	COV
0.82	0.38	0.46	0.58	0.13	0.23	1.06	0.41	0.39

9.5.6. Enhancing the RFLM life predictions

We shall apply our proposed enhancements based on equations (9.14) – (9.18). for the crack growth accounting for the variation of the R ratios shown in Figure 9.8 and residual stresses.

The fracture mechanics model, similar as used for analysis of F class detail presented in section 6, has been used for enhancing the RFLM life predictions. Some details are briefly described below.

The magnification factors applied for the SIFR calculations are the same as used by Zhang and Maddox [59]. Other parameters of the FM model are as follows:

- crack growth parameters: $C=6.64 \cdot 10^{-9}$ and $m=3$ (growth rate in mm/cycle, adopted from [59])
- initial crack depth $a_{ini} = 0.1$ mm
- final crack depth $a_{final} = 12$ mm
- initial crack aspect ratio $a_{ini}/c_{ini} = 0.5$
- no SIFR threshold applied
- reference effective R ratio is assumed 0.6
- residual stress magnitude $\sigma_r = 75$ MPa
- effective SIFR acc. to eq. (9.17) with $\beta = 0.7$

For each specimen the crack growth analysis is first carried out with the reference R ratio for all blocks in the stress spectrum/sequence, cycle by cycle until final crack depth is reached. In the second step, the growth simulation is done with the actual R ratios in each stress block and the assumed residual stress level. The lives predicted by the RFLM crack growth curve are then corrected by factors obtained by comparing predicted lives for constant reference R and actual applied R ratios in the analysed stress spectra. The simulated propagation lives and the correction factors are presented in Table 9.5.

Table 9.5. FM model based life predictions and the obtained correction factors

Specimen	Spectrum		Predicted life [cycles]		Correction factor, N_{pa}/N_{p0}
	Sequence	Min. relative stress range	for reference $R = 0.6$, N_{p0}	for actual R ratios, N_{pa}	
F-03	A	0.25	3.44E+05	2.43E+05	0.71
F-15	A				0.71
F-09	C			3.93E+05	1.14
F-10	B			2.89E+05	0.84
F-04	A	0.2	5.98E+05	3.82E+05	0.64
F-13	A[e] *			5.07E+05**	0.85
F-06	C			6.09E+05	1.02
F-07	B			4.49E+05	0.75
F-05	A	0.15	1.17E+06	6.88E+05	0.59
F-08	A	0.1	2.96E+06	1.61E+06	0.54

* stress ranges in spectrum A[e] are cycled down from a constant maximum stress 147 MPa,
** residual stress level after initial relaxation is assumed to be twice as high as in other tested specimens, σ_r = 150 MPa

Finally, the P-M sums at failure obtained for the corrected life predictions are presented in Table 9.6. As can be seen most of the predictions are improved when applying proposed enhancements. The life predictions are improving such that sequence A get a correction factor about 0.6 – 0.7 on fatigue life. The corrections for sequence B and C are more modest. The change in predictions compared with lives predicted without enhancement are shown in Figure 9.10.

Table 9.6. Statistics for P-M summations – enhanced life predictions

Specimen	Spectrum		P-M sum at failure	
	Sequence	Min. relative stress range	Uncorrected prediction (original RFLM crack growth curve)	Corrected prediction
F-03	A	0.25	0.46	0.66
F-15	A		0.63	0.89
F-09	C		1.60	1.40
F-10	B		0.79	0.94
F-04	A	0.2	0.53	0.83
F-13	A[e] *		0.60	0.71**
F-06	C		1.35	1.33
F-07	B		0.94	1.26
F-05	A	0.15	0.50	0.85
F-08	A	0.1	0.79	1.45
		Mean	0.82	1.03
		SD	0.38	0.30
		CoV	0.46	0.29

* stress ranges in spectrum A[e] are cycled down from a constant maximum stress 147 MPa,
** residual stress level after initial relaxation is assumed to be twice as high as in other tested specimens, σ_r = 150 MPa
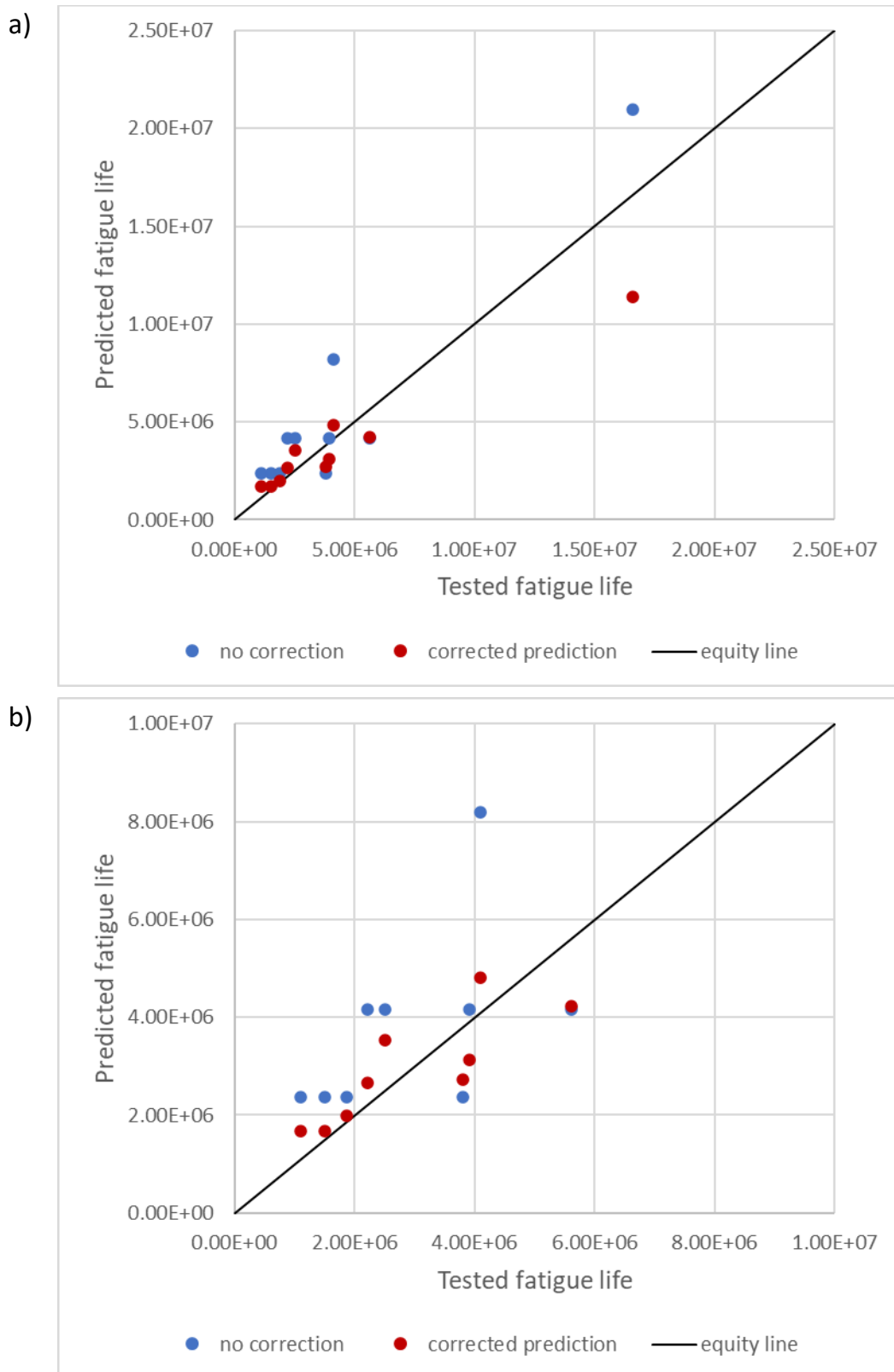
Figure 9.10. P-M summation for conventional method and for enhanced method,
a) all specimens, b) magnification of bottom left corner area

As can be seen both the bias and the scatter in predictions are improved. The P-M sum statistics is also listed in Table 9.6. The average P-M sum at failure for all specimens is close to 1.0 with CoV=0.29, this is a noticeable improvement. When analysing only specimens with sequence A, the average P-M sum is increased from 0.58 to 0.94. The reductions in predicted lives due to the mean stress effect are not enough to fully explain the test results for stress spectrum A. The prediction for test specimen F-08 is significantly poorer. It should be noted that the stress spectrum applied to this specimen consists large number of cycles with low stress range of 21 MPa. It might be the case that the SIFR threshold phenomenon may play a role and thus shall be considered and included in the FM model to obtain further improvements. As only one specimen has been tested with this stress sequence it is not enough to make an explanation and draw conclusions in that matter.

9.5.7. Result summary and conclusions

Based on the analyses carried out it can be concluded that:

- The RFLM predicts that the initiation phase can be neglected. The RFLM then reduces to a one-slope S-N curve with slope parameter $m = 3.072$ This is important information that the conventional S-N curve does not give.

- The life predictions based on the crack growth line of the RFLM must be corrected with the actual effective R ratio to get reliable results. The correction is obtained by carrying out fracture mechanics analysis based on the *unique crack growth rate curve method* using the concept of an effective Stress Intensity Factor.

- The parameter β is chosen such that the accuracy of the life predictions is optimized. A reference value of $R = 0.6$ is applied together with a $\beta = 0.7$. The applied value for β is within the recommendation given by Huang and Moan.

- The obtained improvements in the fatigue life predictions are significant, particularly for the stalactite shaped stress spectrum A. The danger of getting overly optimistic life predictions for this kind of stress spectrum is avoided when the R ratio correction is carried out.

- Despite the excellent numerical results there is still lack of detailed knowledge regarding the damage mechanism for the given stress spectra. Crack growth at very low stress ranges with extremely high R ratio and stress cycle interactions are amongst the topics that should be investigated further.

9.6. Conclusions for enhanced predictions

When the enhancements are applied to modify the basic RFLM predictions, these corrections are larger and more precise than for the conventional S-N curves. In the rule-based S-N predictions it is still common practice to neglect the influence of residual stresses and applied R ratio and use the applied stress range as the only variable. If a correction is carried out it is only allowed when the effective R ratio is negative and low residual stresses can be assumed. Furthermore, the applied correction assumes that a crack growth mechanism is totally dominating. Because the RFLM makes clear distinction between crack initiation and crack growth the corrections become more precise.

The enhancement of the basic RFLM life predictions when crack growth is very dominant damage mechanism is useful, but not straight forward. The present proposed crack growth model captures to some degree the impact of changes in residual stresses and applied R ratio for the three main stress spectra in the test data from Zhang and Maddox [59]. The difference in crack growth for specimens subjected to CA loading and VA loading is not fully understood and may need a more elaborated crack growth model than the present one. The proposed approach seems to be promising and will be further investigated and corroborated by other VA test data found in literature.

10. Concluding remarks

10.1. Introduction to the summing-up

The fatigue damage evolution and life prediction for given welded steel details have been thoroughly studied in this work. The focus has been on transverse and longitudinal welded attachments. Recent advances in fatigue crack growth modelling and probabilistic methods for life prediction have been extensively investigated and corroborated by laboratory test data collected from literature. To summarize the main findings of the present work and answer the research questions that were posed, it is convenient to make a distinction between the damage evolution and the life prediction methodology, Finally, some considerations for VA loading and future work are given.

10.2. The damage evolution

The answers for research questions related to the fatigue damage evolution are as follows:

- From the experimental measurements of crack growth histories, it is observed that the crack initiation phase does exist for as-welded joints. For long lives, typically for in-service conditions, this phase may even be dominant and should not be neglected.

- The crack growth model given by the Paris law and established by testing of wide plates with a central crack can be successfully applied for modelling evolution of semi-elliptically cracks at the weld toe from a crack depth of 0.1 mm up to final failure. However, for smaller crack depths, the early crack evolution determined experimentally was not obtained by the model.

- When determining the SIFR for small semi-elliptical cracks using formulas proposed by Bowness and Lee it is recommended to characterize variable toe geometry by the mean value for the measured toe angle and the extreme minimum value of toe radius which is close to 0.1 mm.

- It is important to consider crack coalescence when modelling damage evolution of a crack emanating at the weld toe. This can be done indirectly by forcing the development of crack aspect ratio when the prediction is based on growth history of a single semi-elliptical crack. The proposed approach gave accurate prediction of a measured growth histories.

- The main differences in the crack growth behaviour between the membrane and the bending loading modes are observed in crack shape evolution and time to crack coalescence. These differences have an impact on crack depth evolution and have an influence on shapes of measured *a-N* curves. The crack coalescence occurs at an earlier stage for the bending loading mode. As a result, the overall growth becomes faster at this stage due to the associated almost immediate decrease in the crack aspect ratio. This effect is in fact more important than the retardation caused by a linear decreasing stress field in the crack depth direction. The crack front at the deepest point is approaching lower stress variations when approaching the neutral axis for bending. This finding was observed in physical testing and was confirmed by crack growth simulations.

10.3. Life prediction methodology

The conclusions regarding questions related to prediction of the entire fatigue life can be summarised as follows:

- The best fit to the fatigue life data at a given stress range of 150 MPa was obtained using the lognormal distribution for an F class detail.
- The RFLM-based resistance curves are suggested as an alternative to the conventional S-N curves. The advantage of the RFLM is that long lives and runouts are easily and logically included in the modelling.
- Because the runouts and long lives ($>5 \times 10^6$ cycles) are neglected in conventional S-N analysis, all information related to such data is not reflected in S-N life predictions. Consequently, the RFLM-based resistance curves give more optimistic life predictions while keeping the same reliability level as conventional S-N curves. It is particularly the long predicted lives that will become longer.
- The principal difference between RFLM-based resistance curves and the conventional S-N curves is visible for life predictions in the regime of lives longer than 10^6 cycles and up to the very high cycle fatigue lives obtained at stress level close to the CAFL. The RFLM is capable of modelling this important area but there is a scarcity of life data available.
- RFLM-based resistance curves fit the test data significantly better than the bi-linear S-N curves, especially in high and very high cycle regime. The RFLM resistance curve does in fact reject the existence of a fatigue limit.

This rejection agrees well with the latest proposal for CA S-N curves from IIW. However, due to lack of data in this very high cycle regime, a conclusion on this matter cannot be drawn.

- The shape of the RFLM resistance curves simplified by two straight lines agrees well with the physical two-phase model for crack initiation and subsequent crack propagation. Consequently, the RFLM can be explained and supported by the physical models for the involved damage mechanisms.

10.4. Considerations for VA loading and future work

The scope of the present work was originally limited to CA loading, whereas the future work will be focused on more accurate life predictions for welded details subjected to VA loading. The preliminary results of the enhanced life predictions for VA stress spectra, as presented in chapter 9, are promising and the procedure will be pursued further to other VA loading applications. One possible extension is to apply the RFLM to girth welded pipes categorized as a D class details. Such welds are applied in offshore steel risers and offshore wind towers. As this type of weld has higher fatigue quality than the welded attachments investigated in the present work, it is expected that the application of the RFLM will be even more effective when it comes to achieving life predictions with high accuracy.

For VA loading conditions two additional papers are under preparation and shall be submitted to international journals:

Paper E Z. Mikulski, T. Lassen, "Enhanced life predictions of welded steel joints subjected to variable amplitude loading". To be submitted to International Journal of Fatigue

Paper F T. Lassen, Z. Mikulski, "Advanced probabilistic models for the fatigue life predictions of girth welded pipes subjected to variable amplitude loading". To be submitted to International Journal of OMAE or Journal of Marine Structures

List of references

[1]   Lassen T, Recho N. FLAWS Fatigue Life Analyses of Welded Structures. ISTE; 2006.

[2]   Mikulski Z, Lassen T. Probabilistic models for the fatigue resistance of welded steel joints subjected to constant amplitude loading. International Journal of Fatigue 2022;155. doi:10.1016/j.ijfatigue.2021.106626.

[3]   EN 1993-1-9:2005. Eurocode 3: Design of steel structures - Part 1-9: Fatigue 2005.

[4]   DNV. DNV-RP-C203: Fatigue Design of Offshore Steel Structures 2021.

[5]   DNV. DNV-RP-C210: Probabilistic methods for planning of inspection for fatigue cracks in offshore structures 2021.

[6]   BS 7910. Guide to methods for assessing the acceptability of flaws in metallic structures 2013.

[7]   Baptista C, Reis A, Nussbaumer A. Probabilistic S-N curves for constant and variable amplitude. International Journal of Fatigue 2017;101:312–27. doi:10.1016/j.ijfatigue.2017.01.022.

[8]   Mikulski Z, Lassen T. Fatigue crack initiation and subsequent crack growth in fillet welded steel joints. International Journal of Fatigue 2019;120:303–18. doi:10.1016/J.IJFATIGUE.2018.11.014.

[9]   Zerbst U, Madia M, Schork B. Fracture mechanics based determination of the fatigue strength of weldments. Procedia Structural Integrity 2016;1:10–7. doi:10.1016/j.prostr.2016.02.003.

[10]   Bremen U. Amélioration du comportement à la fatigue d'assemblages soudés étude et modélisation de l'effet de contraintes résiduelles. EPFL, 1989. doi:10.5075/epfl-thesis-787.

[11]   Mikulski Z, Lassen T. Crack growth in fillet welded steel joints subjected to membrane and bending loading modes. Engineering Fracture Mechanics 2020;235:107190. doi:10.1016/j.engfracmech.2020.107190.

[12]   Lawrence F V., Mattos RJ, Higashida Y, Burk JD. Estimation of fatigue initiation life of weld. STP684 Fatigue Testing of Weldments, Philadelphia: ASTM; 1978, p. 134–58. doi:10.1520/STP33393S.

[13]   Lawrence F V., Burk JD, Yung J. Influence of residual stress on the predicted fatigue life of weldments. In: Throop JF, Reemsnyder HS, editors. Residual Stress Effects in Fatigue, STP 776, ASTM; 1982, p. 33–43.

[14]   Ho N-J, Lawrence F V. The fatigue of weldments subjected to complex loading, FCP Report No. 45. 1983.

[15]   Yung J, Lawrence F V. Analytical and Graphical Aids for the Fatigue Design of Weldments. Fatigue & Fracture of Engineering Materials & Structures 1985;8:223–41. doi:10.1111/j.1460-2695.1985.tb00424.x.

[16]   Fricke W. Fatigue analysis of welded joints: State of development. Marine Structures 2003;16:185–200. doi:10.1016/S0951-8339(02)00075-8.

[17]   DNV. Classification Note No. 30.6: Structural Reliability Analysis of Marine Structures 1992.

[18]   Zerbst U, Ainsworth RA, Beier HT, Pisarski H, Zhang ZL, Nikbin K, et al. Review on fracture and crack propagation in weldments - A fracture

mechanics perspective. Engineering Fracture Mechanics 2014;132:200–76. doi:10.1016/j.engfracmech.2014.05.012.

[19] Verreman Y, Nie B. Early development of fatigue cracking at manual fillet welds. Fatigue and Fracture of Engineering Materials and Structures 1996;19:669–81. doi:10.1111/j.1460-2695.1996.tb01312.x.

[20] Mikulski Z, Lassen T. Fatigue crack initiation and subsequent crack growth in fillet welded steel joints. International Journal of Fatigue 2019;120:303–18. doi:10.1016/j.ijfatigue.2018.11.014.

[21] Lassen T, Recho N. Proposal for a more accurate physically based S-N curve for welded steel joints. International Journal of Fatigue 2009;31:70–8. doi:10.1016/j.ijfatigue.2008.03.032.

[22] Wirsching PH, Chen Y-N. Considerations of probability-based fatigue design for marine structures. Marine Structures 1988;1:23–45. doi:10.1016/0951-8339(88)90009-3.

[23] Schijve J. Fatigue Predictions and Scatter. Fatigue & Fracture of Engineering Materials & Structures 1994;17:381–96. doi:10.1111/j.1460-2695.1994.tb00239.x.

[24] Engesvik K, Moan T. Probabilistic analysis of the uncertainty in the fatigue capacity of welded joints. Engineering Fracture Mechanics 1983;18:743–62. doi:10.1016/0013-7944(83)90122-4.

[25] Wirsching PH. Report no. 17: The statistical distribution of cycles to failure. Paramus, NY: 1984.

[26] Lewis EE. Introduction to Reliability Engineering. Wiley; 1988.

[27] Benjamin JR, Cornell CA. Probability, Statistics, and Decision for Civil Engineers. McGraw-Hill; 1970.

[28] Bastenaire FA. New Method for the Statistical Evaluation of Constant Stress Amplitude Fatigue-Test Results. In: Heller RA, editor. Probabilistic Aspects of Fatigue, West Conshohocken, PA: ASTM International; 1972, p. 3–28. doi:10.1520/STP35402S.

[29] Pascual FG, Meeker WQ. Estimating fatigue curves with the random fatigue-limit model. Technometrics 1999;41:277–89. doi:10.1080/00401706.1999.10485925.

[30] Lassen T, Darcis P, Recho N. Fatigue Behavior of Welded Joints Part 1 - Statistical Methods for Fatigue Life Prediction. Welding Journal 2005;84:183s-187s.

[31] D'Angelo L, Nussbaumer A. Estimation of fatigue S-N curves of welded joints using advanced probabilistic approach. International Journal of Fatigue 2017;97:98–113. doi:10.1016/j.ijfatigue.2016.12.032.

[32] Toasa Caiza PD, Ummenhofer T. General probability weighted moments for the three-parameter Weibull Distribution and their application in S-N curves modelling. International Journal of Fatigue 2011;33:1533–8. doi:10.1016/j.ijfatigue.2011.06.009.

[33] Toasa Caiza PD, Ummenhofer T. A probabilistic Stüssi function for modelling the S-N curves and its application on specimens made of steel S355J2+N. International Journal of Fatigue 2018;117:121–34. doi:10.1016/j.ijfatigue.2018.07.041.

[34] Leonetti D, Maljaars J, Snijder HH (Bert). Fitting fatigue test data with a novel S-N curve using frequentist and Bayesian inference. International Journal of Fatigue 2017;105:128–43. doi:10.1016/j.ijfatigue.2017.08.024.

[35] Drebenstedt K, Euler M. Statistical Analysis of Fatigue Test Data according to Eurocode 3. In: Powers, Frangopol, Al-Mahaidi, Caprani, editors. Maintenance, Safety, Risk, Management and Life-Cycle Performance of Bridges, London: Taylor & Francis Group; 2018, p. 2244–51.

[36] Darcis P, Lassen T, Recho N. Fatigue Behavior of Welded Joints Part 2 : Physical Modeling of the Fatigue Process. Welding Journal 2006;2:19s-26s. doi:10.1111/j.1559-3584.1936.tb03841.x.

[37] Dang-Van K, Griveau B, Message O. On a new multiaxial fatigue limit criterion: theory and application. Biaxial and Multiaxial Fatigue, EGF 3 (Edited by M. W. Brown and K. J. Miller), London: Mechanical Engineering Publications; 1989, p. 479–96.

[38] Huang X, Moan T, Cui W. A unique crack growth rate curve method for fatigue life prediction of steel structures. Ships and Offshore Structures 2009;4:165–73. doi:10.1080/17445300902732370.

[39] Huang X, Moan T. Improved modeling of the effect of R-ratio on crack growth rate. International Journal of Fatigue 2007;29:591–602. doi:10.1016/j.ijfatigue.2006.07.014.

[40] Newman JC, Raju IS. An empirical stress intensity factor equation for the surface crack. Engineering Fracture Mechanics 1981;15:185–92.

[41] Bowness D, Lee MMK. Prediction of weld toe magnification factors for semi-elliptical cracks in T-butt joints. International Journal of Fatigue 2000;22:369–87. doi:10.1016/S0142-1123(00)00012-8.

[42] Stötzel J. Collection and evaluation of fatigue test results - RWTH Aachen, ECCS-TC6-Fatigue, IIW-Working Group JWG XIII-XV. n.d.

[43] Lindqvist A, Nilsson H. Effective notch stress analysis of transverse attachments in steel bridges - a parametric fatigue life assessment. Chalmers, 2016.

[44] Lebas G, Fauve JC. Collection of fatigue data, Elf Aquitaine. Pau: 1988.

[45] Gurney TR. The Fatigue Strength of Transverse Fillet Welded Joints. Woodhead Publishing; 1991.

[46] Gurney TR. Thickness effect in "relatively thin" welded joints; Offshore Technology Report OTH 91 358. 1995.

[47] Berge S. On the effect of plate thickness in fatigue of welds. Engineering Fracture Mechanics 1985;21:423–35. doi:10.1016/0013-7944(85)90030-X.

[48] Lassen T. The effect of the welding process on the fatigue crack growth in welded joints. Welding Journal 1990;February:75s-85s.

[49] Engesvik K, Lassen T. The effect of weld geometry on fatigue life. Proceedings of the 7th International Conference on Offshore Mechanics and Arctic Engineering, OMAE1988, Houston, Texas: ASME Press; 1988, p. 441–5.

[50] Engesvik K. Analysis of Uncertainties in the Fatigue Capacity of Welded Joints, Report UR-82-17. Trondheim: 1982.

[51] Friis LE, Streneroth ER. Fatigue strength of welded joints in mild and high-

strength structural steels. Jernkont Ann 1968.

[52]   Mikulski Z, Hellum V, Lassen T. Modeling the fatigue damage evolution in welded joints. ASME 2017 36th International Conference on Ocean, Offshore and Arctic Engineering, Volume 4: Materials Technology, ASME Press; 2017. doi:10.1115/OMAE201761201.

[53]   Hobbacher AF. The new IIW recommendations for fatigue assessment of welded joints and components - A comprehensive code recently updated. International Journal of Fatigue 2009;31:50–8. doi:10.1016/j.ijfatigue.2008.04.002.

[54]   Haibach E. Discussion paper. The Welding Institute Conference on Fatigue of Welded Structures 1970.

[55]   Gurney TR. Cumulative damage calcuations taking account of low low stresses in the spectrum. TWI Report 2/1976/E. 1976.

[56]   Gurney TR. Cumulative Damage of Welded Joints. Woodhead Publishing; 2006. doi:10.1533/9781845691035.1.

[57]   Manson SS, Freche JC, Ensign CR. Application of a Double Linear Damage Rule to Cumulative Fatigue. In: Grosskreutz J, editor. Fatigue Crack Propagation, West Conshohocken, PA: ASTM International; 1967, p. 384–412. doi:10.1520/STP47237S.

[58]   Zhang B, Moan T. Mean Stress Effect on Fatigue of Welded Joint in FPSOs. 25th International Conference on Offshore Mechanics and Arctic Engineering Volume 3: Safety and Reliability; Materials Technology; Douglas Faulkner Symposium on Reliability and Ultimate Strength of Marine Structures, 2006, p. 403–12. doi:10.1115/omae2006-92056.

[59]   Zhang Y-H, Maddox SJ. Investigation of fatigue damage to welded joints under variable amplitude loading spectra. International Journal of Fatigue 2009;31:138–52. doi:10.1016/j.ijfatigue.2008.04.006.

Appendices

ANNEX A

Present test set-up for details with longitudinal attachments

Test specimen

Plate with non-load carrying longitudinal welded attachment has been chosen for this test campaign. NVE 36 12 mm thick plates are used both as the main plate and the attachment. Flux-Cored Arc Welding procedure has been used.

All specimens have been stress relieved. Non-destructive tests have been caried out for all specimens and no defects were found.
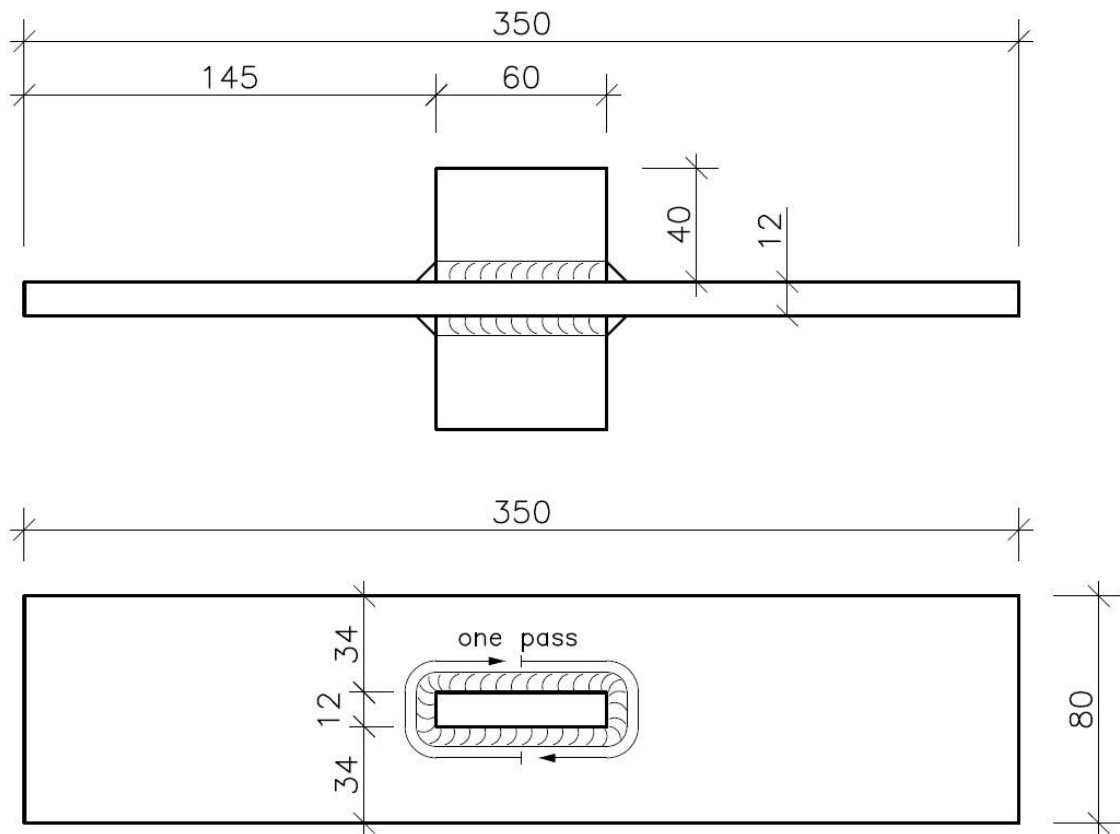
Figure A.1. Geometry of test specimen

Fatigue testing machine

Si-Plan servo-hydraulic universal test machine has been used. The load cell capacity is 25 kN.

Figure A.2. Si-Plan fatigue testing machine with the assembled test rig

Loading frame

Figure A.3. Loading frame for 4-point bending

Figure A.4. Pusher on double hinge to balance the load (uniform loading on both ends)

Crack growth monitoring system

Matelect CGM-7 ACPD Crack Growth Monitor has been used for monitoring crack evolution.

Figure A.5. Matelect CGM-7 ACPD Crack Growth Monitor[1]

Matelect SM-HF Modular Scanner System has been used as a multiplexer for monitoring 8 locations (8 sets of probes, 4 at each end of the attachment)

Figure A.6. Matelect SM-HF Modular Scanners[1]

---

[1] Matelect Product Guide 2016, Matelect Ltd, www.matelect.com

Probe arrangement

Four sets of active and reference voltage probes have been attached to the main plate at each end of the welded attachment using capacitance welder. The probes are made of thin nickel wires (thermocouple wire, type K). The active probes are welded across the weld toe at the expected crack location.

Figure A.7. Probe arrangement
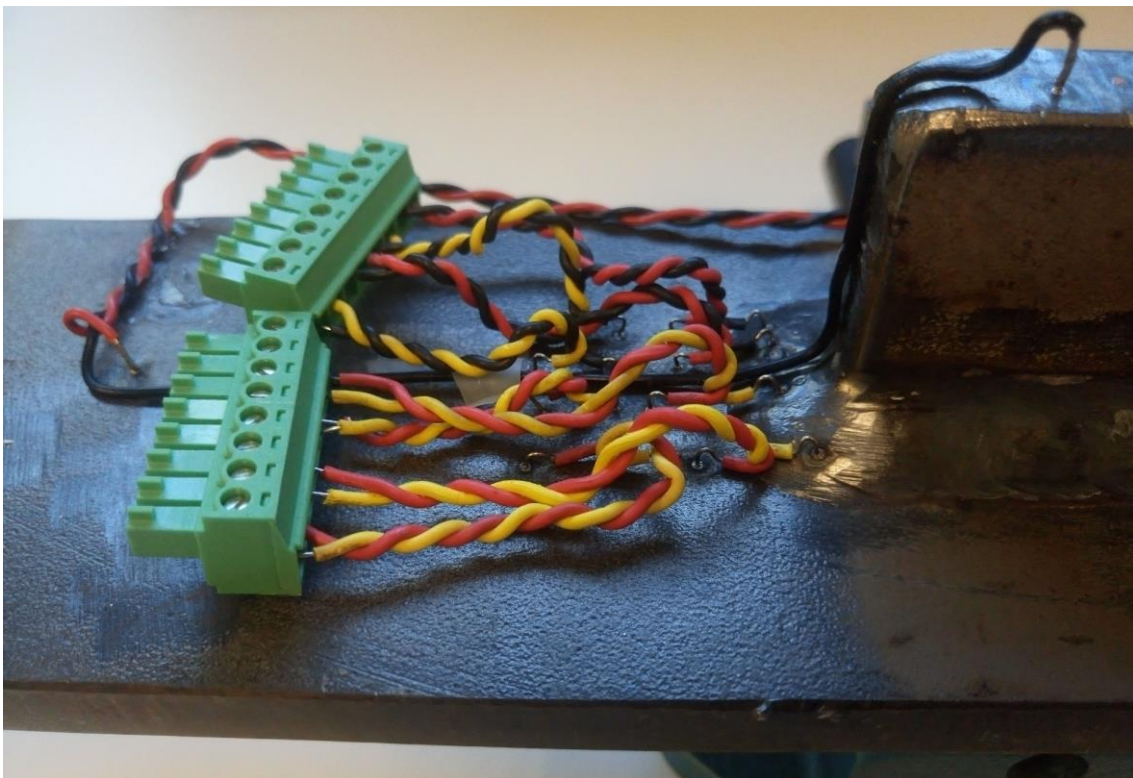
Figure A.8. Probe arrangement – detail view

In order to reduce the induced pick-up voltage effects, the voltage and current leads are tightly twisted and positioned as close as possible to the specimen surface, minimising the lop area enclosed by both the current and voltage leads.

The current probes are installed at each end of the attachment, one at the top of the welded attachment and the second behind the reference voltage probes. The current focused ACPD setup is used in order to improve ACPD sensitivity.

Test setup – selected details

Fatigue testing has been carried out under displacement control with 5 Hz loading frequency. The upper and lower displacement limits have been adjusted several times during course of the test to maintain constant amplitude loading in terms of nominal stresses.

The load cycles have been applied in blocks. ACPD measurements have been taken during a pause between the blocks when the load has been constant and kept at maximum load in the cycle. The AC settings were: 5 Amp and 8 kHz. The readings have been taken consecutively at all monitored locations by switching channels in the modular scanners. After switching the channel and before recording the reading, a settling time of 5 seconds has been set to ensure that reading is taken at stable voltage and current signal.

Appended papers

Paper A

Modelling the fatigue damage evolution in welded joints

Zbigniew Mikulski, Vidar Hellum, Tom Lassen

OMAE2017-61201

MODELING THE FATIGUE DAMAGE EVOLUTION IN WELDED JOINTS

Zbigniew Mikulski
University of Agder
Grimstad, Norway

Vidar Hellum
AS Nymo
Grimstad, Norway

Tom Lassen
[1]University of Agder
Grimstad, Norway
[2]NOV APL, Arendal, Norway

ABSTRACT

The present paper presents a two-phase model for the fatigue damage evolution in welded steel joints. The argument for choosing a two-phase model is that crack initiation and subsequent crack propagation involve different damage mechanisms and should be treated separately. The crack initiation phase is defined as the number of cycles to reach a crack depth of 0.1 mm. This phase is modelled based on the Dang Van multiaxial stress approach. Both a multiaxial stress situation introduced by the acting loads and the presence of the multiaxial welding residual stresses are accounted for. The local notch effect at the weld toe becomes very important and the irregular weld toe geometry is characterized by extreme value statistics for the weld toe angle and radius. The subsequent crack growth is based in classical fracture based on the Paris law including the effect of the Stress Intensity Factor Range (SIFR) threshold value. The unique fatigue crack growth rate curve suggested by Huang, Moan and Cui is adopted. This approach keeps the growth rate parameters C and m constant whereas an effective SIFR is calculated for the actual stress range and loading ratio. The model is developed and verified based on fatigue crack growth data from fillet welded joints where cracks are emanating from the weld toe. For this test series measured crack depths below 0.1 mm are available. The two-phase model was in addition calibrated to fit the life prediction in the rule based S-N curve designated category 71 (or class F). A supplementary S-N curve is obtained by the Random Fatigue Limit Method (RFLM). The test results and the fitted model demonstrated that the crack initiation phase in welded joins is significant and cannot be ignored. The results obtained by the Dang Van approach for the initiation phase are promising but the modelling is not yet completed. The fracture mechanics model for the propagation phase gives good agreement with measured crack growth. However, it seems that the prediction of crack retardation based on a threshold value for the SIFR gives a fatigue limit that is overly optimistic for small cracks at the weld toe. The threshold value has been determined based on tests with rather large central cracks in plates. The validity for applying this threshold value for small cracks at the weld toe is questioned. As the present two-phase model is based on applied mechanics for both phases the parameters that have an influence on the fatigue damage evolution are directly entering into the model. Any change in these parameters can then be explicitly taken into account in logical and rational manner for fatigue life predictions. This not the case with the rule based S-N curves that are based on pure statistical treatment of the bulk fatigue life.

NOMENCLATURE

Symbols
Roman letters:

a	crack depth
a_i	initial crack depth
a_{ini}	initial crack depth
B	fatigue strength exponent
b_0	shear fatigue strength exponent
c	crack length
c	fatigue ductility exponent
C	crack growth rate parameter in Paris equation
c_0	shear fatigue ductility exponent
c_{ini}	initial crack length
$\text{dev}\rho$	deviatoric part of stabilized residual stress tensor
E	module of elasticity

f_w	finite width correction factor
J_2	von Mises norm
k	material parameter in Fatemi-Socie criterion
K'	cyclic strength coefficient
L	attachment length
m	crack growth rate exponent in Paris equation
M_{km}	weld toe magnification factor
M_m	geometrical correction factor
n'	cyclic strain hardening exponent
N	number of cycles
N	total fatigue life
N_i	number of cycles to crack initiation
N_p	number of cycles spent in crack propagation
R	stress ratio
T	thickness of the specimen
W	width of the specimen

Greek letters:

α	material parameter in Dang Van criterion
α_i	material parameter in Dang Van criterion for a life duration N_i
β_0	fatigue curve coefficient in RFLM
β_1	fatigue curve coefficient in RFLM
γ	fatigue limit in RFLM
γ_f'	shear fatigue ductility coefficient
$\Delta\gamma_{max}$	maximum range of shear strain
$\Delta\varepsilon$	local strain range
$\Delta\sigma$	local stress range
ΔK_a	stress intensity factor range for the deepest point of the crack
ΔK_c	stress intensity factor range for the surface points of the crack
ΔK_E	equivalent SIFR at $R=0$
ΔK_{th0}	threshold value for the SIFR at $R=0$
ΔS	nominal stress range
ε_f'	fatigue ductility coefficient
θ	weld toe transition angle
ρ	weld toe transition radius
ρ	stabilized residual stress tensor
ρ_f	fictitious weld toe radius
$\sigma(t)$	stress tensor in mesoscale (mesoscopic stress tensor)
σ_h	maximum hydrostatic stress
$\sigma_h(t)$	hydrostatic stress at time t of the load cycle computed from the stress tensor in mesoscale
σ_f'	fatigue strength coefficient
σ_m	local mean stress
$\sigma_{n,max}$	maximum normal stress
σ_y	yield stress
$\sigma_I(t)$	maximum principal stress of mesoscopic stress tensor
$\sigma_{III}(t)$	minimum principal stress of mesoscopic stress tensor
$\Sigma(t)$	stress tensor in macroscale (macroscopic stress tensor)
τ_a	shear stress amplitude

τ_f'	shear fatigue strength coefficient
$\tau_{max}(t)$	maximum shear stress at time t of the load cycle computed from the stress tensor in mesoscale
τ_0	fatigue limit in simple shear
τ_0	local equivalent shear stress amplitude
$\tau_{0,i}$	local equivalent shear stress amplitude for a life duration N_i
Φ	complete elliptical integral

Abbreviations

ACPD	Alternating Current Potential Drop
COV	Coefficient Of Variation
ESIFR	Equivalent Stress Intensity Factor Range
FCAW	Flux-Cored Arc Welding
FEM	Finite Element Method
IIW	International Institute of Welding
LEFM	Linear Elastic Fracture Mechanics
SAW	Submerged Arc Welding
SCF	Stress Concentration Factor
SIFR	Stress Intensity Factor Range
RFLM	Random Fatigue-Limit Model
TPM	Two Phase Model

1 INTRODUCTION

High reliability against fatigue failure is one of the most important design criteria for welded offshore steel structures. Due to repeated wave loading fatigue cracks may initiate and grow in welds that are important for the integrity of these structures. The final fracture may lead to total collapse for non-redundant structures.

The S-N curve is the common engineering tool for fatigue life predictions in welded steel joints. This coarse bulk approach for predicting the fatigue life is only to a limited extent based on physical understanding of the damage process. It is merely based on descriptive statistics for the fatigue life as a function of the applied stress range. The approach has some disadvantages such as difficulties with handling multiaxial stress situations and accounting for residual stresses in a correct way. The local weld toe geometry is also difficult to handle. A more detailed and accurate physical based model will have the capability to handle these effects in a more rational and logical manner.

As a supplement to the S-N approach applied fracture mechanics has been used to predict the potential crack growth. This model is going more into the detailed fatigue damage mechanism in the welded joint, but it still has the problem of describing the crack initiation and subsequent early growth for high quality joints where the initial crack depth is less than 0.1mm. The crack growth parameters have never been determined for such small cracks. On this background the present two-phase model is proposed. The model is treating the crack initiation phase and the subsequent crack propagation separately. The main argument for this approach is that the two phases involve different damage mechanisms. The model is an

attempt to analyze the damage mechanisms for crack emanating from the weld toe. For the crack initiation phase it is emphasized to take into account the multiaxial stress situation at the weld toe using the approaches set forward by Dang Van, [1-3]. The crack growth phase is modeled by the Paris law by applying the unique crack growth curve approach [4]. The stress intensity factor calculations follow the guidelines in [5-7] that are based on 3D stress analysis. The model is verified and calibrated against crack growth measurements in fillet welded joints where the time to crack initiation is measured during the testing. The following topics are included:

- Both global and local weld toe geometry are easily accounted for. The variable local toe geometry is treated by extreme value statistics.

- Multiaxial stresses including residual stresses can be accounted for in the initiation phase. The initiation phase will often be the dominant part of the fatigue life under in-service stresses.

- S-N curve constructed from the model can be used for life prediction. The curves are obtained without any presumption on the existence of a fatigue limit. The curves will be non-linear for a log-log scale.

- The model gives a tool for risk based inspection planning that is not totally depending on fracture mechanics only. The problem of assuming a fictitious initial crack with very small depth is avoided, and the model gives a more correct response to changes in the applied stress range.

- The model is established for a constant amplitude stress history, but has the capability of handling variable amplitude loading.

The purpose of the present work is to shed some light on the topics listed above, both when it comes to the understanding the fatigue process and the associated form of the S-N curves. The topics are related such that it is possible to demonstrate that long fatigue lives at low stress levels are caused by long initiation lives and not by any threshold phenomenon for the fatigue crack growth. A fatigue limit will as a consequence not exist. This is the hypothesis of the present work. The model results are corroborated by measured crack growth and a large amount of collected life data for fillet welded joints.

2 THE FATIGUE DAMAGE MECHANISM

It is assumed that the total fatigue life consists of two major phases:

$$N = N_i + N_p \qquad (1)$$

where N_i is the number of cycles to crack initiation whereas N_p is the number of cycles spent in the propagation phase. The assumption that the crack initiation phase constitutes an important part of the entire fatigue life has been proven by several experimental test series with fillet welded joints [8]. Modelling the fatigue behaviour by fracture mechanics alone is dubious in such cases. Crack initiation takes place by a shear stress controlled slip-band mechanism at the weld toe notch before crack growth sets in. The nucleation mechanism is modelled by the variation in the mesoscopic shear stress variation at the critical plane at the weld toe. Important materials parameters for the fatigue resistance are related to the yield stress of the steel. The initiation phase becomes very dominant when post weld improvements methods like grinding or needle peening are applied. The subsequent crack growth is governed by the largest principal stress variation. The crack will propagate with the crack planes normal to the applied principal stress. Important material parameters for the fatigue resistance are related to the *E* module of the material and not the yield stress as is the case for the initiation phase.

3 DEFINING THE TWO PHASE MODEL

Based on the discussion in section 2 the number of cycles to crack initiation and the subsequent propagation phase are modeled separately. The proposal was first presented in [9] but the present work includes major extension and improvements. The initiation phase is modeled by the Dang Van multiaxial fatigue approach where the shear stress variation plays a prime role. The subsequent propagation phase is mainly governed by the variation in the largest principal stress. The unique growth rate curve as presented in [4] is adopted. The major topics that have to be addressed are:

- Local toe geometry and stress concentration factor
- The parameters in the Dang Van stress approach
- Transition depth between the two phases
- The validity of the unique crack growth curve for small cracks at the weld toe

The problem with the weld toe geometry is that it may vary considerably along the weld seam. However, it is highly likely that the cracks initiate at a the most unfavourable geometry. If the radius at an arbitrary locus along the weld seam is treated as a stochastic variable, the extreme value distribution for the smallest value among k independent radii can be applied. The Dang Van parameters for the crack initiation phase are not completely determined at the present stage. The planned test series 2 presented in Annex B will provide the necessary data to complete this work. The transition crack depth between the two damage phases may be a crucial number for the model. It has become clear lately that if the entire fatigue life is modelled solely by fracture mechanics this gives initial crack depths below 0.05 mm. This is out of the validity range for the applied geometry functions for the SIFR entering into the Paris law.

These functions are not verified for crack depth less than 0.1 mm. In the test series 1 presented in the next section the number of cycles to reach a crack depth of 0.1 mm is measured. One might even get an estimate of the cycles to reach 0.05 mm, but the accuracy will then decrease. As a consequence a transition depth of 0.1 mm is chosen as a start. However this choice may be changed to a smaller crack depth. The argument for doing so will be to obtain a better fit for the entire fatigue life when comparing the model results with the S-N based fatigue life. For the last topic listed in the bullet points above one should be aware of the fact that small surface cracks at the weld toe may not obey the threshold phenomenon demonstrated for larger central cracks.

4 OVERVIEW OF THE SERIES

The proposed two-phase model shall be calibrated and corroborated against two test series:

- Test series 1 - transverse fillet welded attachment
- Test series 2 - parallel fillet welded attachments

Test series 1 is completed whereas test series 2 is about to start. Some details for the two test series are given in Annex A and B respectively. Test series 1 consist of thirty-four non-load-carrying cruciform and T joints test specimens. All the test specimens were fabricated from C-Mn steel plates with 25 mm thickness. The nominal yield stress was 345 MPa. The welding procedures were taken from normal offshore fabrication practice. The joints were proven free from cracks and undercuts. The test specimens were stress relieved. The specimens were tested under constant amplitude axial loading at $\Delta S = 150$ MPa with a loading ratio of $R = 0.35$. Experimental details are found in [8]. The median life of the series ($N = 460\ 000$ cycles) is only 12% less than the prediction of the F-class ($N = 513\ 000$ cycles). Hence, the test series are of normal quality and comparable with the population pertaining to the F-class and Category 71 in the codes. However, due to the homogeneity of the test series, the Coefficient of Variation (COV) is as expected much smaller, COV=0.22. In addition to recording the fatigue life, crack growth measurements were made during the course of each test for this test series, see Annex A. The depth measurements were carried out by Alternating Current Potential Drop (ACPD) equipment. The most important part of these measured crack depth paths histories is the very beginning of the crack growth as illustrated in Figure 2. As can be seen there is obviously some noise disturbing the measurements from the beginning. Up to 300 000 cycles the crack depth is oscillating between 0.0 and 0.04 mm. But from 300 000 cycles there is a steadily increasing trend in the measurements. The number of cycles to reach 0.1 mm is close to 400 000 cycles for this case. This depth was corroborated physically by ink staining of the crack planes.
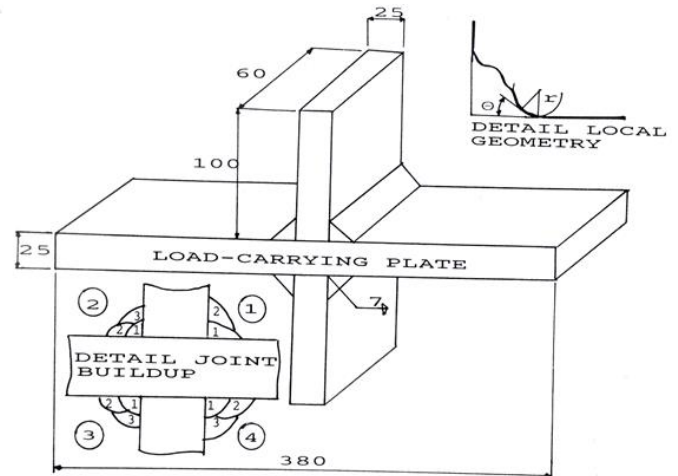
FIGURE 1. Test specimen in test series 1. Local toe geometry up right

The presented case is one of the longest initiation periods recorded. Figure 3 shows a more common case where the initiation period is close to 150 000 cycles. From figures 2 and 3 it is possible to determine the number of cycles to reach a crack depth of 0.1mm. One might even get an estimate of the cycles to reach 0.05 mm.
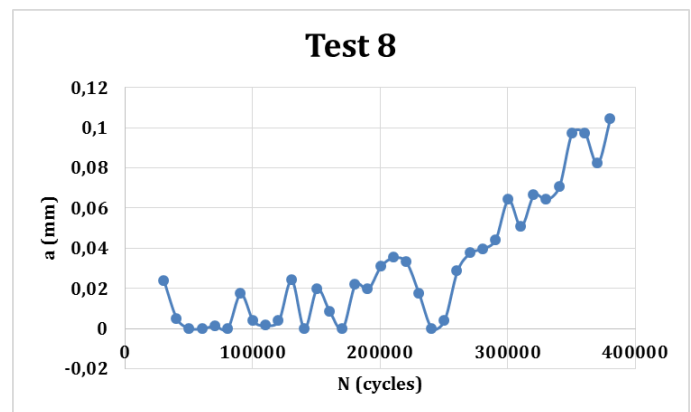
FIGURE 2. Measurements of early crack growth in series 1, test 8
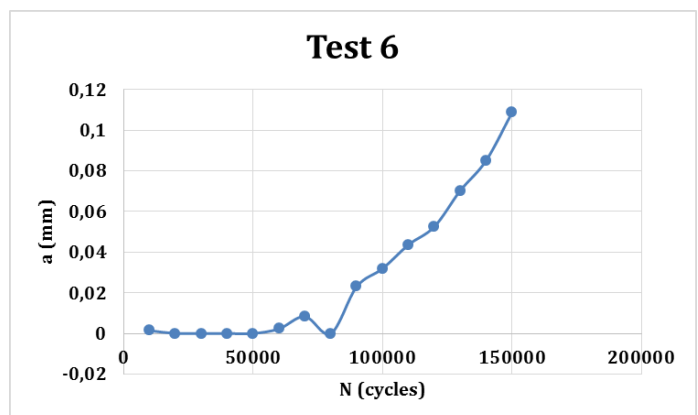
FIGURE 3. Measurements of early crack growth in series 1, test 6

Test series 2 consists 12 specimens. It is a plate with fillet welded longitudinal attachments under four-point bending. Geometry and dimensions are presented in Figure 4. All test specimens were made of NVE 36 steel plate thickness of 12 mm and were fabricated using Flux-Cored Arc Welding procedure (FCAW). The welding process was carried out in the horizontal position and only one passage was made to create the weld. The specimens were manufactured by AS Nymo (Grimstad, Norway). Chemical composition and mechanical properties of the steel are presented in Table 1 and Table 2 respectively. All test specimens are stress relieved at 550 °C.
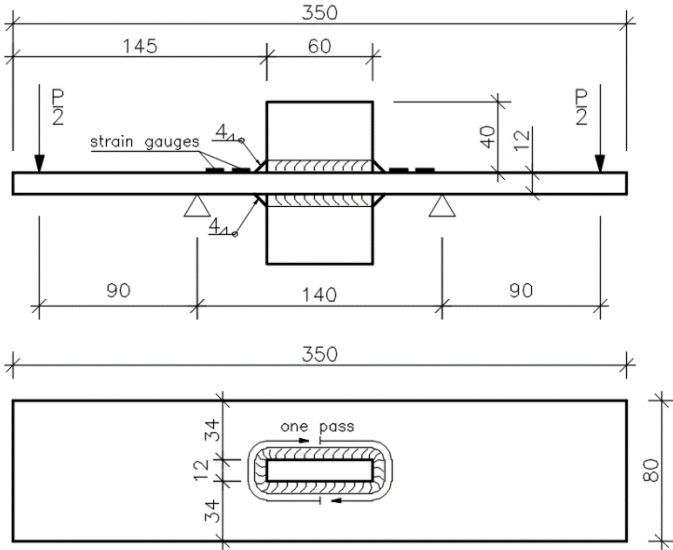
FIGURE 4. Geometry of specimen in test series 2

TABLE 1. Chemical composition

Chemical composition [%]							
C	Mn	Si	S	P	Cr	Ni	Cu
0.16	1.43	0.39	0.011	0.017	0.04	0.022	0.031
Al	N	V	Mo	Ti	As	Nb	C_{eq}
0.041	0.0056	0.0315	0.0026	0.0022	0.003	0.013	0.41

TABLE 2. Mechanical properties

Yield stress	Tensile strength	Elongation
415 MPa	540 MPa	28.5 %

The aim of this test series is to establish a model that predicts the number of cycles to crack initiation based on local approach with multiaxial fatigue criterion. Fatigue testing will be carried out with load ratio $R > 0$, hence, crack is expected to appear on the upper surface of the main plate at ends of the attachment. Thus, there are only two areas of about 20mm long that require crack monitoring. Before fatigue testing local weld toe geometry of these areas will be measured using Alicona optical measurement system. Moreover, profile replica of these areas will be made using polyether impression material and after completed test the mold will be cut exactly at the location of crack initiation and weld toe profile will be obtained utilizing digital camera with high magnification. Detection of crack initiation and crack growth monitoring system based on ACPD

method will be utilized. All these detailed monitoring systems and replica methods will permit us to complete the initiation phase model.

5 MODELING THE TIME TO CRACK INITIATION

The attempt to model the entire damage evolution has thus far mainly been based on applied fracture mechanics. The most common approach is based on Paris law. This procedure assumes existence of initial small crack, which can be true in many welded joints, but the size of this crack is disputed because in real cases the size of initial flaws are so small that cannot be considered using LEFM. On the other hand Paris law is valid only for stress intensity factor ranges greater than the certain threshold value of SIFR, below that value crack growth will not occur. The concept of this threshold value is usually based on experiments with long cracks, typically several mm in a compact tension specimen. However, shallow cracks can growth considerably faster if they develop in notch plasticity area or follow nearly the same growth rate as in stable growth region if they develop in notch elasticity area. This is presented in Figure 5.
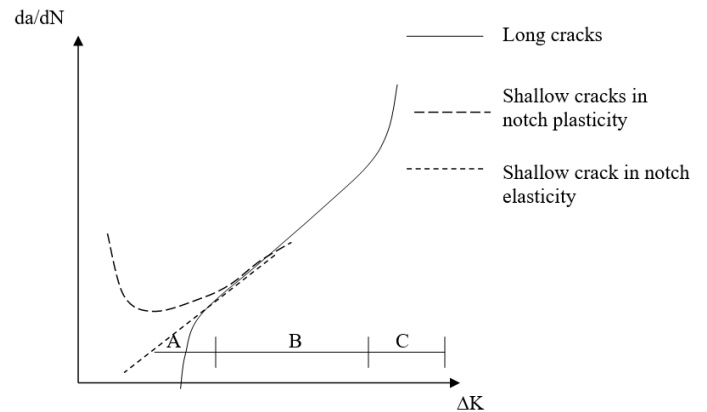
FIGURE 5. Likely growth curves for shallow cracks at weld notches compared with long crack behaviour [10].

The premise for splitting damage evolution process into two phases is fact that different damage mechanism occurs during crack initiation/early crack evolution and crack growth phase. In the first phase damage mechanism is governed by shear stresses whereas normal stresses (perpendicular to crack plane) cause the crack propagation in analyzed loading mode, ie. crack growth mode I (crack opening). The omission of the crack initiation phase results in forced assumption of unreasonable initial crack size and can even lead to the inapplicability of LEFM. It is also desirable to use multiaxial crack initiation criterion (e.g. Dang Van criterion, Fatemi-Socie criterion) in the first phase because stress state in the vicinity of the weld is multiaxial in real structures.

One of the oldest approach for predicting number of cycles to crack initiation in welded joints, used in Two Phase Model, is the Coffin-Manson equation with Morrow's mean stress correction. This model was first proposed by Lawrence and

Young [11] and later modified and calibrated against experimental results (test series 1) by Lassen and Recho [9, 12]. In this model crack initiation criterion can be expressed as:

$$\frac{\Delta\varepsilon}{2} = \frac{(\sigma_f' - \sigma_m)}{E}(2N_i)^b + \varepsilon_f'(2N_i)^c \qquad (2)$$

where $\Delta\varepsilon$ is the local strain range, σ_m is the local mean stress, parameters b and c are the fatigue strength and ductility exponents, and σ_f' and ε_f' are the fatigue strength and ductility coefficients respectively. The local stress-strain behavior is given by the Ramberg-Osgood equation and Massing's hypothesis concerning hysteresis loop, established for stabilized cyclic stress-strain curve:

$$\Delta\varepsilon = \frac{\Delta\sigma}{E} + 2\left(\frac{\Delta\sigma}{2K'}\right)^{\frac{1}{n'}} \qquad (3)$$

where K' and n' are the cyclic strength coefficient and strain hardening exponent respectively. There is one major disadvantage of this approach – Coffin-Manson equation concerns uniaxial stress state whereas at the weld toe region, even under simple loading conditions, stress state is multiaxial. To overcome this disadvantage multiaxial fatigue criterion can be used. As an example a critical-plane-based criterion proposed by Fatemi and Socie for materials exhibiting shear failure mechanisms [13]. The Fatemi-Socie criterion predicts number of cycles to crack initiation in terms of shear fatigue properties as given in the following equation:

$$\frac{\Delta\gamma_{max}}{2}\left(1 + k\frac{\sigma_{n,max}}{\sigma_y}\right) = \frac{\tau_f'}{G}(2N_i)^{b_0} + \gamma_f'(2N_i)^{c_0} \qquad (4)$$

where $\Delta\gamma_{max}$ is the maximum range of shear strain at any plane, $\sigma_{n,max}$ is the maximum normal stress occurring on the same plane during a load cycle, σ_y is the material yield stress, k is a material dependent parameter reflecting the influence of normal stress on fatigue damage, and τ_f', b_0, γ_f', c_0 are shear fatigue properties [14]. However, criteria based on critical plane approach are very computationally expensive, thus, criteria that allow to take into consideration stress multiaxiality in a different manner giving better trade-off between accuracy and computational cost are preferable. As an example Dang Van criterion can be used for this purpose. This criterion will be presented in more detail since it will be used later for analysis test results of both test series.

Dang Van [1-3] proposed crack initiation criterion for multiaxial high cycle fatigue for materials in which cracks are initiated by local plasticity at the level of grains (metallic materials). In the original version it concerns only endurance limit using shear stress amplitude and hydrostatic stress during a loading cycle. However, by introducing equivalent shear stress amplitude it can be also used to predicting crack initiation and establishing S-N curve. The main premise in the Dang Van hypothesis is the fact that crack initiation occurs

within individual grains and it is caused by shear stresses. Moreover, the positive hydrostatic stress causes opening of the microcracks, which facilitates their formation, whereas negative value induces closing of the microcracks. Therefore, these two factors were chosen as having a major influence on crack initiation and linear function of these parameters was proposed. The safety region (endurance domain) can be describe by equation

$$\tau_a + \alpha \cdot \sigma_h \leq \tau_0 \qquad (5)$$

where τ_a is shear stress amplitude, σ_h is maximum hydrostatic stress, α and τ_0 are material parameters which can be determined by simple fatigue tests (τ_0 for instance corresponds to the fatigue limit in simple shear). Thus, the fatigue limit curve is a straight line in the $\tau_a - \sigma_h$ space and proportional loading generates straight line loading paths (Figure 6).
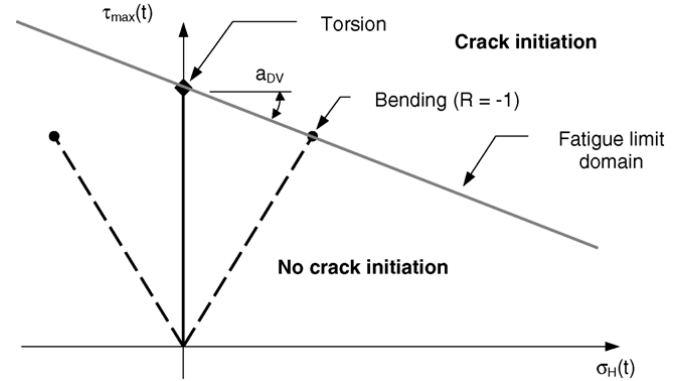
FIGURE 6. The Dang Van diagram: a scheme of typical calibration with bending and torsion fatigue test [15]

For multiaxial non-proportional loading cycle the loading path is a closed curved loop and it should not cross the limit line at any time during the load cycle in order to be in a safety region, it is shown in Figure 7.
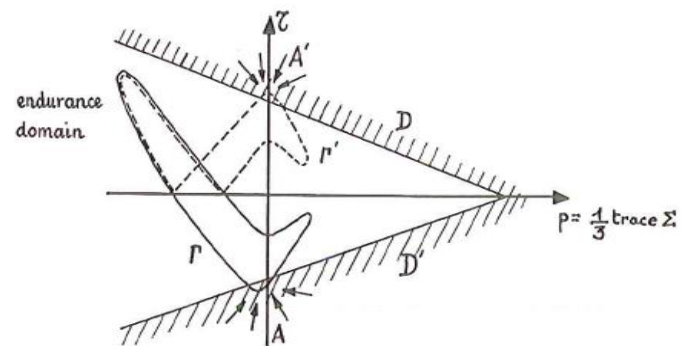
FIGURE 7. Endurance domain and complex loading path [1]

In some cases of complex loading cycle it is difficult to determine what is an amplitude of shear stress and what is a mean value at any moment of the load cycle which causes problems with presentation of the load path in the $\tau_a - \sigma_h$

space. In those cases another formulation of Dang Van fatigue criterion was proposed based on a two-scale approach, macroscale and mesoscale, using new parameter called a mesoscopic stabilized residual stress tensor in the latter scale. The criterion is postulated in mesoscale as

$$\tau_{max}(t) + \alpha \cdot \sigma_h(t) \leq \tau_0 \qquad (6)$$

where $\tau_{max}(t)$ are $\sigma_h(t)$ are the maximum shear stress and hydrostatic stress at time t of the load cycle computed from the stress tensor in mesoscale. The macro- and mesoscale stresses are related as

$$\sigma(t) = \Sigma(t) + \text{dev}\rho \qquad (7)$$

where ρ is the stabilized residual stress tensor, $\sigma(t)$ and $\Sigma(t)$ denotes stress tensor in meso- and macroscale respectively. In equation (7) only deviatoric part of ρ appears because residual stress field may be considered to be purely deviatoric, assuming that only deviator part of stress tensor affects yield. As has been explained in more detail in [16], the determination of the residual stress tensor is achieved by finding the center of the smallest hypersphere in six-dimensional deviatoric stress space which completely circumscribes the load path. Mathematical formulation of this statement is minmax problem

$$\rho = \min_{\rho^*} \max_t \left[J_2(\text{dev}\Sigma(t) - \text{dev}\rho^*) \right] \qquad (8)$$

where J_2 denotes the von Mises norm. Then $-\text{dev}\rho$ represents the center of this hypersphere. Solution of this problem, and thus $\text{dev}\rho$ tensor, can be found numerically using iterative method [16, 17]. According to [18] in proportional loading the residual stress tensor ρ can be computed from the opposite value of the average of two extreme macroscopic stress tensors

$$\rho = -\frac{1}{2}\left(\Sigma(t_1) + \Sigma(t_2)\right) \qquad (9)$$

where t_1 and t_2 designates the two time instants at which the extreme values of the macroscopic stress Σ is obtained.
Maximum mesoscopic shear stress $\tau_{max}(t)$ is determined using Tresca hypothesis and can be expressed as

$$\tau_{max}(t) = \frac{1}{2}|\sigma_I(t) - \sigma_{III}(t)| \qquad (10)$$

where $\sigma_I(t)$ and $\sigma_{III}(t)$ are principal stresses of mesoscopic stress tensor $\sigma(t)$ arranged in descending order, $\sigma_I(t) \geq \sigma_{II}(t) \geq \sigma_{III}(t)$. Mesoscopic hydrostatic stress value equals macroscopic hydrostatic stress and is easy to calculate

$$\sigma_h(t) = \frac{1}{3}\text{trace}\left(\Sigma(t)\right) \qquad (11)$$

Damage lines can be determined by testing for any number of cycles to crack initiation N_i in high cycle fatigue regime (Figure 8). When the fatigue life decreases, there is a substantial decrease in α at the same time as an increase in τ_0 [1] (see eq. (5) and eq. (6)).
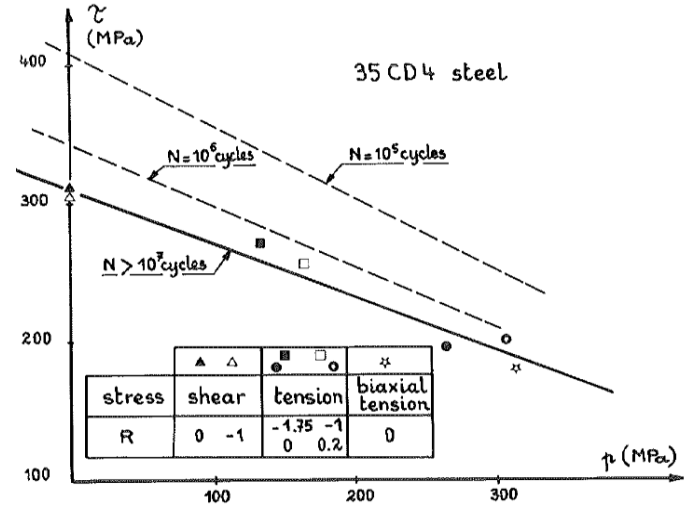
FIGURE 8. Dang Van diagram: damage lines for different number of cycles [1]

According to [3] it is possible to establish S-N curves using local equivalent shear stress $\tau_{0,i}$ for a life duration N_i defined by

$$\tau_{0,i} = \tau_a + \alpha_i \cdot \sigma_h \qquad (12)$$

It is observed that for high cycle fatigue $(N_i > 5 \times 10^5)$ α_i depends weakly on N_i so it can be assumed constant value of $\alpha_i \approx \alpha$ and then we define local equivalent shear stress amplitude by

$$\tau_0 = \tau_a + \alpha \cdot \sigma_h \qquad (13)$$

The second term on the right hand side in equation (11) is also capable of taking into account residual stress situation and/or mean stress effect in a simplified manner - by hydrostatic stress term. An example of such S-N curve is shown in Figure 9. For this case the fatigue life is defined as the number of cycles to reach a crack depth of 0.5 mm. It should be noted that in this example (Figure 5) the entire fatigue life was modelled by applying the Dang Van's stress definition. The intention in the present work is to utilize it only for crack initiation phase in the local weld toe region. The parameters of the local weld toe geometry – transition angle and radius - are supposed to have a substantial influence on crack initiation. The bigger angle and/or the lower radius the higher stress concentration at the weld toe occurs. Since these parameters are randomly distributed there are few approaches to dealing with the variable weld toe geometry. The oldest, proposed by Radaj [19], uses fixed value of the radius $\rho_f = 1$ mm which allows the local stress state to be analyzed directly without requiring actual SCF at the weld toe notch. This fictitious radius can be used for design purposes as the worst case, however, geometry

measurements of test series 1 reveal that the minimum radius found in real weld toes is as low as 0.1 mm.
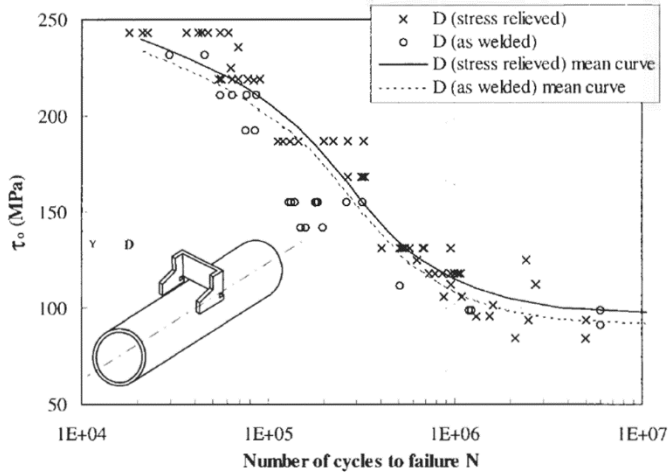
FIGURE 9. S-N diagram for stress relieved and as-welded samples [3]

The second approach is to treat the geometry parameters as random variable and based on extreme value statistics predicts the worst case that most likely may occur. Using this approach minimum radius $\rho = 0.42$ mm was determined and together with mean value of angle θ was used for prediction of the crack initiation. The third, that will be corroborated by test series 2, links the initiation life with weld toe geometry exactly at the location of crack initiation. The advantage of this method is the possibility of taking into account the variety of weld toe geometry generated by different welding procedures as well as post-weld improvement techniques (toe burr grinding) which is very important for high quality welds. Since the parameters of the Dang Van model will be determined by fatigue tests of test series 2, at current stage mean curve was estimated based on a somewhat reverse approach. Number of cycles to crack initiation was found according to the following procedure. For selected nominal stress ranges (45÷240 MPa) total fatigue life predicted by RFLM method were calculated. Subsequently, number of cycles spent in crack propagation phase was estimated and subtracted from total fatigue life. Details of prediction of crack propagation are presented in chapter 6. Crack initiation period is confirmed only for $\Delta S = 150$ MPa by test series 1. For this stress range the mean value from all specimens is used ($N_i = 150\,000$). Afterwards, maximum equivalent shear stress amplitude at the weld toe was calculated using FEM analysis for assumed weld toe geometry ($\rho = 0.5$ mm, $\theta = 55°$) and assumed $\alpha = 0.33$ in the Dang Van's stress definition. Value of this parameter has to be confirmed by test series 2. Obtained data points are marked as red squares in Figure 10. Mean curve of crack initiation based on the same equation type as used in RFLM, obtained by fitting parameters β_0, β_1, μ_v, is also presented in Figure 10. This curve is used later for constructing S-N curve in chapter 7. The curve gradually changes in slope, hence it gives high initiation lives at low stress ranges as expected. This initiation life will be dependent on the steel yield stress. This is not the case with the propagation phase in the next section.
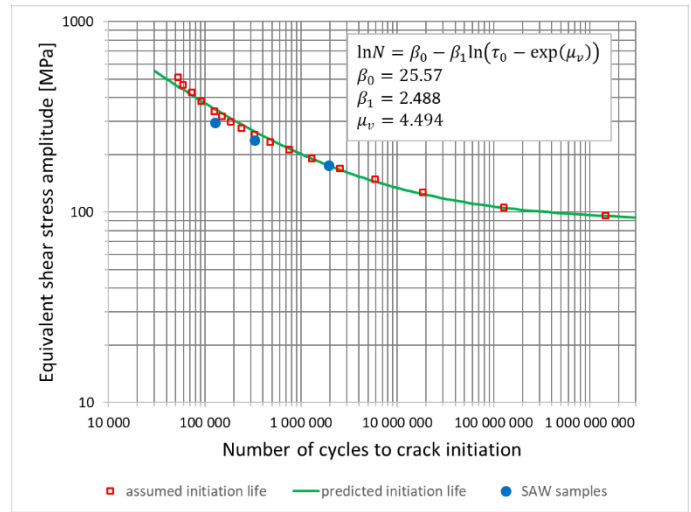
FIGURE 10. Crack initiation mean curve

Specimens in test series 1 were fabricated using four different welding procedures, details are presented in [8]. 10 samples were made using Submerged Arc Welding procedure (SAW). This procedure gave a peculiar local weld toe geometry and for this reason SAW group of samples was excluded from test series 1. Detailed statistics is presented in Table 3.

TABLE 3. Statistics for local weld toe geometry

Test series	Welding procedure	Weld toe angle θ [°]		Weld toe radius ρ [mm]	
		mean	standard deviation	mean	standard deviation
1	FCAW SMAW57 SMAW76	58	9	1.6	0.7
1a	SAW	34	14	0.5	0.3

The mean total fatigue life of this group is 840 000 cycles and the mean initiation life is 330 000 cycles. In this group were some specimens that have very low transition angle $\theta \approx 20°$ while others have $\theta \approx 55°$. The explanation of this difference is that the weld bead, built up using two-passage sequence, in some specimens was not influenced by the second layer at the weld toe on the main plate, it is shown schematically in the left bottom corner of Figure 1. In order to check how crack initiation model behaves to changes in the weld toe geometry the following numerical test was performed. Three cases were simulated – for $\theta = \{34°, 20°, 55°\}$ – and obtained equivalent shear stress amplitudes were linked with mean crack initiation life and minimum/maximum value from testing, respectively. For all three cases mean value of the $\rho = 0.5$ mm was used. Results are plotted in Figure 10 - marked as green dots. As can be seen, results lie not too far from the predicted mean curve. Within test series 2 few specimens will be machined using spherical burr grinders of different radii in order to better fit the crack initiation model to local weld toe geometry effects.

8

6 MODELING THE CRACK PROPAGATION

In the foregoing section the time to reach a crack depth of 0.1 mm was modelled. The Dang Van model that takes account for a multiaxial stress situation including residual stresses was applied. In the present section we shall model the subsequent crack growth from $a = 0.1$ mm to final fracture. For this growth phase we shall apply classical fracture mechanics based on the Paris propagation law. The model is applied for a uniaxial stress situation where the crack planes are assumed to be normal to the largest applied principal stress range. The applied load ratio R will be explicitly taken into account by applying the unique growth rate curve as suggested by Huang, Moan and Cui [4]. Hence, we have reduced our model to be uniaxial and not multiaxial as for the model for the initiation phase. The argument for doing so is that once the crack has nucleated it will be the largest principal stress that is dominant. We are still able to model the influence of the welding residual stresses perpendicular to the crack planes. When adding on the present crack propagation phase to the crack initiation phase, it will be possible to determine the complete evolution of the damage evolution. This will allow us to construct S-N curves that are in agreement with the curves in rules and regulations. The advantage of the present constructed curves is that the influencing parameters are given explicitly by the two-phase model. As a consequence any changes in parameters such as joint geometry, residual stresses of applied R ratio are readily accounted for. Although there are fewer novelties in the present fracture mechanics approach than in the proposed multiaxial initiation phase model, the present propagation model will bring some light on two important topics:

- The applied unique growth rate curve model has been validated by tests carried out with rather large central cracks (5-20 mm) in plate specimens. It is interesting to verify that the model also is capable of modelling the growth of small surface cracks (down to 0.1 mm) emanating from the weld toe

- The influence of threshold value for the SIFR in the unique growth rate curve has also been validated for long central crack in plates. It is particularly interesting to see of this retardation of crack growth remains the same for small cracks at the weld toe.

We will get clear indications on these two issues by fitting the model to the a-N curves obtained from test series 1 described in section 4. Before doing so we will give a short overview of the model.

In available standards and regulations, it is recommended to use Paris Law for modelling of crack propagation after a crack has initiated [20, 21]. The general equations for calculating the crack growth rate of a semi elliptic surface crack is given as:

$$\frac{da}{dN} = C_a (\Delta K_a)^m \qquad (14)$$

$$\frac{dc}{dN} = C_c (\Delta K_c)^m \qquad (15)$$

where a is crack depth and c is crack length. C and m are the crack growth parameters which has slightly different recommendations in different standards. ΔK_a is the stress intensity factor range for the deepest point of the crack and ΔK_c is the stress intensity factor range for the surface points of the crack, see figure 11.

The growth rate of a semi elliptic surface crack at the weld toe is mainly governed by the shape of the crack and the local weld toe geometry, as well as the loading. These are parameters that influence the stress intensity at the crack tips, and are thus accounted for in the SIFR. When considering only membrane loading, the SIFR can be expressed as follows when taken into account the effects of the cracks geometrical deviations from the reference case, M_m, and the weld toe magnification factor M_{km} DNVGL [21]:

$$\Delta K = \Delta \sigma M_m M_{km} \sqrt{\pi a} \qquad (16)$$

The geometrical correction factor M_m, for a semi elliptic surface crack is determined based on the plane plate K values provided by Newman and Raju [5, 6] as:

$$M_m = [M_1 + M_2(a/T)^2 + M_3(a/T)^4] \frac{g \times f_\varphi \times f_w}{\Phi} \qquad (17)$$

where the input parameters M_1, M_2, M_3, g and f_φ are dependent on the a/c ratio.

The finite width correction is given as:

$$f_w = \sqrt{sec\left((\pi c/w) * \sqrt{(a/T)}\right)} \text{ for } 2c/W \leq 0.8 \quad (18)$$

And the complete elliptical integral is given as:

$$\Phi = \sqrt{\left[1 + 1.464(a/c)^{1.65}\right]} \text{ for } 0 \leq a/2c \leq 0.5 \quad (19)$$

and

$$\Phi = \sqrt{\left[1 + 1.464(c/a)^{1.65}\right]} \text{ for } 0.5 \leq a/2c \leq 1.0 \quad (20)$$

The weld toe magnification factor is based on Bowness and Lee who developed this formula during an extensive investigation of stresses at the crack front. The work was done with 3-dimensional solid models, and the resulting formula is dependent on the attachment footprint L, the angle of the weld θ and the depth and length of the crack, a and c.
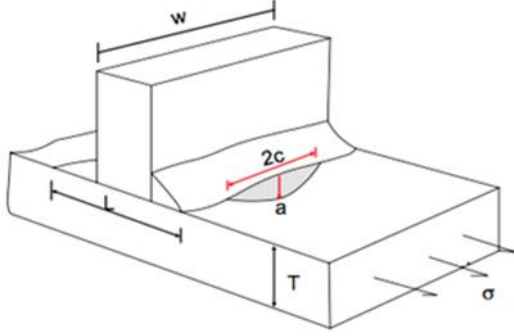
FIGURE 11. Fillet welded joint with elliptical surface crack at the weld toe

The formula reads as follows for the deepest point a and the surface points c:

$$M_{kma} = f_1\left(\frac{a}{T},\frac{a}{c}\right) + f_2\left(\frac{a}{T},\theta\right) + f_3\left(\frac{a}{T},\theta,\frac{L}{T}\right) \qquad (21)$$

$$M_{kmc} = f_1\left(\frac{a}{T},\frac{c}{a},\frac{L}{T}\right) f_2\left(\frac{a}{T},\frac{a}{c},\theta\right) f_3\left(\frac{a}{T},\frac{a}{c},\theta,\frac{L}{T}\right) \qquad (22)$$

The input parameters for Bowness and Lee's formulas are adopted in DNVGL-RP-C210 [21] and are used directly as described therein, based on the physical parameters of the joint subject to investigation.

As can be seen, the a/c ratio has a high influence on the stress intensity factor range. Hence the choice of initial crack sizes a_{ini}, c_{ini}, which is subject to debate amongst scientists, will influence the result. a_{ini} for the crack propagation used in the two-phase model is based on the modelling in chapter 5, which gives the number of cycles to $a = 0.1$ mm. An initial a/c ratio is assumed to be $a/c = 0.2$.

Many recent papers have pointed out that the R-ratio and residual stresses has a significant effect on crack growth rate, and that it is difficult to account for this by using Paris Law as given by equations (14) and (15) [4]. Huang, Moan and Cui has proposed a solution for this by introducing a 'unique crack growth rate equation', which uses the ESIFR or ΔK_E as the driving force. The unique crack growth rate equation is given by the following expressions for the deepest point of the crack, and is similar for the surface points:

$$\frac{da}{dN} = C(\Delta K_E^m - \Delta K_{th0}^m) \qquad (23)$$

$$\Delta K_E = M\Delta K \qquad (24)$$

$$\Delta K_{th0} = M\Delta K_{th} \qquad (25)$$

$$M = \begin{cases} (1-R)^{-\beta_1} & -5 \le R < 0 \\ (1-R)^{-\beta} & 0 \le R < 0.5 \\ (1.05 - 1.4R + 0.6R^2)^{-\beta} & 0.5 \le R < 1 \end{cases} \qquad (26)$$

$$R = \frac{K_{min}+K_R}{K_{max}+K_R} \qquad (27)$$

The proposed value for β for high strength steel is 0.7 whereas $\beta_1 = 1.2\beta$. A general equation for determining β for structural steel has also been proposed:

$$\beta = 0.22 + \frac{0.65}{1 + 0.0035 \cdot \Delta K^4} \qquad (28)$$

Huang, Moan and Cui have calibrated the equations against BS7910 and have recommended the following equation for crack growth rate for welded details (units MPam$^{1/2}$, mm):

$$\frac{da}{dN} = 8.32 \times 10^{-9}\left(\Delta K_E^{2,88} - 7.2^{2,88}\right) \qquad (29)$$

Where 7.2 MPam$^{1/2}$ is the threshold value for the SIFR at R=0. The ΔK_E is the equivalent SIFR at R=0 that will give the same crack growth as ΔK at the given R value. The values of C and m are for all application of the equation pertaining to the R=0 condition.

The model proposed by Huang, Moan and Cui is in the present work fitted to the measured crack propagation data from test series 1 presented in section 4. Paris Law as described in DNVGL-RP-C210 with the crack growth parameters recommended by DNV is also used for comparisons. A typical measured a-N curve close to the mean curve is chosen for comparison. The model is applied both with and without the term containing the threshold term in the growth equations. The goal is to verify if the concept of a fatigue threshold is valid for the small crack growth. The following data are applied:

$L/T = 2.0$
$\theta = 58°$ (mean value)
$\Delta\sigma = 150$ MPa
$R = 0.35$
$\Delta K_{th0} = 0$ MPam$^{0.5}$
$a_0 = 0.1$ mm
$a_0/c_0 = 0.2$

The equation (28) is applied for calculating the β value. The alternative would be to keep it constant at β=0.7. The results obtained by the unique growth rate curve are shown in Figure 12. Both the crack depth and crack length development are in good agreement with the observations from the test. The aspect ratio a/c was set to 0.2 from the beginning and ended at 0.42 when the crack depth reached half the plate thickness. The fatigue life is then exhausted. The predicted growth in the crack length direction seems a bit underestimated. Larger values of c were found in the test specimens, however, the reason may be that several cracks had joined into a larger one by coalescence. The crack depth is compared with measured curves in Figure 13. The total experimental fatigue life was 470 000 and the initiation period was determined to 150 000 cycles. The propagation phase is then 320 000 cycles, whereas the mean

model curve based on equation (29) predicts 370 000 cycles. It is however noticed that the shape of the modelled curve is somewhat different in the way that the experimental curves has a more pronounced acceleration towards the end of the life. A better fit in the crack growth range between $a = 2\,\text{mm}$ and $a = 8\,\text{mm}$ would have been obtained by increasing the m values towards 5 and reducing the C value accordingly to get the final propagation life. But this discrepancy may vary from specimen to specimen due to the variability in weld toe geometry and local material microstructure.
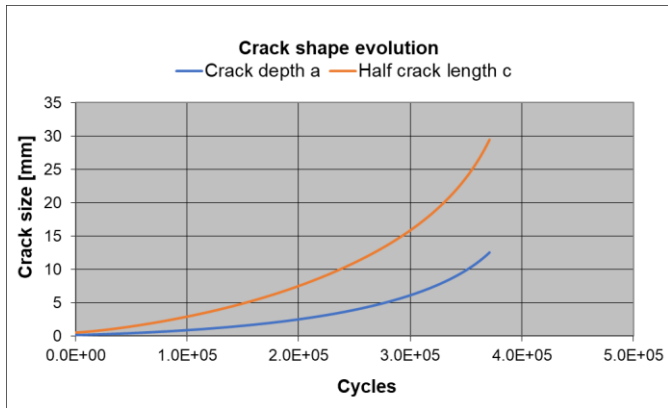
FIGURE 12. Crack growth median prediction with $a_i = 0.1\text{mm}$
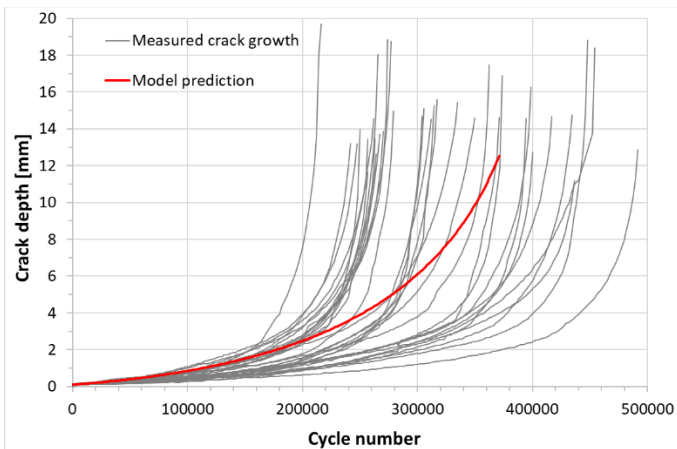
FIGURE 13. Modelled and measured experimental crack depth growth histories with $a_i = 0.1\text{mm}$

If the model is changed to take account for the threshold value for the SIFR, i.e. $\Delta K_{th0} = 7.2\,\text{MPam}^{0.5}$, this will not change the results shown in Figure 12 and Figure 13 significantly. The reason is that the applied SIFR is so much higher than the ΔK_{th0} for the experimental cases that has $\Delta\sigma = 150\,\text{MPa}$. However, if we choose to lower the applied stress range below 150 MPa the propagation life will increase towards infinity already at 118 MPa. If we had kept β constant at 0.7 the corresponding figure will be 100 MPa, i.e. the β value has an important influence on the predicted fatigue limit. If we compare these values with the fatigue limit for the F class this seems too optimistic. We will visualise this in the next section 7 where we

will construct S-N curves by the two-phase model. Hence, this indicates that fatigue crack retardation observed for long central cracks at low values for the SIFR may not take place for small surface cracks at the weld toe. This is a known phenomenon for small cracks under elastic-plastic notch conditions. Small crack under such condition may accelerate even at low a SIFR. The present finding indicates that even under elastic notch condition at the weld toe retardation may not take place, see Figure 5. By overlooking this fact one may overestimate the fatigue propagation life significantly.

7 CONSTRUCTING S-N CURVES FROM THE MODEL

The purpose of the present section is to corroborate the results obtained by the two-phase model against the huge data base that is reflected in the S-N curves found in rules and regulations. This is done in two different manners:

- The category 71 (F class) is applied directly for comparison
- The present test series 1 is supplemented by some additional life data at lower stress levels

The purpose of including life data points directly is to be able to determine our own S-N curves and not be constrained by the bi-linear curves found in rules and regulations. The present two- phase model will give a non-linear S-N curve for a log-log scale. The curve will gradually change slope as the stress range is decreasing towards what earlier on was believed to be the fatigue limit. This shape is in line with the life data analysis carried out by the Random Fatigue Limit Model [23]. The basic equation reads:

$$\ln(N) = \beta_0 - \beta_1 \ln(\Delta S - \gamma) + \varepsilon \qquad (30)$$

where ln denotes the natural logarithm and $\gamma = \Delta S_0$ is the fatigue-limit. The parameters β_0 and β_1 are fatigue curve coefficients.
The advantage of this model is that it is handling both the fatigue life and the fatigue limit as random variables simultaneously. Furthermore, it has the ability of including run outs in a logical manner as it is based on a maximum likelihood technique. For comparison we have chosen the category 71 as suggested by IIW where the former fatigue limit has been replaced by a line segment that has a shallow slope of $m = 22$. We shall confine ourselves to work with the median curves.
The data points and the associated curves are shown in Figure 14. The very upper curve is the one obtained by modeling the crack propagation phase only and including the threshold term in the Paris equation, see the discussion at the end of section 6. As can be seen from the figure this upper curve is too optimistic compared to the collected data points and S-N curves. It has a horizontal asymptote just below a stress range of 118 MPa whereas the knee point of the IIW curve is below 60 MPa. As can be seen from figure 14 the

curves obtained from two-phase model and the RFLM analyses are quite close. The curves fit the data points better than the IIW curve, but more data should be collected.

FIGURE 14. Life data and constructed S-N curves compared with rule based curves

As the present two-phase model is based on applied mechanics for both phases the parameters that have an influence fatigue damage evolution are directly entering into the model. Any change in these parameters can then be explicitly taken into account in logical and rational manner for fatigue life pr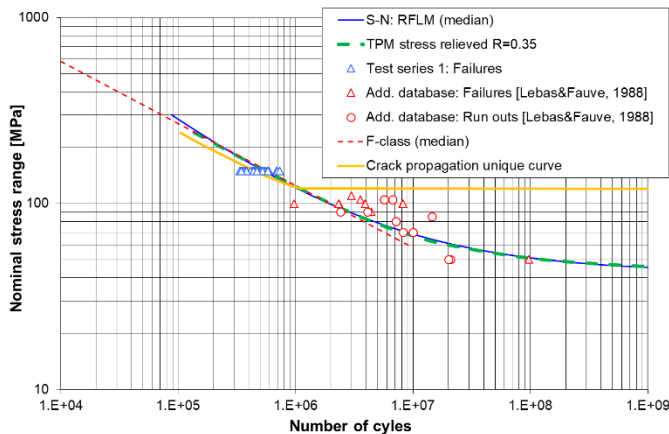edictions. This is not the case with the rule based S-N curves that are based on pure statistical treatment of the bulk fatigue life. For this reason the two-phase model will be kept as it is, the constructed S-N curves are just for verification of the model.

8 DISCUSSSION AND CONCLUSIONS

The common engineering tools for fatigue life predictions and fracture control is the rule based S-N curves and applied fracture mechanics based on the Paris law. The S-N curves are treating the entire fatigue life without making any distinction between the different damage mechanisms involved. Based on linear regression bi-linear curves have been obtained based on the belief that there existed a fatigue limit. Recent re-analyses of life data have proven this this in not likely to be true. Furthermore run-outs are not easy to handle with the traditional statistical approach. In fracture mechanics modelling the assumption is usually also that the entire fatigue life can be modeled by Paris law. The problems that arise with this approach is that one then has to apply an unknown fictitious initial crack depth in the model to get agreement with S-N life data. In general these cracks are so small that the Paris law has never been proven to be applicable for these crack sizes. This is particularly also true for the threshold value for the SIFR. These crack depths are also so small that it is outside the range of the geometry functions entering the calculations of the SIFR. On this background an attempt has been made to model the entire fatigue damage evolution in welded steel joints. The

focus has been on the case where cracks nucleate and subsequently propagates from the notch of the weld toe. The model is based on three approaches:

- The total fatigue life is modelled by the RFLM method.

- The crack initiation phase defined as number of cycles to reach a crack depth of 0.1 mm is modelled by the Dan Van multiaxial stress concept at the local toe notch. The shear stress variation at the critical plane is the prime variable.

- The subsequent crack growth phase from 0.1 mm to final fracture is based on the Paris law and the unique crack growth rate curve method is adopted.

The advantage of the RFLM is that it is easy to include run-outs in the data set. The model gives a non-linear S-N curve for a log-log scale and may reject the existence of a fatigue limit. The obtained curve may continue to drop between 10^7 and 10^8 cycles. This fits the experimental facts given by the collected life data better than the traditional bi-linear curve.

The measured early crack growth in test series 1 has proven that the crack initiation phase as defined above is substantial, typical 30% of the entire fatigue life at a stress range of 150 MPa. At lower stress ranges it is the author's hypothesis that the initiation phase will become dominant. The Dang Van equivalent approach for this phase makes it possible to account for multiaxial stress situations, applied R ratio and the presence of welding residual stresses. It is the author's belief that the Dang Van approach better reflects the actual damage mechanism during this crack nucleation phase. Furthermore, the problem of selecting a small initial fictitious crack depth outside the validity of applied fracture mechanics is circumvented. However, the Dang Van approach makes it very important to characterize the irregular local weld toe geometry accurately. This is a stiff challenge. An extreme value statistics model for the toe radius has been suggested. It remains to complete test series 2 for final determination of all the parameters in the model.

The adopted fracture mechanics model based on the unique crack growth curve seems to fit the measured crack growth in test series 1 quite well at the given R ratio of 0.35. The threshold term in the basic equation in the model has no influence on the growth history at this high stress range level of 150 MPa. However, the model seems to predict the crack retardation at a much too early stage when the stress range is decreased. The model will predict a fatigue limit close to 120 MPa which is too optimistic compared with the category 71 S-N curve and collected life data in the present work. A more proper selection of the parameter β may solve the problem, but as the fatigue limit is decreased, the finite fatigue life for higher stress ranges will also decrease. Huang et al. [4] suggested that R should be set as high as 0.9 for as welded joint to obtain the right threshold value by the model. This is again

verified by measurements with long central cracks. However, if this R value is applied for shallow cracks at the weld toe the growth model will underestimate the fatigue life significantly at higher stress ranges compared with the S-N curves. These matters should absolutely be looked more thoroughly into to clarify the situation. Meanwhile, the present two-phase model will use the unique crack growth rate curve model without the threshold term for small elliptical cracks at the weld toe. Long fatigue lives will then be explained by long time to crack initiation as predicted by the Dang Van approach and not by a crack retardation based on the fracture mechanics threshold concept for the SIFR. Furthermore, when post weld improvements methods such as needle peening are applied the time to crack initiation becomes dominant.

The present work has focused on modelling the mean fatigue life. Probability distributions for the fatigue life shall be obtained at a later stage. For the crack initiation phase this will be obtained by the statistics given for the toe geometry variables and scatter in material properties.

9 SUGGESTIONS FOR FUTURE WORK

The results obtained by the present two-phase seem promising for constant amplitude loading. The model is capable of fitting the time to crack initiation and subsequent crack growth from test series 1 and construct S-N curves that are in agreement with life data at different stress levels. As already stated it remains to elaborate the Dang Van model for the crack initiation phase by the results from ongoing test series 2.

So far the model has been confined to model the fatigue damage evolution under constant amplitude stresses. An important issue will be to address the case with variable amplitude stress histories. At the present the rule based S-N curves give quite large uncertainty for this case, particularly when the applied stress ranges are in the stress regime pertaining to the lower line segment of the S-N curve that starts at $N=10^7$ cycles in air . This line segment has been given an inverse slope of 2m-1 where m is the inverse slope of the upper line segment. Whereas the upper slope is determined with high accuracy by linear regression of constant amplitude life data, the lower slope is determined for variable amplitude stresses under the assumption that there exist a fatigue limit and that this limit can be determined by the threshold concept for the SIFR, Haibach [24]. As has been shown in the present work this hypothesis is questioned. Furthermore, it is the author's intention to improve the accuracy under such variable amplitude stresses by the present proposal with separation of the involved damage mechanisms. This separation will also make it easier to model the effect of post weld improvements techniques. Finally, scatter in fatigue life has to be accounted for by applying reliability functions.

REFERENCES

[1]   Dang Van, K., et al., 1989, "Criterion of High Cycle Fatigue Failure Under Multiaxial Loading", Biaxial and Multiaxial fatigue (Edited by M. W. Brown and K. J. Miller), Mechanical Engineering Publications, London, pp. 459-478

[2]   Dang Van, K., Bignonnet, A., Fayard, J. L., Janosch, J. J., 2001, "Assessment of welded structures by a local multiaxial fatigue approach", Fatigue and Fracture of Engineering Materials and Structures, **24**(5), pp. 369–376

[3]   Dang Van, K., Bignonnet, A., Fayard, J-L., 2003, "Assessment of welded structures by a structural multiaxial fatigue approach", Biaxial/Multiaxial Fatigue and Fracture, (Editors: Carpinteri A., M. de Freitas, Spagnoli A.), ESIS Publication, **31**, Elsevier, pp. 3-21

[4]   Huang, X., Moan, T., Cui, W. A., 2009, "Unique crack growth rate method for fatigue life prediction of steel structures", Ship and offshore structures, **4**(2), pp. 165-173

[5]   Newman, J. C., Raju I. S., 1983, "Stress intensity factor equations for cracks in three-dimensional finite bodies", Fracture Mechanics: 14th Symposium. Vol. I: Theory and Analysis, Philadelphia: ASTM STP 791, pp. 238-265

[6]   Newman, J. C., Raju I. S., 1981, "An empirical stress intensity factor equation for the surface crack", Engineering Fracture Mechanics, **15**(1–2), pp. 185–192

[7]   Bowness, D., and Lee, M.M.K., 2000, "Prediction of weld toe magnification factors for semi-elliptical cracks in T-but joints", International Journal of Fatigue, **22**(5) pp. 389-396

[8]   Lassen, T., 1990, "The effect of the welding process on the fatigue crack growth in welded joints", Welding Journal, pp. 75s-85s

[9]   Lassen, T., Recho, N., 2009, "Proposal for a more physical based S-N curve for welded joints", International Journal of Fatigue, **31**, pp. 70-78

[10] Lassen, T., Recho, N., 2006, "FLAWS Fatigue Life Analysis of Welded Structures", ISTE

[11] Yung, J. Y., Lawrence, F. V., 1985, "Analytical and graphical aids for the fatigue design of weldments", Fatigue and Fracture of Engineering Materials and Structures, **8**, pp. 223-241

[12] Darcis, P., Lassen, T., Recho, N., 2006, "Fatigue behavior of welded joints part 2: physical modeling of the fatigue process", Welding Journal, **85**(1), pp. 19-26

[13] Fatemi, A., Socie, D. F., 1988, "A critical plane approach to multiaxial fatigue damage including out-of-phase loading", Fatigue and Fracture of Engineering Materials and Structures, **11,** pp.149-165

[14] Gates, N. R., Fatemi, A., 2016, "Interaction of shear and normal stresses in multiaxial fatigue damage analysis", Fracture and Structural Integrity, **37**, pp. 160-165

[15] Desimone, H., Bernasconi, A., Beretta, S., 2006, "On the application of Dang Van criterion to rolling contact fatigue", Wear, **260**, pp. 567-572

[16] Dang Van, K., Griveau, B., Message, O., 1989, "On a new multiaxial fatigue limit criterion: theory and application", Biaxial and Multiaxial Fatigue, EGF 3 (Edited by M. W. Brown and K. J. Miller), Mechanical Engineering Publications, London, pp. 479-496

[17] Ciavarella, M., Monno, F., Demelio, G., 2006, "On the Dang Van fatigue limit in rolling contact fatigue", International Journal of Fatigue, **28**, pp. 852-863

[18] Kouhia, R., 2016, "Lecture notes to the course Mechanics of materials", Chapter 6, http://webhotel2.tut.fi/mec_tme/personnel/kouhia/teach/

[19] Radaj, D., 1990, "Design and analysis of fatigue-resistant welded structures", Abington Publishers, Cambridge

[20] BS 7910, 2015, Guidance on Methods for Assessing the Acceptability of Flaws in Fusion Welded Structures, BSI

[21] DNVGL-RP-C210, 2015, "Probabilistic methods for planning of inspections for fatigue cracks in offshore steel structures"

[22] DNVGL-RP-0005, 2014, "Fatigue Strength Analysis of Offshore Steel Structures"

[23] Pascual, F. G., Meeker, W. Q., 1999, "Estimating Fatigue Curves with Random Fatigue–Limit Model", Technometrics, **41**, pp. 277–302

[24] Haibach, E., 1970, Discussion paper, The Welding Institute Conf. on Fatigue of Welded Structures, Brighton

[25] Berge, S., 1985, "Basic Fatigue Properties of Welded Joints", Chapter 4, Fatigue Handbook, Tapir Trondheim,

[26] Lassen, T., Recho, N., 2015, "Risk based inspection planning for fatigue damage in offshore steel structures", Proceedings of the OMAE 2015 conference

[27] Bjørheim, M., Reenskaug, I., 2016, "Laboratory testing of welded joints", Project work, University of Agder

ANNEX A

ILLUSTRATION OF EXPERIMENTAL CRACK GROWTH IN TEST SERIES 1
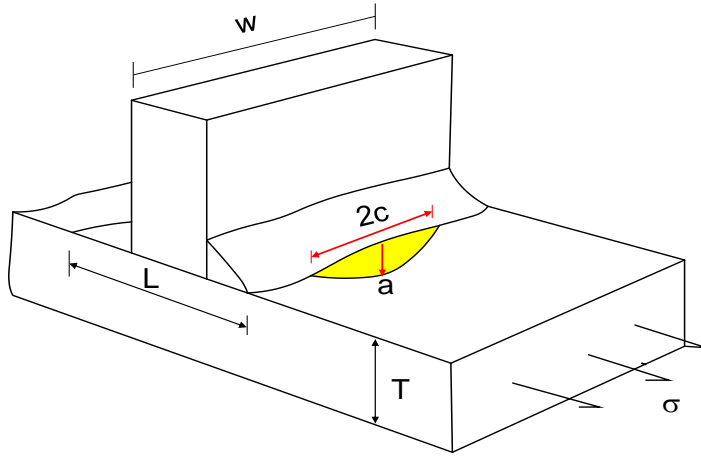
FIGURE A1. Fillet welded joint subject to experiments and modelling
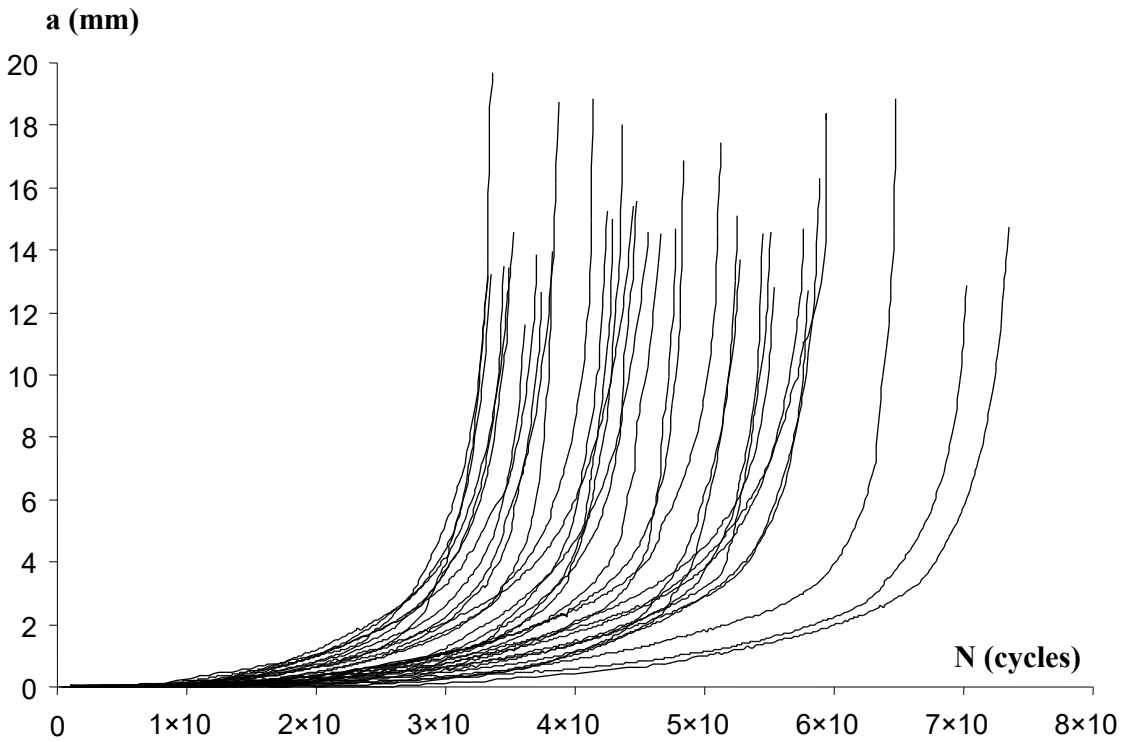
FIGURE A2. Measured crack growth scatter in axial loaded fillet welded joint plate thickness 25 mm constant stress range 150 MPa

ANNEX B

SHORT PRESENTATION OF THE SPECIMENS IN TEST SERIES 2
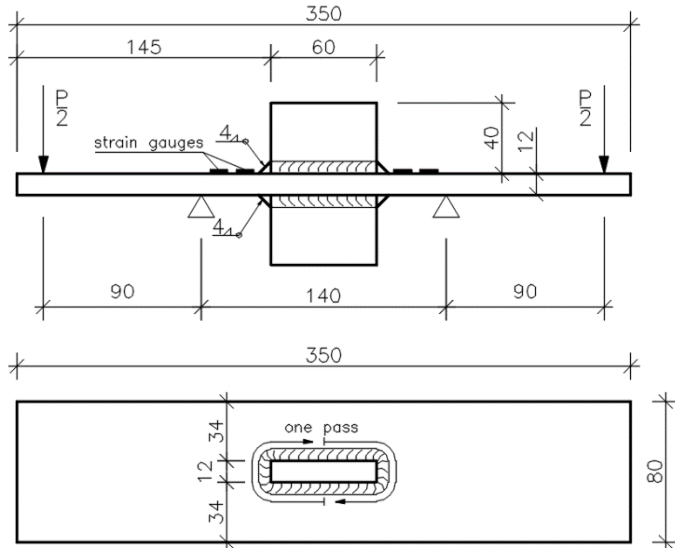
Specifications for test series 2
- Material grade: NVD36
- Weld inspection category 1
- Weld size: What is achievable in one pass, preferably a=5
- Start of weld: as indicated on figure B1.
- Welding method: FCAW
- Detail category 71 (F class)

FIGURE B1. The test specimen and the dimensions for test series 2.

FIGURE B2. Test setup bending loading mode

Paper B

Fatigue crack initiation and subsequent crack growth in fillet welded steel joints

Zbigniew Mikulski, Tom Lassen

Fatigue crack initiation and subsequent crack growth in fillet welded steel joints

Zbigniew Mikulski*, Tom Lassen

University of Agder, Grimstad, Norway

ABSTRACT

The fatigue damage evolution in fillet welded steel joints where cracks are emanating from the weld toe is investigated. Based on existing experimental data for as-welded joints including crack depth measurements of the early crack growth it is proposed to make a distinction between the crack initiation phase and the subsequent crack growth phase. The welded detail in question is an F class detail with plate thickness 25 mm made of medium strength carbon steel. It is found that the crack initiation phase defined at a crack depth of 0.1 mm is close to 25% of the fatigue life even at a relatively high constant stress range of 150 MPa. At lower stress ranges it is concluded that the initiation phase is the dominating part of the fatigue life. The present work is focusing on the crack propagation phase that is defined from a crack depth of 0.1 mm to final failure of the detail. It is demonstrated that the recommendation given in rules and recommendations (DNVGL and BS 7910) for applying Linear Elastic Fracture Mechanics (LEFM) for the crack propagation phase is valid for the propagation of such small surface breaking cracks. A model based on the rule-based formulas for the Stress Intensity Factor Range (SIFR) and the growth parameters C and m in Paris law agree well the with the measured crack growth curves. For these small semi-elliptical cracks at the weld toe notch important topics like the existence of a threshold limit for the SIFR and the influence of the stress ratio R are discussed. Due to the inherent scatter in the variables characterizing the fatigue damage evolution stochastic approaches are applied for the analyses. Observations and measurements are presented by descriptive statistics and simulations are carried out using Monte Carlo techniques.

1. Introduction

The safety margin against fatigue failure is of major concern in design and scheduled inspection planning for dynamically loaded welded steel structures. It is crucial to establish reliable models both for life predictions and for the evolution of the fatigue damage for welded details. A general overview of the fatigue design of welded joints is given by Hobbacher [1] with emphasis on the S-N approach and applied fracture mechanics. The importance of weld imperfections with respect to geometry and initial flaws is underlined in the document. Historically, there have been two schools for how to model the fatigue damage evolution in welded joints and in the way the possible initial flaws are treated. The most common approach is to model the entire fatigue life by fracture mechanics only. Such models are based on the assumption that an as-welded joint will have some initial flaws caused by the welding process that can be regarded as a planar crack-like defect from which the crack growth will start. The existence of an initiation phase is consequently neglected. The entire life mainly consists of crack growth

and the Paris law can be adopted to describe the entire damage from an initial crack with a depth of several tenths of a millimetre [2]. In this approach, the choice of initial crack depth is often based on back calculations, i.e. the crack does not represent a real initial defect. This approach was used by Haibach [3] to explain the fatigue limit in the S-N curves by the threshold value for the SIFR under Constant Amplitude (CA) loading. Based on this work the flatter slope of the S-N curves in rules and regulations for Variable Amplitude (VA) loading has been determined based on fracture mechanics and on the assumption on the size of an initial crack depths. The other school of modelling is based on the belief that even for an as-welded joint there exists an initiation phase that represents a significant part of the fatigue life, specially at low stress ranges. Initial flaws - although they may exist - are not treated as crack-like defects. Consequently, this initiation phase must be modelled separately before using a fracture mechanics model for the subsequent crack growth phase. This line of thought was historically advocated primarily by Lawrence et al. [4]. A good integrated overview of these topics can be found in the text books by Radaj [5,6] and Lassen

---

[7]. In the present work an analysis of available crack growth data from a large fatigue test series is carried out. The test specimens are non-load-carrying fillet welded transversal attachments where the cracks are emanating from the weld toe. In addition to the final fatigue life, the damage evolution was monitored in detail. Based on the crack growth data, fracture mechanical modelling is carried out for the growth phase. The purpose is to validate the recent recommendations found in rules and regulations DNVGL [8], BS 7910 [9] for the Stress Intensity Factor Range (SIFR) calculations and the given values for the growth parameters *C* and *m* in the Paris law. In these references the SIFR is based on the calculations recommended by Newman and Raju [10] and Bowness and Lee [11]. The given equations have been established based on FEA for idealized geometries of the welded joints. The purpose of the present work is to apply these equations to realistic geometries with variable and irregular local geometry of the weld toe. The growth parameters *C* and *m* in the Paris law are also subject to investigation. The values given in rules and regulations are based on the measurements made for the growth rates of rather long central cracks in smooth specimens [12]. In the present work the purpose is to verify if these parameters are applicable for the growth of small semi-elliptical cracks close to a weld toe notch. The existence of the threshold value for the SIFR for such small cracks is questioned. An important part of the study is also to determine the impact of the applied stress ratio *R*. This part of the work is related to the proposal made by Huang et al. [13] who presented a so called unique linear elastic crack growth model valid for any given value of the *R* ratio. In the present work this model is further investigated together with the rule-based models. The discussed models are evaluated based on the following acceptance criteria:

- The model shall be able to fit the crack depth history curves measured at a constant stress range of 150 MPa
- The model shall be applicable for predicting the fatigue life in agreement with the F class S-N curves as one approaches lower constant stress ranges close to the fatigue endurance limit

The final objective is to include the crack growth model in a two-phase model that can explain and simulate the data points pertaining to the S-N curve both with respect to the mean life and the inherent scatter. Such a two-phase model will have the ability to predict the fatigue behavior of other joint geometries than the F class. Furthermore, the model will be an important tool when planning scheduled inspections for welded details in service. Knowledge about the damage evolution is at the essence during such planning. The obtained model shall strike the balance between accuracy and simplicity such that it can be useful for practical engineering applications.

2. Crack growth modelling of the fatigue cracks in welded joints

2.1. Discussion of crack development in various phases

The fatigue damage processes related to cracking from the weld toe are quite complicated and involve in fact several sub-phases. A good overview of the crack stages is given by Baptista et al. [14] and can be summarized as shown in Fig. 1. As can be seen from the figure, the three major phases are:

- Crack initiation
- Microcrack propagation
- Macrocrack propagation

It is essential to make a distinction between crack initiation and subsequent crack growth. The distinction is important as these two phases involve different damage mechanisms. The crack initiation phase is driven by cyclic shear stress variation and the resistance against this damage mechanism is related to the yield stress of the steel. The growth phase is usually driven by the cyclic principal stresses perpendicular to the crack planes (mode 1 case) and the resistance against crack growth is not related to the yield stress, but to the *E* module of the steel. Hence, a distinction between the two phases is crucial to establish a correct model for the entire damage evolution. Each phase must be modelled separately to capture the characteristics of the damage mechanism involved.

In the present work the two early phases designated as nucleation and micro crack propagation are simplified to be a crack initiation phase. The subsequent macro crack growth is then modelled separately. The crack initiation is defined by the number of cycles to reach a fatigue crack depth of 0.1 mm. This initiation phase is likely to be influenced by initial flaws created by the welding process. These flaws are not possible to measure and are not regarded as crack-like defects in the present work. Hence, separation of this phase into micro-crack growth modelling as suggested by Zerbst [15] is avoided. This simplification is chosen to obtain a model that may not be completely correct, but accurate enough and useful for the practicing engineer. The subsequent crack growth is simplified as one simple stable crack propagation phase based on the common engineering fracture mechanics approach. It remains to verify if the defined initial crack depth of 0.1 mm is an appropriate choice for the transition crack depth between the two main phases. Furthermore, it should be verified if the subsequent growth can really be modelled by the common models applied in engineering. The key question to be answered is if an engineering approach based on Paris law with SIFR calculation and growth rate parameters as found in the literature are applicable for small semi elliptical cracks emanating from the weld toe. The crack initiation phase will not be handled in any detail in the present work. The chosen crack transition depth of 0.1 mm is more based on practical considerations than on theoretical arguments. This crack depth is within the measuring uncertainty of the monitoring equipment that was applied during testing. Furthermore, for the test specimens with plate thickness 25 mm the formulas for the SIFR are valid down to a depth 0.125 mm so we are just below the application range with the chosen transition crack depth of 0.1 mm. The theoretical argument is that the applied Paris law has never been proven for such small semi elliptical cracks. Attempts in this field have been made, Ref. [16]. However, no results from such studies have yet entered rules and recommendations (DNVGL, BS 7910).
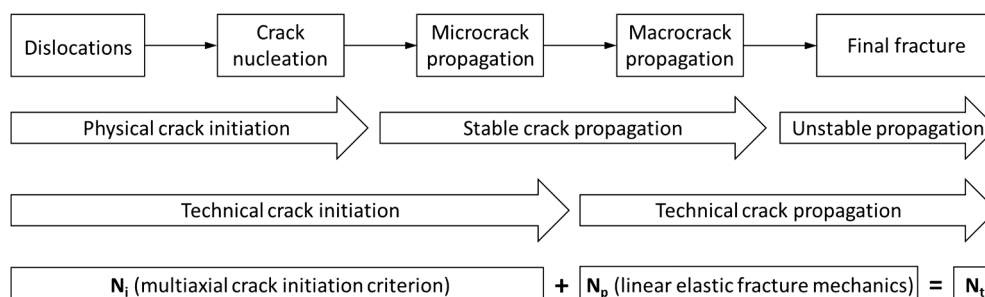

Fig. 1. Schematic crack stages for the two-phase model [14].

2.2. Basic concepts – the Paris law

Fracture mechanics models are usually based on applied LEFM. The Paris law is adopted in rules and regulations for predicting fatigue crack growth in welded joints. The basic concept is linear relation between crack growth rate and stress intensity factor range, for a log-log scale, given by the growth parameters C and m. Furthermore, it is assumed that there exists a threshold value for the SIFR below which a crack does not propagate. This model is suggested in DNVGL-RP-0001 [8]. In BS 7910 bi-linear model is proposed for better prediction of the crack behavior at an early crack growth stage. Both approaches do not take account the influence of the stress ratio R explicitly. BS 7910 distinguishes only between two cases, $R < 0.5$ and $R \geq 0.5$, and gives different values for the C and m material parameters for each of them. An attempt to explicitly take into account the R ratio has been made by Huang et al. [13]. The model is denoted a unique crack growth model. The model applies an equivalent SIFR definition and 'a unique crack growth rate curve method'. Like the previously mentioned models it also contains a threshold term and crack growth rate can be expressed as:

$$\frac{da}{dN} = C\left(\Delta K_E^m - \Delta K_{th0}^m\right) \tag{1}$$

where ΔK_E is the effective SIFR for the given R ratio, whereas the ΔK_{th0} is the threshold value for the SIFR at $R = 0$. The R ratio is defined by the applied SIF:

$$R = \frac{K_{min} + K_R}{K_{max} + K_R} \tag{2}$$

The parameters are given by the equations:

$$\Delta K_E = M\Delta K$$
$$\Delta K_{th0} = M\Delta K_{th}$$

$$M = \begin{cases} (1 - R)^{-\beta_1} & -5 \leq R < 0 \\ (1 - R)^{-\beta} & 0 \leq R < 0.5 \\ (1.05 - 1.4R + 0.6R^2)^{-\beta} & 0.5 \leq R < 1 \end{cases} \tag{3}$$

where β and β_1 are parameters dependent on material property and environment, satisfying the following relationship: $0 \leq \beta \leq \beta_1 \leq 1$. Proposed values for medium and high strength steels are: $\beta = 0.7$ and $\beta_1 = 0.84$ ($\beta_1 = 1.2\beta$). A general equation for determining β for structural steels has the following form:

$$\beta = 0.22 + \frac{0.65}{1 + 0.0035\Delta K^4} \tag{4}$$

β_1 is typically equal to a constant value of 0.84 for many examined materials [17]. Although the parameters β and β_1 are treated as material properties, proposed empirical formula (4) for structural steels assumes a dependency on the stress intensity factor range. It gives higher values in the early crack growth stage and then tends rapidly to a constant value of 0.22. This gives a change in the M factor used in computation of the effective SIFR that, in the case of $R = 0.35$, starts from 1.45 for a low nominal SIFR and becomes close to 1.1 for $\Delta K > 10 \, \text{MPa m}^{0.5}$. The β factor vs. the nominal SIFR is plotted in Fig. 2 together with the M factor computed for $R = 0.35$ and $R = 0.5$.

Finally, a unique crack growth rate curve equation recommended for analysis of welded steel structures (mean curve) is given:

$$\frac{da}{dN} = 8.32 \times 10^{-9}(\Delta K_E^{2.88} - 7.2^{2.88}) \tag{5}$$

In the present work we shall use a differential equation like (5) both in the crack depth direction and in the crack length direction at the surface. This will give both the crack depth increase and shape development for a single crack case. Eq. (5) has so far only been established for the depth direction.

In summary, the experimental results analyzed in the present work will be compared to the three fracture mechanics models shortly
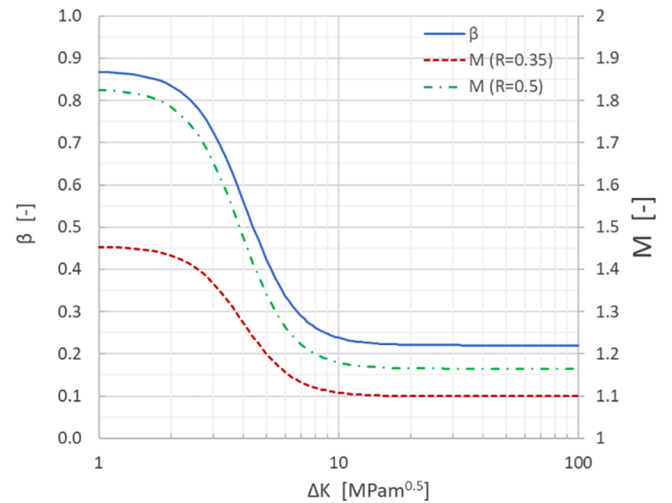
Fig. 2. β coefficient for structural steels and corresponding M factor for $R = 0.35$ and $R = 0.5$.

presented above, for a fixed R-ratio:

- Model 1: DNVGL – One linear growth curve for a log-log scale
- Model 2: BS 7910 – Bi-linear growth curve for a log-log scale
- Model 3: Unique growth model – Non-linear growth curve for a log-log scale

All models get an extension #a if the threshold value is neglected and extension #b if the threshold value is included. The crack growth parameters C and m for these models are presented in Table 1 together with possible values for ΔK_{th0}. These values are referred to as the original values for the models.

Graphical representation of those models is shown in Fig. 3. The unique model is drawn for $R = 0.35$ which is the ratio for the present test series. As can be seen from the figure the curves almost coincide when ΔK is larger than $10 \, \text{MPa m}^{0.5}$. Furthermore, the unique model can be regarded as non-linear version close to the two linear segments given in BS 7910. The unique model is somewhat more optimistic regarding the level of the threshold value for the SIFR. The DNVGL curve is the most pessimistic one in the way that it keeps a straight line until ΔK reaches a threshold value of $2 \, \text{MPa m}^{0.5}$.

2.3. Calculation of the SIF according to rules and regulations

In the present work the formulas adopted in DNVGL [8] are used for determining the SIF. It is based on empirical equations proposed by Newman and Raju [10] for surface crack in plates under membrane and bending loading and extended to the case of a crack in weld toe notch area by applying magnification factors proposed by Bowness and Lee [11]. The formulas proposed by Bowness and Lee have been obtained from FE simulations of the elliptical cracks at the weld toe notch in T-butt joints under membrane and bending loading modes. Stress intensity factors at the deepest crack point and the surface points have been computed utilizing J-integral approach and magnification factors have been defined by comparison to the similar cracks in a flat plate.

Table 1
Original C and m constants in basic models, for $R = 0.35$.

FMM	C (resultant rate in mm/cycle, ΔK in MPa m$^{0.5}$)	m	ΔK_{th0} MPa m$^{0.5}$
Model 1a or 1b	$5.79 \cdot 10^{-9}$	3	0 or 2
Model 2a or 2b	$8.32 \cdot 10^{-9}$	2.88	0 or 2
Model 3a or 3b	$8.32 \cdot 10^{-9}$	2.88	0 or 7.2
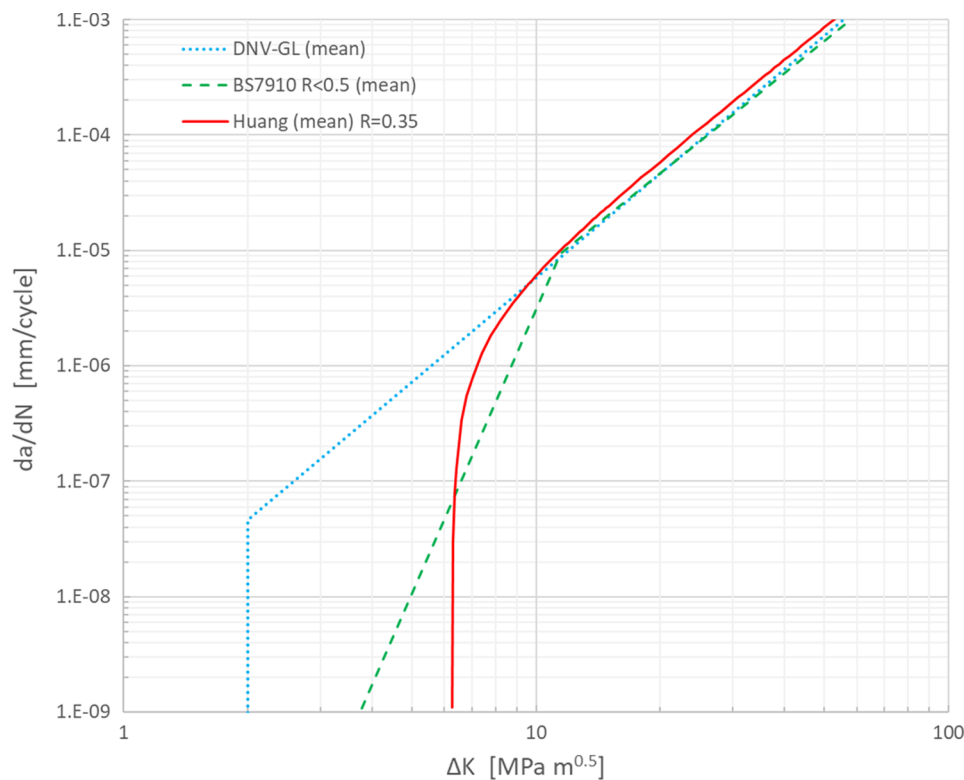
Fig. 3. Prediction of growth rates for various models (model type #b).

Influence of the local weld toe geometry has been modelled, however, only the weld flank angle θ is taken into account explicitly in the proposed formulas. The weld toe radius ρ is specified separately for two cases with $\rho = 0$ and $\rho = 0.1\ T$ (T being the load-carrying plate thickness) which are assumed to correspond to the as-welded and toe ground joints, respectively. As the assumption of $\rho = 0$ is the most conservative and, hence, acceptable from the design point of view, it may not be sufficient for accurate modelling of the early crack growth phase. A short discussion about influence of the weld toe radius on the SIF calculations for shallow cracks will be presented in the next section. In all fracture mechanics models presented in the present paper the stress intensity factors are computed utilizing the methodology adopted in DNVGL. It is important to be aware of its limitations and simplifications, see the analyses and discussion in next section.

2.4. The influence of the local toe geometry on the SIF for small cracks

To corroborate the formulas given in DNVGL for extreme values of θ and ρ an extensive FE parametric study of a non-load carrying fillet welded transversal attachment was carried out in the present work. The DNVGL document is used because the formulas in BS 7910 are only given for a fixed value of 45 degrees for θ. The angle is variable in the formulas given by DNVGL but limited to an upper bound of 60 degrees. The present analysis was carried out in the 2D plane and the local weld toe geometry was described by toe radius and flank angle under membrane loading and plane strain conditions. A short illustration of the applied FEA model is shown in Appendix A. The analysis was carried out to investigate the influence of a local stress concentration and stress gradient on the SIF calculation. Distributions of the maximum principal stresses along the likely crack path starting at weld toe surface and going into the depth direction for an un-cracked plate are presented in Figs. 4 and 5. The stresses are normalized by dividing them by the applied nominal stress. The first point marked on each curve (for x/t = 0) represents the Stress Concentration Factor (SCF) that corresponds to the given local weld toe geometry. Two main conclusions can

be drawn when analyzing these stress distributions. First, from Fig. 4 where radius is kept constant at any θ value, the stress distributions do not differ significantly for angles higher than 60°. Second, from Fig. 5, the influence of the weld toe radius while the angle is kept constant is visible only up to the depth of about 2% of the plate thickness. In the present case this means that cracks with less depth than 0.5 mm will be influenced by variations in the weld toe radius. At crack depths close to the chosen initial crack depth of 0.1 mm the impact will be substantial.

The influence of the local weld toe geometry on the SIF was investigated by analyzing the geometry correction factor that accounts for nonuniform distribution of the opening stresses utilizing the methodology proposed by Albrecht and Yamada [18]. Based on the stress distribution shown in Figs. 4 and 5 it was found that the weld toe radius has a significant impact on the SIF estimation, especially for shallow cracks close to the present transition crack depth of 0.1 mm. Although the present results are obtained by a simplified 2D analysis, the relative changes in SIF are regarded as reliable. In conclusion the upper limit on the flank angle given by 60° in the DNVGL document is not an obstacle for applying the given formulas for the present fatigue crack analysis. Steeper angles will not give a substantial increase of the SIF. However, various values of the toe radius will have an important influence on the SIF for cracks down to the present transition depth of $a = 0.1$ mm. This is neglected in formulas in DNVGL based on the work by Bowness and Lee. Finally, it is emphasized that both the angle and the radius are random variables varying along the length of the weld seam. Characteristic values must be chosen based on statistical considerations.

2.5. The likely development of semi-elliptical crack at the weld toe

From in-service experience and observations given by the crack monitoring system described in the next section the following crack behavior is likely:

- Micro cracks initiate at locations where there is a combination of unfavorable weld toe geometry giving a high notch factor and the

a)

b)

c)

Fig. 4. Influence of weld toe angle on the normalized stress distribution through the plate thickness for different weld toe radii.

presence of initial flaws. The number of cracks that initiate per length of the weld seam is by nature random. These micro cracks will at a given stage exceed the defined transition depth of 0.1 mm

- The cracks along the weld seam that have passed a depth of 0.1 mm will have a semi-elliptical shape and their aspect ratio a/c is by nature random
- Each of these cracks can be modelled by a single crack fracture mechanics model predicting the crack size and crack shape

evolution until crack coalescence takes place
- After crack coalescence the cracks join to form one edge crack that rapidly propagates to failure.

The goal of the present work is to model all the stages except the first one. The ability of the fracture mechanics models in Table 1 will be demonstrated by both comparing the crack depth growth rate and the crack shape evolution with experimental data.

3. Short presentation of the test specimens and the test set-up

3.1. Test specimens and test set-up

The experimental work has been carried out earlier and is well documented in [19]. In the present section only a short resume of the characteristics of test series are given. A total number of 34 non-load-carrying cruciform and T joint specimens were tested. All the test specimens were fabricated from C-Mn steel plates with 25 mm thickness. The nominal yield stress was 350 MPa and the tested yield stress close to 420 MPa. Weldments were fabricated using welding procedures taken from normal offshore fabrication practice: Flux-Cored Arc Welding (FCAW) and Shielded Metal-Arc Welding (SMAW) with two different electrodes.

The joints were proven free from cracks and undercuts and comply with quality level B acc. to EN ISO 5817:2014 [20]. The test specimens were stress relieved in an oven at 570 °C for 1 h. The specimens were tested under constant amplitude axial loading at $\Delta S = 150$ MPa with a loading ratio of $R = 0.35$. In addition to recording the fatigue life, crack growth measurements were made during each test for this test series. Compared to former analyses [19,21] of these experimental data the progress in the present work is:

- A correction of the measured ACPD crack depths by direct readings on the fractured surfaces is carried out (Appendix B).
- The focus is on measured crack growth rates for small cracks depths in the range between 0.05 mm and 0.5 mm.
- Recent fracture mechanics models recommended in rules and regulations supplemented by the unique growth model are fitted to the measured crack growth histories (models in Table 1).
- The inherent scatter in crack growth is treated in a logical and consistent manner by Monte Carlo simulations.

3.2. Global geometry and local weld toe geometry

Global geometry of the test specimen and dimensions are presented in Fig. 6. Parameters of the local weld toe geometry – toe radius r and flank angle θ - were measured using a profile replica method. Measurements were taken for each specimen at the locations of ACPD pin probes (10 recordings per specimen) and statistics are presented in Table 2.

3.3. Fatigue life results compared with the F-class S-N curve predictions

According to DNVGL [22] the tested detail can be classified as an F-class. This gives the following design and mean S-N curves for N < 10^7 cycles:

design: $\log N = 11.855 - 3\log\Delta\sigma$
mean: $\log N = 12.255 - 3\log\Delta\sigma$ (6)

The predicted fatigue life is 210 000 cycles when using the F-class design S-N curve. The F-class mean S-N curve gives 530 000 whereas the mean fatigue life from test series is 470 000. All samples are within scatter bounds of the F-class, however, as expected, scatter in test series is smaller than scatter included in F-class definition, standard deviation of logN is 0.1 for the present test series, whereas it is close to 0.2 for the
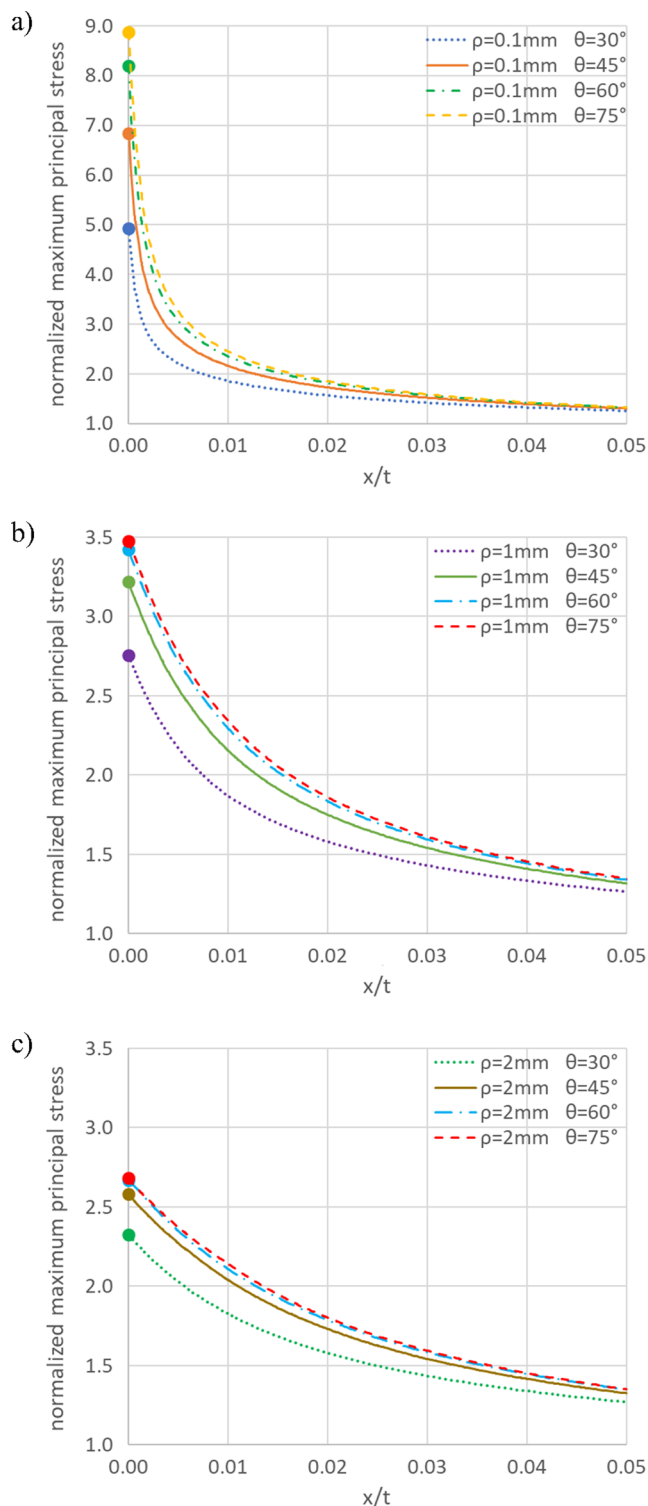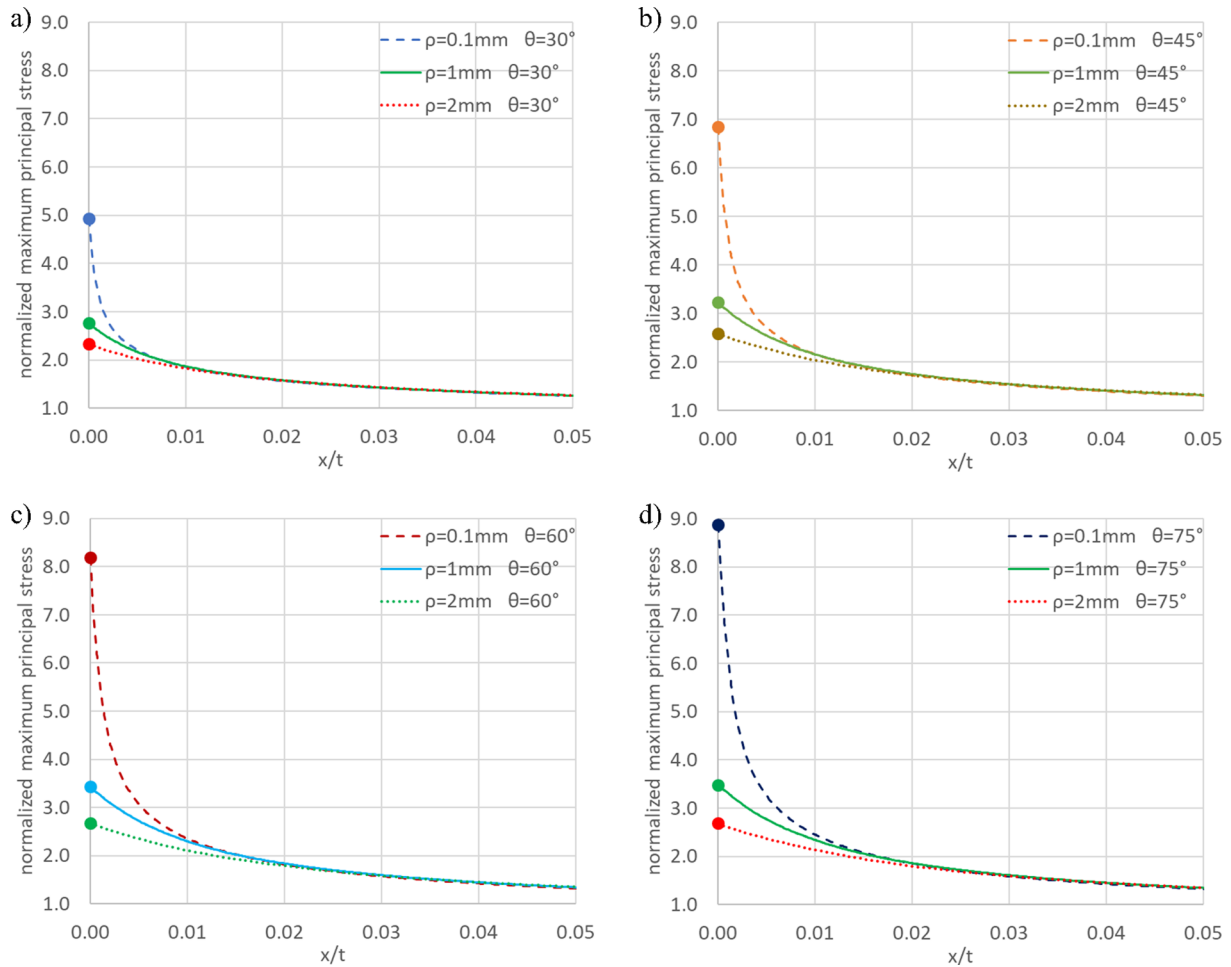
Fig. 5. Influence of weld toe radius on the normalized stress distribution through the plate thickness for different weld flank angles.
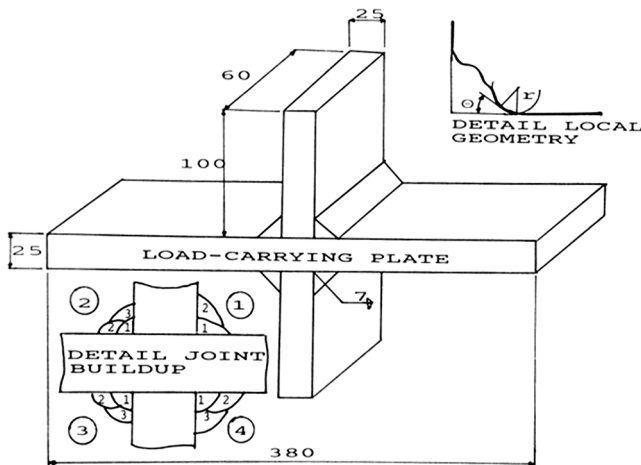
Fig. 6. Test specimen and local weld toe geometry (top right corner) [19].

Table 2
Statistics for local weld toe geometry.

Welding procedure	Number of specimens	Weld flank angle θ [°]		Weld toe radius ρ [mm]	
		Mean	Standard deviation	Mean	Standard deviation
FCAW	11	54	10	1.3	0.6
SMAW57	12	53	9	1.6	0.7
SMAW76	11	69	8	1.8	0.9
Whole test series	34	58	9	1.6	0.7

influence. We will come back to this question in Section 7. We will use the F-class curve as a reference when we choose to lower the stress range to investigate the model behavior for decreasing stress ranges.

4. Monitoring the crack initiation phase

4.1. Measurements of early crack growth

Crack initiation and subsequent crack growth were monitored using the ACPD system based on the Krautkramer U8 Microgauge. The voltage signals were interpreted as crack depth according to the simple linear relation between voltage drop and crack depth. The following equation, called ACPD first estimate, was used:

F class. Hence, the test series are of normal quality and comparable with the population pertaining to the F-class in the codes. However, the present test series do not contain short lives close to the F-class design line, the shortest tested life is 310 000 cycles. The shortest lives found in the F-class population could be caused by a more abrupt local weld toe geometry and/or by larger initial flaws than found in the present test series. This is an important topic when establishing a fatigue life simulation model for welded joints. The present work is based on the hypothesis that the local toe geometry has the most important

$$a_{est1} = \frac{e}{2}\left(\frac{V_c}{V_r} - \frac{V_{c0}}{V_{r0}}\right)$$

(7)

Fig. 7. Early crack growth history for representative specimens of each welding procedure.

Fig. 8. Distribution for the number of cycles to reach given crack depth for the whole sample set.

where V_c and V_r are measured potential at cross-crack and at uncracked surface, respectively, whereas V_{c0} and V_{r0} are initial values at the same positions. The parameter e is the distance between the pin probes. This first estimate given by (7) is in principle only an estimate for the depth increase and will consequently be somewhat less than the true crack depth, see discussion in Section 5.1 and Appendix B. The ACPD system was surprisingly sensitive to early crack growth, see Fig. 7. In this figure, the three specimens are chosen as being a representative of each of the three welding procedures. The voltage signals had a stable increase long before a crack depth of 0.1 mm was reached. As can be seen from Fig. 7 it should be possible to make a qualified guess of the number of cycles to reach a crack depth even as low as 0.05 mm.

4.2. Statistics for number of cycles to reach crack depths a = 0.05 mm, a = 0.1 mm and a = 0.5 mm

For the very early crack growth histories a power function was fitted to the measured *a-N* curves as shown in Fig. 7. All data points are obtained by linear estimates of the crack depths. The number of cycles to reach the crack depths of 0.05 mm, 0.1 mm and 0.5 mm was estimated. Statistics for the whole sample set are presented in Table 3. Lognormal distributions were fitted to the histograms for the number of cycles to reach the given crack depths, see Fig. 8.

One can conclude from Fig. 8 that the time spent to reach very small crack depths represents a significant part of the total fatigue life, even at the high stress range of 150 MPa. The number of cycles spent to reach 0.05 mm and 0.1 mm is 113 000 cycles and 142 000 cycles respectively. This is 24% and 30% respectively of the entire fatigue life. The scatter given in number of cycles is important and the COV is 0.40 and 0.36 respectively for the two cases above. If we increase the crack depth to 0.5 mm the COV decreases further to 0.29. This indicates that the large scatter for the fatigue life in welded joints has an important contribution from the initiation phase. This is owed to the high variability of the

Table 3
Statistics of cycles to reach given crack depth for the whole sample set (34 specimens).

Statistical parameter	Number of cycles to reach		
	$a = 0.05$ mm	$a = 0.1$ mm	$a = 0.5$ mm
Mean	113,000	142,000	239,000
Standard deviation	46,000	51,000	70,000
Coefficient of variation	0.40	0.36	0.29
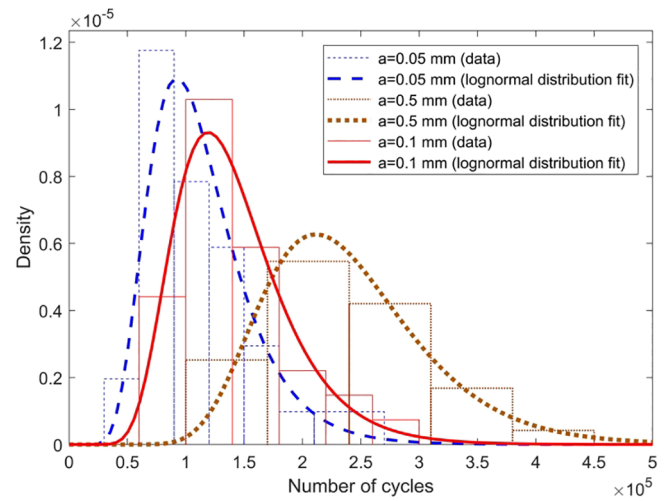
local weld toe geometry. The influence of this variability is higher the smaller the crack is. All the numbers discussed above pertain to crack depth determined by a linear relation between the potential drop at crack locus and the crack depth. If a correction is made for the bias in this calculation, the number of cycles to reach a true crack depth of 0.1 mm will decrease from 142 000 cycles as given in Table 3 to approximately 120 000 cycles, i.e. a reduction of the initiation phase of 15% only. Hence, a corrected distribution for the time to reach 0.1 mm will be found between the two left curves in Fig. 8 for linear crack depths estimates of 0.05 mm and 0.1 mm respectively. Details on this correction are found in Section 5.1 and Appendix B. Furthermore, if the 95% lower confidence limit for the mean number of cycles to reach a true crack depth of 0.1 mm is determined, one will get 62 000 cycles based on Student t statistics. This is still 13% of the entire fatigue life of 470 000 cycles. This is a demonstration of the fact that the crack initiation phase for welded joints cannot be neglected.

4.3. Discussion of the size of a possible initial flaw

As can be seen from Fig. 8 and particularly from Table 3 the number of cycles to reach a crack depth of 0.05 mm has a mean value of 113 000 cycles with a standard deviation of 46 000. Even when subtracting two standard deviations for the time to reach 0.05 mm, there is still a remaining initiation part of the fatigue life. This finding implies that if the unknown initial flaws are defined as crack-like defects, the size of these defects will be smaller than 0.05 mm. This supports the recommendations given in DNVGL-RP-0001 [8] that suggests a mean value for the initial crack depth as small as 0.043 mm and an exponential probability distribution to account for the scatter in the crack depth. The DNVGL document suggests that this initial crack depth can be entered in a fatigue crack propagation model based on Paris law. However, the present observation may also support the argument in the present work that the initial flaws cannot be modelled as an initial fatigue crack. Consequently, the initiation phase should be modelled quite differently than by a fracture mechanics approach, see next section.

4.4. Modeling the crack initiation phase

It is outside the scope of the present work to carry out detailed modelling of the crack initiation phase. Our goal is to pursue the subsequent crack propagation phase by an engineering fracture mechanics models and compare results with the models in codes. Hence, the crack initiation model proposed by Lassen and Recho [21] has been adopted for simulation of the number of cycles to crack initiation under constant

amplitude fatigue loading. The model is based on a local strain-life approach with the use of the Coffin-Manson-Basquin formula, including the Morrow mean stress correction. The number of cycles N_i to crack initiation can be found from:

$$\frac{\Delta \varepsilon}{2} = \frac{(\sigma_f' - \sigma_m)}{E}(2N_i)^b + \varepsilon_f'(2N_i)^c \tag{8}$$

where $\Delta \varepsilon$ is the local strain range, σ_m is the local mean stress, parameters b and c are the fatigue strength and ductility exponents, and σ_f' and ε_f' are the fatigue strength and ductility coefficients respectively. The local stress-strain behavior is given by the Ramberg-Osgood equation and Massing's hypothesis concerning the hysteresis loop, established for stabilized cyclic stress-strain curve:

$$\Delta \varepsilon = \frac{\Delta \sigma}{E} + 2\left(\frac{\Delta \sigma}{2K'}\right)^{\frac{1}{n'}} \tag{9}$$

where K' and n' are the cyclic strength coefficient and strain hardening exponent, respectively. Parameters of that model have been established and validated on the results of presented test series. More details can be found in [7,21].

5. Monitoring the crack propagation phase

5.1. Crack depth measuring uncertainty

The number of cycles to reach given crack depths is shown in Fig. 9 for each test specimen. The curves represent the crack growth only, starting from crack depth of 0.1 mm. The mean curve for all the samples is also drawn.

These curves are based on the simple linear relation given in Eq. (7). To improve the accuracy the first estimated depths were calibrated against true crack depth measurements. The following equation is used for correction:

$$a_{ets2} = a_{est1} + g(a_{ets1}) \tag{10}$$

Details are found in Appendix B. The proposed correction formula has been established based on measurements carried out on the entire sample set, and not for each specimen separately. Hence, it can only be used for correction of the mean propagation curve. The corrected mean a-N curve is presented in Fig. 10. As can be seen the difference between the uncorrected and the corrected curve is not very large, but important when determining the parameters C and m.

5.2. Analyzing the crack growth phase from a crack depth of 0.1 mm up to final fracture

In the analyzed test series cracks are initiated at several positions along the weld toe, then they grow as shallow semi-elliptical cracks. A sketch of the plate cross-section is shown in Fig. B1 (Appendix B). Crack coalescence was observed at a depth between 2.5 and 3.5 mm. At this stage an edge crack is formed. In the presented crack growth model that sequence is simulated using the following two stages:

1. Growth of a single semi-elliptical crack both in depth and length direction starting from initial crack depth and an assumed initial crack aspect ratio a/c,
2. From a specified depth a_1, treated as a starting point for crack coalescence, only the crack depth follows the crack growth law. The crack length will then be determined by the formation of an edge crack. Numerically the crack aspect ratio decreases exponentially reaching a value of 0.01 at crack depth a_2, and continuing to the asymptote of a/c = 0.001.

The forcing function that controls the crack aspect ratio evolution in the second stage of the crack growth model has the form:

$$\frac{a}{c} = p \ \exp(-q(a - a_1)) \tag{11}$$

where p and q are coefficients determined based on experimental observations.

Example of the crack aspect ratio evolution is presented in Fig. 11. The first part is determined by the depth and length propagation model, whereas the last part is obtained by the above empirical forcing function. The first part obtained by the growth model agrees well with experimental observations, although considerable scatter in shape has
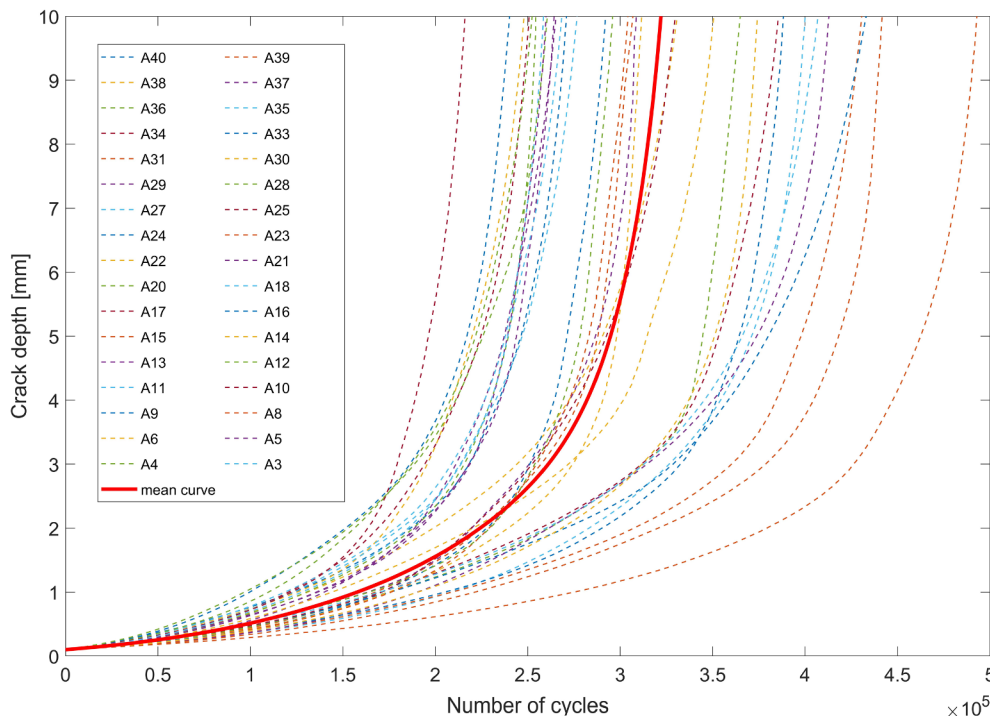
Fig. 9. Mean a-N curve and a-N curves measured for all samples (FCAW, SMAW57 and SMAW76, 0.1 ÷ 10 mm, ACPD first estimate).
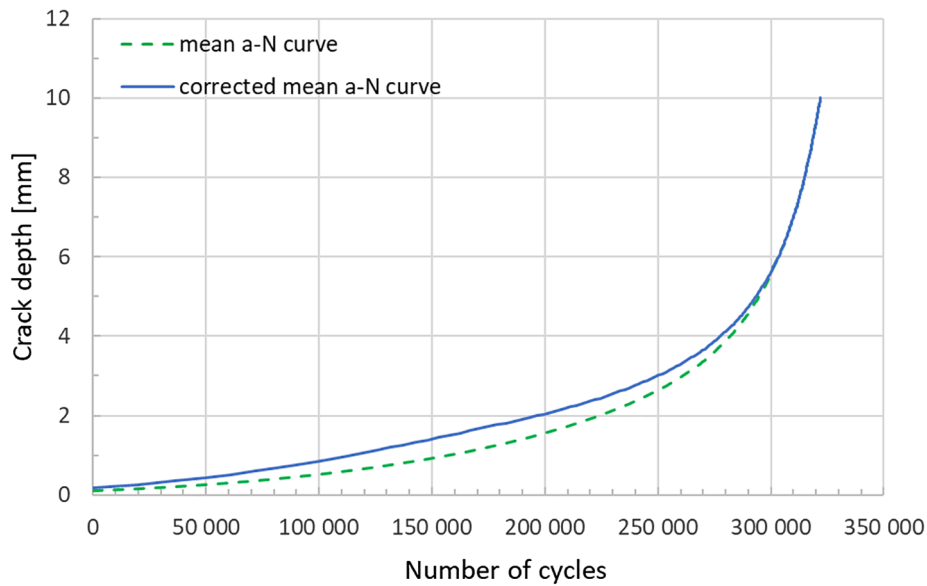
Fig. 10. Uncorrected (ACPD first estimate) and corrected mean a-N curve.
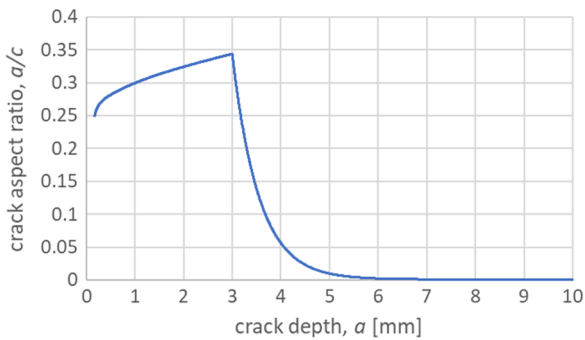
Fig. 11. Crack aspect ratio evolution, $a_1 = 3$ mm, $a_2 = 5$ mm.

been observed. Similar observations of crack shape development and coalescence have been reported by other researchers: Bell et al. [23], McFadyen et al. [24], Frise et al. [25].

Using the above described model for the crack aspect evolution, the three models were fitted to the corrected mean propagation curve:

Model 1a: The basic model is based on DNVGL, no threshold for the SIFR.

Model 3a: A unique crack growth rate curve method with account for the R ratio value only (no threshold for the SIFR).

Model 3b: A unique crack growth rate curve method with account for the R ratio value and SIFR threshold value ($\Delta K_{th0} = 7.2$ MPa m$^{0.5}$).

For all models the SIFR is calculated according to DNVGL [8]. The described models will first be applied with the original growth parameters C and m given in Table 1. Then C and m will be modified to obtain the best fit to the experimental curves. The parameters a_1 and a_2 are set to fixed values of 3 mm and 5 mm, respectively, as those values are found to be close to the optimum values in each model that fits best to the measured mean curve. This choice agrees also well with experimental observations. An initial crack aspect ratio of a/c = 0.25 was assumed. The objective function in the fitting procedure is the sum of relative errors between predicted and measured corrected mean number of cycles to reach a given crack depths. Fitted crack growth parameters C and m together with the obtained model predictions are presented in Figs. 12–14. The curves obtained by models with original
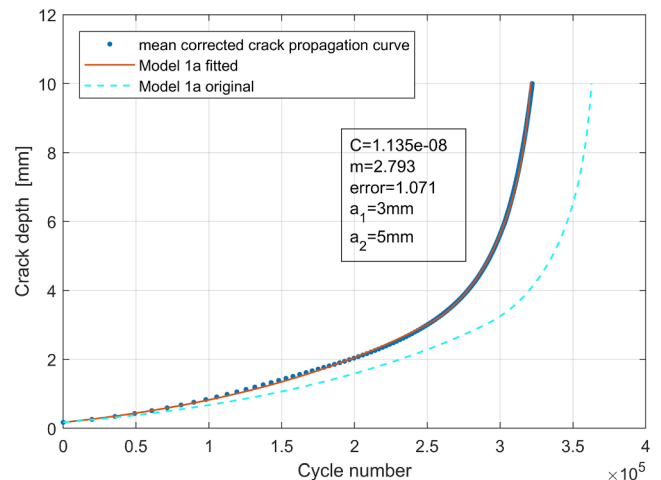
Fig. 12. Mean corrected *a-N* curve and best fit using Model 1a.
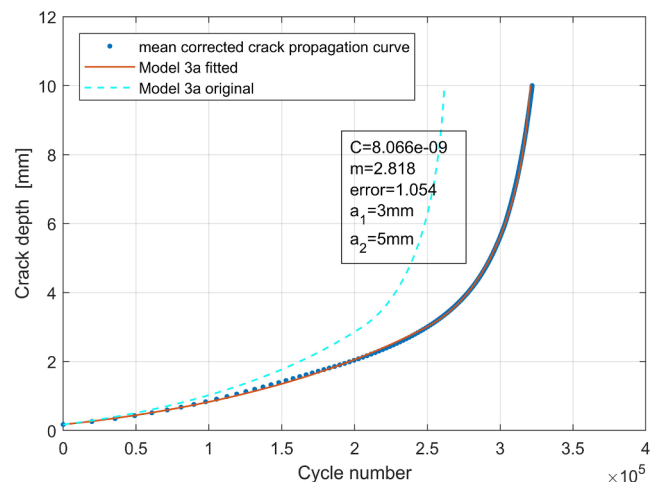
Fig. 13. Mean corrected *a-N* curve and best fit using Model 3a.

parameters as given in Table 1 are also drawn on these figures.

As can be seen from the figures the obtained C and m parameters give a very good fit to measured data for each model. Furthermore, the
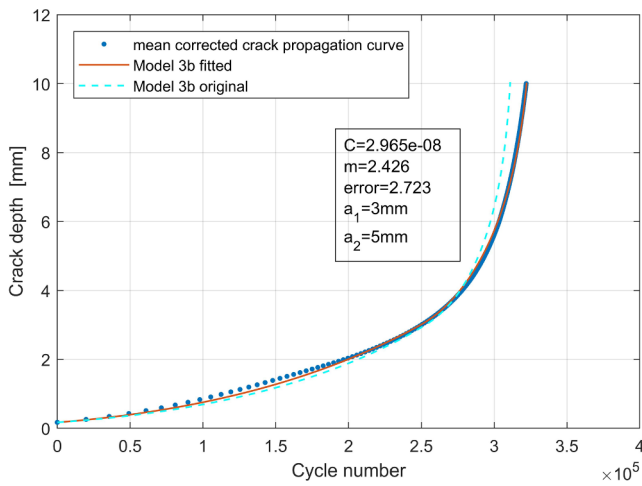
Fig. 14. Mean corrected *a-N* curve and best fit using Model 3b.

parameters C and m giving the best fit are quite close to the original recommended values given in rules and regulations. The recommended values will in fact give results within $\pm 15\%$ of the number of cycles to reach the final crack depth. Regarding the fitted parameter values, the only outlier is found in model 3b for which the m exponent is as low as 2.43 for the best fit. This is a substantially lower value for m than what is recommended in rules and regulations. It may indicate that the threshold value of $7.2\,\mathrm{MPa\,m^{0.5}}$ at $R = 0$ for this model is too high for small surface breaking cracks. This issue will be pursued further during the simulation models when the stress range is decreased towards the fatigue limit given by the S-N curve. The presented models were fitted directly to the corrected mean *a-N* curve, however a better overview of the goodness of fit can be obtained by comparing crack growth rates predicted by the models.

5.3. Crack growth rates predicted by the models

Crack growth rates derived from the corrected mean *a-N* curve are plotted versus the SIFR in Fig. 15. The crack aspect ratios used for the SIFR calculations were taken from the crack shape evolution obtained from Model 1a. The model predicts the propagation both in the crack depth and in the crack length direction for semi elliptical cracks before crack coalescence. The model predicted aspect ratios are as shown to the left in Fig. 11. For larger cracks the growth in the depth direction is still calculated by the model, whereas the crack length is controlled by the forcing function, Eq. (11). As can be seen the obtained curves in Fig. 15 are quite close to a smooth straight line for a log-log scale. However, there is a small zig-zag shape for the SIFR between 12 and $15\,\mathrm{MPa\,m^{0.5}}$ This is likely to be an effect from the method that was used to correct ACPD readings with true crack depth measurements using the ink injection method, see equation B-1 in Appendix B. As can be seen from Fig. 15 all three models fit the measured growth rates well. When comparing to mean curves from the codes, both these curves – DNVGL and BS 7910 - are close to measured rates. However, the mean curve for $R < 0.5$ based on the BS 7910 underestimates measured rates at the early crack growth when the SIFR is below $10\,\mathrm{MPa\,m^{0.5}}$. This is an important observation.

The parameters C and m in the linear models (Model 1a and Model 3a) can also be fitted to measured growth rates using a log-log scale regression method. Results are presented in Table 4. For Model 3b an effective SIFR that takes account for the R ratio correction must be used when estimating the C and m parameters. The obtained value for the m exponent gives 6% lower values than found in Section 5.2. The obtained values are also somewhat lower than values given in the codes. Hence, estimating parameters by finding the best fit directly to the experimental *a-N* curve seems to be a better procedure than fitting them to the
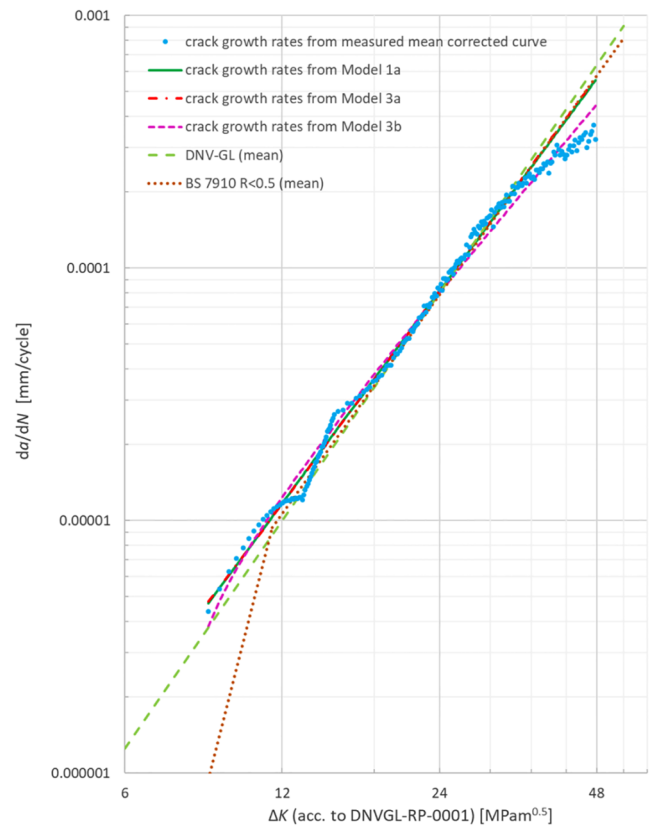
Fig. 15. Crack growth rates from the corrected mean propagation curve with predictions from the three models.

Table 4
C and m parameters fitted using two methods.

Method	Model 1a		Model 3a	
	C	m	C	m
Fit to *a-N* curve	$11.35 \cdot 10^{-9}$	2.79	$8.066 \cdot 10^{-9}$	2.82
Fit to growth rates	$17.54 \cdot 10^{-9}$	2.64	$13.27 \cdot 10^{-9}$	2.65
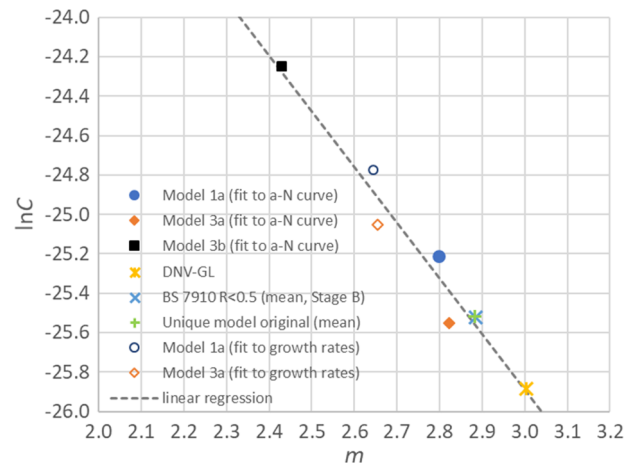
Fig. 16. ln$C$ vs. m for all models.

derived growth rates.

All determined growth parameters together with parameters proposed in codes and in the original 'unique model' are plotted in Fig. 16. Linear regression, even if its usage is not clearly justified in this case,

gives the relation $\ln C = -2.823m - 17.42$ for the present analysis. This strong negative correlation between $\ln C$ and m is close to relations found by other researchers.

6. Crack growth simulations by the Monte Carlo method at various constant stress ranges

6.1. Introduction to the simulation

The purpose of the Monte Carlo simulation is to simulate the results obtained in the test series and the results pertaining to an F class detail to which the specimens belong. It is particularly interesting to see if the fracture mechanics models predict rational crack behavior when the constant stress range decreases towards the fatigue limit given by the F class. The existence of a fatigue limit can be explained by very long initiation life and/or by cracks that are not growing due to the threshold phenomenon related to the SIFR. It is the latter phenomenon that is investigated in the present section. We do assume that the crack initiation will take place, but that the fatigue crack may subsequently stop growing if the SIFR is below the threshold value. The long initiation life is added on in Section 7.

The first important step in the Monte Carlo simulation is to choose and define the random variables that enter explicitly to the model and have an influence on the predicted propagation life. Among all model variables we can make a distinction between measurable and non-measurable source variables. The variability of the measurable variables was estimated based on measurements from the presented test series and the assumptions regarding their values and distributions are shown in Table 5. The measured variation in the weld toe radius in not included as this variation does not have an impact on the applied SIFR calculations.

The crack growth parameters, C and m, are treated as non-measurable variables in the present context as they are obtained from the mean growth curve only. In accordance with a common rule adopted in codes, the m exponent is kept constant whereas variability is added to the C parameter. The following models are analyzed:

- Model 1b-original: Original DNVGL model (with SIFR threshold value and scatter in C as given in DNVGL-RP-0001 [8]).
- Model 3a-fitted: A unique crack growth rate curve method with account for the R ratio value only (fitted parameters C and m are presented in Fig. 13, Section 5.2).
- Model 3b-fitted: A unique crack growth rate curve method with account for the R ratio value and the SIFR threshold value (fitted parameters C and m are presented in Fig. 14, Section 5.2).

As can be seen, the standard deviation for C was kept at its original value for model 1b. For model 3a and 3b with fitted parameters the standard deviation was determined such that the observed scatter in propagation life from the testing was reproduced during the simulation. The obtained logarithmic standard deviation for $\log C$ was determined to be just below 0.1. This is somewhat less than what is recommended in the rules and regulations. Values and distributions of the non-measurable parameters for the above models are presented in Table 6.

The SIFR threshold value in Model 1b-original and Model 3b-fitted is $2\,\text{MPa}\,\text{m}^{0.5}$ and $7.2\,\text{MPa}\,\text{m}^{0.5}$, respectively. These parameters were

Table 5
Measurable variables.

Variable	Value	Distribution type
Initial crack aspect ratio, a_0/c_0	$0.05 \div 0.3$	Uniform
Beginning of coalescence, a_1	$1 \div 3\,\text{mm}$	Uniform
End of coalescence (edge crack, $a/c = 0.01$), a_2	$a_2 = a_1 + 2\,\text{mm}$	Uniform (dependent)
Weld flank angle, θ	Mean = 58° SD = 9°	Normal

Table 6
C and m parameters used in MC simulations based on optimized fit.

Model	Parameter	Value	Distribution type
Model 1b-original	C	Mean = $5.79 \cdot 10^{-9}$, log SD = 0.11	Lognormal
	m	3.0	Deterministic
Model 3a-fitted	C	Mean = $8.07 \cdot 10^{-9}$, log SD = 0.090	Lognormal
	m	2.82	Deterministic
Model 3b-fitted	C	Mean = $2.97 \cdot 10^{-8}$, log SD = 0.085	Lognormal
	m	2.43	Deterministic

kept as fixed constants in the above simulation models. A better approach would probably be to treat the threshold value as a random variable. This approach could in particular be interesting for model 3b to improve this model ability to fit the S-N curve data. However, there is at present a lack of data for defining the threshold value as a random variable. In BS 7910 the mean values and scatter are given for the parameter C, whereas only a lower bound is given for the threshold value.

Output from the MC simulation - number of cycles spent in crack propagation from initial crack depth $a_0 = 0.1\,\text{mm}$ to final depth $a_f = 10\,\text{mm}$ is compared to the results obtained in the presented test series.

6.2. Simulation of the crack growth phase at the test stress range 150 MPa

Simulated results obtained with the use of the models defined in Section 6.1 are presented in Table 7 together with test data for a stress range of 150 MPa. The lognormal distribution fits well the simulated results, see Fig. 17.

As can be seen the original DNVGL model (Model 1b-original) gives a reasonable prediction of the mean propagation life for the F-class detail. The mean value of 374 000 cycles is only 24 000 cycles longer than the value observed in the present test series. This is a smaller difference than what was observed between mean total fatigue life in the present test series and the prediction from the median F-class S-N curve (see Section 3.3). It is however noted that the Coefficient of Variation (COV) in simulated propagation fatigue life is 0.25 only. This is relatively small when considering that the F class has a COV = 0.5 for the entire life range. All the specimens that are defining the F class do obviously have large scatter in the measurable fatigue source variables given in Table 5. For Model 3a-fitted and Model 3b-fitted there is no discrepancy between test results and simulated life results. Both the mean value and the scatter are simulated accurately as expected when fitted values are applied. If the variability in C is suppressed, the predicted mean value for the propagation life is still close to measured value, but the scatter is much lower – the standard deviation is only 18 000 cycles, i.e. COV = 0.05. This scatter is the contribution from the measurable variables (geometry parameters) on the predicted propagation life. One may suspect that this scatter should have been larger, as we have discussed the SIFR calculations may not capture the influence of extreme values in the weld toe geometrical variables θ and ρ. The

Table 7
Results of simulations of the crack growth phase at $\Delta\sigma = 150\,\text{MPa}$.

	Model 1b-original	Model 3a-fitted	Model 3b-fitted	Test series
Mean	374 000	329 000	338 000	350 000
Standard deviation	93 000	73 000	72 000	72 000
Min	144 000	167 000	169 000	216 000
Max	801 000	708 000	630 000	493 000
Number of samples	1000	1000	1000	34
Number of run-outs	0	0	2	0
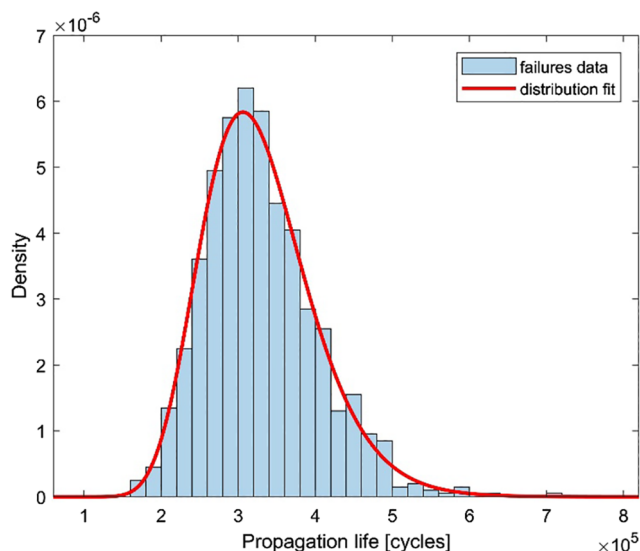
Fig. 17. Lognormal distribution fitted to the data from simulations for Model 3a.

Table 8
Results in number of cycles for simulations at $\Delta\sigma = 100$ MPa.

	Model 1b-original	Model 3a-fitted	Model 3b-fitted
Mean	1 247 000	975 000	–
Standard deviation	313 000	218 000	–
Min	533 000	484 000	–
Max	2 525 000	1 795 000	–
Number of samples	1000	1000	1000
Number of runouts	0	0	1000

extreme values are outside the validity range for the given formulas for the SIFR. As already mentioned Model 3b (with the threshold value for SIFR) will give some run-outs already at this high stress level (150 MPa). This is not in agreement with the present test nor with other S-N test data for similar details, see Fig. 18. As can be seen run outs do not occur before one approaches a stress range of 100 MPa. This confirms our assumption that the threshold value of SIFR = 7.2 MPa m$^{0.5}$ for the unique model is too high.

6.3. Simulation of the crack growth phase at stress range of 100 MPa

The next stress level for simulation was chosen at a stress range of 100 MPa. This is the stress regime where physical testing starts to give some few run outs, see Fig. 18. We must bear in mind that at this stress

level the initiation life has increased significantly and that our simulation only predicts the crack growth. Nevertheless, it is interesting to see if initiated fatigue cracks will stop to grow due to stress intensity factor ranges that are below the given threshold values in the models. The results are given in Table 8.

As can be seen Model 1b with original parameters does still not predict any runouts at this stress level. This is regarded to be a reasonable result compared with experimental data bearing in mind that the initiation life has increased substantially. The mean initiation life has increased to close to $1.3 \cdot 10^6$ cycles at this stress range, ref. [21]. With the measured COV of 0.35 for the initiation life this will give some long initiation lives between 3 and $4 \cdot 10^6$ cycles. Adding the longest propagation lives from Table 8 this gives total maximum lives up to $6 \cdot 10^6$ cycles. These specimens may during physical testing very well be defined as run-outs, see Fig. 18. For Model 3b-fitted all simulated samples were run-outs at 100 MPa, hence, the high threshold value for this model must be rejected.

6.4. Simulation the crack growth phase at stress range of 50 MPa

The stress range of 50 MPa is just below the mean fatigue limit of 56 MPa, see Eq. (6) and Fig. 18. The initiation life has now a mean value as long as $5 \cdot 10^8$ cycles and is totally dominating the fatigue life, Ref. [21]. Again, if the scatter in initiation life is accounted for some of these specimens will last far longer than 10^9 cycles. Hence, the initiation life alone can explain the concept of the fatigue limit during testing. This
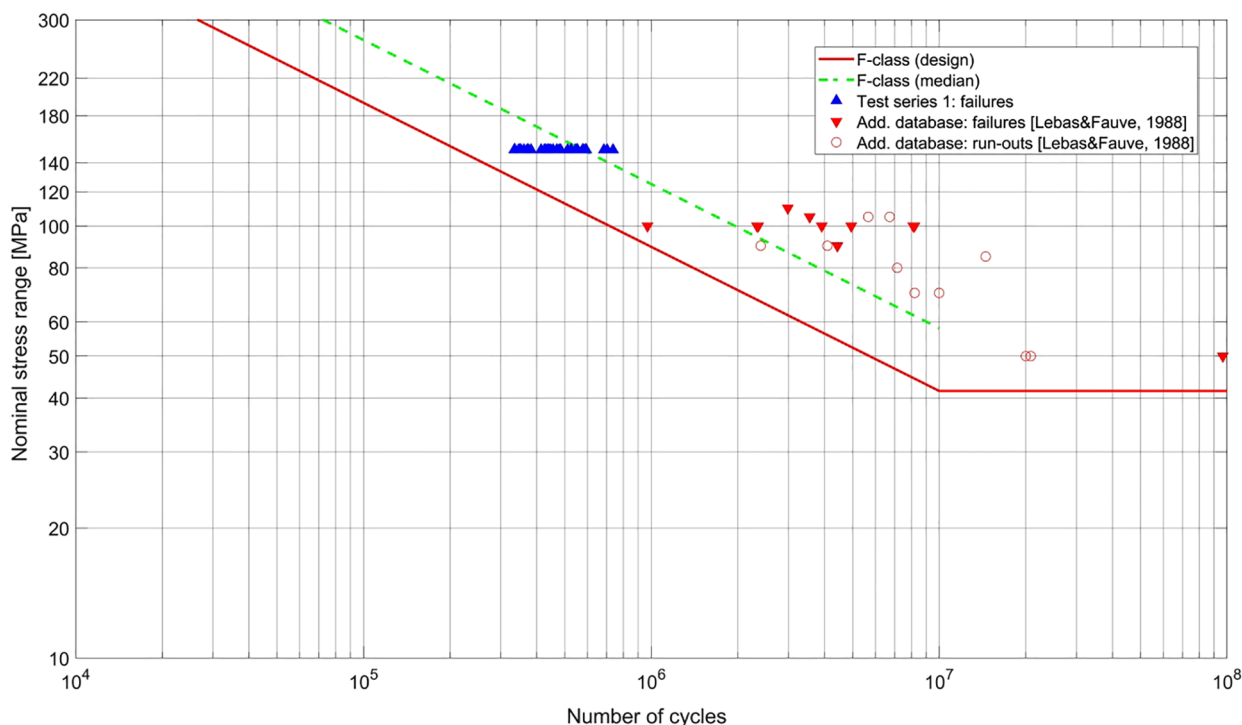
Fig. 18. Total fatigue life in test series and other data for similar detail found in literature.

Table 9
Results of simulations of the crack growth phase at $\Delta\sigma = 50$ MPa.

	Model 1b-original	Model 3a-fitted	Model 3b-fitted
Mean	9 960 000	5 230 000	–
Standard deviation	2 630 000	1 160 000	–
Min	4 270 000	2 310 000	–
Max	21 660 000	11 020 000	–
Number of samples	1000	1000	1000
Number of runouts	0	0	1000
Number of failures longer than $10 \cdot 10^6$ cycles	456	2	–

fact will be pursued in Section 7. As for the crack propagation life, Model 1b does still not predict any run-outs for the crack propagation related to the SIFR threshold value of 2 MPa m$^{0.5}$, however, nearly 50% of the simulations have propagation life longer than 10^7 cycles. Hence, Model 1b predicts very slow crack growth without any crack arrest.

The results confirm that the fatigue limit should be explained mostly by long initiation lives and not by the threshold value of the SIFR, ref. [21]. Explanation of the fatigue limit in the S-N curves by the threshold value for the SIFR was proposed by Haibach [3]. However, as has been shown, care should be taken by using the SIFR threshold values determined for large long cracks in uniform plates when analyzing small semi-elliptical cracks at the weld toe notch. A unique crack growth rate curve model without SIFR threshold (Model 3a) gives acceptable results when added on to an initiation phase. The total life when the initiation life is added exceeds the common limit of 10^7 cycles where most tests without failure are stopped and defined as run-outs. Results for the given stress range of 50 MPa are given in Table 9 and Fig. 19.

7. Simulation of the total fatigue life based on a two-phase model

So far, we have only simulated the crack propagation phase. Simulation of the total fatigue life using a two-phase model can give more insight on the model's ability to construct an S-N curve. For that purpose, the crack initiation model, shortly described in Section 4.4, has been used for simulation of the number of cycles to crack initiation under constant amplitude fatigue loading. The simulation of the total fatigue life is carried out with the following steps:

- The crack initiation period is simulated using the mean value

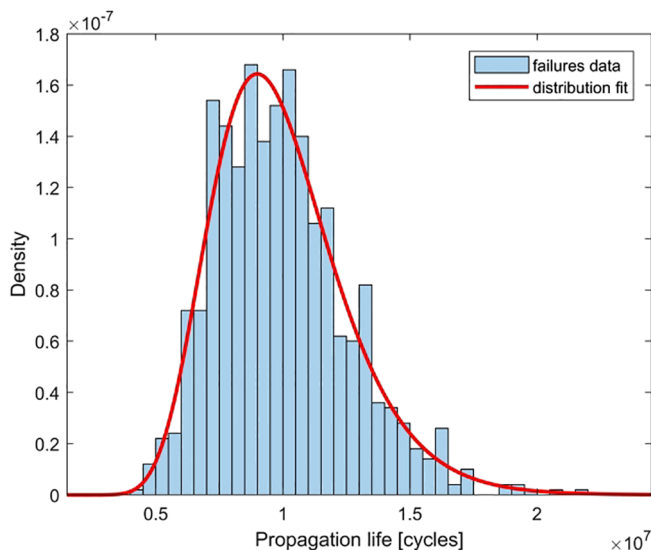**Fig. 19.** Lognormal distribution fitted to the data from simulation of Model 1b-original at stress range 50 MPa.

predicted by the crack initiation model and with a COV = 0.35 as was measured at a stress range of 150 MPa. A lognormal distribution for the initiation life is assumed. The scatter for the initiation period is strongly related to the variation in the weld toe angle and radius, particularly the toe radius. The variation of the size of small non-measurable initial flaws may also come into the play and contribute to the observed scatter.

- The crack growth is simulated with the use of Model 3a-fitted with $R = 0.35$. A negative correlation of 0.5 is applied between the initiation life and the C parameter in the propagation law. This assumption is based on the observed positive correlation between the initiation life and propagation life in the tests. ($\rho_{xy} = -0.5$, x = logN_i, y = log$C$). The variation of the weld toe radius is as before neglected for the crack growth phase.

Results from the simulations are presented in Fig. 20. As can be seen at high stress ranges, $\Delta\sigma > 100$ MPa, the simulated lives are in accordance with F-class predictions both regarding mean value and scatter. It is noted that the simulation gives some short lives that are close to the F class design line. Hence, our model is fully capable of simulating the F class data without the existence of larger initial crack depths than 0.1 mm. In fact, if initial crack depths larger than 0.1 mm had been assumed, the model would predict overly pessimistic data compared with experimental results. At the design curve fatigue limit, $\Delta\sigma = 42$ MPa, the simulated lives are typical longer than 10^9 cycles which is in accordance with experimental facts. In many situations, tests at such low stress levels are stopped before 10^9 cycles and defined as run-outs. At these lower stress ranges we can see deviations compared with the F class curve in the way that simulated results tend to be non-linear for a log-log scale. This effect is also strongly visible in fatigue tests, however, due to simplicity and high level of conservatism, bi-linear curves are commonly used in the building codes. More advanced nonlinear S-N curves can be used to establish more accurate predictions at low stress ranges. Such curves must be based on more enhanced statistical treatment of the test data. This can be obtained by the approach designated the Random Fatigue Limit Model proposed by Pascual and Meeker [26]. The model has been applied for welded joints by Lassen [27]. The model has been further elaborated by Leonetti et al. [28]. One characteristic property of these models is that both the finite life and the fatigue limit are treated as random variables simultaneously. This approach coincides with the idea that the threshold value for the SIFR should be treated as a random variable, see discussion in Section 2.1. To summarize, both experimental data and simulated data support the suggestion that the bi-linear S-N curve for a log-log scale should be replaced by a continues non-linear curve. The curve can be obtained by the Random Fatigue Limit Model.

The applied propagation model (Model 3a-fitted) with the results given in Fig. 20 does not include any threshold value for the SIFR. If a $\Delta K_{th} = 2$ MPa m$^{0.5}$ is included in the propagation phase this will give infinite propagation lives for stress ranges between 30 MPa and 40 MPa. However, for these stress ranges the initiation lives have already exceeded 10^8 cycles as can be seen from Fig. 20. Hence, neglecting the SIFR threshold is without importance for practical calculations. One may argue that the present two-phase model represents a shift in the explanation of the very long lives at low stress ranges. The earlier explanation based on the threshold value for SIFR is replaced by the very long and dominant initiation lives. The present model also supports the fact that the fatigue limit does not exist; even at low stress ranges the welded joints will eventually fail, see Fig. 20. This is in accordance with the findings made by International Institute of Welding (IIW) that now recommends a shallow line slope of $m = 22$ in the high cycle regime instead of a horizontal fatigue limit. However, from a practical engineering point of view the concept of a fatigue limit may still be useful.
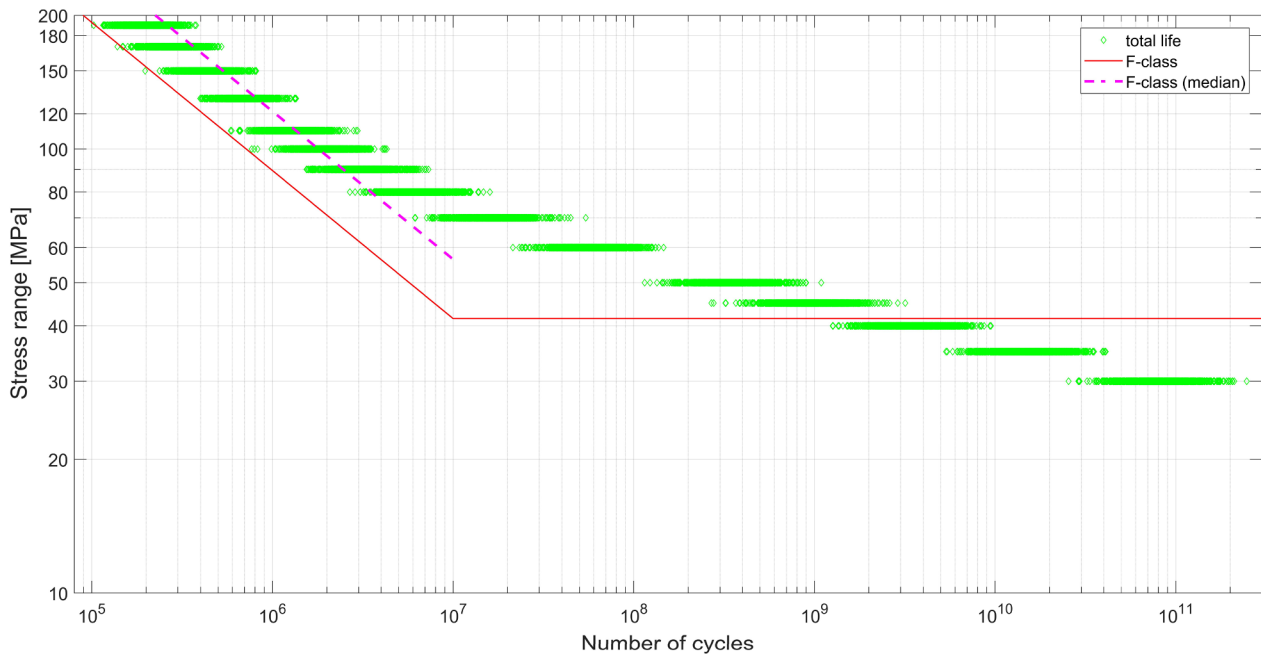
Fig. 20. Total life predictions by TPM simulations.

8. Conclusions

The fatigue damage evolution in welded joints where cracks emanate from the weld toe has been investigated by comparing experimental observations with engineering fracture mechanics modelling. The investigation was carried out for non-load carrying fillet welded transverse gussets attached to a central load-carrying plate with a thickness of 25 mm. The welded detail belongs to an F class population and both early crack growth histories and final lives were available at an applied stress range of 150 MPa. The effective R ratio was 0.35.

For the applied stress range it was found that the mean number of cycles to reach a crack depth of 0.1 mm was close to 120 000 cycles when accounting for crack depth measuring uncertainties. This is close to 25% of the entire mean fatigue life. Even at a 95% lower confidence limit the mean number of cycles to reach a depth 0.1 mm was 62 000 cycles, i.e. 13% of the entire fatigue life. This phase of the damage evolution was defined as the crack initiation phase.

The remaining fatigue life after a crack depth of 0.1 mm had been reached was defined as crack propagation. The mean number of cycles in this phase was 350 000 cycles and this phase had only a weak positive correlation of 0.5 with the time to crack initiation. This is taken as support for the argument that there are two different damage mechanisms involved in the two phases. Hence, the two phases should be modelled separately.

The crack propagation phase was modelled by the formulas and recommendations found in rules and regulations (BS 7910 and DNVGL). The recommended equations for calculation of the SIFR and the prescribed growth parameters agree with the behavior of the cracks during testing. The best fit parameters C and m were close to the recommended mean values when the SIFR calculations were based on the mean weld toe angle and the expected crack shape. However, for small cracks the weld toe radius, which is not included in the formulas for the SIFR, will play a role between depths of 0.1 mm and 0.5 mm.

Amongst the deviations found between measured growth rates and model predictions the lower crack growth rates given by BS 7910 for low values of the SIFR were found to be too optimistic compared with the measured rates. This is explained by the fact that the rate curve given by BS 7910 is based on measurements with long central cracks. In the present work it was found that small semi elliptical surface breaking cracks do not slow down in the same manner as the SIFR decreases.

For deeper cracks a correct prediction of the crack growth rate is dependent on an appropriate modelling of crack coalescence. Crack coalescence of multiple cracks will take place at crack depths close to 10% of the plate thickness. The SIFR will then increase substantially and speed up the growth rate when the multiple cracks form one single edge crack. Neglecting this transition by continuously using a two-directional single crack growth model will overestimate the time spent in crack propagation when using the given SIFR formulas and recommended growth rates.

In addition to the models given by DNVGL and BS 7910, the unique crack growth model proposed by Huang et al. seems to have an advantage over other models because it explicitly takes account of the R ratio for the applied stresses. However, the measured crack growth does not seem to slow down as the models predicts when ΔK reduces below 10 MPa m$^{0.5}$. The model recommendation of a threshold value of 7.2 MPa m$^{0.5}$ at $R = 0$ seems too high. Again, the explanation seems to be that small surface breaking elliptical cracks at the weld notch do not slow down for low values of the SIFR as is the case for long cracks in components without notches.

The applied models were finally verified by Monte Carlo simulation of the propagation fatigue lives compared with the F class S-N curve. Observations were made regarding when run-outs start to occur when the stress range was decreased towards the fatigue limit. This confirmed that the threshold value for the SIFR pertaining to the unique model is too high. Future work will focus on how to model this value. An appealing approach can be to model it as a random variable.

The Monte Carlo simulation was also carried out with a complete two-phase model by adding on the initiation life. It was demonstrated that this model represents a shift in the explanation of the very long lives at low stress ranges. The earlier explanation based on the threshold value for SIFR is replaced by the occurrence of very long initiation lives. Furthermore, both experimental data and simulated data support the suggestion that the linear S-N curve with two-line segments for a log-log scale should be replaced by a continuous non-linear curve. The curve can be obtained by the Random Fatigue Limit Model. This will be pursued in future work.

Acknowledgments

Appendix A. Finite element model of welded joint

A parametrized FE model was built by applying the Abaqus/CAE software. The local weld toe geometry was described by the flank angle θ and the toe radius ρ. The attachment length to the thickness ratio was kept constant at $L/T = 2$. A static analysis was carried out in 2D and plane strain conditions were assumed. Linear elastic material properties with $E = 206$ GPa and $\nu = 0.3$ were used. Due to symmetry, only a quarter of the specimen was modelled and symmetrical boundary conditions were applied. The membrane loading mode was simulated by applying uniformly distributed load to the end of the load-carrying plate. 8-node biquadratic plane strain quadrilateral elements (CPE8) were used. In the notch region element size was about 5% of the toe radius. Visualization of the FE model is presented in Fig. A1.
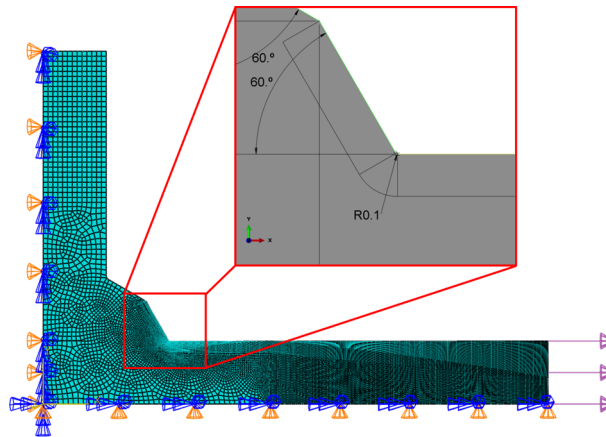
Fig. A1. FE model visualization.

Appendix B. Correction of the ACPD measurements

The ACPD monitoring system was based on the application of a conventional U8 Microgauge. The nickel pin probes were spot welded to the weld toe region. At selected locations one pair of probes was straddling over the potential crack location with a reference pair of probes nearby. There were 10 measurement locations along the weld seam of each specimen. The ACPD measurements can only estimate crack depth increase, the measurements were related to true crack depths at a chosen number of cycles by two different techniques:

- at given stages where the ACPD measurements had passed a linear estimate a_{est1} of 0.1 mm crack depth, ink was injected into the fatigue crack.
- for larger crack depths beach marking was carried out by reducing the stress range.

Both techniques made it possible to read the true crack depth on the fractured surface after the failure of the specimen at the end of the test. A sketch of such readings is shown in Fig. B1. Based on these readings the first linear estimate a_{est1} was corrected to a value a_{est2} that agreed better with post surface depth readings. The true crack depth was always deeper than the first estimate. The following correction function was obtained:

$$a_{est2} = a_{est1} + g(a_{est1})$$

$$g(a_{est1}) = \begin{cases} \dfrac{a_{est1}}{\varphi^2} e^{-\frac{a_{est1}^2}{2\varphi^2}} & for\ \ 0 \leq a_{est1} \leq a_{th} \\[2ex] a_{th} + \dfrac{a_{th}}{\varphi^2} e^{-\frac{a_{th}^2}{2\varphi^2}} + b(a_{est1} - a_{th}) - a_{est1} & for\ \ a_{th} < a_{est1} \leq a_{end} \end{cases}$$

$\varphi = 1.17$
$a_{th} = 1.33$ mm
$a_{end} = 6$ mm
$b = 0.891$ (B-12)

Correction function $g(a_{est1})$ is shown in Fig. B2. This rather peculiar correction was chosen because it gave better fit to the depth readings than any polynomial function. No correction has been imposed to cracks deeper than 6 mm as the formula used for first linear estimation gives very accurate results in this crack regime.
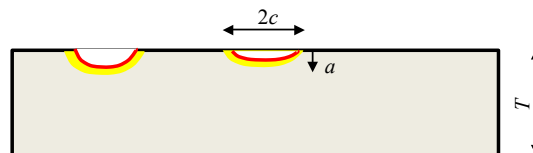
Fig. B1. Elliptical surface flaws along the weld toe.
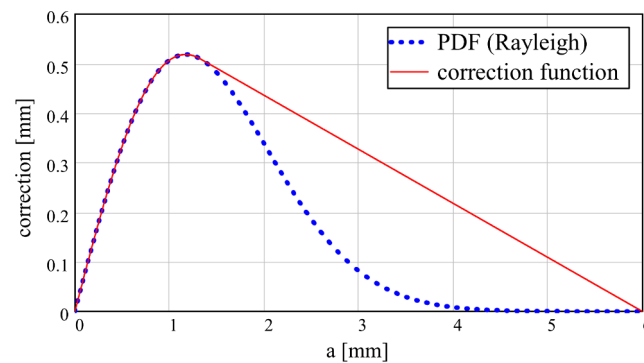
Fig. B2. Correction function used for the estimation of crack depth.

References

[1] Hobbacher A. Recommendations for fatigue design of welded joints and components; 2016.

[2] Almar-Naess A. Fatigue handbook: offshore steel structures. Trondheim: Tapir; 1985.

[3] Haibach E. "Discussion paper," The welding institute conference on fatigue of welded structures, Brighton; 1970.

[4] Lawrence FV, Burk JD, Mattos RJ, Higashida Y. Estimating the fatigue crack initiation life of welds. STP648 fatigue testing of weldments. 1978. p. 134–58.

[5] Radaj D. Design and analysis of fatigue resistant welded structures. Cambridge: Abington Publishing; 1990.

[6] Radaj D, Sonsino CM, Fricke W. Fatigue assessment of welded joints by local approaches. Elsevier Science; 2006.

[7] Lassen T, Recho N. FLAWS fatigue life analyses of welded structures. ISTE; 2006.

[8] DNVGL-RP-0001. Recommended practice: probabilistic methods for planning of inspection for fatigue cracks in offshore structures. DNV GL AS; 2015.

[9] BS 7910. Guide to methods for assessing the acceptability of flaws in metallic structures. BSI; 2013.

[10] Newman JC, Raju IS. An empirical stress intensity factor equation for the surface crack. Eng Fract Mech 1981;15(1–2):185–92.

[11] Bowness D, Lee MMK. Prediction of weld toe magnification factors for semi-elliptical cracks in T-butt joints. Int J Fatigue 2000;22(5):369–87.

[12] King RN. A review of fatigue crack growth rates in air and seawater. Health and Safety Executive; 1998.

[13] Huang X, Moan T, Cui WA. A unique crack growth rate method for fatigue life prediction of steel structures. Ship Offsh Struct 2009;4(2):165–73.

[14] Baptista C, Reis A, Nussbaumer A. Probabilistic S-N curves for constant and variable amplitude. Int J Fatigue 2017;101:312–27.

[15] Zerbst U, Madia M, Schork B. Fracture mechanics based determination of the fatigue strength of weldments. Proc Struct Integr 2016;1:10–7.

[16] Bremen U. Amélioration du comportement à la fatigue d'assemblages soudés étude et modélisation de l'effet de contraintes résiduelles. Lausanne: EPFL; 1989.

[17] Huang X, Moan T. Improved modeling of the effect of R-ratio on crack growth rate. Int J Fatigue 2007;29(4):591–602.

[18] Albrecht P, Yamada K. Rapid calculation of stress intensity factors. J Struct Div Proc ASCE 1977;103(ST2):377–89.

[19] Lassen T. The effect of the welding process on the fatigue crack growth in welded joints. Weld J 1990;February:75s–85s.

[20] EN ISO 5817:2014 Welding - Fusion-welded joints in steel, nickel, titanium and their alloys (beam welding excluded) - Quality levels for imperfections; 2014.

[21] Lassen T, Recho N. Proposal for a more accurate physically based S-N curve for welded steel joints. Int J Fatigue 2009;31(1):70–8.

[22] DNVGL-RP-C203: fatigue design of offshore steel structures; 2016.

[23] Bell R, Vosikovsky O, Bain SA. The significance of weld toe undercuts in the fatigue of steel plate T-joints. Int J Fatigue 1989;11(1):3–11.

[24] McFadyen NB, Bell R, Vosikovsky O. Fatigue crack growth of semi- elliptical surface cracks. Int J Fatigue 1990;12(1):43–50.

[25] Frise PR, Bell R. Fatigue crack growth and coalescence at notches. Int J Fatigue 1992;14(1):51–6.

[26] Pascual FG, Meeker WQ. Estimating fatigue curves with the random fatigue-limit model. Technometrics 1999;41(4):277–89.

[27] Darcis P, Lassen T, Recho N. Fatigue behavior of welded joints Part 2: physical modeling of the fatigue process. Weld J 2006;2:19s–26s.

[28] Leonetti D, Maljaars J, (Bert) Snijder HH. Fitting fatigue test data with a novel S-N curve using frequentist and Bayesian inference. Int J Fatigue 2017;105:128–43.

Paper C

Crack growth in fillet welded steel joints subjected to membrane and bending loading modes

Zbigniew Mikulski, Tom Lassen

Crack growth in fillet welded steel joints subjected to membrane and bending loading modes

Zbigniew Mikulski*, Tom Lassen

University of Agder, Jon Lilletuns vei 9, 4879 Grimstad, Norway
National Oilwell Varco (APL Norway), Arendal, Norway

ABSTRACT

The present paper presents the results from extensive studies of the fatigue damage evolution in fillet welded steel joints subjected to Constant Amplitude (CA) stress under membrane and bending loading modes. The welded joints in question are F class details (category 71) with plate thicknesses ranging from 25 to 32 mm. The steel quality is a medium strength carbon manganese steel. Crack growth histories for the shallow semi-elliptical shaped cracks emanating from the weld toe are obtained by an Alternating Current Potential Drop (ACPD) technique. These growth histories are presented in detail and modelled by Linear Elastic Facture Mechanics (LEFM). The calculations follow the recent recommendations found in rules and regulations based on different formats of the Paris law. The uncertainties related to a multiple cracks situation and the variability in the weld toe geometry are discussed. The measured crack growth was modelled from an initial crack depth of 0.1 mm to final fracture. The recommended rule-based parametric formulas for the Stress Intensity Factor Range (SIFR) for small surface cracks at the weld notch are examined and supplemented by results from finite element modelling. Recommendations are given on how to make decision regarding uncertainties related to a correct characterization of the local weld toe geometry and the crack coalescence. Finally, an attempt is made to capture the influence of the applied stress ratio R and the applicability of a threshold value for the SIFR is discussed.

1. Introduction

The reliability against fatigue failure is of vital importance both in the design and in the planning of scheduled inspections for welded details in steel structures. The fatigue resistance of welded joints is characterized by random variations caused by the uncertainties related to imperfections such as the possible presence of initial flaws and irregular weld toe geometries. These variables cause significant scatter in fatigue crack growth and final fatigue lives. Consequently, statistical analysis of crack growth data and associated reliability models for the fatigue life must be applied to handle the problem in a consistent and rational manner. Fatigue lives must be predicted, and safety margins must be chosen for a given target service life. In addition, in-service inspection must be planned and carried out for the most critical details to maintain the reliability against fatigue failure. For the offshore industry in Norway it was a great advance in knowledge in these areas when the Fatigue Handbook was published in 1985 [1]. New methodology and models were presented and explained for the practicing engineer both regarding the S-N approach and for applied fracture mechanics. Both fields have of course been developed further since then, particularly the fracture mechanics modelling. A good overview of the recent progress is given by Hobbacher [2], Radaj et al. [3], Lassen and Recho [4] and Lotsberg [5]. This engineering

Nomenclature

SymbolsRoman letters:

a	crack depth
a_{est1}	first ACPD estimate of crack depth
a_{est2}	corrected depth
a_{ini}	initial crack depth
a_1	crack depth at the start of crack coalescence
a_2	crack depth at which a/c ratio is assumed to reach value of 0.01
c	crack half-length
c_{ini}	initial crack half-length
C	crack growth rate parameter in Paris equation
e	distance between pin probes
E	module of elasticity
F_{tot}	total geometry factor
g	correction function
K_I	stress intensity factor for crack opening mode (mode I)
L	attachment length
m	crack growth rate exponent in Paris equation
M_{km}	weld toe magnification factor
p	parameter in forcing function of the crack shape evolution
q	parameter in forcing function of the crack shape evolution
R	stress ratio
t	thickness of the specimen
V_c	measured potential over the crack
V_{c0}	measured initial potential over the crack
V_r	measured potential over the reference surface
V_{r0}	measured initial potential over the reference surface
Y	geometrical correction factor

Greek letters:

α_i	material parameter in Dang Van criterion (slope)
ΔK_E	effective SIFR at $R = 0$
ΔK_{th0}	threshold value for the SIFR at $R = 0$
θ	weld toe transition angle
ρ	weld toe transition radius
σ_0	nominal stress
σ_h	maximum hydrostatic stress
τ_a	shear stress amplitude
τ_{0i}	material parameter in Dang Van criterion (intercept)

Abbreviations

ACPD	Alternating Current Potential Drop
CA	Constant Amplitude
COV	Coefficient of Variation
CT	Compact Tension
ERR	Energy Release Rate
ESIFR	Effective Stress Intensity Factor Range
FCAW	Flux-Cored Arc Welding
FE	Finite Element
FM	Fracture Mechanics
FMM	Fracture Mechanics Model
HAZ	Heat Affected Zone
IIW	International Institute of Welding
LEFM	Linear Elastic Fracture Mechanics
SAW	Submerged Arc Welding
SCF	Stress Concentration Factor
SIF	Stress Intensity Factor
SIFR	Stress Intensity Factor Range
SMAW	Shielded Metal Arc Welding
RFLM	Random Fatigue-Limit Model
TPM	Two Phase Model
VA	Variable Amplitude
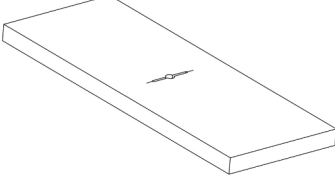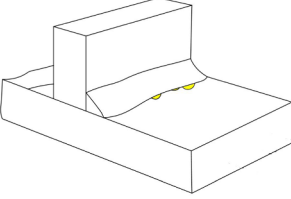
fracture mechanics approach has matured into applicability in recent years based on the work of Newman and Raju [6] and Bowness and Lee [7]. These works give the necessary formulas for calculating the Stress Intensity Factors (SIF) at the weld notch. These formulas are now presented in the guidelines given by DNVGL-RP-C210 [8] and BS 7910 [9]. An alternative model is the unique fracture mechanics model suggested by Huang et al. [10]. This model has the appealing feature that it explicitly considers the effect of the applied R ratio for the stress variation on crack growth. However, there are still problems regarding the size of the initial flaws and the characterization of the irregular toe geometry when applying these models to small semi-elliptical cracks with a typical depth of 0.1 mm. General practical guidelines and acceptance criteria for weld imperfections are given in [11], but the information given is not detailed enough to provide data for a LEFM model.

The established LEFM models with the Paris propagation law as basis are usually based on the experimental results obtained from testing with standard specimens such as Compact Tension (CT) specimens or wide plates with a long central crack. The objective of the present work is to provide data for the fatigue crack growth evolution leading to the final failure in more realistic joint geometries as found in structural welded details. The work includes the influence of possible weld imperfections and the variability in the local weld toe geometry. How to model the behavior of multiple cracks along the weld seam is also addressed. The various types of uncertainties that are introduced when analyzing a welded joint compared with a wide plate standard specimen are listed in Table 1. A distinction is made between physical, measurement, statistical and model uncertainty, as per [12].

The physical uncertainty in Table 1 reflects the uncertainty in physical variables. For the present joints this type of uncertainty is given by the variability in the local toe profile (i.e. toe angle and radius) and the size of possible initial crack depths. The growth parameters characterizing the steel quality may also change along the crack path as the steel microstructure changes when going from the HAZ into the base plate. For this reason, these parameters are treated as random variables [8,9]. The measurement uncertainty is caused by the fact that the exact position of the crack front is hidden during the testing of the joints. The crack depths in the present case are obtained by ACPD estimates that must be calibrated against true crack depths observed on the fatigue crack planes after the test of the joints. The statistical uncertainty listed in Table 1 is related to the limited number of observations available when determining the random variables involved in the crack propagation model. This gives uncertainty when determining the mean values

Table 1

Overview of the sources of uncertainties in the fatigue crack growth in welded joints compared with standard wide plate test specimens.

Type of uncertainty	Standard test specimen: Wide plate with a single long central crack	Present test specimen: Welded detail with multiple shallow semi-elliptical cracks emanating from the weld toe
Physical	The global geometry and steel properties are well defined and easy to control. The initial crack length is known	The global geometry is well defined. There are large variabilities in the local toe geometry. The steel properties may change during the crack growth. The initial crack depth is unknown
Measurement	The crack growth of a single crack can be measured precisely	The ACPD measurements of the crack depth must be calibrated. Crack coalescence has an important impact. The definition and the measurement of the weld toe geometry are sometimes difficult
Statistical	Little uncertainty due to the many tests carried out	The limited number of tests available give lower confidence in the random variables
Model	The Paris law has a proven validity for these large crack sizes. The threshold value for the SIFR exists and can be determined	The validity of the Paris law for small semi-elliptical cracks at the weld toe is questionable. The threshold value for the SIFR has never been proven. Different loading modes may occur

and the associated standard deviations for these variables. This uncertainty is often dealt with by specifying a confidence interval for the estimated mean and variance of the variable. Finally, the model uncertainty is the most important part of the present investigation. The Paris law applicability has been proven for rather long cracks in well-defined test objects. The law's applicability for very shallow semi-elliptical crack in the weld toe notch stress field is still uncertain. For such small cracks special models must be developed. A good overview of the topic can be found in [13,14]. On this background the research questions to be answered by the present work are:

- Does there exist a fatigue crack initiation phase for as-welded joints or do there exist crack-like defects already from the start?
- Can the growth model given by the Paris law and established by testing of wide plates with a central crack be applied for these small semi-elliptically shaped cracks at the weld toe?
- For the crack growth phase, what is the best way to characterize the variable weld toe geometry when determining the SIFR for small semi-elliptical cracks?
- What is the impact of crack coalescence and how shall the coalescence of multiple cracks be accounted for in the crack growth model?
- What are the most important differences in the crack growth behavior under the membrane and the bending loading modes?

The authors find these questions of vital importance as the uncertainties listed in the right column of Table 1 are the same as the uncertainties encountered for a similar structural detail in a load bearing structure in service. An important additional physical uncertainty for structural details in service is of course the magnitude of the acting stresses. Furthermore, significant additional model uncertainty is also introduced caused by the Variable Amplitude (VA) loads often occurring in service. Nevertheless, the uncertainties given in the right column of Table 1 must be understood, characterized and modelled in the first place before these additional in-service uncertainties can be dealt with.

The present work is carried out with non-load-carrying fillet welded transversal attachments where the cracks are emanating from the weld toe. The joints were made of medium strength C-Mn steel with a typical plate thickness of 25–32 mm. The results are representative of an F-class detail according to DNV RP-C203 (2001) [15] or category 71 in ENV 1993-1-9: 1992 [16]. For all the test specimens the crack growth histories were very accurately monitored and logged from an initial crack depth below 0.1 mm up to final failure at a crack depth in the range of 12–15 mm. Based on the crack growth data, fracture mechanical modelling is carried out for the growth phase in specimens subjected to the membrane and the bending loading mode respectively.

2. Modelling the crack growth in welded joints

2.1. Discussion of the crack development in various phases

From a material science perspective, the fatigue damage process in metallic components involves several phases, starting from dislocations at the atomic scale, through crack nucleation and crack propagation until final fracture occurs. For welded joints the damage process is often modelled by the following three phases [13,17]:

- Phase 1: Crack nucleation. The cracks initiate due to repeated irreversible plastic deformation at irregularities in the

microstructure, e.g. at dislocations and grain boundaries. The cracks may initiate close to the surface or at the surface.

- Phase 2: Growth of short cracks with sizes down to the grain size of the microstructure typically in the range from 10 to 100 μm.
- Phase 3: Growth of larger cracks with depths beyond 100 μm.

It is generally accepted that the crack nucleation is an important part of the fatigue damage evolution in high quality machined parts with a smooth surface. It has been a usual assumption that this phase could be neglected for welded joints. However, in the absence of weld imperfections such as slag intrusions, cold laps or undercuts the natural nucleation phase may play an important role even for welded joints. This is a fact for welded joints with post weld treatment such as grinding, but the phase may also be important for as-welded joints at low stress ranges. Phase 1 can be modelled by a local stress–strain approach based on the notch stress situation at the weld toe. This approach is often limited to a uniaxial stress situation using the largest principal stress range as a key to the crack initiation life. The approach does not consider the presence of any initial flaws caused by weld imperfections. The most common calculation scheme is to determine the number of cycles to crack initiation by applying the Coffin-Manson equation with the Morrow mean stress correction [3]. An alternative to this approach is to use the Dang Van equivalent shear stress criterion to determine the crack initiation life [18]. According to this approach, for any number of cycles N_i to crack initiation under constant amplitude loading, a critical state can be described as:

$$\tau_{0i} = \tau_a + \alpha_i \sigma_h \tag{1}$$

where τ_a is the shear stress amplitude, σ_h is the maximum hydrostatic stress, α_i and τ_{0i} are material parameters obtained by testing. This approach is more in line with the fact that the crack nucleation is driven by the shear stress variations. The Dang Van approach can also take account for a multiaxial stress situation at the weld toe through the hydrostatic stress component occurring in combination with the acting shear stress amplitude. Welding residual stresses often give a multiaxial stress situation. This methodology was originally proposed for determining the fatigue limit for non-welded components [18]. The approach has later been applied for modeling the initiation life for the present test series I in an earlier publication by the present authors [19]. The numerical results are not repeated in the present paper.

A fracture mechanics approach can be applied to model the short crack growth that takes place in phase 2. The SIFR calculations must be carried out such that the particularities for short crack behavior are accounted for. The SIFR calculation does not follow linear elastic theory because the crack tip plasticity cannot be ignored. An effective SIFR must be calculated and crack arrest at grain boundaries must be considered [20]. This makes the calculation scheme substantially different from models based on LEFM that are applied for cracks with larger size.

For as-welded joints subjected to a stress situation for which both phase 1 and 2 are a modest part of the entire fatigue life it is a temptation to simplify phase 1 and 2 by merging them together into one single phase. One must then choose between the local stress–strain approach and the short crack growth approach described above to model this hybrid phase. None of the two approaches will be theoretically correct but they may both be accurate enough for a practical engineering crack growth prediction. Zerbst et al. [20] chose to develop a methodology based on short crack behavior. An elastic–plastic crack driving force is defined, and the gradual build-up of the crack closure effect is determined. An initial crack size based on a crack arrest criterion is obtained. Fictitious initial crack sizes close to 10–20 μm are obtained by the model. Based on this methodology a fatigue stress limit as defined by an S-N curve was determined. The proposal was based on an effective SIFR under loading mode I. The possibility that the early short cracks may grow in a shear mode involving loading mode II (the tearing loading mode) was not considered. An alternative to this fracture mechanics approach for this hybrid phase is to use the Dang Van notch stress approach as discussed above.

Phase 3 is in most cases the last and most important phase for crack propagation in welded joints. A review of this propagation phase is given by Fricke [21]. This is the phase that is given emphasis to in the present work. The applicability of the models, the formulas and the growth parameters recommended in rules and regulations for this phase is at the essence of the present investigation. This approach gives the necessary tool for an engineering critical assessment of welded structural members with crack like defects. Furthermore, the approach is a necessity when carrying out risk-based inspection planning for welded structures.

2.2. Basic concepts – The Paris law

The crack growth models recommended for phase 3 in rules and regulations (DNVGL-RP-C210 [8] and BS 7910 [9]) are based on Linear Elastic Fracture Mechanics (LEFM). The main premise of this approach is a linear relation between the crack growth rate and the stress intensity factor range for a log–log scale. The growth parameters C and m are obtained from this linear curve and these parameters are often treated as material properties. However, it has been observed that these parameters are dependent on the applied stress ratio R. Hence, in the BS 7910 document different values for the C and m are proposed for $R < 0.5$ and $R \geq 0.5$. The DNVGL document neglects this difference. Another approach is to treat C and m as material constants and use them together with the effective stress intensity factor range that explicitly considers the influence of the R ratio. These crack growth models often utilize the concept of an effective SIFR in combination with a threshold value. This approach goes back to the theoretical work by Elber [22] who introduced the crack closure concept. However, the influence of R on the effective SIFR is given by parametric formulas that are obtained empirically from test results with wide plates. Such an approach, designated 'a unique crack growth rate curve method' has been proposed by Huang et al. [10]. The crack growth rate equation can be expressed as:

$$\frac{da}{dN} = C(\Delta K_E^m - \Delta K_{th0}^m) \tag{2}$$

where ΔK_E is the effective SIFR for the given R ratio, whereas the ΔK_{th0} is the threshold value for the SIFR at $R = 0$. More details regarding this method, with the definition of ΔK_E including the underlying formulas and parameters, can be found in [23]. Some remarks regarding the application of this approach for modelling crack growth in welded joints under membrane loading mode were also presented in [24]. For the unique model the parameters m and C can be treated as true material parameters independent of the R ratio. This is also true for the threshold value as the influence of the applied R ratio is accounted for in the calculation of the effective SIFR. The method proposed by Huang is also interesting in the way that the factor used in the definition of the effective SIFR has also been applied as a multiplication factor on the nominal stress range when predicting the fatigue life based on S-N curves, [25,26]. This is an attempt to explicitly take into account the mean stress effect for life predictions based on S-N curves. However, in the present work we shall focus on the application of this factor in the crack growth model.

In summary, the experimental results in the present work will be analysed by two fracture mechanics models, for a given R-ratio:

- Model 1: DNVGL – One linear growth curve for a log–log scale applying the nominal value for the SIFR
- Model 2: Unique crack growth rate curve model – Non-linear growth curve for a log–log scale applying the effective value for SIFR

All models get an extension 'a' if the threshold value is neglected and extension 'b' if the threshold value is included. The crack growth parameters C and m for these models are presented in Table 2 together with possible values for ΔK_{th0}. These values are referred to as the original values for the models.

A graphical representation of the two models is shown in Fig. 1. The unique model is drawn for $R = 0.35$ and $R = 0.1$ which are the stress ratios for the present test series I and series II respectively, see Section 3. As can be seen from the figure the curves almost coincide when ΔK is larger than 10 MPam$^{0.5}$. The BS 7910 growth curve is included for comparison. This curve is not applied in the present analysis because the unique model can be regarded as non-linear version close to the two linear segments given in BS 7910. The unique model is somewhat more optimistic regarding the level of the threshold value for the SIFR. The DNVGL curve is the most pessimistic one in the way that it keeps a straight line until ΔK reaches a threshold value of 2 MPam$^{0.5}$.

2.3. Calculation of the SIF according to rules and regulations

The nominal S-N approach does not make a distinction between the membrane and bending loading mode, but the SIF calculation in a fracture mechanics model does. Before applying the models in Section 2.2 we will investigate the difference between the SIFR for these two modes particularly for small cracks. In the present work the formulas adopted in DNVGL-RP-C210 [8] are used for calculating the SIF. The general expression for the SIF for a given loading mode can be written in the form:

$$K_I = \sigma_0 Y(a, c) M_k(a, c) \sqrt{\pi a} \tag{3}$$

where a is the crack depth, $2c$ is the crack surface length and σ_0 is the applied nominal stress. The function Y gives the influence of the global plate and crack geometry, whereas M_k takes account for the effect of the weld notch. The functions Y and M_k also take account for the loading mode. The notch factor M_k is dependent on the crack depth and shape, the welded attachment length and the local toe geometry, see DNVGL-RP-C210 [8] for further details. The formulas given to determine the geometry factor Y are based on the work of Newman and Raju [6] who proposed empirical parametric equations for the stress intensity factors for semi-elliptical surface cracks in flat plates subjected to membrane and bending loads. These equations have been obtained from a 3D FE analysis. 20 years later Bowness and Lee [7] proposed empirical formulas for a weld toe magnification factors M_k which, together with Newman and Raju formulas, allows us to obtain SIF values for surface breaking semi-elliptical shaped cracks located in the weld toe notch area. Weld toe magnification factors were obtained for the membrane and bending loading modes using the J-integral approach and 3D FE simulations. The M_k factor is obtained at the deepest point and at the surface points along the crack front by comparing SIFs for a given crack in a T-butt joint and in a flat plate. Hence, the influence of the local weld toe geometry was determined by comparing the two cases. Only the weld toe flank angle θ is explicitly entering the obtained formulas. The influence of the weld toe radius ρ is considered in a simplified way, by two separate sets of formulas for $\rho = 0$ and $\rho = 0.1 t$ (t being the load-carrying plate thickness) corresponding to an as-welded and a ground joint respectively. The assumption of $\rho = 0$ is in most cases overly pessimistic as the transition between the weld bead and the plate usually is smoother with $\rho > 0$. Hence, although the assumption may be acceptable from the design point of view, it may not be sufficiently accurate for modelling the early crack growth of shallow elliptical cracks. For this reason, a short discussion regarding the influence of the weld toe radius on the SIF calculations for shallow cracks will be presented in Section 2.4. The parametric formulas for the weld notch magnification factor M_k proposed by Bowness and Lee were developed by multiple regression analysis and thus the authors did not recommend extrapolating them outside the validity limit for the crack depth. The lower limit value of the crack depth to thickness ratio in the given formulas is $a/t = 0.005$ [7]. This corresponds to a crack depth of 0.125 mm for a plate thickness of 25 mm. In the need of using the formulas below the given validity limit they

Table 2
Original C and m constants in the basic models.

FMM	C (mean value with rate in mm/cycle and ΔK in MPam$^{0.5}$)	m	ΔK_{th0} [MPam$^{0.5}$]	SIFR based on R
Model 1a or 1b	5.79·10^{-9}	3	0 or 2	No
Model 2a or 2b	8.32·10^{-9}	2.88	0 or 7.2	Yes
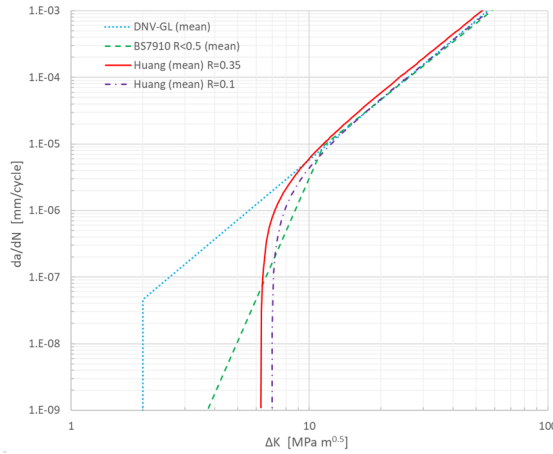
Fig. 1. Prediction of growth rates for various models (model type #b).

suggested to use the M_k value at the given lower limit for the crack depth. As the factor M_k has a strong bearing on the calculation of the SIF this aspect is particularly important when dealing with shallow cracks at the weld toe. The problem is illustrated in Fig. 2. As can be seen from the curves the weld notch magnification factors have a steep gradient when extrapolation is carried out below the validity limit of $a/t = 0.005$. If one chooses to keep the factors constant below $a/t = 0.005$ this will make an important difference compared to using the extrapolated values when predicting the very early crack growth. Consequently, if fracture mechanics are to be applied to these small cracks it is obviously a need to clarify which values are to be used for the magnification factors when $a/t < 0.005$.

From Fig. 2 it is also seen that for the deepest crack point the magnification factors are higher for the bending loading mode than for the membrane loading mode. This is observed for flank angles higher than 35°, for lower angles the situation is opposite. The maximum differences reach about 10% and may be caused by inaccuracy of the approximation formulas proposed by Bowness and Lee. For plates without a notch it is the membrane loading mode that gives the highest value at the deepest point. A comparison of the total geometry factors, YM_k for the membrane and bending loading mode is presented in Fig. 3.

The magnification factors and the total geometry factors presented in Fig. 2 and Fig. 3 are obtained for the constant crack shape given by the a/c ratio. In practical cases, the shape of the crack changes while the crack is growing. According to the applied model the shape evolution of a single semi-elliptical crack will be as presented in Fig. 4 for the two loading modes. The initial shape of the crack is set to $a/c = 0.25$ and the growth parameters C and m for model 1 are applied.

As can be seen from Fig. 4 at the very beginning of the crack growth both the loading modes have increasing aspect ratio a/c. It means that the cracks grow relatively faster in the depth direction than in the length direction. Subsequently the a/c ratio is decreasing during the growth history for the bending loading mode whereas it continues to increase for the membrane loading mode. The explanation is that for the bending loading mode the deepest point at the crack front is growing away from the maximum bending stresses and the associated weld toe stress concentration at the surface as the crack front approaches the neutral axis for bending. The surface ends of the crack are subjected to these maximum stresses during the entire crack evolution. This explains the somewhat
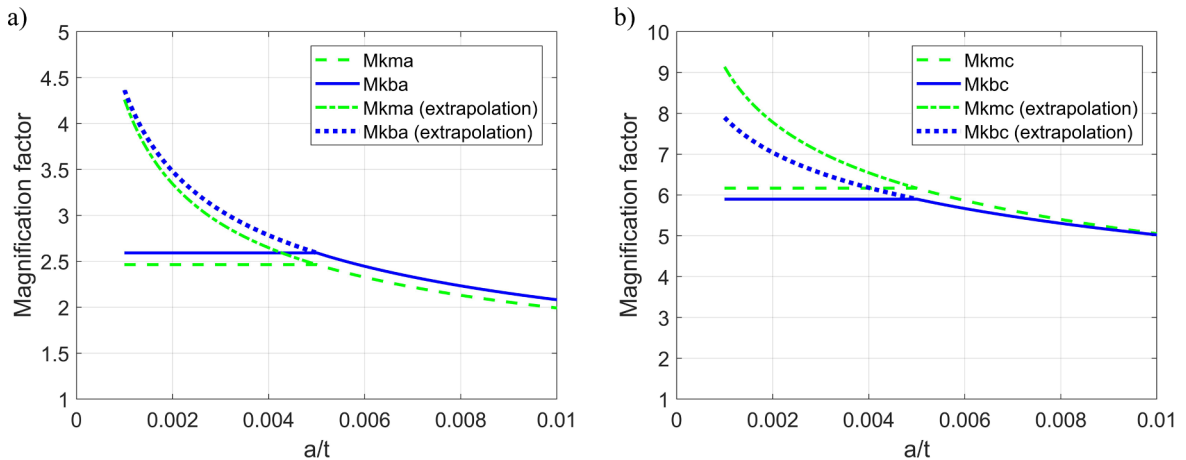
Fig. 2. Magnification factors, M_k, for shallow cracks for membrane and bending loading: a) at the deepest point, b) at the crack ends; (constant $a/c = 0.2$, $L/t = 2$, $\theta = 45°$, $\rho = 0$).
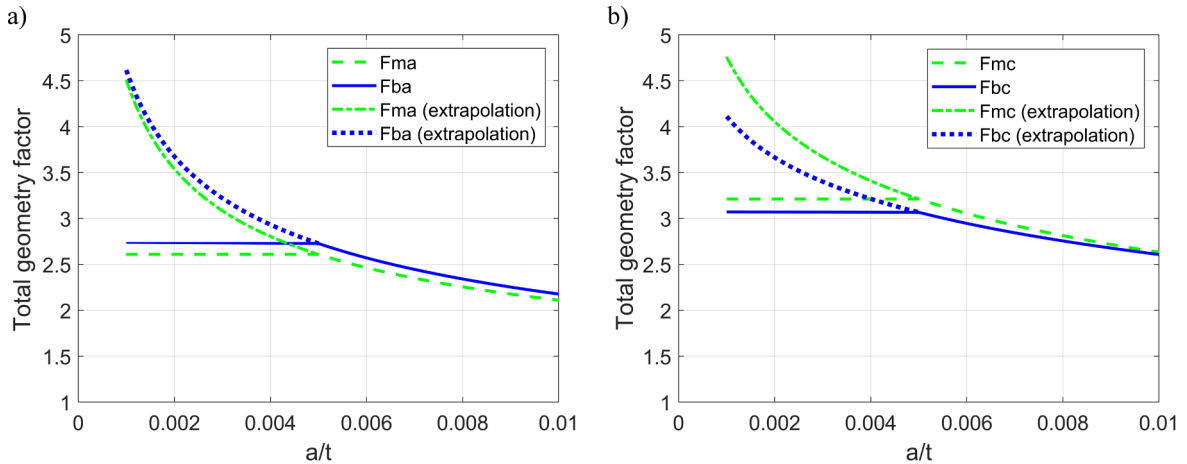
Fig. 3. Total geometry factors, $F_{tot} = Y \cdot M_k$, for shallow cracks for membrane and bending loading: a) at the deepest point, b) at the crack ends; (constant $a/c = 0.2$, $L/t = 2$, $\theta = 45°$, $\rho = 0$).
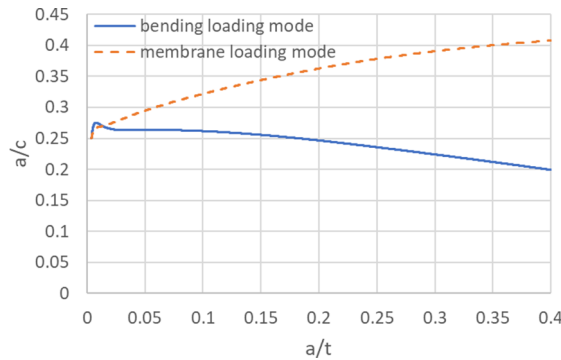
Fig. 4. Crack shape evolution of a single semi-elliptical crack for the membrane and bending loading mode ($a_0/c_0 = 0.25$, $L/t = 2$, $\theta = 45°$).

peculiar shift in the crack shape evolution at the early crack growth for the bending loading mode. We shall compare this theoretical behavior of the shape evolution with a more realistic multiple-cracks situation including crack coalescence in Section 5.1. We will also compare the shape evolution with the aspect ratios measured on the test specimens.

2.4. Additional analysis for determining the SIF for small shallow cracks at the weld toe

The parametric formulas developed by Bowness and Lee are, as suggested by them, not applicable for smaller crack than $a/t = 0.005$. For as welded joints the toe radius ρ was set to 0 mm, whereas the maximum toe angle θ was set to 60°. The problem of the influence of local geometry on the stress concentrations and stress gradients at the weld toe notch area in an un-cracked joint has been thoroughly investigated in [24]. Based on the through-thickness stress distribution in the plate without the presence of a crack, the weld toe magnification factors were obtained. It was done utilizing the approach proposed by Albrecht and Yamada [27] which is based on the correction factor that accounts for nonuniform opening stresses along the crack faces. It was reported that local weld toe geometry has a significant impact on the SIF values for shallow cracks close to the present transition crack depth of 0.1 mm. It was also verified that the upper limit on the flank angle given by 60°, as suggested by Bowness and Lee and adopted in the DNVGL document, is not an obstacle for applying the given formulas for the present fatigue crack analysis. Steeper angles will not give a substantial increase of the SIF. However, various values of the toe radius will have an important influence on the SIF for cracks down to the present transition depth of 0.1 mm. This is neglected in formulas in DNVGL based on the work by Bowness and Lee. To corroborate the qualitative assessment made in [24] a direct calculation of SIF based on FEA for a joint containing a crack was carried out in the present work. The same procedure as used by Bowness and Lee was applied, but to limit the computational effort the analysis was made for an edge crack only. In the present paper a crack spanning the entire width of the plate is called an edge crack. The 2D FE model with a crack at the weld toe notch has been built in Abaqus software and the magnification factors have been obtained by comparing SIFs with similar cracks in a flat plate. SIF values have been obtained using J-integral approach utilizing solution of the stress distribution around the crack tip. Cracks with depth to thickness ratio from 0.002 to 0.01 have been analysed. The model includes local weld toe geometry described by toe radius and flank angle and the analysis is carried out under plane strain conditions. All results discussed and presented in this section are obtained for the membrane loading mode. Bowness and Lee propose

not to extrapolate M_k factors outside the validity limits of the dependent parameters (a/t, a/c, L/t, θ) and use the closest limit value. This recommendation has been used by Lotsberg [28,29] when using a fictitious small initial crack size distribution that enters into the crack growth model. The goal for the proposed model was to obtain a total fatigue life consistent with the S-N based predictions. However, based on results from the present FE model this seems to be incorrect for shallow cracks with $a/t < 0.005$. The exact crack location and orientation are very important when computing SIF for such small cracks. In the simplest model the crack planes are assumed to be perpendicular to the plate surface and located at the starting point of the weld toe. However, the exact location of a hot spot is somewhat higher up on the weld toe profile. If we assume crack location at the point of maximum principal stress (in an un-cracked state) and that crack planes orientation are perpendicular to the principal stress direction, then a difference in SIF estimation is observed, especially for very shallow cracks. The results given by the stress distribution for a cracked joint and the associated total geometry factor $Y \cdot M_k$ are presented in Fig. 5. As can be seen, the difference in the SIF increases when toe radius increases. In the present work we shall choose the crack path perpendicular to the plate surface at the start of the toe radius. This agrees with common practice and observation of the crack initiation spot in laboratory testing.

M_k factors have been extracted from FE simulations and compared with results based on Bowness and Lee formulas. First the M_k factors from Bowness and Lee formulas have been computed assuming no extrapolation outside validity limits. This implies that for $a/t < 0.005$ M_k is constant. Moreover, M_k factors have been computed for $a/c = 0.1$ as the lower limit value, whereas the results from the present FE simulations are obtained for an edge crack case (2D model, plane strain). Results for the case where the crack locus is at the starting point of the toe radius are presented in Fig. 6. The present results are compared with extrapolated Bowness and Lee formulas. To do the comparison with the present edge crack results the a/c ratio is set as low as 0.001 in the in the Bowness and Lee formulas.

As can be seen from Fig. 6 the curves have a significant gradient as a/t decreases, particularly for small values of the radius ρ. This gradient cannot be ignored. In conclusion, it is a better choice to extrapolate the Bowness and Lee M_k curves below $a/t = 0.005$ than let them level off. The latter choice will significantly underestimate the acting stress intensity factor for small cracks. It is also noted that the Bowness and Lee results are typically 10% lower than the present results for the smallest analysed radius $\rho = 0.1$ mm. The discrepancy is likely owed to the fact that we have used a 2D model for a true edge crack under plane strain condition, whereas Bowness and Lee have applied a 3D model with a small a/c ratio. A similar discrepancy between M_k results obtained from 2D and 3D analysis models was found in [13]. In the present work it is noted that the slope of the two upper curves in Fig. 6 are almost the same although they were obtained by 2D and 3D analysis models. This demonstrates that there is a significant increase in the magnification factor as a/t decreases below the given limit value of 0.005. An important issue is the singularity in the stress field at the weld toe for $\rho = 0$. This makes the FEA based calculations of the SIF more difficult for very small cracks. The singularity can be handled by using the V-notch approach as proposed by Lazzarin and Livieri [30]. This analytical approach determines the Energy Release Rate (ERR) at the weld toe geometrical discontinuity by modelling it like a V-notch angle in the continuum of the joint. The approach has been applied by Lazzarin et al. [30,31] and Recho et al. [32] for calculating the SIF for steel welded joints. Fig. 6 also includes magnification factors obtained by this approach for $a/t = 0.004$ and $a/t = 0.008$ that corresponds to crack depth 0.1 mm and 0.2 mm
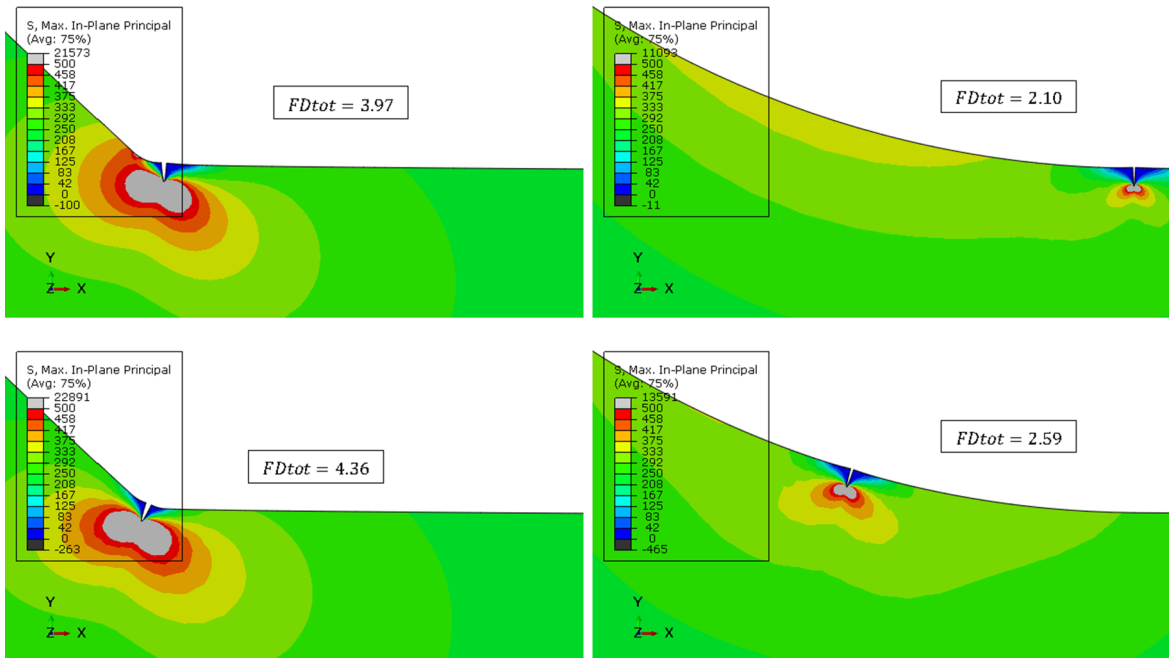

Fig. 5. Influence of the crack locus and orientation on the SIF; upper/lower figures – different crack location; left/right figures – different toe radius ($FDtot = Y \cdot M_k$ is the total geometry factor, membrane loading mode).
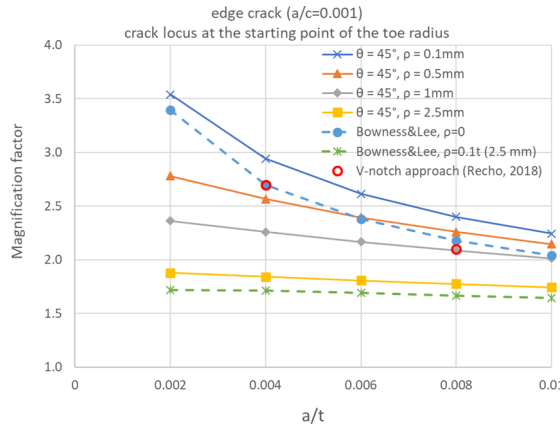
Fig. 6. Influence of the weld toe radius on the magnification factors M_k for different crack depths for the membrane loading mode. Comparison to extrapolated Bowness and Lee formulas and V-notch results. Crack locus at the starting point of the toe radius.

respectively for a 25 mm plate thickness. As can be seen these results are very close to the Bowness and Lee solution. These results can be taken as a support to the Bowness and Lee parametric formulas for a crack depth down to $a/t = 0.004$. The slopes of the curves are also substantiated by this analysis.

2.5. Characterizing the irregular weld toe geometry

The significant influence of the weld toe geometry on the SIFR for small cracks was demonstrated in Section 2.4. The weld toe geometry is often so irregular and abrupt that it can, in some cases, be regarded as an imperfection. This may give a problem with defining the local geometry by an idealized flank angle and toe radius applied when determining the SIFR. Furthermore, the variability of the geometry along the weld seam needs to be characterized by descriptive statistics. Consequently, these two parameters are treated as random variables and both measuring uncertainty and statistical uncertainty is a challenge when determining these variables. When analysing the scatter occurring at different phases of the damage evolution, one may notice that the scatter of the total life mostly comes from the crack initiation period and the early crack growth phase. The large variation in the local weld toe geometry may be used to explain this observation. Hence, in order to model these phases accurately, a local stress approaches are recommended. The classical approach has been to measure the local toe geometry by using various replica techniques [33]. For the test series investigated in the present paper the replica method was used to determine the toe geometry. The weld toe profile can also be determined by using an advanced optical systems and 3D laser scanning. This methodology allows us to analyse precisely the local weld toe geometry and its variability along the weld seam. An example of the measurements of the local weld toe geometry carried out by laser scanning is shown in Fig. 7. On the left in this figure a top view of the weld at the end of the longitudinal attachment is shown. The blue line represents the weld toe, whereas the red lines indicate cutting planes at which weld profiles were extracted and the local weld toe geometry was analysed.

Both parameters, ρ and θ, have a strong influence on the stress concentration occurring at the weld toe notch. However, the toe radius has a more pronounced impact than the angle for smaller cracks. Hence, some combinations of those parameters should be considered for more accurate life predictions. When the statistical distributions of ρ and θ are known, they may be used for predicting the most likely profile at the crack initiation locus utilizing extreme value statistics. The distribution for the weld toe radius will give very low extreme value within a given weld length, typically close or inferior to 0.1 mm. This supports the assumptions made by Bowness and Lee in their analyses. Hence, for design purposes the assumption of $\rho = 0$ is justified and this observation also justifies the application of a V-notch approach at the weld toe. However, for more accurate life predictions, especially regarding scatter of the predicted fatigue life, some larger realistic values for ρ should be included. Analysis of the local weld toe geometry is essential in

Fig. 7. Local weld toe geometry for a longitudinal attachment, a) 3D laser scan overview, b) extracted profile, c) local weld toe geometry - fitted simplified profile to determine θ and ρ (scale: mm).

order to establish an accurate model for fatigue damage evolution.

2.6. The likely development of semi-elliptical crack at the weld toe

From in-service experience and the following crack behaviour is likely under a nominal stress range of 150 MPa:
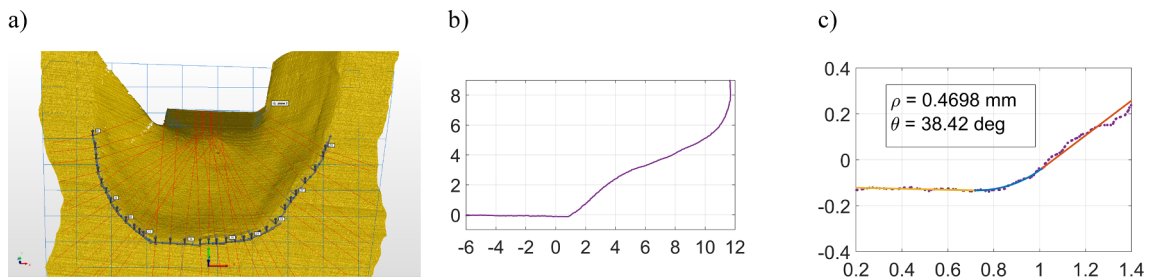
- Multiple micro cracks initiate at locations where there is a combination of an unfavourable weld toe geometry and a presence of initial flaws. The number of cracks that initiate per length of the weld seam for a given stress range is by nature random and depends on load level. These micro cracks will grow and at a given stage exceed the defined transition depth of 0.1 mm. Based on observations given by the crack monitoring system described in the next section the number of cracks that initiate along the width of a specimen (60 mm) is between 2 and 3 at an applied stress range of 150 MPa (see examples in Appendix C). The number of cracks can be randomized according to a Poisson distribution. The number of cracks will have an influence on when the a/c transition towards an edge crack takes place. At lower stress ranges the number of cracks along the weld seam will decrease.
- The cracks along the weld seam that have passed a depth of 0.1 mm will have a semi-elliptical shape and their aspect ratio a/c is by nature random.
- Each of these cracks can be modelled by a single crack fracture mechanics model predicting the crack size and crack shape evolution until crack coalescence takes place.
- After crack coalescence the cracks join to form one edge crack that rapidly propagates to failure.

The goal of the present work is to model all the stages except the first one. The ability of the fracture mechanics models in Table 2 will be demonstrated by both comparing the crack depth growth rate and the crack shape evolution with experimental data. The likely difference in shape evolution for the membrane and bending loading mode is shown in Fig. 4 at the end of Section 2.3.

3. Short presentation of the test specimens and test results

3.1. Test specimens and results for the total fatigue life

Life data points are collected for non-load-carrying fillet welded steel joints at a constant stress range of 150 MPa. All results are for medium strength C-Mn steel with a plate thickness of 25 and 32 mm. The typical joint configuration is shown in Fig. 8. As can be seen the semi-elliptical cracks are emanating from the weld toe. For all the test specimens very frequent and detailed crack depth measurements were carried out during each test. This gives a unique database containing both life data and associated crack growth histories. For further details regarding test set-up and crack growth measurements the reader may follow the references given in the right column in Table 3. The results for the specimens subjected to the bending loading mode are presented for the first time in the present work.

For series I the effective R ratio was equal to 0.35, whereas it was 0.1 for test series II. Descriptive statistics for the weld toe geometry for the present test series are given in Table 4. The fitted frequency functions follow a lognormal distribution for both the geometry variables. In the fracture mechanics analyses the mean value was used for the toe angle, whereas an extreme minimum value was used for the toe radius. Based on extreme value statistics the minimum value of the radius was close to 0.1 mm which is quite close to the Bowness and Lee's assumption with $\rho = 0$.

According to DNVGL [35] the tested detail can be classified as an F-class. This gives the following design and mean S-N curves for $N < 10^7$ cycles regardless of the applied R ratio:

design: $\log N = 11.855 - 3\log\Delta\sigma$

mean: $\log N = 12.255 - 3\log\Delta\sigma$ (4)
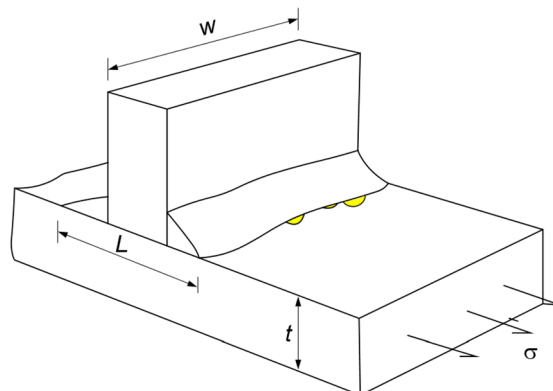
Fig. 8. Typical configuration of test specimen with multiple cracks along the weld seam (T-joint specimen).

Table 3
Overview of test series.

Test data identification	Geometry	Number of specimens	Thickness [mm]	Steel grade	Welding procedure	Loading mode	R ratio	References
Series I-A	Cruciform	34	25	S355	SMAW, FCAW	Membrane	0.35	1) Mikulski and Lassen [24] 2) Lassen [34]
Series I-B	Cruciform	10	25	S355	SAW	Membrane	0.35	Lassen [34]
Series II	T-joint	10	32	S355	SMAW	Bending	0.1	Present work

Table 4
Statistics of the local weld toe geometry.

Test data identification	Flank angle, θ [°]		Toe radius, ρ [mm]	
	mean	standard deviation	mean	standard deviation
Series I-A	58	9	1.6	0.7
Series I-B	34	14	0.5	0.3
Series II	69	8	1.8	0.9

When S-N data are analysed using the nominal stress approach no distinction is usually made between the membrane and the bending loading mode. Statistics of the total fatigue life for the entire data collection (54 samples) are presented in Table 5. As can be seen the collected data are very close to the S-N curve statistics for an F class.

Before proceeding to the measurements and the models for crack growth, the very long lives pertaining to the fully automated SAW test specimens (series I-B, 10 samples) are excluded from the present data set. These long lives are explained by the fact that the mean flank angle for these specimens is as low as 34° as can be seen in Table 4. The reason for excluding these long lives is that we shall focus on the results at the left tail of the life distribution for an F class detail. Hence, abnormal long lives on the right tail are not of interest. This reduction of the membrane sample size reduces the standard deviation given in Table 5 by a factor close to 2. The mean value remains almost the same. Our selected data set will now be representative for fillet welded joints made by manual and semi-manual welding procedures. The focus is on the crack growth for medium and shorts lives.

4. Monitoring the crack initiation phase

4.1. Measurements of the early crack growth

The crack growth monitoring system based on the ACPD technique was used to detect crack initiation and to determine the subsequent crack growth. The voltage signals were interpreted as crack depth according to a simple linear relation between voltage drop and crack depth:

$$a_{est1} = \frac{e}{2}\left(\frac{V_c}{V_r} - \frac{V_{c0}}{V_{r0}}\right)$$

(5)

where V_c and V_r are the measured potential over the crack and the plate surface respectively, while e is the distance between the pin probes. V_{c0} and V_{r0} are the initial readings. Typical crack depth evolution based on first estimates for three specimens of series II subjected to the bending loading mode is shown in Fig. 9. For this loading mode the crack growth data before a depth of 0.1 mm is reached are not available for all specimens as was the case for the membrane loading mode. However, for specimen B3 where very early measurements are available it can be seen that the voltage signals do not start to increase before 1.5×10^5 cycles is reached. This is close to 25% of the entire fatigue life.

The registered first estimate growth data for specimen B3 (test series II) are included in Appendix B. The growth data for a specimen representative for the membrane loading mode (specimen A9, test series I-A) are presented in Appendix A.

Table 5
Statistics of the total fatigue life at nominal stress range of 150 MPa.

Statistical parameter	All present test data (54 samples)	DNVGL (F-class)
Median	518,000	533,000
Standard Deviation	326,000	288,000
Minimum	319,000	–
Maximum	2,074,000	–
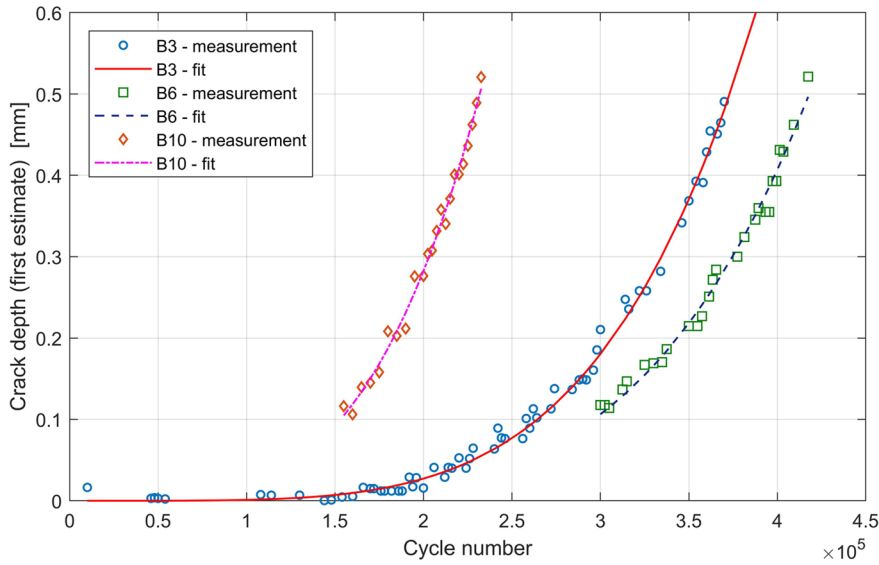
Fig. 9. Early crack growth for selected specimens subjected to the bending loading mode (test series II in Table 3).

4.2. Statistics for number of cycles to reach crack depths below a = 0.5 mm

For the very early crack growth histories based on the first estimate depths a power function was fitted to the measured *a-N* curves to obtain smooth curves as shown in Fig. 9. The number of cycles to reach the crack depths of 0.1 mm, 0.2 mm and 0.5 mm were estimated. Statistics for reaching these crack depths are given in Table 6. Lognormal distributions were fitted to the histograms for the number of cycles to reach the given crack depths, see Fig. 10. Detailed results for the membrane loading mode were presented and discussed in [24].

For the membrane loading mode it was possible to establish a distribution for reaching a crack depth as small as 0.05 mm as shown in Fig. 10a. The fitted probability distributions for the number of cycles to reach given crack depths of 0.1, 0.2 and 0.5 mm for the bending loading mode (Series II) are presented in Fig. 10b. As can be seen there is a certain increase in number of cycles to reach the given crack depths compared to the membrane loading mode. For a crack depth of 0.1 mm the number of cycles has increased from 142,000 cycles for the membrane load case to 176,000 cycles for the bending load case, i.e. an increase of 24%. As for the membrane load case, the scatter in number of cycles decreases when crack depth increases. Based on the analysis of the results from both loading modes it can be concluded that the large scatter for the fatigue life in welded joints has a significant contribution from the initiation phase. This is owed to the high variability of the local weld toe geometry. Furthermore, the results demonstrate that the crack initiation phase for welded joints cannot be neglected.

4.3. Discussion of the early crack growth and the size of possible initial flaws

For the membrane loading mode it was shown that even when subtracting two standard deviations for the time to reach 0.05 mm, there is still a remaining initiation part of the fatigue life. This will also be true for the bending loading mode as the number of cycles to reach 0.1 mm in fact has increased compared to the membrane loading mode case. The crack growth histories obtained for the bending loading mode supports the finding made for the membrane loading mode. One may argue that if the unknown initial flaws are defined as crack-like defects, the size of these defects will be smaller than 0.05 mm for an F-class detail. This supports the recommendations given in DNVGL-RP-C210 [8] that suggest a mean value for the initial crack depth as small as 0.043 mm and an exponential probability distribution to account for the scatter in the initial crack depth. The present findings are also close to the initial crack depths determined by Zerbst [20], by applying the model briefly discussed in Section 2.1. The DNVGL document suggests that this initial crack depth can be entered in a fatigue crack propagation model based on the Paris law to obtain life results consistent

Table 6
Statistics of cycles to reach given crack depths for bending loading mode (Series II, 10 specimens).

Statistical parameter	Number of cycles to reach		
	$a = 0.1$ mm	$a = 0.2$ mm	$a = 0.5$ mm
Mean	176,000	213,000	267,000
Standard deviation	73,000	83,000	93,000
Coefficient of variation	0.41	0.39	0.35

a)

b)

Fig. 10. Distribution for the number of cycles to reach given crack depth: a) for the membrane loading mode (Series I-A, first estimates), b) for the bending loading mode (Series II, first estimates).
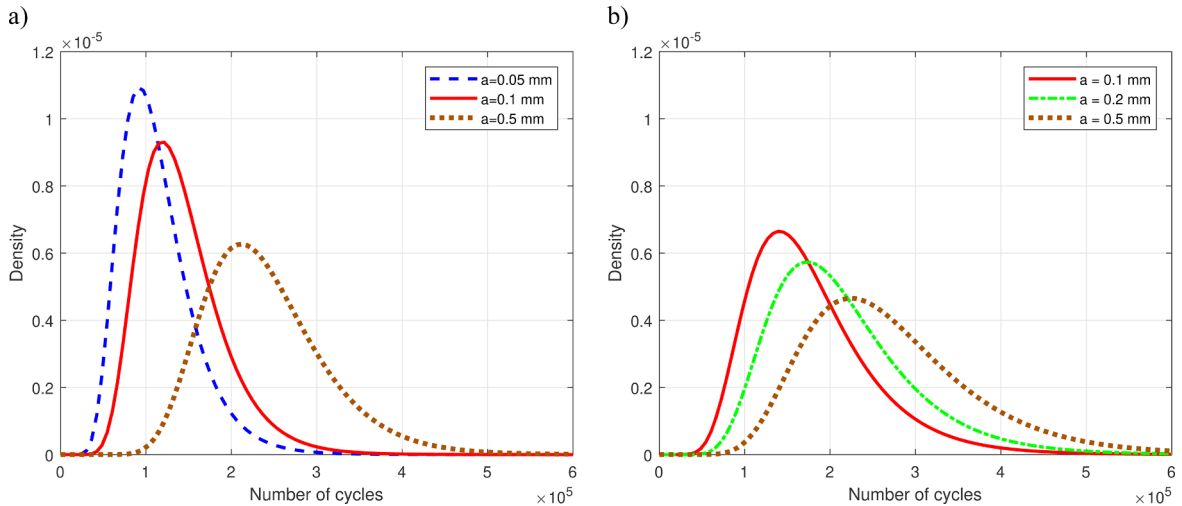
with S-N life predictions. Hence, the experimental findings in the present work as visualized in Fig. 10 corroborate this back-calculation for determining the size of the initial crack depths. This contradicts the proposals made by other researchers where initial crack depths with a size in the range from 0.2 up to 0.5 mm have been suggested [1,36]. However, even if the model for propagation of long cracks recommended by DNVGL can simulate the total fatigue life, the model is not capable of describing the very early crack growth correctly. An attempt was made in the present work to obtain the number of cycles to reach 0.1 mm by using the DNVGL recommended exponential distribution for the initial crack depths. The life distributions given in Fig. 10 were not obtained. Consequently, the application of the proposed distribution for the fictitious small initial crack size in conjunction with LEFM is questioned. The conclusion is that other models should be used to physically describe the damage mechanism at this early stage, see the discussion given in Section 2.1. However, these models are not within the scope of the present work. Our goal shall be to pursue the subsequent crack propagation phase by an engineering fracture mechanics model and compare the results with the measurements carried out in the test.

5. Experimental results and models for the crack propagation phase

5.1. Fracture mechanics modelling of measured crack growth

In the present section we shall use the rule-based models and the unique model defined in Table 2 to model the measured crack growth. In Section 2.6 we discussed the likely development of the crack growth. In contrast to the analysis of crack growth results from a defined standard specimen (e.g. central cracks in plate, CT specimens) we must in the present case address the uncertainties listed in Table 1 before applying a facture mechanics models defined in Table 2. We have circumvented the problem of choosing the magnitude of an initial crack depth as we are looking at crack growth beyond a given crack depth 0.1 mm. As for the local toe geometry we have applied the mean values for θ and $\rho = 0$ when determining the SIFR. The alternative would be to use extreme value statistics for both these parameters. The choice has an important impact on the SIFR for small crack as discussed in Section 2.4. The crack shape evolution is based on the observation that cracks are initiated at several positions along the weld toe within a specimen and in the beginning these cracks grow as individual shallow semi-elliptical cracks. At a later stage these cracks will coalesce as described by Pang and Gray [37]. In the present tests the crack coalescence was observed at a depth between 2 and 3.5 mm (see examples in Appendix C). In this depth range a rectangular edge crack is formed and the growth rate is accelerated. In the presented crack growth model that sequence is simulated using the following two stages:

1. Growth of a single semi-elliptical crack both in depth and length direction starting from initial crack depth and an assumed initial crack aspect ratio a/c,
2. From a specified depth a_1, treated as a starting point for crack coalescence, only the crack depth follows the crack growth law. The crack length will then be determined by the formation of an edge crack. Numerically the crack aspect ratio decreases exponentially reaching a value of 0.01 at crack depth a_2, and continuing to the asymptote of $a/c = 0.001$

The forcing function that controls the crack aspect ratio evolution in the second stage of the crack growth model has the form:

$$\frac{a}{c} = p\exp(-q(a - a_1)) \tag{6}$$

where p and q are coefficients determined based on experimental observations. There is an important difference in the timing for the crack coalescence for the two loading modes. The coalescence takes place at an earlier stage for the bending loading mode. This was observed experimentally and can also be shown theoretically. Based on the SIF calculations and FM model designated 1a the crack aspect ratio evolutions are as presented in Fig. 11 for both loading modes. The first part of the curves is determined by the depth and length propagation model, whereas the last part, with a significant drop in a/c due to assumption of crack coalescence, is obtained by the above empirical forcing function given by equation (6). Before the final failure of the specimen, the crack shape will be rectangular over the entire width of the cross-section.

The difference in the crack depth where the drop in the a/c ratio starts is explained by the fact that cracks in specimens subjected to bending grow faster in the length direction than in the depth direction. This was discussed in the end of Section 2.3. Consequently, these specimens develop a larger major axis $2c$ such that multiple cracks will coalesce earlier. This is illustrated in Fig. 12 at different crack depths for a single crack for the two loading modes. In the multiple cracks case this will give an earlier crack coalescence for the bending loading mode.

As can be seen from Fig. 11 crack coalescence will start at $a_1 = 3$ mm for the membrane loading mode, whereas it starts at $a_1 = 2$ mm for the bending loading mode. These are assumed values, consistent with observations during testing. It is also very close to the case when parameter a_1 in equation (6) has been set as free variable to obtain the best fit to the crack history.

Using the above described model for the crack shape evolution, the two LEFM models described in Section 2.2 were fitted to the corrected mean propagation curve for membrane and bending loading mode separately:

Model 1a and b: The basic model based on DNVGL.
Model 2a and b: A unique crack growth rate curve model with account for the R ratio.

For all models the SIFR is calculated according to DNVGL-RP-C210 [8]. The described models were first applied with the original growth parameters C and m given in Table 2. Then C was modified to obtain the best fit to the experimental curves. The parameters a_1 and a_2 are set to fixed values of 3 mm and 5 mm, and 2 mm and 5 mm for membrane and bending mode respectively. Some observations of the crack front for selected specimens from series I-A are presented in Appendix C. An initial crack aspect ratio of $a/c = 0.25$ was assumed based on observations on the test specimens. Observations of the a/c ratios occurring on the test specimens were carried out during the testing by ink staining or by a beach marking technique. Ink was injected at an early stage, when the ACPD measurements indicated the onset of crack growth, see Fig. 9. These measurements are included in Fig. 11. For the smallest cracks ($a < 0.2$ mm) it was difficult to define and measure the semi-elliptical shape. Hence, the aspect ratio remains uncertain for such small cracks. As can be seen from Fig. 11 there is a large scatter in the measured a/c ratios. This can partly be explained by the fact that the measurements were carried out randomly at different stages and on various specimens. Nevertheless, the observed scatter is regarded as realistic and as one of the sources for the large scatter in final fatigue life. Compared to the model prediction shown in Fig. 4 it is obvious that the aspect ratio of the initial cracks is by nature completely random. Despite the large scatter in observed shapes it can be seen that the applied mean model curve for the aspect ratio lies close to the center of the data points. Hence, the suggested theoretical mean relation given in equation (6) for the aspect ratio evolution is supported by the experimental measurements (see also Appendix C). However, it must be borne in mind that the scatter is lost in this model that is established to obtain the mean measured $a-N$ curve as shown in Fig. 13 and Fig. 14 in the next section.

5.2. Comparing model-based crack growth with experimental results

The number of cycles to reach given crack depths is shown in Fig. 13 for each test specimens from the membrane loading mode. These experimental curves represent the crack growth only, starting from crack depth of 0.1 mm. The mean curve for the growth histories is also drawn. The $a-N$ curves obtained by FM model 1a is also included using $m = 3.0$ and with the magnitude of the C parameter at the mean value and the mean value plus two standard deviations (growth parameters from DNVGL-RP-C210 [8]). As can
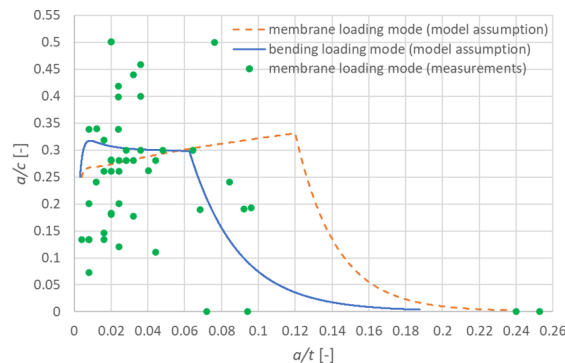
Fig. 11. Fitted crack shape evolution for the membrane and bending loading modes (all parameters specific for the present test series, θ = 58°, L/t = 2 and °θ = 69°, L/t = 1.6 respectively for the membrane and bending loading mode, a_{ini}/c_{ini} = 0.25).
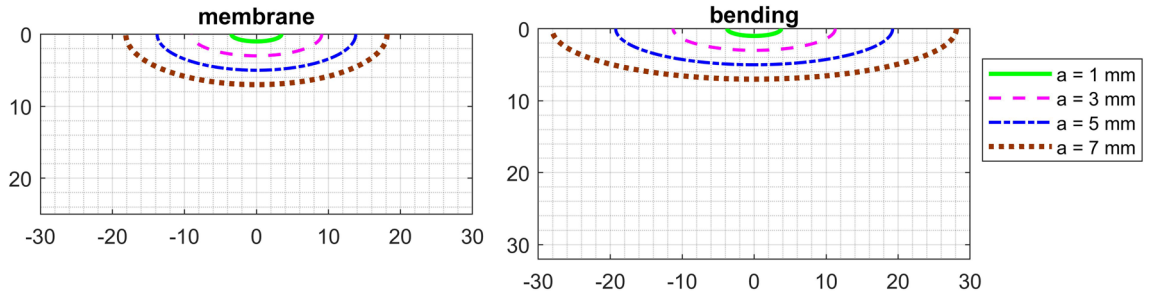
Fig. 12. Shape evolution of a single semi-elliptical crack under membrane and bending loading modes at different growth stages.
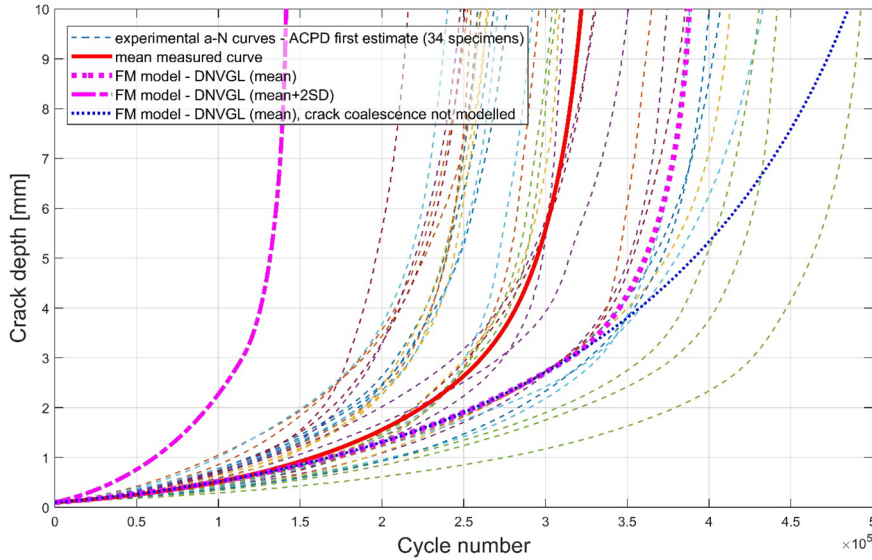
Fig. 13. Measured individual a-N curves together with the mean curve for all specimens subjected to membrane loading mode (Series I-A, crack depths from 0.1 ÷ 10 mm, ACPD first estimate) and model predicted growth histories.
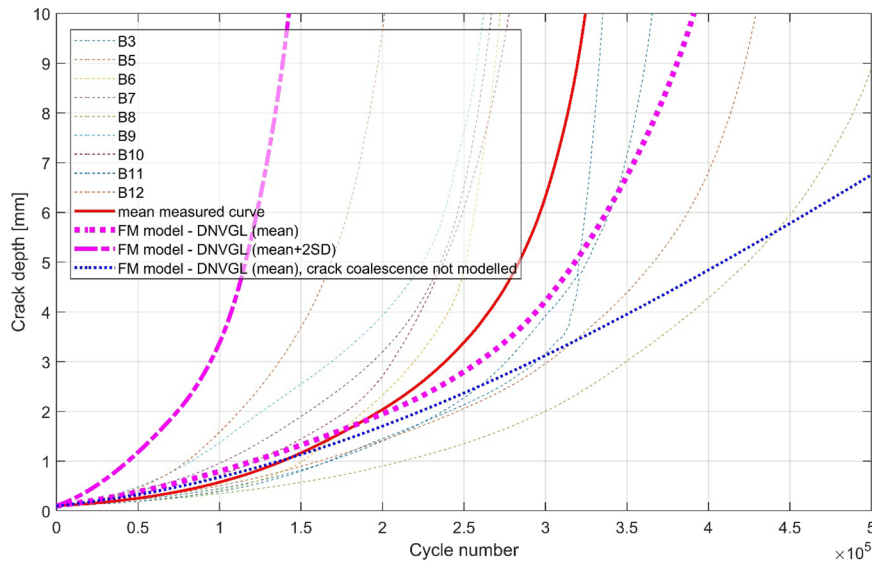
Fig. 14. Measured individual a-N curves together with the mean curve for all specimens subjected to bending loading mode (Series II, crack depths from 0.1 ÷ 10 mm, ACPD first estimate) and model predicted growth histories.

be seen the curve obtained from the model using the mean value for C is not very different from the experimental mean curve. The model-based mean curve gives typical 20% longer propagation life. As for the model curve obtained by the mean plus two standard deviations for the C parameter the curve gives significantly shorter propagation life than all the experimental curves. This model-based curve can be regarded as a design curve and the closest experimental curve gives about twice as long propagation life. Similar curves are given for the bending loading mode in Fig. 14. As can be seen the trend is the same as for the membrane loading mode, the model mean curve gives close to 20% longer propagation life than the experimental mean curve. The design model curve to the left is now closer to the nearest experimental curve. The experimental curve with the shortest propagation life gives now only 1.4 longer life the design curve. In conclusion the model-based curves describe the experimental data very well and the safety margin obtained by the design curve is judged as acceptable. When comparing the experimental mean curves for the two loading modes it is seen that growth histories are not very different. Both test series give a mean propagation life slightly longer than 3×10^5 cycles based on the first estimated crack depths. This is close to 75% of the total fatigue life. However, it must be borne in mind that the growth curve for the bending loading mode is obtained with test specimens that have a main plate thickness of 32 mm, whereas the test specimens subjected to membrane loading have plate thickness of 25 mm. If the thickness is reduced to 25 mm for the bending loading mode, the propagation life will increase by 30% due to the thickness effect according to the fracture mechanics model. Hence, the bending loading mode generally gives longer lives when the geometry is the same. Finally, it should be noted that the agreement between the curves obtained by the models and the experimental curves is dependent on a correct modelling of the multiple crack coalescence phenomenon. If only a single semi-elliptical crack is modelled, then the predicted crack growth curves will give lives that are far too long. This is shown by the blue dotted lines in Fig. 13 and Fig. 14. For the membrane loading mode the fatigue life will be over-estimated by close to 30% if the crack coalescence is neglected. As can be seen from Fig. 14 the single crack model gives almost the double propagation life of the test specimen compared to the final propagation life of the measured mean curve for the bending loading mode.

5.3. Obtaining a mean crack growth curve by calibration of crack depth measurements

The crack growth curves discussed so far for each test are based on a linear relation between the increase in the potential drop and the crack depth. There are several sources of uncertainty in this simplified relation. The two most important sources are:

- The relation is valid for a long rectangular shaped crack, not for a smaller semi-elliptical crack
- The increase in potential drop is related to depth increase, not the absolute value of the depth

To enhance the accuracy of the crack growth histories the estimated crack depths were calibrated against true crack depth readings on the fractured surfaces. The true crack depths were obtained by ink staining or beach marking carried out during the testing of a specimen [34]. The first estimates for the crack depths and the true crack readings are shown in Fig. 15.

Based on the data shown in Fig. 15 the following equation is used for the correction:

$$a_{est2} = a_{est1} + g(a_{est1}) \tag{7}$$

where a_{est1} is the first ACPD estimate crack depth and a_{est2} is the corrected depth. The detailed expression for $g(a_{est1})$ function can be
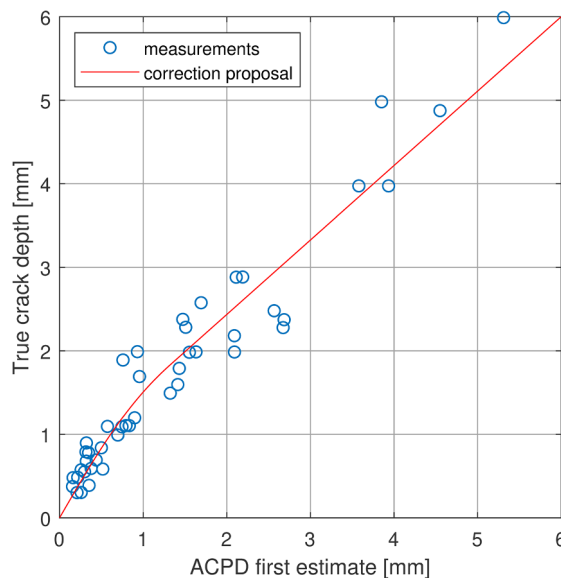

Fig. 15. True crack depth vs 1st estimate based on ACPD.

found in [24]. As can be seen from Fig. 15 the corrected depth a_{est2} is always larger than a_{est1} for small and medium sized cracks. For cracks larger than 6 mm there is hardly any difference between the two estimates. Hence, once the crack coalescence has taken place with the formation of an edge crack there will be no correction of the first estimated crack depth. The proposed correction formula has been established based on measurements carried out on chosen specimens in the test series. It is a correction for the average value of the depth and not for the depth measured for individual specimens as these curves may exhibit substantial random deviations. This is clearly illustrated in Fig. 15. Hence, equation (7) can only be used for correction of the mean experimental propagation curves shown in Fig. 13 and Fig. 14. The corrected mean *a-N* curve is presented in Fig. 16 for the bending loading mode. It represents crack growth from the estimated true crack depth of 0.1 mm up to 10 mm. The uncorrected crack depth is also shown. The consequence of the correction is that the transition depth of 0.1 mm is reached at an earlier stage when the crack depth is corrected. Hence, the initiation phase becomes somewhat shorter, and therefore the propagation life becomes slightly longer than the results obtained by the first estimated ACPD depths. The propagation life increases from $3.2 \cdot 10^5$ to about $3.5 \cdot 10^5$ cycles when the crack depths estimates are corrected. As can be from Fig. 16, the difference between the first estimate and the corrected curve is largest for intermediate crack depths between 1 and 4 mm. It is also noted that the difference between the uncorrected and the corrected curve is not very large, but it is nevertheless important when determining the parameters *C* and *m* when using a fracture mechanics model to fit the experimental curves. A more detailed analysis of this topic is presented in the next sections.

5.4. Mean crack growth rates predicted by model 1

The crack growth histories obtained by the presented fracture mechanics-based models have been compared directly to the experimental *a-N* curves in the foregoing sections. To gain more knowledge on the involved growth parameters *C* and *m*, an analysis based on the growth rates versus the applied SIFR for a log–log scale was carried out. Crack growth rates obtained from the corrected mean *a-N* curves for both loading modes are plotted versus the SIFR in Fig. 17. The crack aspect ratios used for the SIFR calculations were taken from the crack shape evolution obtained from Model 1a. The model predicted aspect ratios are as shown in Fig. 11. As can be seen the obtained data plots in Fig. 17 are quite close to a smooth straight line for a log–log scale for both the loading modes. There are some unexpected irregularities in the mid part of the curves that reflects a perturbation related to the calibration equation that was established and discussed in Section 5.3. The straight-line pattern for the data points supports the decision made regarding the uncertainties listed in in the right column of Table 1. However, based on the shape of the curves it is convenient to make a separation between three different sections before going into detailed analysis:

- Lower section given by a SIFR < 10 MPam$^{0.5}$
- Mid-section with SIFR between 10 and 20–25 MPam$^{0.5}$
- Upper section given by a SIFR larger than 20–25 MPam$^{0.5}$

The upper part of the mid-section is defined by a crack depth of 6 mm, see the experimental curves in Fig. 13 and Fig. 14. This corresponds to a SIFR close to 20 MPam$^{0.5}$ for the bending loading mode and 25 MPam$^{0.5}$ for the membrane loading mode. The upper section of the data points has been excluded from the fitting calculations. The crack growth in this region, occurring just before the onset of the final ductile fracture, is very accelerated and does not follow the applied fracture mechanics models. As this final phase represents only a small portion of the propagation life (5–7%) these data are not analysed in detail. A linear regression analysis was first carried out for mid-section of the curves. To obtain the growth parameter *C* pertaining to the two test series it was chosen to keep *m* constant at the values given in Table 2. The argument for keeping *m* constant is twofold. This choice agrees with the approach in rules and regulations, statistical variations in crack growth parameters are accounted for by the *C* parameter only. Furthermore, especially for the bending loading mode, the number of tests is so few that letting *m* be a free variable will introduce large statistical uncertainty. The results from the linear regression analysis when *m* is fixed are given in Table 7. As can be seen the fitted values for *C* are quite close to the mean values given in rules and regulations, see Table 2. The discrepancy compared with recommended mean values from the BS7910 and the DNVGL codes is also given as fractions in Table 7. As can be seen the discrepancy is small, typically
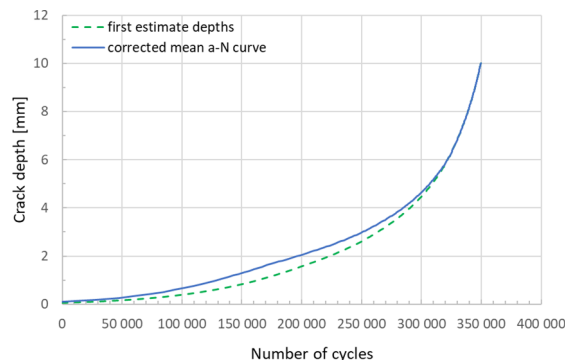
Fig. 16. Corrected experimental mean a-N curve for the bending loading mode. Uncorrected crack depths are shown for comparison.
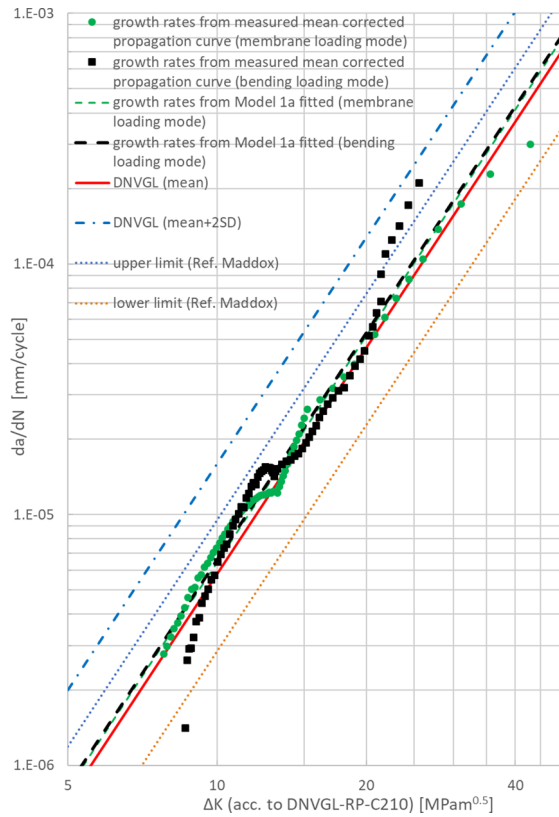
Fig. 17. Experimental crack growth rates, model 1a predicted growth rates, DNVGL curves and lower/upper bounds acc. to Maddox [38].

Table 7
Comparison of FM model parameters (fitted values to the mid-section of Fig. 17).

Loading mode	Model 1a			
	m	C	$C_{fitted}/C_{original}$	R^2
All data	3	$6.54 \cdot 10^{-9}$	1.13	0.96
membrane	3	$6.45 \cdot 10^{-9}$	1.11	0.97
bending	3	$6.62 \cdot 10^{-9}$	1.14	0.95

10–20% only. The standard deviation for C is not possible to determine from the present tests as the results are based on the calibrated mean experimental curves only. Given that the standard deviation for the final propagation fatigue life is less than 20% of the mean propagation life, much of this scatter is caused by variations in the local toe profile. Hence, one can conclude that the scatter in growth rate in Fig. 17 is in average substantially less than 20%. As can be seen from Fig. 17 the present data are well in between the boundary limits given by Maddox [38]. As can be seen from Table 7 the correlation factor was as high as 0.98 when all the present data were grouped together. This is close to the same correlation obtained when the two test series are analyzed separately. For the membrane test series the numbers given in Table 7 will not change significantly if the data points in the lower section are included in the analysis. This is not the case for the bending loading mode.

With a closer look at the lower sections of the growth curves it is observed that the data points would be best described by a two-slope curve for the bending loading mode, but not for the membrane loading mode. Fig. 17 also reveals a slight difference in the experimental growth rates between the two loading modes. The growth rates are typically 10–12% higher for the membrane loading mode in the mid-section of the data. However, the curves are relatively close compared to the usual scatter found in growth rates, see the scatter bands drawn in Fig. 17. The observed difference in the present case is of course not explained by the difference in the applied loading mode. The applied SIFR calculations shall take care of this difference. To explain the observed benign difference in the growth rates between two loading modes one must bear in mind the difference between test specimens in the two series. These differences are summarized in Table 3.

As can be seen the there is a difference in plate thicknesses and the applied welding procedures for the two test series. The thickness effect is taken care of by the SIFR calculation. However, the increased thickness may affect the microstructure of the HAZ and hence the growth parameter C in Paris law. Furthermore, and more important, there is a difference in the applied R ratio in the

way that the test specimens subjected to membrane loading mode has a higher R ratio. For the same nominal SIFR one should then expect that this loading mode should have the highest growth rate. This agrees with the experimental data in the mid-section of the curves in Fig. 17. This can also explain the difference in the lower section of the data where the bending loading mode data indicate a threshold value for the SIFR, whereas this is not clearly indicated for the membrane loading mode. It is only in the excluded upper sections of the data that the growth rates for the bending loading mode are higher. In the third column of Table 3 we have listed the number of specimens that implies that there is larger statistical uncertainty related to the line obtained for the bending loading mode. In conclusion these physical and statistical differences between the two test series can very well explain the benign difference in the data plots in Fig. 17.

5.5. *Mean crack growth rates predicted by model 2*

To study if the influence of the R ratio an effective SIFR was determined as recommended in the unique model 2a. The associated growth rate plots are shown in Fig. 18 and numerical details are given at the left side of Table 8. As expected, the membrane loading mode curve is moved more to the right than the bending loading mode curve due to the fact the membrane test specimens have the highest R ratio. Consequently, the obtained curves for the two loading modes have shifted position, when using the effective SIFR the bending growth rate curve will be higher than the curve for the membrane loading mode. Ideally the curves should now be in the same position if the test specimens were identical. But given the differences and uncertainties in Table 3 the new discrepancy shown in Fig. 18 is still acceptable. However, one cannot disregard that the empirical parameters entering the calculation formulas for the effective SIFR in model 2a should be adjusted for the present shallow semi-elliptical cracks. These parameters are originally obtained for long central cracks.

Finally, the fitting to the growth rate data was done by model 2b with an effective SIFR and with the threshold value include as a free variable. For this case both the mid-section data and the lower section data were included. The results are shown in Fig. 19 and the right side of Table 8. The threshold value for the bending load case was determined to be 7.8 MPam$^{0.5}$ which is quite close to the recommended value of 7.2 MPam$^{0.5}$ for model 2b. The correlation factor is still as high as 0.98. However, there are too few data points close to the threshold value to claim high confidence regarding this finding. For the same reason the threshold value for the membrane load case was determined with very large confidence bounds and hence should not be trusted. The existence of a threshold value for the SIFR in the lower region of the data remains an open question.

6. Discussion and conclusions

The fatigue crack growth in fillet welded steel joints has been investigated experimentally and modelled by engineering fracture mechanics. The joints are all made of medium strength C-Mn steel with various manual and semi-automatic welding techniques. The plate thickness was 25 mm for the test specimens subjected to the membrane loading mode and 32 mm for the bending loading mode. The test results are representative for an F class detail (category 71 in Eurocode). All the tests were carried out at a constant stress
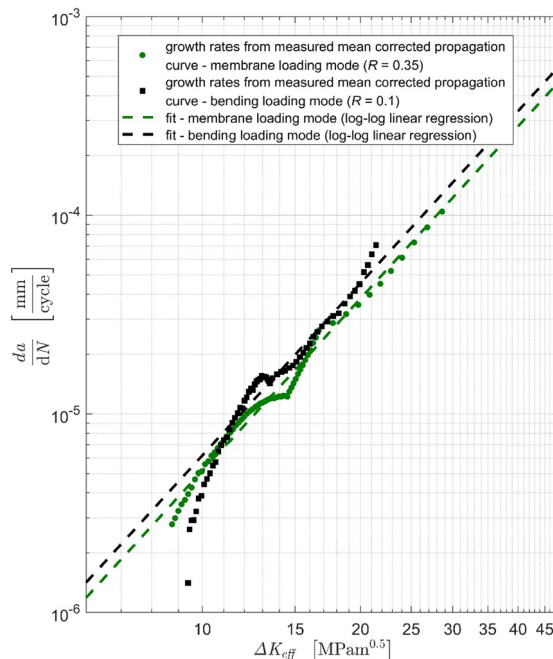
Fig. 18. Experimental crack growth rates and growth rates predicted by Model 2a.

Table 8

Comparison of FM model parameters for model 2a and 2b. (Model 2a is fitted values to the mid-section of Fig. 18, model 2b is fitted to both the mid-section and the lower section).

Loading mode	Model 2a				Model 2b				
	m	C	$C_{fitted}/C_{original}$	R^2	m	C	ΔK_{th0} [MPam$^{0.5}$]	$C_{fitted}/C_{original}$	R^2
All data	2.88	$7.47 \cdot 10^{-9}$	0.90	0.95	2.88	$8.22 \cdot 10^{-9}$	6.1	0.99	0.95
membrane	2.88	$6.83 \cdot 10^{-9}$	0.82	0.98	2.88	$6.82 \cdot 10^{-9}$	2.8	0.82	0.99
bending	2.88	$8.14 \cdot 10^{-9}$	0.98	0.96	2.88	$10.38 \cdot 10^{-9}$	7.8	1.25	0.96
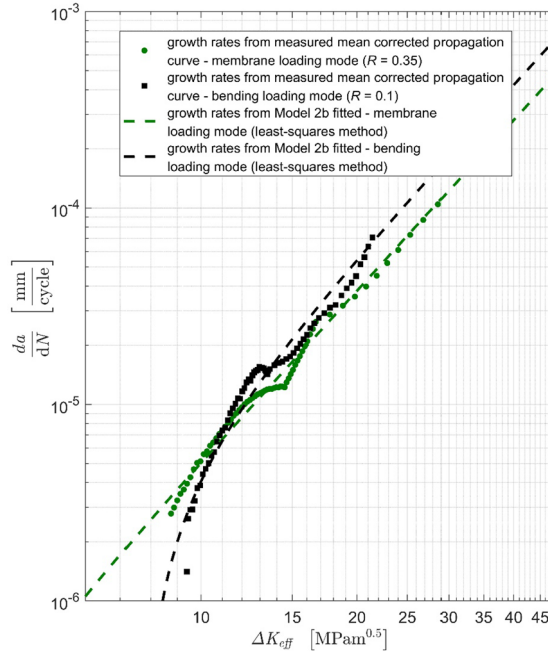
Fig. 19. Experimental crack growth rates and growth rates predicted by Model 2b.

range of 150 MPa and the following conclusions are drawn for the research questions given in the introduction of this paper:

- At the given stress range there exists a substantial crack initiation period before crack propagation starts to occur. The captured voltage signals in the ACPD system monitoring the depths did not start to increase before about 20% of the total fatigue life was spent. This was the case for all specimens in both loading modes.
- If the crack initiation phase is defined by a crack depth of 0.1 mm the number of cycles to reach this crack depth is typically 25–30% of the total fatigue life. The crack depths obtained by the ACPD signals were calibrated by readings on the fractured specimens to corroborate the findings.
- An attempt to model the very early crack growth before a depth of 0.1 mm was reached by a LEFM model failed. The early crack evolution determined experimentally was not obtained by the model.
- The fatigue crack growth from a crack depth of 0.1 mm up to final failure was successfully modelled by applying a model based on LEFM. The SIFR calculations were based on the parametric formulas suggested by Bowness and Lee. These formulas are also recommended in rules and regulations.
- The Bowness and Lee formulas are obtained by 3D FEA models of a welded joint with a crack applying the concept of the J-integral to determine the SIF. The results from the formulas were compared and found in good agreement with the results from the more analytically based V-notch approach.
- When calculating the SIFR entering the fracture mechanics models the weld toe profile shall be characterized by the mean value for the measured toe angle, whereas the toe radius shall be kept at the extreme minimum value close to 0.1 mm.
- The Bowness and Lee formulas should be extrapolated and verified for crack depths below $a/t = 0.005$. There is a significant increase in the SIF as a/t decreases below this given limit. However, as a/t gets smaller the application of LEFM becomes dubious as concluded above.
- The variation in the toe radius has a significant impact on the crack initiation and early crack growth. This variation is not included in any of the formulas established by Bowness and Lee. These formulas are obtained by setting the radius equal to zero.

- The mean *a-N* curves from a crack depth of 0.1 mm to failure were modelled by LEFM using the C and m parameters as recommended in rules and regulations. The obtained curves are very close to the experimental mean curves for both the present loading modes. Furthermore, the model design curves based on a growth parameter *C* defined by the mean value plus two standard deviations are significantly on the safe side of all the experimental curves for both loading modes.
- For the applied test stress range of 150 MPa the number of crack initiation points along the weld seam is a random variable with an average value between 2 and 3 for the given length of 60 mm. A Poisson distribution can be applied to model this discrete variable. As the applied stress range decreases the average number of crack initiation points will decrease.
- At high stress ranges it is essential to model the effect of crack coalescence of multiple cracks initiating along the weld seam. If crack coalescence is neglected for the tested specimens the fatigue propagation life will be overestimated by close to 30% for the membrane loading mode and up to 100% for the bending loading mode. The significant difference between the loading modes is caused by the different crack shape evolution and associated time to reach crack coalescence for the two loading modes.
- The mean fatigue growth rate parameter *C* obtained from the present measured growth rates is close to the suggested values given in rules and regulations if the exponent *m* is kept fixed at recommended values. If both *m* and *C* are treated as free variables the membrane loading mode will still give parameters *m* and *C* close to the recommendations, whereas the exponent *m* will be too high for the bending load mode, typically close to 3.5. This could be explained by the depth measuring uncertainty or inaccuracy in the SIFR calculations for this loading mode. The number of tests is also fewer for the bending loading mode and this gives a higher statistical uncertainty.
- The model fitted to the measured growth data did not get significantly better when applying the unique model (Huang et al. [10]) with the concept of an effective SIFR depending on the applied *R* ratio. Introducing a threshold value for the effective SIFR seems to give overly optimistic results for crack retardation of small semi-elliptical cracks. However, these topics must be investigated further.

Availability of data

Examples of crack growth data are given in Appendix A and B. The interested reader may get the entire database for all specimens from the authors at request.

Declaration of Competing Interest

The authors declare that they have no known competing financial interests or personal relationships that could have appeared to influence the work reported in this paper.

Acknowledgments

Appendix A. First estimate crack growth data for test specimen A9 (test series I-A)

Cycle number	Depth [mm]	Cycle number	Depth [mm]	Cycle number	Depth [mm]	Cycle number	Depth [mm]
10,005	0.0014	295,005	0.6256	382,635	1.1894	464,633	2.4123
20,006	0	297,506	0.6256	384,634	1.2071	466,633	2.4928
30,005	0	300,007	0.6493	386,633	1.2309	468,635	2.5197
40,004	0	302,507	0.6331	388,632	1.249	470,632	2.5765
50,006	0	305,006	0.6731	390,635	1.255	472,633	2.5408
60,003	0.0023	307,503	0.6849	392,635	1.2669	474,635	2.7174
70,004	0.0083	310,006	0.6849	394,632	1.2906	476,634	2.7749
80,005	0	312,507	0.7132	396,635	1.314	478,633	2.8014
90,001	0.023	315,007	0.7371	398,635	1.368	480,635	2.8711
100,006	0.0319	317,506	0.716	400,631	1.3803	482,629	2.9412
110,006	0.0436	320,006	0.749	402,634	1.3918	484,635	2.9913
120,008	0.0525	322,505	0.7728	404,633	1.4156	486,635	3.0514
130,007	0.0702	325,003	0.78	406,631	1.4577	488,631	3.1115
140,007	0.085	327,503	0.7966	408,634	1.4696	490,635	3.1836
150,008	0.1086	330,005	0.8491	410,636	1.5293	492,632	3.2557
160,005	0.126	332,505	0.8226	412,632	1.5347	494,636	3.3508
170,006	0.1432	335,002	0.8442	414,634	1.5466	496,632	3.436
180,007	0.1763	337,507	0.8799	416,631	1.6009	498,634	3.6283
190,007	0.1731	340,007	0.8799	418,634	1.5808	500,633	3.8327
200,007	0.1999	342,505	0.9037	420,634	1.6486	502,635	3.9412
210,006	0.2793	342,551	0.8603	422,636	1.6775	504,636	4.0496
220,005	0.2706	344,543	0.8868	424,633	1.6894	506,632	4.1831
225,006	0.2872	346,543	0.9088	426,634	1.7441	508,633	4.3401

230,005	0.2978	348,546	0.9207	428,635	1.7799	510,634	4.5212
235,005	0.2942	350,546	0.9377	430,628	1.8085	512,635	4.6541
240,005	0.345	352,544	0.9513	432,632	1.8323	514,632	4.8377
245,006	0.365	352,638	0.9632	434,633	1.8607	516,635	5.0344
250,006	0.3805	354,631	0.9684	436,632	1.9037	518,633	5.2286
255,007	0.416	356,634	0.9856	438,632	1.9439	520,630	5.431
260,005	0.4514	358,634	0.9975	440,632	1.9947	522,635	5.7019
265,004	0.4593	360,634	1.0215	442,631	2.0109	524,635	6.0296
270,007	0.4987	362,635	1.0334	444,635	2.0424	526,632	6.3694
272,506	0.5027	364,635	1.0228	446,634	2.0782	528,633	6.9063
275,006	0.4987	366,635	1.052	448,633	2.11	530,632	7.2516
277,505	0.5146	368,636	1.0813	450,632	2.1578	532,636	7.6409
280,006	0.5424	370,632	1.0878	452,634	2.1937	534,635	8.112
282,506	0.5383	372,630	1.0942	454,632	2.2498	536,632	8.6495
285,005	0.5501	374,632	1.1236	456,634	2.2774	538,632	9.2868
287,505	0.5899	376,631	1.107	458,632	2.3182	540,631	10.2128
290,006	0.5738	378,631	1.1537	460,633	2.3492	542,631	11.573
292,504	0.6018	380,635	1.2009	462,635	2.409	544,635	14.5333

Appendix B. First estimate crack growth data for test specimen B3 (test series II)

Cycle number	Depth [mm]	Cycle number	Depth [mm]	Cycle number	Depth [mm]	Cycle number	Depth [mm]
10,017	0.0164	240,016	0.0637	426,018	0.9443	552,019	3.4375
46,016	0.0029	242,013	0.0892	438,020	1.0686	554,011	3.4725
48,006	0.0037	244,010	0.0773	440,013	1.0895	556,006	3.6529
50,014	0.0029	246,022	0.0764	444,018	1.1259	558,004	3.6817
52,004	−0.0001	254,019	−0.0100	446,014	1.1485	560,018	3.7728
54,021	0.0022	256,022	0.0764	448,006	1.1779	562,005	3.8618
56,013	−0.0015	258,018	0.1011	450,008	1.2143	564,013	3.9401
66,022	−0.0037	260,015	0.0892	452,021	1.2583	566,012	4.0542
84,015	−0.0044	262,016	0.1130	460,019	1.3436	568,012	4.0968
94,005	−0.0037	264,004	0.1020	466,015	1.4126	570,011	4.1999
100,018	−0.0051	272,005	0.1130	468,009	1.4742	572,021	4.1530
104,017	−0.0044	274,019	0.1378	474,010	1.5432	574,014	4.3046
108,020	0.0075	284,004	0.1367	478,006	1.6166	576,009	4.3401
114,020	0.0068	288,013	0.1486	480,006	1.6363	578,005	4.4879
118,019	−0.0058	290,006	0.1497	484,017	1.7144	580,016	4.5310
130,020	0.0068	292,004	0.1486	488,005	1.7980	582,010	4.2932
132,013	−0.0065	296,020	0.1605	492,015	1.8296	584,007	4.7101
134,004	−0.0058	298,013	0.1854	494,009	1.8963	586,020	4.8255
140,011	−0.0093	300,011	0.2104	500,014	1.9492	588,015	5.0139
144,011	0.0003	314,004	0.2475	502,012	1.9812	590,015	5.1194
148,015	0.0010	316,019	0.2356	504,019	2.0196	592,016	5.1332
154,022	0.0046	322,005	0.2581	506,013	2.0611	594,012	5.2344
160,010	0.0053	326,016	0.2581	508,009	2.1146	596,010	5.3914
166,011	0.0164	334,016	0.2820	510,020	2.1528	598,008	5.5944
170,014	0.0149	346,012	0.3417	512,013	2.1664	600,022	5.6460
172,007	0.0149	350,018	0.3687	514,015	2.2611	602,015	5.8683
176,005	0.0120	354,004	0.3927	516,005	2.3121	604,009	6.0729
178,017	0.0120	358,005	0.3911	518,014	2.3503	606,014	6.1423
180,014	−0.0004	360,018	0.4287	520,003	2.3772	608,005	6.3768
182,010	0.0120	362,011	0.4545	522,016	2.4201	610,022	6.6894
186,005	0.0120	366,018	0.4509	524,004	2.4834	612,011	6.7891
188,020	0.0120	368,011	0.4647	526,022	2.5672	614,013	7.0001
192,015	0.0290	370,004	0.4906	528,009	2.5953	616,006	7.4007
194,012	0.0172	390,005	0.6107	530,004	2.6896	618,019	7.6973
196,008	0.0283	392,008	0.6348	532,019	2.7486	620,015	8.0131
200,022	0.0157	398,007	0.6973	534,012	2.7646	622,009	8.3420
206,019	0.0409	402,002	0.6949	536,012	2.8721	624,017	8.6737
212,012	0.0290	404,013	0.7480	538,012	2.9531	626,013	9.0920
214,014	0.0409	406,010	0.7601	540,005	3.0091	628,010	9.4665
216,011	0.0401	408,007	0.7455	542,017	3.0823	630,019	10.0799
220,005	0.0527	412,020	0.7937	544,018	3.0767	632,011	10.5392
224,018	0.0401	418,011	0.8567	546,006	3.1695	634,007	11.2287
226,011	0.0519	420,005	0.8660	548,004	3.2326	636,004	12.0851
228,014	0.0646	422,015	0.8929	550,018	3.3210		

Appendix C. Schematic representation of crack size and location at selected growth stages

Illustration of shallow multiple cracks along the weld seam obtained from ink staining. For deeper cracks crack fronts are drawn based on beach marking (see Figs. C1–C6).

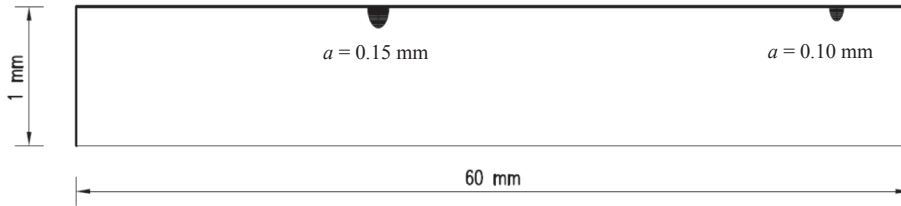**Fig. C1.** Specimen A5 (test series I-A) at N = 121000 cycles (figure is scaled 10 times in vertical direction; crack length was not measured).
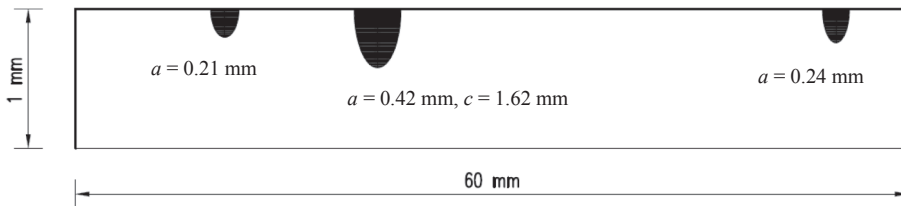

Fig. C2. Specimen A6 (test series I-A) at N = 150000 cycles (figure is scaled 10 times in vertical direction).
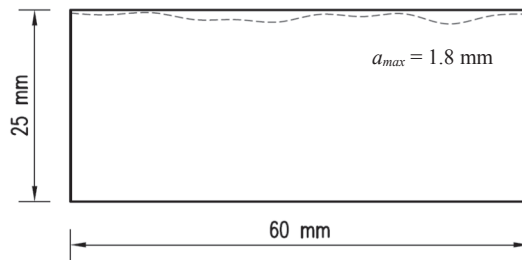

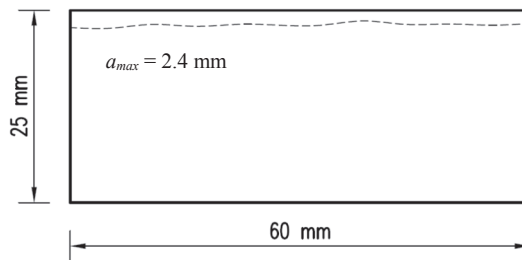**Fig. C3.** Specimen A9 (test series I-A) at N = 352000 cycles.

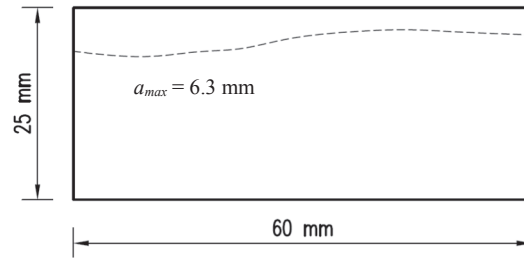**Fig. C4.** Specimen A10 (test series I-A) at N = 258000 cycles.

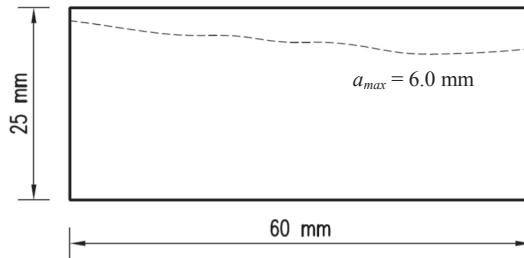**Fig. C5.** Specimen A3 (test series I-A) at N = 355000 cycles.

Fig. C6. Specimen A4 (test series I-A) at N = 332000 cycles.

References

[1] Almar-Naess A. Fatigue handbook: offshore steel structures. Trondheim: Tapir; 1985.

[2] Hobbacher A. Recommendations for Fatigue Design of Welded Joints and Components. Springer 2016. https://doi.org/10.1007/978-3-319-23757-2.

[3] Radaj D, Sonsino CM, Fricke W. Fatigue Assessment of Welded Joints by Local Approaches. Elsevier Science; 2006.

[4] Lassen T, Recho N. FLAWS Fatigue Life Analyses of Welded Structures. ISTE; 2006.

[5] Lotsberg I. Fatigue Design of Marine Structures. Cambridge: Cambridge University Press; 2016. http://doi.org/10.1017/CBO9781316343982.

[6] Newman JC, Raju IS. An empirical stress intensity factor equation for the surface crack. Engng Fract Mech 1981;15:185–92.

[7] Bowness D, Lee MMK. Prediction of weld toe magnification factors for semi-elliptical cracks in T-butt joints. Int J Fatigue 2000;22:369–87. https://doi.org/10.1016/S0142-1123(00)00012-8.

[8] DNVGL. DNVGL-RP-C210: Probabilistic methods for planning of inspection for fatigue cracks in offshore structures. 2015.

[9] BS 7910. Guide to methods for assessing the acceptability of flaws in metallic structures 2013.

[10] Huang X, Moan T, Cui WA. A unique crack growth rate curve method for fatigue life prediction of steel structures. Ship and Offshore Structures 2009;4:165–73.

[11] EN ISO 5817:2014 Welding - Fusion-welded joints in steel, nickel, titanium and their alloys (beam welding excluded) - Quality levels for imperfections; 2014.

[12] DNV. Classification Note No. 30.6: Structural Reliability Analysis of Marine Structures; 1992.

[13] Zerbst U, Ainsworth RA, Beier HT, Pisarski H, Zhang ZL, Nikbin K, et al. Review on fracture and crack propagation in weldments - A fracture mechanics perspective. Engng Fract Mech 2014;132:200–76. https://doi.org/10.1016/j.engfracmech.2014.05.012.

[14] Verreman Y, Nie B. Early development of fatigue cracking at manual fillet welds. Fatigue Fract Engng Mater Struct 1996;19:669–81. https://doi.org/10.1111/j.1460-2695.1996.tb01312.x.

[15] Recommended DNV. practice RP-C203: Fatigue Strength Ananlysis of Offshore. Steel Structures 2001.

[16] ENV 1993-1-1: 1992, Eurocode 3: Design of steel structures; 1992.

[17] Baptista C, Reis A, Nussbaumer A. Probabilistic S-N curves for constant and variable amplitude. Int J Fatigue 2017;101:312–27. https://doi.org/10.1016/j.ijfatigue.2017.01.022.

[18] Dang-Van K, Griveau B, Message O. On a new multiaxial fatigue limit criterion: theory and application. Biaxial and Multiaxial Fatigue, EGF 3. In: Brown MW, Miller KJ, editor. London: Mechanical Engineering Publications; 1989, p. 479–96.

[19] Mikulski Z, Hellum V, Lassen T. Modeling the fatigue damage evolution in welded joints Technology, ASME Press; 2017. https://doi.org/10.1115/OMAE201761201.

[20] Zerbst U, Madia M, Schork B. Fracture mechanics based determination of the fatigue strength of weldments. Procedia Struct Integrity 2016;1:10–7. https://doi.org/10.1016/j.prostr.2016.02.003.

[21] Fricke W. Fatigue analysis of welded joints: State of development. Mar struct 2003;16:185–200. https://doi.org/10.1016/S0951-8339(02)00075-8.

[22] Wolf E. Fatigue crack closure under cyclic tension. Engng Fract Mech 1970;2:37–45. https://doi.org/10.1016/0013-7944(70)90028-7.

[23] Huang X, Moan T. Improved modeling of the effect of R-ratio on crack growth rate. Int J Fatigue 2007;29:591–602. https://doi.org/10.1016/j.ijfatigue.2006.07.014.

[24] Mikulski Z, Lassen T. Fatigue crack initiation and subsequent crack growth in fillet welded steel joints. Int J Fatigue 2019;120:303–18. https://doi.org/10.1016/j.ijfatigue.2018.11.014.

[25] Zhang B, Moan T. Mean Stress Effect on Fatigue of Welded Joint in FPSOs. 25th International Conference on Offshore Mechanics and Arctic Engineering Volume 3: Safety and Reliability; Materials Technology; Douglas Faulkner Symposium on Reliability and Ultimate Strength of Marine Structures, 2006, p. 403–12. http://doi.org/10.1115/omae2006-92056.

[26] Syahroni N, Berge S. Fatigue Assessment of Welded Joints Taking Into Account Effects of Residual Stress. J Offshore Mech Arct Engng 2012;134.. https://doi.org/10.1115/1.4004519.

[27] Albrecht P, Yamada K. Rapid calculation of stress intensity factors. J Struct Divis, Proc ASCE 1977;103:377–89.

[28] Lotsberg I, Sigurdsson G. A New Recommended Practice for Inspection Planning of Fatigue Cracks in Offshore Structures based on Probabilistic Methods. Proceedings of the ASME 2014 33rd International Conference on Ocean, Offshore and Arctic Engineering OMAE2014, 2014.

[29] Lotsberg I, Sigurdsson G, Fjeldstad A, Moan T. Probabilistic methods for planning of inspection for fatigue cracks in offshore structures. Mar Struct 2016;46:167–92. https://doi.org/10.1016/j.marstruc.2016.02.002.

[30] Lazzarin P, Livieri P. Notch stress intensity factors and fatigue strength of aluminum and steel welded joints. Int J Fatigue 2001;23:225–32. https://doi.org/10.

1016/S0142-1123(00)00086-4.

[31] Lazzarin P, Lassen T, Livieri P. A notch stress intensity approach applied to fatigue life predictions of welded joints with different local toe geometry. Fatigue Fract Engng Mater Struct 2003;26:49–58. https://doi.org/10.1046/j.1460-2695.2003.00586.x.

[32] Recho N, Lassen T, Mikkelsen ON. Fatigue crack growth in welds based on a V-notch model for the short crack propagation at the toe. Procedia Engng 2018;213:239–54. https://doi.org/10.1016/j.proeng.2018.02.025.

[33] Engesvik K, Lassen T. The effect of weld geometry on fatigue life. Houston, Texas: ASME Press; 1988. p. 441–5.

[34] Lassen T. The effect of the welding process on the fatigue crack growth in welded joints. Welding Journal 1990;February:75s–85s.

[35] DNVGL. DNVGL-RP-C203: Fatigue Design of Offshore Steel Structures; 2016.

[36] Cui W, Wang F, Huang X. Towards a Unified Fatigue Life Prediction (UFLP) Method for Marine Structures. Springer 2014. https://doi.org/10.1115/OMAE2010-21007.

[37] Pang HLJ, Gray TGF. Fatigue Analysis of Surface Cracks At Fillet Welded Toes. Fatigue Fract Engng Mater Struct 1993;16:151–64. https://doi.org/10.1111/j.1460-2695.1993.tb00750.x.

[38] Maddox SJ. Assessing the significance of flaws in welds subject to fatigue. Welding J 1974;53.

Paper D

Probabilistic models for the fatigue resistance of welded steel joints subjected to constant amplitude loading

Zbigniew Mikulski, Tom Lassen

Probabilistic models for the fatigue resistance of welded steel joints subjected to constant amplitude loading

Zbigniew Mikulski [*], Tom Lassen

NOV APL, Arendal, Norway
University of Agder, Grimstad, Norway

ARTICLE INFO

ABSTRACT

S-N curves found in various rules and regulations are the basic tool for the practicing engineer when carrying out life predictions for welded details in dynamically loaded structures. The present work is investigating the expected fatigue life and associated scatter for welded steel joints subjected to Constant Amplitude (CA) loading. The objective is to obtain more reliable life predictions based on advancements in the probabilistic model fitted to collected life data. A Random Fatigue Limit Model (RFLM) is proposed to obtain fatigue resistance curves at given probability levels of survival. As a distinction to more conventional statistical methods, the model is treating both the fatigue life and the fatigue limit as random variables. The focus is on high cycle fatigue and long-life data and runouts are included in a rational and logical manner by using a maximum likelihood method. Life data for a transverse fillet welded attachment originally designated as a category 71 detail in Eurocode 3 Part 1-9 are collected and analysed. The plate thickness of the specimens ranges from 20 mm to 32 mm and the steel quality is mild and medium strength Carbon-Manganese steel. The results are compared with the results obtained by conventional S-N curves. The compatibility between the fitted probabilistic models and the underlying fatigue damage mechanisms is emphasized.

1. Introduction

1.1. Design of welded details and the reliability against fatigue failure

The reliability against fatigue failure of welded details is of vital importance in the design of dynamically loaded welded steel structures. When welded joints are subjected to dynamic repetitive loading a potential fatigue failure will always be an issue of concern. Risk reduction measures must be implemented both in the detailed design of the joints and by planning of scheduled in-service inspections during the target service life. It is a major problem that the fatigue behaviour of welded joints is characterized by random variations caused by uncertainties related to residual stresses, imperfections such as the possible presence of initial flaws, and irregular weld toe geometries. These variables are often not possible to measure but they cause significant scatter in the

fatigue damage evolution and final fatigue lives. Consequently, statistical analysis of life data and reliability models must be applied to handle the problem in a consistent and rational manner. Fatigue lives must be predicted at an acceptable probability of failure during the target service life for the structure. Typical examples are bridge structures, large cranes, and offshore structures.

The basic tool for engineering design is the S-N curves found in rules and recommendations. These curves are based on an exponential relationship between the applied stress range S and the number of cycles to failure N. The historical background for the development of these S-N curves has been neatly described by Murakami et al. [1] and will not be repeated herein. The curves are based on experiments with welded joints that have similar characteristics regarding the fatigue resistance. The specimens in such a test series are usually subjected to Constant Amplitude (CA) loading. This gives the necessary data for obtaining the life endurance at different stress ranges for the type of welded joint in

Nomenclature

Roman letters

a	crack depth
b	fatigue strength exponent
c	crack half-length
C	crack growth rate parameter in the Paris equation
$f(t)$	frequency function
L	spacing of the weld base points
$\log a$	intercept parameter of S-N curve
m	slope parameter of S-N curve
m	crack growth rate exponent in the Paris equation
m_1	slope parameter of upper part of S-N curve
m_2	slope parameter of lower part of S-N curve
n	number of specimens
N	number of cycles to failure
N_i	number of cycles to crack initiation
$\mathbf{Q}$	vector containing RFLM model parameters
R	stress ratio
$R(t)$	reliability function
S	nominal stress range

t	time to failure
T	thickness of the specimen
W	width of the specimen

Greek letters

α	significance level
β_0, β_1	fatigue curve coefficients in RFLM
γ	fatigue limit defined as random variable
$\Delta\sigma$	notch stress range at the weld toe
ΔK	stress intensity factor range
ΔK_0	threshold value for the SIFR
ΔS	nominal stress range
ΔS_0	fatigue limit
$\lambda(t)$	failure rate function
$\widehat{\mu}_t$	sample mean
μ_v	mean value of the fatigue limit (logarithmic)
$\sigma_f^{'}$	fatigue strength coefficient
σ_m	notch mean stress at the weld toe
$\widehat{\sigma}_t$	sample standard deviation
σ_v	standard deviation of the fatigue limit (logarithmic)
σ_x	standard deviation of the fatigue life (logarithmic)

question. Due to the inherent scatter in life data, both a mean curve and a characteristic curve used in design are given. The S-N curves may be based on the nominal stress range or the geometrical hot spot stress range. A more detailed overview of these topics is given by Hobbacher [2], Radaj et al. [3], Lassen et al. [4], Lotsberg [5] and Maddox [6]. Important rules and recommendations are Eurocode 3 Part 1-9 [7], HSE Offshore rules [8], DNVGL-RP-C203 [9], ABS [10] and IS0 12107 [11]. In the present work the limitations and shortcomings of this conventional statistical methodology for obtaining an S-N curve are discussed. An alternative probabilistic model based on the Random Fatigue-Limit Model (RFLM) in combination with a Maximum Likelihood Method (MLM) is investigated.

1.2. Characteristics and shortcomings of the conventional S-N curves

The present work is shortly reviewing the background and the recommended analyses for conventional bi-linear S-N curves. This is worthwhile doing because the applied methodology can still be a bit confusing for the experimentalist and the practicing engineer. The conventional procedure for establishing S-N curves for CA loading are usually characterized by:

- An elementary reliability model with the fatigue life as the single random variable is assumed to be valid at any applied stress range above what is believed to be a fatigue limit.
- The linear regression analysis carried out results in a log-normal distribution of the fatigue life because of the central-limit theorem.
- Long-lasting failures and runouts are excluded from the analysis.

The methodology is summarized in the Background Documentation 9.01a [12] for Eurocode 3 Part 1-9 [7]. Given that the fatigue damage mechanism changes as the stress range decreases it is not obvious that the same reliability model gives the best description of the scatter in fatigue life at all stress levels. It is essential to make a distinction between crack initiation and the subsequent crack growth. The distinction is important as these two phases involve different damage mechanisms. The crack initiation phase is driven by cyclic shear stress variation and the resistance against this damage mechanism is related to the yield stress of the steel. The growth phase is usually driven by the cyclic principal stresses perpendicular to the crack planes (stress mode 1) and the resistance against crack growth is not related to the yield stress, but

rather to the *E*-modulus of the steel. Each phase must be modelled separately to capture the characteristics of the damage mechanism involved (Schijve [13]). This point of view is also supported and elaborated in the more recent work carried out by Murakami et al. [1]. The assumptions that there exists a fatigue limit may not be true. In the last proposal from IIW the fatigue limit has been rejected for the CA curves, Hobbacher [14]. IIW suggested that the lower line segment shall be given a shallow slope with a slope parameter $m = 22$ based on the work of Sonsino [15].

Furthermore, the log-normal distribution may not always be the most appropriate function for the model fitted to the life data, a competing distribution is the Weibull function, Schijve [13], Wirsching [16], Engesvik et al. [17]. Although the log-normal model is widely applied in rules and recommendation the authors have not found any formal proof that this is the best choice based on hypothesis testing. Finally, it is the present author's opinion that the long-lasting failures and runouts must not be excluded from the statistical analyses. In fact, these stress ranges are usually much closer to the magnitude of the stress ranges acting in service than the higher stress ranges applied in the linear regression for the conventional S-N curves. From that perspective the excluded data give more important information for an in-service load condition than the stress ranges that enter the linear regression analysis. Although an in-service stress spectrum gives significant additional uncertainty due to Variable Amplitude (VA) stresses the above arguments are still valid. Modification of the curve to handle VA loading must be carried out at a later stage in the same way as it is done for the conventional S-N approach. Hence, the damage accumulation under VA loading will be pursued when the life curve for CA loading has been properly understood and modelled.

1.3. The random fatigue limit model and its advantages

In the present context the expression *reliability model* is used if the model involves one random variable only such as described in the foregoing section. If several variables are involved the model shall be labelled as a *probabilistic model*. The RFLM gives a probabilistic resistance curve where both the fatigue life and the fatigue limit are treated as random variables simultaneously. The advantages of the model when compared with the conventional S-N approach are:

- The life model may change as a function of the applied stress range because of the interaction between the two random variables in the model.
- The probabilistic model can also assume any frequency function for both variables, e.g. log-normal and Weibull functions.
- An a-priori assumption regarding the existence of the fatigue limit is avoided.
- The model parameters are found based on the MLM such that long lives and runouts are included in a logical and rational manner.
- The resistance curves can be extrapolated into the very high cycle area without necessarily losing validity, although very few test results exist in this area.

1.4. Research questions and the objectives of the present work

Based on the above background the objectives and the research questions for the present work are:

1) Starting with the elementary reliability model for the finite fatigue life at a given stress range, can a conclusion be reached regarding the distribution function that gives the best fit to the life data?
2) When establishing the S-N curves with associated lower bounds based on CA life data, what are the principal differences between the conventional curves in rules and recommendations and the present resistance curve obtained by RFLM? What will be the practical outcome for fatigue life predictions based on the two approaches?
3) The focus of the present analysis will be in the high cycle regime where the RFLM includes all available data whereas the conventional S-N curves do not include these data. How is the RFLM-based resistance curve fitting these experimental data? Can any conclusion be reached regarding the existence of the fatigue endurance limit?
4) Finally, there shall be a mutual agreement between the RFLM resistance curve and the underlying damage mechanisms. Can the probabilistic curves be explained and supported by physical models for these mechanisms?

In the present study a population defined by a non-load-carrying fillet welded transverse attachment is investigated. This type of joint is designated category 71 in ENV 1993-1-9: 1992 [18] and class F in the offshore fatigue recommendations given by DNV [19]. According to current version of these standards [7,9] the proposed categorization is one level higher. The recommended categorization of such details has changed over the year, see the discussion in Section 4.3. The number that identifies the category in Eurocode 3 is defined as the fatigue strength at $N = 2 \times 10^6$ cycles. To answer research question 1 above a large amount of life data is collected at a given CA stress range of 150 MPa. The aim is to choose between the log-normal distribution and the Weibull distribution for the finite fatigue life under the same loading condition. Furthermore, a huge database at various stress ranges for the joint in question is applied to establish the conventional S-N curve and the RFLM resistance curve to answer research questions 2 and 3. In order to answer the last question 4 the underlying damage mechanisms for various phases in the fatigue damage evolution are modelled and discussed. The present work is based on the hypothesis that the understanding of the damage mechanism and which probabilistic model to select are inter-related problems.

2. Conventional S-N curves based on elementary statistical methods

2.1. Defining a population and a life model

The welded joint investigated in the present analysis is shown in Fig. 1. The applied stresses are in the main plate perpendicular to the welding direction of the transverse attachment. The multiple fatigue cracks that may appear at the weld toe are indicated with one large crack
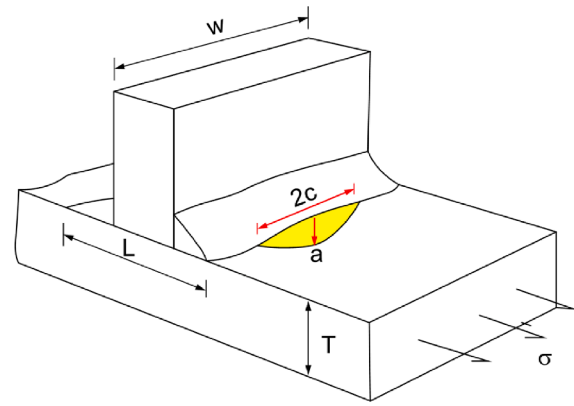

Fig. 1. Steel plate with transverse welded attachment.

only. The most important global geometry parameters with respect to fatigue are the plate thickness T and the spacing of the weld base points L. The fatigue life will increase if this distance decreases. Hence, for small attachment lengths the category changes from category 71 to category 80. The reason for this change is that the stress concentration at the weld toe decreases when the parameter L decreases. This is accounted for in Eurocode 3 Part 1-9 by a differentiation in detail category depending on the distance L when using the nominal stress range in the plate as the key to the life prediction. An alternative to this approach that circumvents this categorization problem is to use the hot spot method where the stress concentration due to the stiffener is explicitly accounted for. In the present work we shall focus on the S-N approach based on the nominal stress range. A more detailed discussion of the present category is given in Section 4.3 where the collected data are discussed. Important details for the damage evolution in the chosen welded detail is given by Mikulski and Lassen [20,21].

The consequence of the large scatter observed in test data is that the fatigue life t for a given welded joint must be treated as a random variable. For fatigue life predictions the time t is usually given in number of cycles N to failure. The associated reliability model gives the design engineer the possibility to predict the fatigue life at a chosen probability of survival. It is an advantage if enough test results are available at a given constant stress range, such that the model can be determined regarding the type of frequency function. This will also give modest statistical uncertainty for the model parameters. Unfortunately, to limit the testing efforts, the tests are usually carried out at various stress ranges with rather few tests at each stress range level. The data are then analysed directly by an S-N approach as we shall discuss in the next section. However, before pursuing the S-N approach it is important to study the behaviour of the fatigue life at a given constant stress range to understand the basic ideas of reliability modelling. In the cases where enough data are collected at a given stress range this can also give important background information for the subsequent S-N analysis at various stress range levels.

The basic characteristics for a reliability model at a given stress range are illustrated in Fig. 2. Based on the histogram fitted to the life data the frequency function $f(t)$ with associated parameters can be determined. Subsequently the reliability function $R(t)$ and the failure rate function $\lambda(t)$ are obtained. The basic mathematical equations for the model are found in Appendix A. It must be borne in mind that the reliability model shown in Fig. 2 is valid for:

- A defined damage mechanism (high cycle fatigue in the present case)
- A given quality of the welded joint (joint geometry, steel quality, welding procedures, post-weld inspections and post-weld improvement methods)
- A given operating condition (the direction of the stresses, variations of the stresses)
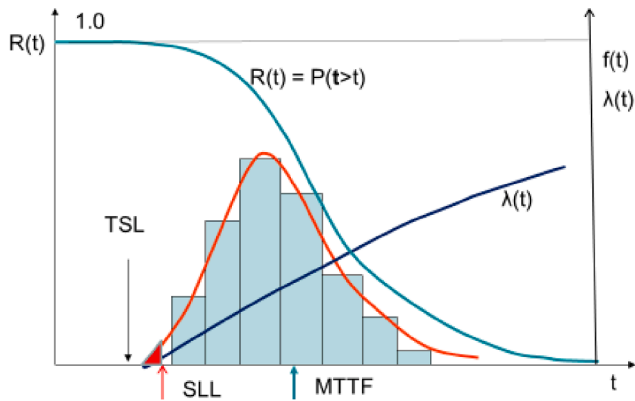
Fig. 2. Definition of a reliability model for the fatigue life.

Fig. 3. An illustration of the basic concepts for the S-N curve.

The damage mechanism in the present case is high cycle fatigue, but to make things more subtle one may benefit from making a distinction between crack initiation and subsequent crack growth (Mikulski and Lassen [20,21], Lassen et al. [22]). The quality of the joint is usually given by the definition of the categories in Eurocode 3 Part 1-9. However, a category also includes considerations for the direction of the applied stresses relative to the welding direction. Finally, the given operating condition is the stress spectrum to which the welded detail is subjected during service. However, it is quite common to simplify the operating condition by applying various levels of CA stress ranges in laboratory tests. The reliability model is then conditional on an independent free variable such as the CA nominal stress range S.

In practice the design engineer must work with estimates for the true mean value μ=MTTF and the true standard deviation σ for the time to failure. These model parameters can be found by:

- The method of moments
- The least square method
- The maximum likelihood method

For a description of the two first methods the reader may look into [23]. The estimates are then generally given by a point estimate and an associated confidence interval. For the mean value the interval is determined from Student's t statistics, whereas chi-square statistics are used to determine an interval for the standard deviation. If the life data contain runouts none of the two methods are applicable. For this case a Maximum Likelihood Method (MLM) can be applied to determine the model parameters. A pioneer work for the application of the MLM for fatigue life data was carried out by Bastenaire [24].

2.2. The basic concept of an S-N curve

To obtain a life model as described in Section 2.1 at any constant stress range an S-N curve must be established. The time to fatigue failure given in number of cycles N is obtained for any CA nominal stress range S. The basic Basquin equation reads:

$$logN = loga - m \cdot logS + \varepsilon \tag{1}$$

The basis for this equation is shown in Fig. 3. The figure includes the data points and the fitted mean curve. In the central part of the diagram the relation between S and N is assumed linear for a log-log scale as given by Eq. (1). The fatigue damage mechanism in this area is mainly crack growth governed by the stress intensity factor range pertaining to a crack. For higher stress ranges the linear relation is overly optimistic as indicated by the dotted upper curve. This is explained by the fact that the damage mechanism changes to low cycle fatigue which is mainly governed by the plastic strain variation. For lower stress ranges the linear assumption is overly pessimistic as indicated by the dotted lower curve.
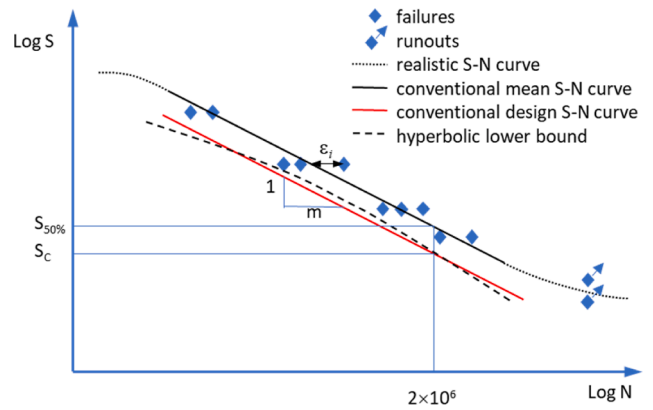
Again, the explanation is related to the change in damage mechanism as the fatigue life for these low stress ranges is dominated by a crack initiation phase. Based on the data points in the mid region of the diagram a linear regression analysis is carried out for a log-log scale. The intercept parameter $log a$ and the slope parameter m give the mean life at any stress range. A third parameter defined as the standard error is defined by the discrepancy ε for each individual data point relative to the obtained mean curve. The squared sum of the residuals will give an estimate for the standard error defining the standard deviation in the fatigue life. The standard deviation is assumed constant for all stress ranges and the design curve is found by subtracting a chosen number of standard deviations from the mean curve such that the probability of failure is regarded as acceptable. This curve is shown to the left in Fig. 3. In some cases, this design curve is chosen to be hyperbola shaped to reflect the increased confidence interval for stress ranges for which the available life data are scarce. This curve is given by the left dashed line in Fig. 3.

2.3. Some details for the conventional statistical analysis

Whereas there are no problems related to the conventional linear regression analysis, there is still some debate on how to obtain the design curves at defined probabilities of survival. Hobbacher [25,26] recommends that both the mean value and the standard deviation are chosen at an 87.5% one sided confidence level. Subsequently, these estimates are applied to determine the design curve at a 95% probability of survival. The calculations will result in a design curve that is parallel to the straight mean curve as shown by the fully drawn line in Fig. 3.

An alternative and more direct way to determine the design curve by a lower *prediction bound* is given by the equation:

$$logN_{k,limit} = logN_k - t_{\alpha,dof}\widehat{\sigma}\sqrt{1 + \frac{1}{n} + \frac{\left(logS_k - \overline{logS}\right)^2}{\sum_i \left(logS_i - \overline{logS}\right)^2}} \tag{2}$$

where n is the number of data points given by $log S_i$ and $log N_i$ which define the parameters $log a$ and m for the mean regression line. N_k is the mean life for the considered stress range S_k. $\overline{logS}$ is the mean of the n values of $log S_i$. The parameter $\widehat{\sigma}^2$ is the best estimate for the variance about the regression line which is equal to the sum of squared residuals divided by the number of degrees of freedom dof. In the case that both the parameters $log a$ and m have been estimated from the data, the dof is equal to n-2. As can be seen from Eq. (2) the Student's t-distribution still plays a central role when determining the design curve, but the chi-square distribution is no longer explicitly applied. This approach was originally based on the work by Cooper [27]. It has also been applied by Euler and Kuhlmann [28] and by Drebenstedt and Euler [29]. The shape

of the lower limit according to Eq. (2) will be a hyperbola. In the outer part of the database both the uncertainty of the mean value and the slope parameter m of the curve will be added up in life predictions. The Background Documentation 9.01a [12] uses Eq. (2) when determining the fatigue strength at 2×10^6 cycles. To facilitate the calculations the term $\log S_k$ in Eq. (2) is replaced by $\log S_{50\%}$ which is determined at $N_k = 2 \times 10^6$ cycles at the mean S-N curve. When introducing this term Eq. (2) becomes linear for a log-log scale. This linear curve is subsequently applied to define a design curve at a probability of survival chosen at 95% in the Background Documentation 9.01a. This curve is parallel to the mean curve and the characteristic fatigue strength S_C at 2×10^6 cycles can be determined. This procedure is illustrated in Fig. 3 where both $S_{50\%}$ and S_C are indicated. As can be seen the stress range S_C is slightly above the corresponding point on the hyperbola for $N = 2 \times 10^6$ cycles.

A more simplified procedure uses the line obtained in the central area of the data given in Fig. 3. This straight line is subsequently used for any applied stress range such that the hyperbola shaped curve is replaced by a straight line from the very beginning. This means that the third term under the square root in Eq. (2) is ignored. Furthermore, as the sample size increases the second term under the square root can also be neglected. This can be justified for sample sizes larger than 20. For even larger sample sizes and with a required probability of survival equal to 97.5% the value of t will approach 1.96, i.e. for $\alpha = 2.5\%$. A very informative description of these matters is given by Schneider and Maddox [30]. These simplifications are usually accepted when establishing the S-N design curves in the rules and regulations for offshore structures. This is for a limited sample size somewhat non-conservative, but this is compensated by the requirement of a high probability of survival equal to 97.5%. One may say that the offshore rules are relaxed regarding the hyperbola shape of the lower boundary line, whereas the rules are strict regarding the required survival probability level. Therefore, in these rules and regulations it has become common practice to simply subtract 1.96 standard deviations from the mean S-N curve to define the design curve.

2.4. Examples of obtained design curves for various calculation procedures

The differences in current rules and regulations regarding the type of confidence interval, how to handle the hyperbola shaped lower bound and finally the chosen probabilities of survival are summarized in Table 1.

To study the results from the two approaches recommended by the Background Documentation 9.01a and the common approach in offshore rules, the simple data sample presented by Drebenstedt and Euler [29] is applied. This data sample consists of 10 finite lives and 5 runouts, see Appendix C. Following the prescribed recommendations, the 10 finite lives were analysed by the two approaches given in Table 1. The results are given in Table 2. As can be seen the two approaches applied in civil engineering and offshore engineering give the same design curve for all practical considerations.

When determining the conventional design S-N curves for the present collected data the approach used by the offshore industry will be applied, i.e. the hyperbola shape is neglected, and the probability of

Table 2
Design S-N curves based on Eurocode and the offshore recommendations.

Approach	log a (mean value)	Standard deviation	log a (design)	S at $N = 2 \times 10^6$
Eurocode 3 Offshore rules	12.104	0.116	11.838 11.829	70.1* 69.6**

*At survival probability 0.95. **At survival probability 0.975.

survival is set to 97.5%.

2.5. Assessing the conventional S-N approach in relation to involved damage mechanisms

As we have discussed the S-N curves assume that there is a single damage mechanism dominated by crack growth for any stress range. The curve is then cut off at a stress range that is designated the endurance fatigue limit. The damage mechanisms are indeed more complicated. The damage mechanism will mainly be crack growth at high stress ranges, whereas for low stress ranges the crack initiation damage mechanism will be dominant. This is in fact an objection to the basic idea of an S-N curve that assumes the same type of reliability model for any CA stress range level. Schijve [13] argued that scatter in crack initiation and crack growth are different issues. Baptista et al. [31] simulated the damage process in welded joints by three possible phases: crack initiation, micro crack growth and associated crack arrest and the final growth of larger cracks. These possible shifts in damage mechanisms explain why the long life and runout data must be excluded in the conventional analysis. These data do not obey the simple reliability model assumed to be valid for the relatively high stress range levels. This gives doubt with respect to the general validity of the S-N curves when extrapolating them down to lower stress ranges. This is also the reason why the present authors advocate the application of a RFLM as an alternative to the conventional S-N curves.

3. Resistance curves based on the random fatigue limit model (RFLM)

3.1. Basic theory and numerical procedure

The present work is based on the RFLM approach as presented by Pascual and Meeker [32]. The methodology was first applied for welded joints by Lassen et al. [33]. Similar analyses have also been carried out by D'Angelo and Nussbaumer [34] that included a Monte Carlo simulation based on the model. Toasa and Ummenhofer [35] applied a modified approach based on a general formulation of the probability weighted moments using the three-parameter Weibull distribution. This work was further developed by the authors in [36] where the focus was on how to include the result from retesting of former runouts. Leonetti et al. [37] used the RFLM for welded cover plates on girders. The work suggested to introduce more parameters to the RFLM to enhance the model fitting. Furthermore, the possibility of applying Bayesian inference is emphasized.

Table 1
Characteristics for the fatigue design S-N curves in civil engineering and offshore structures.

Rules	Application area	Type of lower bound	Hyperbolic lower bound line	Chosen probability level of survival
Background Documentation 9.01a	Civil engineering	Prediction limit	Yes	0.95
ABS	Ship and Offshore structures	Prediction limit	No	0.975
HSE				
DNVGL-RP-C203				

The basic equation of the RFLM curve reads:

$$\ln N = \beta_0 - \beta_1 \ln(\Delta S - \gamma) + \varepsilon \tag{3}$$

where $\gamma = \Delta S_0$ is the fatigue-limit defined a random variable. The parameters β_0 and β_1 are fatigue curve coefficients. As can be seen, Eq. (3) s fundamentally different from Eq. (1). The life data are transformed by x = ln(ΔS) and w = ln(N). For a sample of data for x_i and w_i obtained from various test specimens $i = 1, n$, the model parameters can be determined by the Maximum Likelihood (ML) function:

$$L(\boldsymbol{Q}) = \prod_{i=1}^{n} [f_w(w_i; x_i \boldsymbol{Q})]^{\delta_i} [1 - F_W(w_i; x_i \boldsymbol{Q})]^{1-\delta_i} \tag{4}$$

where $\delta_I = 1$ if w_i is a failure and $\delta_I = 0$ if w_i is a censored observation (runout).

The vector $\boldsymbol{Q}$ contains the model parameters:

$$Q = (\beta_0, \beta_1, \sigma_x, \mu_v \sigma_v,) \tag{5}$$

Once these parameters have been determined from optimization of Eq. (4), the corresponding confidence intervals can be obtained by a profile likelihood method using the profile ratio of the variables together with chi-square statistics. The basic equations are given in Appendix B and further details for these calculations can be found in Pascual and Meeker [32]. The optimization of Eq. (4) and the necessary integration of the involved functions must be done numerically. The problem with local maxima may occur. In the present work an algorithm is developed in Matlab to obtain the global maximum of the object function with high accuracy. For that purpose, a multivariable object function is defined based on Eq. (4). Numerically this is carried out by searching for the minimum of the function -log($L(\boldsymbol{Q})$). This nonlinear optimization problem is solved using the *fmincon* built-in function in Matlab. This is a gradient-based method dependent on the specified initial point. Hence, the global maximum is found using semi-manual procedure by comparing results for many different sets of initial values. When the parameters are determined we can calculate the fatigue life for a chosen probability p of failure, see Eq. (B4) in Appendix B. Hence, the median curve and percentile curves for design purpose are obtained.

3.2. Illustrating example

To illustrate the differences between the conventional S-N curves and the present RFLM resistance curves the data given by Drebenstedt and Euler [29] (see Appendix C and Table 2) are plotted in Fig. 4 together with the two types of curves. As can be seen the curves from the two models are quite close in the upper left region of the diagram. The RFLM curve does not deviate much from a linear line and may be approximated by a straight line if the number of finite life data increases. In the lower region the conventional curve is still linear until it stops at $N = 5 \times 10^6$ or 10^7 cycles where it is assumed to change to a horizontal line (not shown). This is in accordance with the Background Documentation 9.01a [12]. In this region of the diagram the RFLM curve captures the influence of the runouts. The fact that these test specimens could have lasted even longer gives a RFLM curve that changes slope gradually such that predicted lives will be longer. The mean RFLM curve is significantly more optimistic than the conventional curve because of the 5 runouts that are included in the sample. These runouts represent 1/3 of the entire sample of 15 specimens. Nevertheless, the RFLM design curve at a PoF of 2.5% is on the safe side of all the failures. It is seen from Fig. 4 that the RFLM-based curve does not become horizontal in the area where the fatigue limit is assumed to exist in the conventional analysis. At $N = 10^7$ cycles the RFLM curve is still falling with a shallow slope. The non-linear shape of the RFLM resistance curve is quite like the original S-N curve proposed by Weibull back in the nineteen fifties. This model was revisited by D'Antuono in a recent publication [38]. However, that model has not included a random variable for the fatigue limit and does not apply the maximum likelihood method such that runouts can be included.

4. Data analysis and choice of reliability model

4.1. Present data collection at a given constant stress range of 150 MPa

In the present section the problem of selecting an appropriate distribution for the fatigue life model at a given stress range is pursued. The issue was discussed in Section 2 and illustrated in Fig. 2. Life data are collected at a constant stress range of 150 MPa (see Table 3 and Appendix D). All results are for mild and medium strength C-Mn steel with a plate thickness of 25 and 32 mm. The typical joint configuration was shown in Fig. 1. For some of the test specimens very frequent and detailed crack depth measurements were carried out during each test. This gives a unique database containing both life data and associated crack growth histories (Mikulski and Lassen [21]). The tests were carried out at rather low R ratios. For Series 1 the effective R ratio was equal to 0.35, whereas it was 0.1 for the other test series. For further details regarding test set-up and crack growth measurements the reader may follow the references given in the right column in Table 3. A total number of 138 life data were collected for the same given stress range
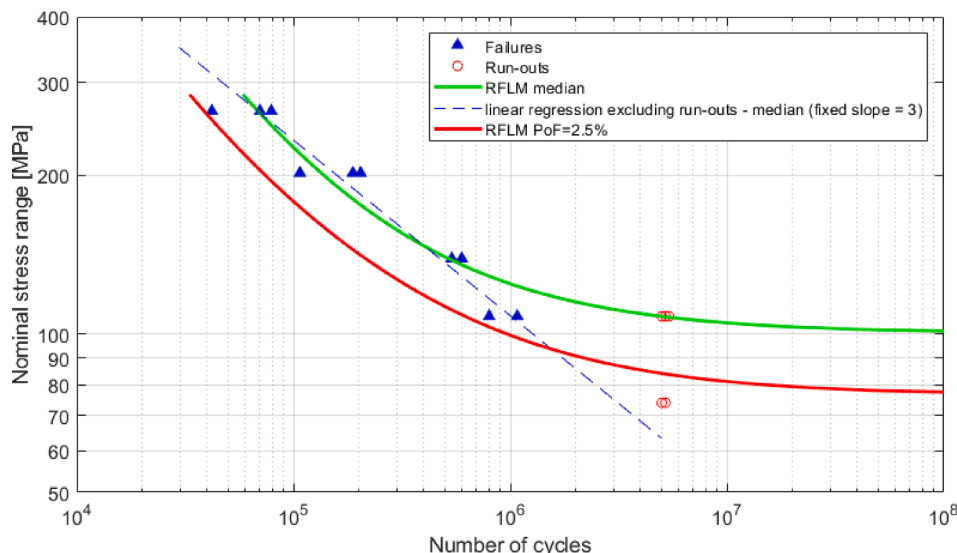

Fig. 4. S-N curves fitted to the data applied by Drebenstedt and Euler, see Appendix C.

Table 3

Overview of test series at a given applied stress range of 150 MPa.

Test data identification	Geometry	Number of specimens	Thickness	Steel grade	Welding procedure	Loading mode	Life data	Crack growth data	References
Series 1a	cruciform	34	25	S355	SMAW, FCAW	axial	x	x	1) Mikulski and Lassen [20] 2) Lassen [39]
Series 1b	cruciform	10	25	S355	SAW	axial	x	x	Lassen [39]
Series 2	cruciform	42	25	S355	SMAW	axial	x		Engesvik and Lassen [40]
Series 3	cruciform	42	32	S235	SMAW	axial	x		1) Engesvik [41] 2) Engesvik and Moan [17] 3) Engesvik and Lassen [40]
Series 4	T-joint	10	32	S355	SMAW	bending	x	x	Mikulski and Lassen [19]

and this collection permits the authors to seek the most appropriate distribution type for the life model.

4.2. Present data collection at various stress ranges

Fatigue life data at various stress ranges, besides the data presented in Section 4.1, were taken from the literature. The data collection presented in [42–44] were examined and results that were representative for the present population were included. The runout data was available only in [44]. Some fatigue life data come originally from [45–47]. These additional fatigue life data consist of 88 specimens in total, of which 15 are runouts.

4.3. Categorization and conventional life predictions for the chosen test specimen

Categorization of the welded detail in question has been changed over the years in the design standards. An overview of these changes in Eurocode 3 and DNV offshore rules is presented in Table 4. As can be seen, most of the specimens investigated in the present analysis are at the boundary given for the categorization according to the current rules. But when using the original version of these standards, the present detail has category 71 or class F undoubtedly, and this detail category is chosen in the present analysis. Moreover, the results from the present analysis of the collected life data corroborate that the chosen categorization is correct.

The following design and mean S-N curves [9] for $N < 10^7$ cycles regardless of the applied R ratio for the F class welded detail are given:

$$
\begin{aligned}
\text{design}: \quad & \log N = 11.855 - 3\log\Delta S \\
\text{mean}: \quad & \log N = 12.255 - 3\log\Delta S
\end{aligned}
\tag{6}
$$

It should be mentioned that the results for test series 3 and 4 are treated as-is without any thickness correction. A minor thickness correction would not change our conclusions from the present analyses. Statistics of the total fatigue life for the entire data collection (138 specimens) are presented in Table 5. As can be seen the collected data are very close to the S-N curve statistics for an F class. The F-class mean

Table 4

Categorization of the present welded detail in the design standards.

Standard	Governing parameter	Detail category and limitation	
ENV 1993-1-9: 1992	attachment plate thickness, T	80 for $T \leq$ 12 mm	71 for $T > 12$ mm
EN 1993-1-9: 2005	spacing of the weld base points, L	80 for $L \leq$ 50 mm	71 for $50 < L \leq$ 80 mm
DNV RP-C203 (2001)	attachment plate thickness, T	E for $T \leq 12$ mm	F for $T > 12$ mm
DNVGL RP-C203 (2016)		E for $T \leq 25$ mm	F for $T > 25$ mm

Table 5

Statistics of the total fatigue life at stress range 150 MPa.

Statistical parameter	All present test data (138 specimens)	DNVGL (F-class)
Median	455,000	533,000
Standard Deviation	278,000	288,000
Minimum	189,000	–
Maximum	2,074,000	–

S-N curve gives a median life of 533,000 cycles whereas the corresponding value from the test series is 455,000 cycles. The scatter for the present test series is given by a standard deviation of log N equal to 0.185, whereas it is close to 0.21 for the F class. Hence, the present collected test data have normal fatigue quality and are representative for the population pertaining to the F-class or category 71 in the codes.

4.4. Determining the distribution type for the life model at a stress range of 150 MPa

Before determining the distribution type for the life model, the very long lives pertaining to the fully automated SAW test specimen (Series 1b) are excluded from the present data base. These specimens had a peculiar shape of the weld toe and very long lives. The reason for excluding these results is that we shall focus on the results at the left tail of the fitted life distribution models. Hence, abnormal long lives on the right tail are not of interest. Our selected data population will consequently be representative for manual and semi-manual welding procedures. The SAW specimens are outliers in this respect. In the present work the following types of probability distributions were fitted to the collected data sample:

- The 2-parameter log-normal distribution
- The 2-parameter Weibull distribution
- The 3-parameter Weibull distribution

Results from the present analysis and the fitted distributions are illustrated in Fig. 5.

Only the 2-parameter log-normal distribution and the 3-parameter Weibull distribution passed the chi-square goodness-of-fit test at a 5% significance level. The log-normal distribution gave a better fit than 3-parameter Weibull distribution. Furthermore, as can be seen from Fig. 5, the log-normal distribution gives a better fit at the left tail where the safe life limit is determined. The main conclusion to be drawn from the present descriptive statistical analysis is that the 2-parameter log-normal distribution applied in rules and regulations is an appropriate choice for characterizing the life model for the collected life data. The competing model based on the 2-parameter Weibull model did not pass the chi-square test. Furthermore, the 3-parameter Weibull distribution gave a poorer fit to the data than the log-normal distribution,
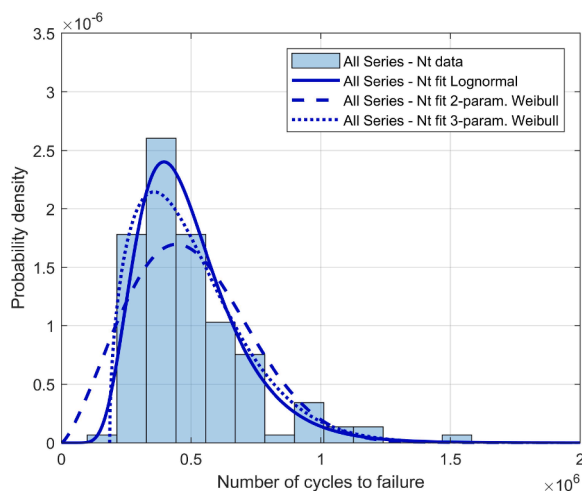
Fig. 5. Fitted probability distributions (128 samples, SAW excluded).

particularly to the important left tail of the distribution. The failure rate functions pertaining to the various distributions are shown in Fig. 6. As can be seen the Weibull model is highest in the very beginning before the log-normal failure rate increases and passes. However, the failure rate function for the log-normal model levels off when the median value for the life has been passed. This difference is generally not emphasized in engineering but gives important information for welded details in aging structures.

As conclusive remark it should be added that the model is validated at a stress range of 150 MPa and it may not represent the correct model for substantial lower stress ranges.

5. Resistance curves obtained by the RFLM

5.1. Analysis of CA fatigue lives

In the present section the RFLM methodology described in Section 3 is applied to establish fatigue resistance curves under CA loading. For the present analyses a large portion of data (216 samples) were collected at various stress ranges, particularly at lower stress ranges [42–47]. Some of these data are runouts such that the conventional linear regression analysis is not capable of including them. An RFLM analysis is carried out and the results are shown in Fig. 7. The three curves in Fig. 7 are 1) the rule-based curve, 2) the conventional S-N curves for the present data and 3) the RFLM resistance curve for the present data. The rule-based curve designated F class and is equal to the 71 category and is based on a larger amount of data. A resume of the model parameters is given in Table 6. As can be seen from the numbers in Table 6, the difference between the present conventional curve and the curves

Fig. 6. Failure rate function of the Weibull and lognormal life models.

pertaining to the F class is benign and is owed to the fact that the present data is limited compared to the huge database pertaining to the curves in rules and regulations. On this background we shall emphasize the differences found between the present conventional S-N curve and the RFLM curve as they are both based on the same collected data. But it should be commented that the all the three mean curves in Fig. 7 do coincide when the number of cycles is below 2×10^6. The design curves defined at a 97.5% probability of survival are also quite close in the same area. The small differences in these curves are caused by a small difference in the scatter of the applied data. As can be seen from Fig. 7 the present conventional mean curve and the RFLM mean curve are parallel at about 3×10^5 cycles. The discrepancy in the upper left region of the diagram is caused by the lack of data for the RFLM in this high stress regime. More data could be provided to force the RFLM curve to become almost linear in this area, but this area is not the primary stress range area of the present investigation. Above the given parallel point at 3×10^5 cycles, the conventional straight line will be accepted. The design curves in Fig. 7 are somewhat more separated than the mean curves in the same stress cycle region. However, the curves are not very different before 10^6 cycles are passed. If we focus on fatigue lives longer than 10^6 cycles it is interesting to compare the stress ranges for the two curves at 2×10^6 cycles. This is the fatigue life that is used for defining the fatigue strength and the associated fatigue category in Eurocode 3 Part 1-9. Following the procedures described in Section 2, the fatigue strength is 69 MPa for the present conventional curve whereas it is 74 MPa when defined at the RFLM curve. The increase in the fatigue strength found by the RFLM curve is reflecting the optimism inherent in the long-life data and the runouts. This gives a hyperbola curve that has the opposite curvature compared to the hyperbola used in the conventional theory. This optimism is lost when these data are excluded by the conventional analysis. The increase in fatigue strength is close to 7% and the increase in predicted fatigue life will be close to 20% in this stress region. These increases are substantial. In the high cycle regime, it is noticed that the RFLM design line continues to drop between $N = 10^7$ cycles and $N = 10^8$ cycles. This is in contradiction with the assumption of the existence of a fatigue limit in this area. Parameters of the fitted S-N curves and the S-N curves from codes are presented in Table 6. Only parameters that exist in basic equations are listed. The complete set of parameters of the fitted RFLM model is shown in Fig. 7.

Fig. 7 also shows that the RFLM design curve predicts significantly longer lives beyond 2×10^6 cycles before the stress ranges decrease to the conventional fatigue limit of 48 MPa defined at 5×10^6 cycles according to Eurocode 3 Part 1-9 for detail category 71. The RFLM curve crosses this conventional horizontal fatigue limit line at about 2×10^7 cycles. Beyond this life the RFLM model will in fact predict shorter fatigue lives than the conventional design curve given by Eurocode 3. This is an important nonconformity when comparing with the conventional curves. If we compare with the conventional design curve where it is assumed that the fatigue limit is given at 10^7 cycles the RFLM curve will predicts longer lives up until 10^9 cycles is reached.

5.2. Defining the RFLM design curve for CA loading

Based on the discussion in Section 5.1, the final CA design curve obtained by the RFLM can be defined. The proposed design curve is shown in Fig. 8 together with the conventional S-N curve obtained from the present data. In the illustration the latter linear curve is chosen to have a fatigue limit at 10^7 cycles and not at 5×10^6 cycles as in Eurocode 3 Part 1-9. The RFLM design curve is defined at 97.5% probability of survival. The obtained resistance curve is accepted as it is; however, to the left of 3×10^5 cycles, the RFLM curve shall be parallel with the conventional linear S-N curve, i.e. $m = 3.0$. The chosen point is where the RFLM curve is close to tangential to the conventional linear curve. The argument for this choice is that there is no reason to question the conventional analysis in this high stress range regime. This part of the conventional S-N curve is in the gravity centre of the data included in the
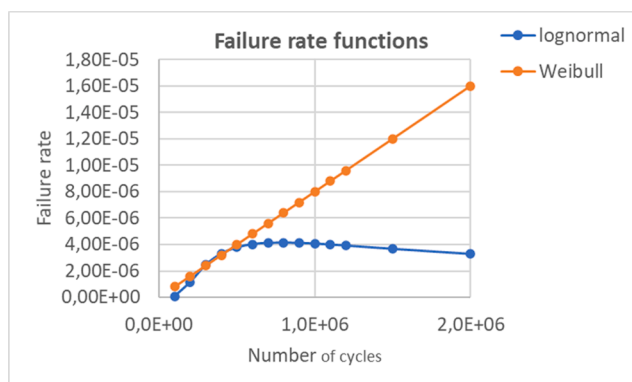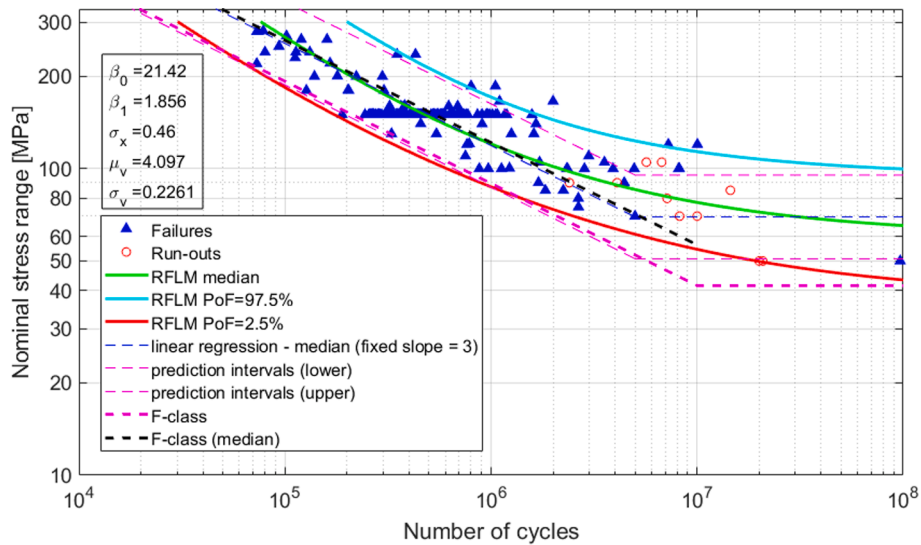
Fig. 7. RFLM fitted to all available data with plate thickness 20–32 mm, (SAW samples excluded).

Table 6
S-N curve parameters.

S-N curve	Mean curve	Design curve
Category 71 (Eurocode 3, part 1-9)	Not given	$\log a_1 = 11.855$ $m_1 = 3$
F-class (DNV)	$\log a_1 = 12.255$ $m_1 = 3$	$\log a_1 = 11.855$ $m_1 = 3$
Conventional S-N curve for the present data	$\log a_1 = 12.227$ $m_1 = 3$	$\log a_1 = 11.817$ $m_1 = 3$
RFLM for the present data	$\beta_0 = 21.42$ $\beta_1 = 1.856$ $\gamma = \exp(\mu_v) =$ $\exp(4.097) =$ 60.2	no direct parameters for probabilistic model, can be found by fitting to the numerical results with approximation function of the same type as basic RFLM Eq. (3)

linear regression analysis. The conventional design S-N curve gives a fatigue limit of 40 MPa for the present data. As can be seen from the figure the RFLM curve will predict longer CA lives than the conventional curve between 10^6 cycles and 10^9 cycles. For stresses below the conventional fatigue limit of 40 MPa the RFLM will predict finite long lives beyond 10^9 cycles, but not infinitely long as is the case for the conventional curve predictions.

It is obvious that the non-linear RFLM curve is more in agreement with the lower data points than the conventional S-N curve. But the RFLM curve has increased uncertainty at very low stresses due to the scarcity of data in this long-lasting life area. As shown, the RFLM curve will give more optimistic CA life predictions than the conventional curve if the fatigue limit is defined at 10^7 cycles. However, this is not the case if the conventional fatigue limit had been drawn at 5×10^6 cycles as recommended in Eurocode 3 Part 1-9. The design curve suggested by IIW is also included in Fig. 8. As this curve is keeping $m = 3$ down to the knee point at 10^7 cycles and has a constant slope parameter of $m = 22$ beyond this point, the curve becomes significantly more pessimistic than the present RFLM curve. It must be born in mind that the two curves are not obtained from the same data sample.

6. Considerations for the underlying damage mechanisms

As discussed in Section 2.5 the chosen probabilistic models and the
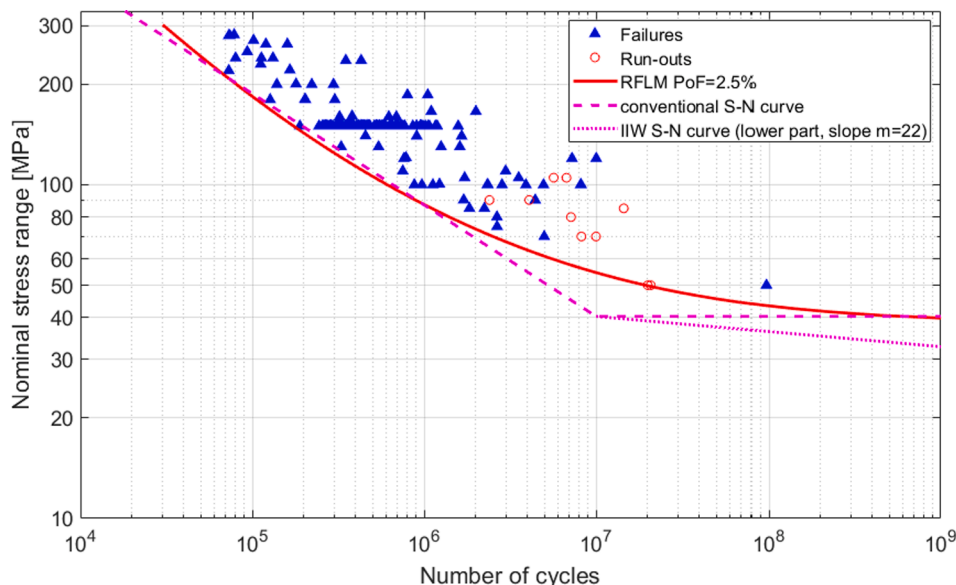

Fig. 8. Design S-N curves based on RFLM for CA loading together with the conventional S-N curve.

involved damage fatigue mechanisms shall be compatible. For the high stress ranges the present analysis confirms what is accepted as common knowledge, the upper linear S-N curve has a slope parameter m that coincides with the exponent m in the Paris crack propagation law:

$$\frac{da}{dN} = C(\Delta K)^m \, for \, \Delta K \geq \Delta K_0 \tag{7a}$$

$$\frac{da}{dN} = 0 \, for \, \Delta K < \Delta K_0 \tag{7b}$$

Hence, the fatigue life in this area consists mainly of crack growth as described by Eq. (7a). The RFLM curve continues to fall at lower stress ranges, but the slope of the curve gets more and more shallow. However, the RFLM curve does not turn into a horizontal line. This observation does in fact reject the hypothesis that a fatigue limit exists. The traditional explanation for such a fatigue limit has been that the stress intensity factor range ΔK for a given initial cracklike defect is less than the threshold value ΔK_0, i.e. as explained by Eq. (7b). Variations of such models have been used by Haibach [48] and Gurney [49,50] to establish S-N curves both for CA and VA loading. This results in an abrupt knee-point of the conventional S-N curve. In the present work the shape of the lower part of the RFLM curve demonstrates that the fatigue damage mechanism is changing gradually from crack growth to a crack initiation mechanism such that the crack initiation phase becomes the dominant part of the fatigue life. It is the present authors opinion that this shift in damage mechanisms is a better description of the physical realities than a cut-off given by the threshold value based on LEFM and Eq. (7b). To investigate this topic further the RFLM curve is split into two parts. One part is defined by a crack growth mechanism only. The corresponding curve is obtained by extrapolating the upper linear curve with slope parameter m down to a low stress range level of 1 MPa. When subtracting this crack growth life curve from the total RFLM curve given in Fig. 8 the other phase of the damage mechanism is obtained. The result is shown in Fig. 9. A conspicuous finding is that the curve obtained by subtracting the crack growth is also very close to being a straight line for a log-log scale. This curve agrees with common mechanic models for time to crack initiation such as the Coffin-Manson equation. If the present curve is linearized between 10^7 and 10^8 cycles the slope parameter m is close to $m_2 = 10$. This is in good agreement with the inverse value of the fatigue strength exponent $(-1/b)$ of the elastic part of the Coffin-Manson equation. The equation can be written:

$$\frac{\Delta \sigma}{2} = \sigma_f' (2N_i)^b \tag{8}$$

where $\Delta \sigma$ is now the weld notch stress range, $2N_i$ is the number of reversals to crack initiation, σ_f' is the fatigue strength coefficient and b is the fatigue strength exponent. The equation can be written:

$$N_i = \frac{1}{2} \frac{\left(2\sigma_f'\right)^{-1/b}}{(\Delta \sigma)^{-1/b}} \tag{9}$$

The notch stress range $\Delta \sigma$ at the weld toe is directly linear proportional to the nominal stress S under linear elastic conditions. This is assumed to be the case when the number of cycles to failure is longer than 10^7 cycles. The mean stress effect can be modelled by adding the Morrow correction to Eq. (9):

$$N_i = \frac{1}{2} \frac{\left(2\left(\sigma_f' - \sigma_m\right)\right)^{-1/b}}{(\Delta \sigma)^{-1/b}} \tag{10}$$

where σ_m is the local mean stress at the weld toe notch. The formula allows to take into account the magnitude of the residual stresses.

It should be added that the random variations in the strength exponent b can be substantial such that other results for the second slope parameter of the S-N curve are possible. Baptista et al. [31], found a value close to 12, and even the slope parameter of 22 suggested by Sonsino [15] cannot be completely rejected. However, Sonsino did not consider the possibility that the slope of the S-N curve may change gradually beyond 10^6 cycles. One should also be aware of that if the Coffin-Manson equation is adopted as the governing equation in this low stress regime it will lead to different slopes of the S-N curves for various steel grades. High strength steels will have the shallowest slope, i.e. the highest parameter m. This is well known for welded joints that have been subjected to post weld improvement techniques. However, the phenomenon is usually neglected for as-welded joints. The present discussion is summarized in Table 7. The low cycle fatigue phenomenon with number of cycles to failure less than 10^4 cycles is not included. These short lives are not within the scope of the present study. In the medium cycle area with lives between 10^4 and 10^6 cycles both the mechanical models pertaining to the S-N curve and the RFLM curve is given by the Paris propagation law. In the high cycle area where N is between 10^6 and 10^7 cycles the S-N curve is still assuming that the Paris propagation law alone is governing the damage evolution, but now a possible cut-off given by the threshold value for the SIFR is included. In this stress region the RFLM curve is supported by a two-phase model where both the time to crack initiation and the time spent in crack growth play an important role.

The model for the conventional S-N curve that ignores the crack initiation phase will result in an S-N curve that gives overly pessimistic life predictions in this curve segment. Finally, in the very high cycle regime with $N > 10^7$ cycles, the S-N curve will predict infinite lives supported by the threshold value for the SIFR, whereas the RFLM will predict very long lives with the same two-phase model as before. The only difference for the underlying physical model for the RFLM curve is that the initiation part of the fatigue life has become dominant. It is the authors opinion that the LEFM applied to explain the fatigue endurance limit given by the S-N curves should be rejected. Extensive testing has shown that there exists a significant initiation period in the fatigue lives even at stress levels as high as 150 MPa and with lives less than 10^6 cycles (Mikulski and Lassen [20,21]). The test series in this work had an initiation period close to 20% of the total fatigue life when defined as the time to reach a crack depth of 0.1 mm. This becomes even more pronounced at stress ranges giving fatigue lives beyond 10^7 cycles. The life data from the test series were typical for an F class detail such that the fatigue quality of the joint is representative for this category. The same investigation also demonstrated that the involved welding imperfections do not have a size large enough such that LEFM can be directly applied from the very beginning of the damage process such as assumed when constructing the conventional S-N curves. An objection to the present underlying physical model for the RFLM curve is that it does not
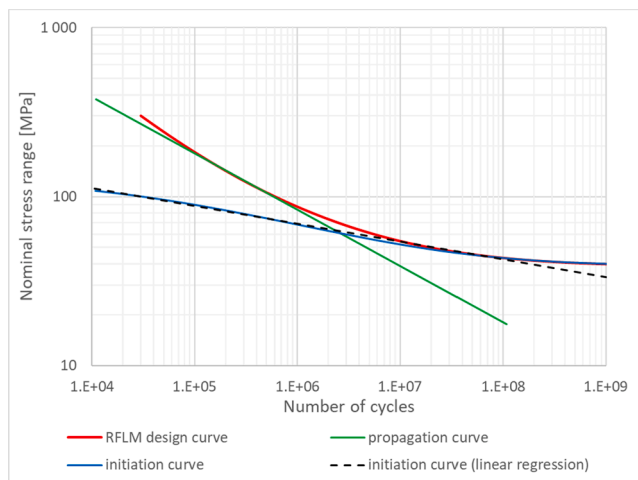

Fig. 9. Splitting the RFLM design curve into two straight lines for crack initiation and crack growth.

Table 7
The reciprocal relation between the probabilistic model and the mechanical models.

Fatigue type categorization	Damage mechanisms	Segment of conventional S-N curve	Basic physical equation S-N curve	Segment of RFLM resistance curve	Basic physical equation RFLM
medium cycle fatigue 10^4–10^6 cycles	mainly crack growth	upper straight line	Paris law	upper straight line	Paris law
high cycle fatigue 10^6–10^7 cycles	crack initiation and crack growth	lower part of straight line	Paris law	transition segment with maximum curvature	Coffin- Manson equation and Paris law
very high cycle fatigue longer than 10^7 cycles	mainly crack initiation	lower horizontal line from knee point	threshold cut-off in Paris law	lower segment which approaches a straight line	Coffin-Manson equation

explicitly model the influence of weld imperfections such as micro defects and non-metallic inclusions. A good review of possible weld imperfections is given by Hobbacher [14]. Hence, our model does not include possible micro crack nucleation, subsequent crack growth and possible crack arrest. Zerbst et al. [51] have modelled such micro crack behavior in welded joints and LEFM is not applicable. In the present case these topics would have given a physical three-phase model which also could have agreed with the shape of the RFLM resistance curve. However, the present authors have been reluctant to include this third phase, as the underlying model would become more complicated. It is our opinion that the present two-phase model strikes the balance between accuracy in life prediction and model simplicity. The possible weakness is that the initiation life model is developed for a theoretical microstructure without weld imperfections such as small defects. However, the crack initiation curve is in the present case obtained directly from experimental life data by subtracting the crack growth phase, such that any initial defects or flaws are indirectly accounted for in the initiation model. Consequently, the parameters in the physical model will reflect the presence of such possible flaws although the theoretical model was originally developed for a flawless microstructure.

7. Discussion and conclusions

The results from descriptive statistical analysis and probabilistic modelling for the fatigue life in fillet welded steel joints subjected to CA loading have been presented. The plate thicknesses are ranging from 20 to 32 mm and the steel qualities are mild and medium strength C-Mn steel. The welded details are originally designated category 71 in Eurocode 3 Part 1-9, whereas same population is designated as an F class in offshore rules and regulations. Various elementary life models at a given stress range are studied and the construction of conventional S-N curves is included. Finally, the more advanced resistance curves obtained by the RFLM are fitted to the test data. The results from the various models are compared and discussed. Based on the obtained results the following conclusions can be drawn:

1) For the fatigue life data collected at a constant stress range of 150 MPa it is demonstrated that the two-parameter log-normal distribution gives the best fit to the test results. The Weibull distribution gives a poorer fit to the life histogram. This finding supports the common life model applied for the S-N curves in current rules and regulations where the underlying linear regression analysis implies a normal distribution for a log-log scale.

2) The acceptance of the log-normal distribution for the fatigue life gives more optimistic safe life predictions than a Weibull distribution does. Furthermore, the log-normal distribution gives a failure rate function that will decay after the mean time to failure (MTTF) has been reached. This is not the case for a Weibull model that gives a steadily increasing failure rate function. The shape of the log-normal failure rate function indicates that when a welded joint has survived many cycles, it has proven its fatigue quality and may continue to be fit for purpose. This is interesting information for aging structures that have passed their fatigue design

lives. If the structure has been kept in service by a scheduled program with frequent detailed inspections up to the MTTF one does not necessarily have to increase the inspection frequency during a further life prolongation. However, the decrease in the failure rate function should not be used as an argument for omitting in-service scheduled fatigue inspection for such structures.

3) More life data were collected for the actual detail at various stress ranges to establish S-N curves. The conventional linear regression analysis was carried out using the lower prediction bound as basis for defining the design curves at chosen probability of survival. A comparison between the design curves given by the building codes for civil engineering (e.g. Eurocode 3 Part 1-9) and the codes for marine structures (e.g. DNVGL-RP-C203) was performed. Although somewhat different statistical analysis procedures are applied in the two codes, no significant differences were found in the obtained design curves. The lower prediction bound defined by a 95% probability of survival is recommended when defining the design curve in Eurocode 3 Part 1-9. If the statistical procedure accounts for the hyperbola shape of the prediction interval, this will give the same design curve as the one obtained when the probability of survival is set to 97.5% with the hyperbola shape neglected. The latter procedure is the basis for DNV recommendations. Both procedures give the same design curve.

4) At lower stress levels the linear regression has the unfortunate limitation that it excludes the long-life failures and the runout results. These data are essentially important in the way that they usually are closer to the magnitude of the acting stress ranges in-service than the finite life data entering the linear regression analysis. The short-comings of the conventional S-N curves were eliminated by using the Random Fatigue Limit Model.

5) The design curve obtained by the RFLM is non-linear for a log-log scale. The RFLM design curve is defined at a 97.5% probability of survival. The obtained resistance curve is accepted as it is; however, to the left of 3×10^5 cycles, the RFLM curve shall be parallel with the conventional linear S-N curve. The chosen point is where the RFLM curve is close to tangential to the conventional linear curve. The RFLM fatigue resistance curve will as a result coincide with the conventional linear S-N curve in the medium cycle fatigue range for stress ranges above 80 MPa. Both curves have a slope parameter $m = 3$. This part of the curve is the area where the gravity centre of the test data is found. At lower stresses where the conventional S-N curve has a knee point, the non-linear RFLM curve has its maximum curvature. This shape gives far better agreement with the long-life data in this area. Below the conventional S-N knee point the RFLM curve continues to fall with an increasing slope parameter m with a decreasing curvature. The curve becomes almost linear when 10^7 cycles are passed, but the curve does not become horizontal.

6) When comparing with a conventional S-N curve that has a CA fatigue limit at 10^7 cycles, the RFLM curve is very close to tangential to both the upper line segment and the fatigue limit when approaching 10^8 cycles. Consequently, the RFLM curve will

almost always give more optimistic CA life predictions compared to predictions based on the conventional curves found for offshore structures.

7) When comparing with a conventional S-N curve that has a CA fatigue limit at 5×10^6 cycles (as the category 71 in Eurocode 3 Part 1-9 for civil engineering), the RFLM curve is still very close to tangential to the upper line segment, but the RFLM curve has a more pessimistic shape compared to the conventional fatigue limit. For a large band of stress ranges the RFLM curve will in fact predict shorter fatigue lives than the conventional curve.

8) The comparison with the conventional curves from the offshore industry and Eurocode 3 Part 1-9 indicates that a fatigue limit drawn at 10^7 cycles is a better choice than drawing it at 5×10^6 cycles for a detail category 71. However, the RFLM resistance curve does in fact reject the existence of a fatigue limit before 10^9 cycles is reached. This rejection agrees well with the latest proposal for CA S-N curves from IIW. However, the IIW curve predicts significantly shorter fatigue lives close to its knee-point. There is still a lack of data in this very high cycle regime to support a final conclusion on this matter.

9) Based on the above observations the present RFLM resistance curve is not envisioned to replace the conventional S-N curves found in rules and regulations. However, the RFLM curve gives an important supplement for fatigue assessment in the high cycle regime.

10) It has been demonstrated that the shape of the obtained RFLM resistance curve agrees well with a two-phase model for the involved damage mechanisms. An initiation model based on the Coffin-Manson equation and a crack growth model based on the Paris propagation law have been proposed. These models will support the RFLM resistance curve to handle changes in important variables such as the applied stress ratio and the magnitude of the residual stresses.

11) Future work will be focusing on how to handle VA loading with the present RFLM resistance curves. The split into two separate curves and the conclusion drawn in clause 9) above will play an important role in this work. The support from the underlying physical equations is expected to increase the accuracy of the calculated damage accumulation. This will be the hypothesis for the future work.

Declaration of Competing Interest

The authors declare that they have no known competing financial interests or personal relationships that could have appeared to influence the work reported in this paper.

Acknowledgements

Appendix A. Summary of the mathematics for an elementary life model

The probability of failure pertaining to the SLL on the left tail in Fig. 2 in the main text is theoretically obtained by the equation:

$$P(t \leq t) = F(t) = \int_0^t f(t') dt' \tag{A1}$$

The reliability $R(t)$ is defined by the probability of surviving the SLL which is the complementary probability to the expression in Eq. (A1):

$$P(t > t) = R(t|\mu, \sigma, S|) \tag{A2}$$

The failure rate function is defined by, Lewis [52]:

$$\lambda(t) = \frac{f(t)}{R(t)} \tag{A3}$$

The failure rate function is a conditional probability function. It gives the probability of failure per time unit just after the time t is reached, given that the joint has survived up to the time t.

Appendix B. Summary of the mathematics for the RFLM curves

With Eq. (3) in the main text as basis, it is assumed that $v = \ln(\gamma)$ has a Probability Density Function (PDF) given by:

$$f_V(v) = \frac{1}{\sigma_v} \varphi_V\left(\frac{v - \mu_v}{\sigma_v}\right) \tag{B1}$$

with location parameter and scale parameter μ_v and σ_v, respectively. $\phi_v(\cdot)$ is the normal frequency function. Let $x = \ln(\Delta S)$ and $W = \ln(N)$. Assuming that V is given and that $V < x$, $W|V$ then has a frequency function:

$$f_{W|V}(w) = \frac{1}{\sigma_x} \varphi_{W|V}\left(\frac{w - [\beta_0 - \beta_1 \ln(\exp(x) - \exp(v))]}{\sigma_x}\right) \tag{B2}$$

with the location parameter $\beta_0 - \beta_1 \ln(\exp(x) - \exp(v))$ and scale parameter σ_x. The marginal frequency function of W is given by:

$$f_W(w) = \int_{-\infty}^x \frac{1}{\sigma_x \sigma_v} \varphi_{W|V}\left(\frac{w - [\beta_0 - \beta_1 \ln(\exp(x) - \exp(v))]}{\sigma_x}\right) \varphi_V\left(\frac{v - \mu_v}{\sigma_v}\right) dv \tag{B3}$$

The marginal Cumulative Distribution Function (CDF) of W is given by:

$$F(w) = \int_{-\infty}^{x} \frac{1}{\sigma_v} \Phi_{W|V}\left(\frac{w - [\beta_0 - \beta_1 \ln(\exp(x) - \exp(v))]}{\sigma_x}\right) \varphi_V\left(\frac{v - \mu_v}{\sigma_v}\right) dv \tag{B4}$$

where $\Phi_{W|V}(\cdot)$ is the CDF of W|V. Further details are found in [32,33].

Appendix C. Life data for the Drebenstedt and Euler example

Life data from [28,29]

Stress range [MPa]	Cycles	failure/runout
265	42,000	failure
265	70,000	failure
265	79,000	failure
202	107,000	failure
202	188,000	failure
202	204,000	failure
139	537,000	failure
139	597,000	failure
108	800,000	failure
108	1,077,000	failure
108	5,000,000	runout
108	5,200,000	runout
108	5,400,000	runout
74	5,000,000	runout
74	5,200,000	runout

Appendix D. Life data at a stress range of 150 MPa

Series 1a		Series 1b		Series 2		Series 3		Series 4	
A3	387,235	A11	999,119	S2-1	323,520	S3-1	326,810	B2	1,578,652
A4	370,248	A15	603,314	S2-2	262,950	S3-2	551,000	B3	636,004
A5	436,426	A23	523,562	S2-3	259,310	S3-3	552,900	B5	599,388
A6	483,540	A27	523,656	S2-4	270,510	S3-4	416,860	B6	571,395
A8	647,939	A28	505,000	S2-5	454,300	S3-5	632,400	B7	376,006
A9	544,635	A31	1,490,400	S2-6	265,970	S3-6	1,073,630	B8	658,011
A10	336,070	A35	2,073,554	S2-7	314,480	S3-7	707,270	B9	410,012
A12	576,732	A40	651,503	S2-8	323,290	S3-8	387,380	B10	446,519
A13	428,970	A43	1,074,052	S2-9	286,650	S3-9	370,620	B11	590,574
A14	374,064	A48	1,008,050	S2-10	189,270	S3-10	1,016,410	B12	318,504
A16	512,159			S2-11	305,120	S3-11	859,160		
A17	424,542			S2-12	282,630	S3-12	679,950		
A18	334,876			S2-13	283,220	S3-13	650,260		
A20	588,573			S2-14	388,710	S3-14	984,700		
A21	414,214			S2-15	330,070	S3-15	771,560		
A22	352,006			S2-16	312,400	S3-16	522,390		
A24	553,546			S2-17	244,490	S3-17	729,880		
A25	478,004			S2-18	327,230	S3-18	582,590		
A29	702,468			S2-19	294,680	S3-19	705,180		
A30	594,047			S2-20	255,400	S3-20	905,440		
A33	456,790			S2-21	367,388	S3-21	432,050		
A34	361,002			S2-22	390,560	S3-22	647,280		
A36	551,015			S2-23	472,230	S3-23	954,790		
A37	527,270			S2-24	305,266	S3-24	484,140		
A38	332,513			S2-25	425,700	S3-25	693,870		
A39	734,505			S2-26	376,390	S3-26	379,470		
A41	525,507			S2-27	268,250	S3-27	1,163,580		
A42	349,059			S2-28	404,030	S3-28	549,230		
A44	580,007			S2-29	276,320	S3-29	522,380		
A45	382,012			S2-30	319,820	S3-30	323,960		
A46	447,015			S2-31	374,080	S3-31	1,191,670		
A47	445,007			S2-32	310,590	S3-32	565,680		
A49	465,717			S2-33	362,750	S3-33	947,660		
A50	345,074			S2-34	356,300	S3-34	455,550		
				S2-35	326,170	S3-35	463,760		
				S2-36	367,110	S3-36	530,000		
				S2-37	365,450	S3-37	736,780		
				S2-38	288,810	S3-38	527,320		
				S2-39	380,690	S3-39	754,890		
				S2-40	334,540	S3-40	532,700		
				S2-41	346,350	S3-41	901,850		
				S2-42	366,210	S3-42	713,450		

References

[1] Murakami Y, Takagi T, Wada K, Matsunaga H. Essential structure of S-N curve: Prediction of fatigue life and fatigue limit of defective materials and nature of scatter. Int J Fatigue 2021; 146. doi:10.1016/j.ijfatigue.2020.106138.

[2] Hobbacher A. Recommendations for Fatigue Design of Welded Joints and Components. Springer; 2016. doi:10.1007/978-3-319-23757-2.

[3] Radaj D, Sonsino CM, Fricke W. Fatigue Assessment of Welded Joints by Local Approaches. Elsevier Science; 2006.

[4] Lassen T, Recho N. FLAWS Fatigue Life Analyses of Welded Structures. ISTE 2006.

[5] Lotsberg I. Fatigue Design of Marine Structures. Cambridge: Cambridge University Press; 2016. doi:10.1017/CBO9781316343982.

[6] Maddox SJ. Fatigue Strength of Welded Structures (Second Edition). Second Edi. Woodhead Publishing; 1991. doi:10.1016/B978-1-85573-013-7.50002-1.

[7] EN 1993-1-9:2005. Eurocode 3: Design of steel structures - Part 1-9: Fatigue; 2005.

[8] HSE. Offshore rules; 1991.

[9] DNVGL. DNVGL-RP-C203: Fatigue Design of Offshore Steel Structures; 2016.

[10] ABS. Guide for Fatigue Assessment of Offshore Structures. Standardization 2003; 2014:1–56.

[11] ISO 12107:2012. Metallic materials — Fatigue testing — Statistical planning and analysis of data; 2012.

[12] ECCS Technical Committee 6 - Fatigue. Background Documentation 9.01a: Background information on fatigue design rules – Statistical evaluation – 3rd Draft; 2018.

[13] Schijve J. Fatigue Predictions and Scatter. Fatigue Fract Eng Mater Struct 1994;17: 381–96. https://doi.org/10.1111/j.1460-2695.1994.tb00239.x.

[14] Hobbacher AF. The new IIW recommendations for fatigue assessment of welded joints and components - A comprehensive code recently updated. Int J Fatigue 2009;31:50–8. https://doi.org/10.1016/j.ijfatigue.2008.04.002.

[15] Sonsino CM. Course of SN-curves especially in the high-cycle fatigue regime with regard to component design and safety. Int J Fatigue 2007;29:2246–58. https://doi.org/10.1016/j.ijfatigue.2006.11.015.

[16] Wirsching PH. Report no. 17: The statistical distribution of cycles to failure. Paramus, NY: 1984.

[17] Engesvik K, Moan T. Probabilistic analysis of the uncertainty in the fatigue capacity of welded joints. Eng Fract Mech 1983;18:743–62. https://doi.org/10.1016/0013-7944(83)90122-4.

[18] ENV 1993-1-1: 1992, Eurocode 3: Design of steel structures; 1992.

[19] DNV. Recommended practice RP-C203: Fatigue Strength Ananlysis of Offshore Steel Structures; 2001.

[20] Mikulski Z, Lassen T. Fatigue crack initiation and subsequent crack growth in fillet welded steel joints. Int J Fatigue 2019;120:303–18. https://doi.org/10.1016/j.ijfatigue.2018.11.014.

[21] Mikulski Z, Lassen T. Crack growth in fillet welded steel joints subjected to membrane and bending loading modes. Eng Fract Mech 2020;235:107190. https://doi.org/10.1016/j.engfracmech.2020.107190.

[22] Lassen T, Recho N. Proposal for a more accurate physically based S-N curve for welded steel joints. Int J Fatigue 2009;31:70–8. https://doi.org/10.1016/j.ijfatigue.2008.03.032.

[23] Benjamin JR, Cornell CA. Probability, Statistics, and Decision for Civil Engineers. McGraw-Hill; 1970.

[24] Bastenaire FA. New Method for the Statistical Evaluation of Constant Stress Amplitude Fatigue-Test Results. In: Heller RA, editor. Probabilistic Asp. Fatigue, West Conshohocken, PA: ASTM International; 1972, p. 3–28. doi:10.1520/STP35402S.

[25] Hobbacher A. Fatigue Design of Welded Joints and Components. Woodhead Publishing; 1996. doi:10.1533/9780857093189.34.

[26] Hobbacher A. Recommendations for fatigue design of welded joints and components. Doc. XIII-1251-07, XV-1254-07. 2007.

[27] Cooper BE. Statistics for Experimentalists. Oxford: Pergamon Press; 1969.

[28] Euler M, Kuhlmann U. Statistical intervals for evaluation of test data according to Eurocode 3 Part 1-9. ECCS Technical committee 6 - Fatigue, Contribution to working group 6.3 Statistical analysis of fatigue data; 2013.

[29] Drebenstedt K, Euler M. Statistical Analysis of Fatigue Test Data according to Eurocode 3. In: Powers, Frangopol, Al-Mahaidi, Caprani, editors. Maintenance, Safety, Risk, Manag. Life-Cycle Perform. Bridg., London: Taylor & Francis Group; 2018, p. 2244–51.

[30] Schneider CRA, Maddox SJ. Best practice guide on statistical analysis of fatigue data; 2003.

[31] Baptista C, Reis A, Nussbaumer A. Probabilistic S-N curves for constant and variable amplitude. Int J Fatigue 2017;101:312–27. https://doi.org/10.1016/j.ijfatigue.2017.01.022.

[32] Pascual FG, Meeker WQ. Estimating fatigue curves with the random fatigue-limit model. Technometrics 1999;41:277–89. https://doi.org/10.1080/00401706.1999.10485925.

[33] Lassen T, Darcis P, Recho N. Fatigue Behavior of Welded Joints Part 1 - Statistical Methods for Fatigue Life Prediction. Weld J 2005;84:183s–7s.

[34] D'Angelo L, Nussbaumer A. Estimation of fatigue S-N curves of welded joints using advanced probabilistic approach. Int J Fatigue 2017;97:98–113. https://doi.org/10.1016/j.ijfatigue.2016.12.032.

[35] Toasa Caiza PD, Ummenhofer T. General probability weighted moments for the three-parameter Weibull Distribution and their application in S-N curves modelling. Int J Fatigue 2011;33:1533–8. https://doi.org/10.1016/j.ijfatigue.2011.06.009.

[36] Toasa Caiza PD, Ummenhofer T. A probabilistic Stüssi function for modelling the S-N curves and its application on specimens made of steel S355J2+N. Int J Fatigue 2018;117:121–34. https://doi.org/10.1016/j.ijfatigue.2018.07.041.

[37] Leonetti D, Maljaars J, Snijder HH (Bert). Fitting fatigue test data with a novel S-N curve using frequentist and Bayesian inference. Int J Fatigue 2017; 105: 128–43. doi:10.1016/j.ijfatigue.2017.08.024.

[38] D'Antuono P. An analytical relation between the Weibull and Basquin laws for smooth and notched specimens and application to constant amplitude fatigue. Fatigue Fract Eng Mater Struct 2020;43:991–1004. https://doi.org/10.1111/ffe.13175.

[39] Lassen T. The effect of the welding process on the fatigue crack growth in welded joints. Weld J 1990; February: 75s-85s.

[40] Engesvik K, Lassen T. The effect of weld geometry on fatigue life. Proc. 7th Int. Conf. Offshore Mech. Arct. Eng. OMAE1988, Houston, Texas: ASME Press; 1988, p. 441–5.

[41] Engesvik K. Analysis of Uncertainties in the Fatigue Capacity of Welded Joints, Report UR-82-17. Trondheim: 1982.

[42] Stötzel J. Collection and evaluation of fatigue test results - RWTH Aachen, ECCS-TC6-Fatigue, IIW-Working Group JWG XIII-XV. n.d.

[43] Lindqvist A, Nilsson H. Effective notch stress analysis of transverse attachments in steel bridges - a parametric fatigue life assessment. Chalmers 2016.

[44] Lebas G, Fauve JC. Collection of fatigue data. Pau: Elf Aquitaine; 1988.

[45] Gurney TR. The Fatigue Strength of Transverse Fillet Welded Joints. Woodhead Publishing; 1991.

[46] Gurney TR. Thickness effect in "relatively thin" welded joints; Offshore Technology Report OTH 91 358; 1995.

[47] Berge S. On the effect of plate thickness in fatigue of welds. Eng Fract Mech 1985; 21:423–35. https://doi.org/10.1016/0013-7944(85)90030-X.

[48] Haibach E. Discussion paper. Weld Inst Conf Fatigue Welded Struct 1970.

[49] Gurney TR. Cumulative damage calcuations taking account of low low stresses in the spectrum. TWI Report 2/1976/E. 1976.

[50] Gurney TR. Cumulative Damage of Welded Joints. Woodhead Publishing; 2006. doi:10.1533/9781845691035.1.

[51] Zerbst U, Madia M, Schork B. Fracture mechanics based determination of the fatigue strength of weldments. Procedia Struct Integr 2016;1:10–7. https://doi.org/10.1016/j.prostr.2016.02.003.

[52] Lewis EE. Introduction to Reliability Engineering. Wiley; 1988.